C–O Bonds Formation Using Transition Metal Alkyl or Aryl Complexes

Jiajun Mei

B.S. Chemistry, Peking University, 2008

A Dissertation Presented to the Graduate Faculty of the
University of Virginia in Candidacy for the Degree of
Doctor of Philosophy

Department of Chemistry

University of Virginia

Jan 23, 2015

ABSTRACT

MEI, JIAJUN C–O Bond Formation using Transition Metal Alkyl or Aryl Complexes. (Under the direction of Professor T. Brent Gunnoe.)

The selective catalytic oxidation of hydrocarbons is an important but challenging process. Transition metal catalysts for partial oxidation of alkanes to form alcohols must be able to perform two key steps: C–H bond activation and C–O bond formation. One strategy is to activate the C–H bond of hydrocarbons (RH) by a metal–alkoxide (M–OR) complex to produce the alcohol and a metal–alkyl (M–R) complex ($\boldsymbol{RH + M{-}OR \rightarrow M{-}R + ROH}$), followed by net O-atom insertion into the newly formed M–R bond by an oxygen donor (YO) to regenerate the M–OR complex ($\boldsymbol{M{-}R + YO \rightarrow M{-}OR}$). With examples of both steps reported, relatively little is known about the O-atom insertion step. Two pathways for the O-atom insertion step are under investigation. One is an organometallic Baeyer-Villiger (OMBV) type reaction involving the migration of the nucleophilic R$^{\delta-}$ to the bound OY ($\boldsymbol{M{-}R^{\delta-} + OY \rightarrow R^{\delta-}{-}M{-}O^{\delta+}{-}Y \rightarrow M{-}OR + Y}$), the other pathway involves the migration of the nucleophilic R$^{\delta-}$ to a M≡O$^{\delta+}$ intermediate ($\boldsymbol{M{-}R^{\delta-} + OY \rightarrow R^{\delta-}{-}M{\equiv}O^{\delta+} + Y \rightarrow M{-}OR + Y}$). Stoichiometric reactions are utilized to extend the O-atom insertion reaction to a range M–R complexes and to demonstrate the transition series between different nucleophilicity of the M–C$^{\delta-}$ bond.

Extension of the O-atom insertion to the middle transition W^{VI}–R complexes has been studied. Cp*W(O)$_2$(CH$_2$SiMe$_3$) (Cp* = η^5-pentamethylcyclopentadienyl) reacts with oxygen atom donors (*e.g.*, H$_2$O$_2$, PhIO, IO$_4^-$) in THF/water to produce high yield TMSCH$_2$OH (TMS = trimethylsilyl). Mechanism studies reveal an OMBV type O-atom insertion for this conversion.

Attempts of O-atom insertion into late(r) transition 3d Fe^{II}–R and Co^{I}–R complexes have been presented. $Cp^*Fe(P(OCH_2)_3CEt)_2Ph$ reacts with Me_3NO to produce high yield PhOH in the presence of Brønsted acid. All the other ligands are also oxidized by Me_3NO during this conversion. Computational mechanism studies suggest a R to M=O migration pathway. Low yield of MeOH is produced from $(N_3)CoMe$ (N_3 = triamine ligand) with oxidants. Decomposition of the Co–Me complex occurs during this conversion.

ACKNODGEMENTS

So many people deserve thanks for their support and direction for this dissertation.

Thank you to my collaborators who have directly helped in the completion of this dissertation. Thank you to Dr. Cundari, Kurtis, Cody and Daniel for your theoretic and computational work to this dissertation. Thank you to Dr. Jeff Elena for the support in NMR technique. Thank you to Dr. Michal Sabat for solving crystal structures. Thank you to my CCHF collaborators for helping with the projects.

Thank you to my committee members Dr. Dean Harman, Dr. Pu Lin, Dr. Cassandra Fraser, and Dr. Bob Davis for answering questions, reading annual reports and providing constructive suggestions for my research.

Thank you to the Gunnoe group who truly understand what I do, It has been a pleasure to work together with you: Samantha, Chong, Steve, Mike, Tristan, Kathleen, Ben, Junqi, Nicole, John, Bridgette, Zuming, Huimin, Yan, Shaojin, Max, Edmund, Anna, Nate, Michael, Thomas, Paige. Thanks to old members and postdocs for mentoring and answering questions: Mark (training me), Brad, Joanna, Evan, Vijay, Jeremy, Brandon, Ted, George, Mat, Sarah and Dominik.

So many Thanks to my advisor Brent Gunnoe. Thank you for accepting me to the group. Thank you for your patience whenever I have questions. Thank you for your encourage whenever I was frustrated. Your enthusiasm, optimism, passion in Chemistry and your persistence, diligence in work have been a perfect example what a scientist should be. Your integrity, knowledge, patience and considerateness have been a perfect

example what a teacher and mentor should be. I have learnt so many qualities from you beyond chemistry. I could not work for anyone better.

Thank you to my parents and my brother for understanding me as a graduate student studying abroad. Thanks for your doubtless support. Thank you to all my family members for understanding my barely visits to you.

Most importantly, thank you to my fiancée Qian for transferring to UVa and going through this with me for five straight years. Without your sacrifice and support I could not finish all of this.

TABLE OF CONTENTS

LIST OF SCHEMES……viii
LIST OF FIGURES……xii
LIST OF TABLES……xvi

1 Introduction……1
1.1 Methane to Methanol (MTM)……1
  1.1.1 Rationale and Direction for Methane to Methanol……1
  1.1.2 Heterogeneous Catalyzed Methane Oxy-functionalization……4
  1.1.3 Methane Functionalization by Homogeneous Transition Metal-Mediated Catalysts-The Shilov and Related systems……8
  1.1.4 Other Approaches to Oxy-functionalization of Hydrocarbons……13
1.2 C–H Activation by Metal–alkoxide Bonds (M–OR)……18
1.3 C–O bond Formation by Oxygen Atom Insertion……23
  1.3.1 Oxygen Atom Insertion by Radical Pathway……24
  1.3.2 Oxygen Atom Insertion by Non-radical Pathways……25
    1.3.2.1 Oxygen Atom Insertion by Migration of R to M(η^2-O2) …… ……25
    1.3.2.2 Oxygen Atom Insertion into M–R bonds by Migration of R to M=O……27
    1.3.2.3 Oxygen Atom Insertion by Migration of R to M–OY……31
    1.3.2.4 Computational Study of Oxygen Atom Insertion into Late Transition Metal–alkyl Complexes……36
  1.3.3 Previous work by Gunnoe group……39
1.4 Summary and Directions……47

2 Variable Pathways for Oxygen Atom Insertion into Metal–Carbon Bonds: The Case of Cp*W(O)$_2$(CH$_2$SiMe$_3$)……58
2.1 Rationale for Study of Oxygen Atom Insertion into W–C bonds……58
2.2 Results and Discussion……66
  2.2.1 Reaction of Cp*W(O)$_2$(CH$_2$SiMe$_3$) (2.1) with NaIO$_4$……66
  2.2.2 Reaction of Cp*W(O)(η^2-O$_2$)(CH$_2$SiMe$_3$) (2.2) with NaOH……85
  2.2.3 Reaction of Cp*W(O)(η^2-O$_2$)(CH$_2$SiMe$_3$) (2.2) with Brønsted Acid……91
  2.2.4 Reaction of Cp*W(O)$_2$(CH$_2$SiMe$_3$) (2.1) with Hydrogen Peroxide in the Presence of Hydroxide……96
2.3 Summary and Discussions……99
2.4 Experimental Section……101
2.5 References……108

3 Oxygen Atom Insertion into Iron(II) Phenyl and Methyl Bonds……109
3.1 Rationale for Study of Oxygen Atom Insertion into Fe–C bonds……109
3.2 Results and Discussion ……122
  3.2.1 The Reaction of Cp*Fe(CO)(NCMe)Ph (3.1) with Oxidants……122
  3.2.2 The reaction of Cp*Fe(P(OCH$_2$)$_3$CEt)$_2$Ph (3.3) with Me$_3$NO……125
  3.2.3 The Reaction of Cp*Fe(P(OCH$_2$)$_3$CEt)$_2$Ph (3.3) with Other Oxidants……142
  3.2.4 The reactivity of Cp*Fe(P(OCH$_2$)$_3$CEt)$_2$Me (3.5)……148
3.3 Summary and Conclusions……151

3.4 Experimental Section……………………………………………………………….152
3.5 References…………………………………………………………………….158

4 Oxygen Atom Insertion into Cobalt(I) Methyl Bond…………………..………..…164
4.1 Rationale for Study of Oxygen Atom Insertion into Co–C bonds………………….164
4.2 Results and Discussion……………………………………………………..…168
  4.2.1 Synthesis of (N_3)CoMe (4.1)………………………………..………......168
  4.2.2 Reactions of (N_3)CoMe (4.1) with Oxidants…………………..…………….169
4.3 Summary and Discussion………………………………………………………175
4.4 Experimental Section……………..…………………………………………...176
4.5 References………………………………………………………………………..178

5. Summary and Outlook…………………..……………………………………182
5.1 Early 3d *vs* Late 4d and 5d (Nucleophilicity of the $R^{\delta-}$ *vs* Electrophilicity of $O^{\delta+}$)..182
5.2 OMBV *vs* R to M=O………………………………………………………..184
5.3 Trends for the O-atom Insertion into Middle and Late Metal–Carbon Bonds….185
5.4 Ligands………………………………………………………………………...188
5.5 Outlook and Directions…………………………………………………...189
5.6 References……………………………………………………………………..190

LIST OF SCHEMES

Scheme 1.1. Advantages of partial oxidation of methane-to-methanol (MTM) process …………………………………………………………………………… 2

Scheme 1.2. Catalytic cycle for the oxidation of CH_4 to CH_3OOH using H_2O_2, catalyzed by a binuclear Fe species in ZSM-5. The overall charge in each case is formally +2 as the species acts as an extra-framework cation within the zeolite….. 6

Scheme 1.3. Selective oxidation of methane to methanol by bipyrimidinylplatinum polyoxometalate hybrid compound catalyst…………... 7

Scheme 1.4. Structure of supported Periana catalyst on covalent triazine-based framework (CTF)…………………………………………………………………… 8

Scheme 1.5. General catalytic cycle for selective functionalization of hydrocarbons (X = OH, Cl)……………………………………………………… 10

Scheme 1.6. Proposed catalytic cycle for methane functionalization by Shilov system…………………………………………………………………………..... 12

Scheme 1.7. Selective oxidation of CH_4 using $(bpmy)Pt(Cl)_2$ in concentrated sulfuric acid (OP = Cl, HSO_4)…………………………………………………… 13

Scheme 1.8. Two possible pathways for oxidation of hydrocarbons (RH) involving C–H activation via 1,2-addition across metal-heteroatom bonds…………………... 15

Scheme 1.9. Generic mechanisms for the organic Baeyer-Villiger reaction and the analogous organometallic Baeyer-Villiger reaction (OMBV)…………….......... 17

Scheme 1.10. Electronic properties for the C–X bond formation in the Shilov-type systems and C–O bond formation via organometallic Baeyer-Villiger reaction (OMBV)…………………………………………………………………………….. 18

Scheme 1.11. Proposed mechanism and calculated results (PH_3 for PMe_3) for C–H activation of benzene by $TpRu(PMe_3)_2OH$……………………………………… 20

Scheme 1.12. Statistically corrected results for the H/D exchange reaction of $TpRu(PMe_3)_2OH$ in toluene-d_8.. 21

Scheme 1.13. proposed mechanism for C–H activation by (κ^2-*O,O*-acac)$_2$Ir(HOMe)(OMe) (acac = acetylacetonate)…………………………………… 22

Scheme 1.14. Proposed mechanism for C–H activation of arenes by (PNP)Ph(OR). 23

Scheme 1.15. Proposed mechanism for C–H activation of indene by [(COD)Rh(μ-OH)]$_2$…………………………………………………………………………... 24

Scheme 1.16. Proposed mechanism for O-atom insertion into Zr–R bond via radical pathway……………………………………………………………... 26

Scheme 1.18. Proposed mechanism for O-atom insertion into Ta–C bond catalyzed by electrophiles……………………………………………………... 27

Scheme 1.19. Proposed mechanism for O-atom insertion into Cr–Ph bond……….. 28

Scheme 1.20. O-atom insertion into Re–Ar bonds by migration of Ar to Re^V=O…. 29

Scheme 1.22. Comparison of the migrations in the R to M=O, Organometallic Baeyer-Villiger (OMBV) reaction and Shilov-type reaction……………………….. 30

Scheme 1.23. Oxygen atom insertion into Ni–C bond in the Hillhouse system…… 31

Scheme 1.24. Calculated pathway for oxygen atom insertion into Ni–C bond…….. 32

Scheme 1.25. O-atom insertion form [2-((dimethylamino)methyl)-3-naphthyllpalladium complex and tBuOOH via formation of P^{IV}=O intermediate…. 32

Scheme 1.26. O-atom insertion into Pd–Ar bond…………………………………... 33

Scheme 1.27. The kinetics of the reaction of MTO and H_2O_2 to release MeOH in aqueous solution…… 33
Scheme 1.28. Proposed mechanism for the O-atom insertion into MTO with various oxidants…… 34
Scheme 1.29. Two possible pathways for the reaction of MTO with IO_4^- to produce MeOH…… 35
Scheme 1.30. O-atom insertion into $ArReO_3$ and related complex via organometallic Baeyer-Villiger (OMBV) pathway…… 36
Scheme 1.31. Proposed mechanism for flavins catalyzed oxidation (S = Substrate) 37
Scheme 1.32. Reaction of MTO with flavins peroxide and hydroperoxide anions via a BV transition state (R = flavins or H; $\Delta\Delta G^{\ddagger} = 4.8$ kcal/mol)…… 38
Scheme 1.33. The model reaction and metals that are studied computationally for the OMBV O-atom insertion reactions…… 39
Scheme 1.34. Transitions for the nucleophilicity of the $M–C^{\delta-}$ bond or the electrophilicity of the bound $O^{\delta+}$ in the periodic table…… 42
Scheme 1.35. Reaction of $[(^t\text{bpy})\text{Pt(Ph)(THF)}][\text{BAr'}_4]$ with YO (YO = $Me_2S=O$, $ONMe_3$ or PyO) to form coordinated YO products $[(^t\text{bpy})\text{Pt(Ph)(YO)}][\text{BAr'}_4]$ without the generation of the O-atom insertion products upon heating…… 44
Scheme 1.36. Synthesis of $[(^t\text{bpy})_2\text{Rh(Me)(OTf)}][\text{BAr'}_4]$…… 45
Scheme 1.37. Reactions of $[(^t\text{bpy})_2\text{Rh(Me)(OTf)}][\text{BAr'}_4]$ with H_2O, $ONMe_3$ and PyO (80 °C) to form the coordinated products…… 46
Scheme 1.38. Reactivity of $[(^t\text{bpy})_2\text{Rh(Me)(ONMe}_3)][\text{BAr'}_4][\text{OTf}]$ at 160 °C…… 47
Scheme 1.39. Reactivity of $[(^t\text{bpy})_2\text{Rh(Me)(PyO)}][\text{BAr'}_4][\text{OTf}]$ under thermolysis and photolysis…… 48
Scheme 1.40. Summary of the O-atom insertion reactions into transition M–R bonds…… 50
Scheme 2.1. Proposed catalytic cycle for methane functionalization by Shilov system…… 59
Scheme 2.2. Proposed pathways for partial oxidation of hydrocarbon involving oxygen atom insertion into a M–R bond and 1,2-CH-additon across a M–OR bond…… 60
Scheme 2.3. Proposed mechanism for O-atom insertion into Ta–C bond catalyzed by electrophiles…… 61
Scheme 2.4. The kinetics of the reaction of MTO and H_2O_2 to release MeOH in aqueous solution…… 62
Scheme 2.5. Generic mechanisms for the organic Baeyer-Villiger reaction and the analogous organometallic Baeyer-Villiger reaction (OMBV)…… 64
Scheme 2.6. Proposed mechanism for the O-atom insertion into MTO with various oxidants 64
Scheme 2.7. Two possible pathways for the reaction of MTO with IO_4^- to produce MeOH…… 65
Scheme 2.8. $Cp^*W(O)_2(CH_2SiMe_3)$ (**2.1**) reacts with H_2O_2 (30%) to generate $Cp^*W(O)(\eta^2\text{-}O_2)(CH_2SiMe_3)$ (**2.2**)…… 67
Scheme 2.9. Reactions of $Cp^*W(O)(\eta^2\text{-}O_2)(CH_2SiMe_3)$ (**2.2**) with oxidants or water do not result in O-atom insertion into W–R bond…… 68
Scheme 2.10. Proposed mechanism for the formation of $TMSCH_2OH$ from the

reaction of Cp*W(O)$_2$(CH$_2$SiMe$_3$) (**2.1**) and NaIO$_4$ in 1:1 THF-d_8:D$_2$O (v:v)........ 72

Scheme 2.11. Reactions monitored in the kinetic simulation........................... 73

Scheme 2.12. Calculated free energy for the production of TMSCH$_2$OH in the reaction of Cp*W(O)$_2$(CH$_2$SiMe$_3$) (**2.1**) with periodate. Numbers are free energies (kcal/mol) for 1,4-dioxane (top, bold) and water (bottom, italics), and are relative to complex **2.1** and IO$_4^-$... 78

Scheme 2.13. Possible pathways for alcohol release from the reaction of Cp*W(O)(η^2-O$_2$) (CH$_2$SiMe$_3$) (**2.2**) with NaOH in 1:1 THF-d_8:D$_2$O (v:v). Mechanism studies are consistent with Pathway C..................................... 88

Scheme 2.14. Calculated free energy for the reaction of Cp*W(O)(η^2-O$_2$) (CH$_2$SiMe$_3$) (**2.2**) with OH$^-$. Numbers are free energies (kcal/mol) for 1,4-dioxane (top, bold) and water (bottom, italics), and are relative to complex **2.2** (Cp* = κ^1-Cp*).. 91

Scheme 2.15. Two possible pathways for the alcohol release reaction of Cp*WO(η^2-O$_2$) (CH$_2$SiMe$_3$) (**2.2**) with HCl.. 94

Scheme 2.16. Calculated free energy for the reaction of Cp*WO(η^2-O$_2$) (CH$_2$SiMe$_3$) (**2.2**) with H$^+$. The Eigen Cation (H$_9$O$_4^+$) was used to model the proton. Numbers are free energies (kcal/mol) for 1,4-dioxane (top, bold) and water (bottom, italics) and are relative to complex **2.2**.. 95

Scheme 2.17. Comparison of alcohol release from Cp*W(O)$_2$(CH$_2$SiMe$_3$) (**2.1**) with H$_2$O$_2$ in the presence of H$^+$ and OH$^-$.. 98

Scheme 2.18 . Calculated free Energy for the conversion of Cp*W(O$_2$) (CH$_2$SiMe$_3$) (**2.1**) and H$_2$O$_2$ to Cp*WO(η^2-O$_2$) (CH$_2$SiMe$_3$) (**2.2**). Numbers are free energies (kcal/mol) for 1,4-dioxane/water and are relative to complex **2.2** (Cp* = κ^1-Cp*)... 99

Scheme 2.19. Summary of pathways for the oxygen atom Insertion into W–C bonds of Cp*W(O)$_2$(CH$_2$SiMe$_3$) (**2.1)** and Cp*W(O)(η^2-O)$_2$(CH$_2$SiMe$_3$) (**2.2**)...... 100

Scheme 2.20. Comparison of transition states for base- and scid-promoted conversion of Cp*W(O)(η^2-O)$_2$(CH$_2$SiMe$_3$) (**2.2**) to the oxy-insertion products..... 101

Scheme 3.1. Proposed pathways for partial oxidation of hydrocarbons involving oxygen atom insertion into a M–R bond and 1,2-CH-Addition across a M–OR bond... 115

Scheme 3.2. Generic mechanisms for the organic Baeyer-Villiger reaction and the analogous organometallic Baeyer-Villiger reaction (OMBV).......................... 115

Scheme 3.3. Proposed mechanism for the O-atom insertion into MTO with various oxidants... 116

Scheme 3.4. Electronic properties for the C–X bond formation in the Shilov-type systems and C–O bond formation via organometallic Baeyer-Villiger reaction (OMBV).. 116

Scheme 3.5. Proposed mechanism for the formation of TMSCH$_2$OH from the reaction of Cp*W(O)$_2$(CH$_2$SiMe$_3$) (**2.1**) and NaIO$_4$ in 1:1 THF-d_8:D$_2$O (v:v)........ 117

Scheme 3.6. O-atom insertion into Re–Ar bonds by migration of Ar to Re^V=O...... 118

Scheme 3.7. O atom insertion into Re–Ar bonds by migration of Ar to Re=O 119

Scheme 3.8. Comparison of the migrations in the R to M=O, Organometallic Baeyer-Villiger (OMBV) reaction and Shilov-type reaction........................... 119

Scheme 3.9. Transitions for the nucleophilicity of the M–C$^{\delta-}$ bond or the electrophilicity of the bound O$^{\delta+}$ in the periodic table……………………………… 120
Scheme 3.10. Hydrocarbon functionalization involving a C–H bond breaking by M=O step and a C–O bond forming "rebound" step…………………………….. 121
Scheme 3.11. Activation of aromatic C–H bond by Cp*Fe(CO)(NCMe)Ph (**3.1**)… 121
Scheme 3.12. O-atom insertion into Cp*M(CO)(NCMe)R via formation of the M=O…………………………………………………………………………... 122
Scheme 3.13. Calculated (Cundari group, U. of North Texas) free energies for the reaction of Cp*Fe(CO)(NCMe)Ph (**3.1**) and pyridine-*N*-oxide (PyO) in THF-d_8. Numbers are free energies (kcal/mol) relative to Cp*Fe(CO)(ONMe$_3$)Ph. Lowest energy spin states are labeled in the boxes on the top left of structures……………. 124
Scheme 3.14. Synthesis of Cp*Fe(P(OCH$_2$)$_3$CEt)$_2$Ph (**3.3**)………………………... 125
Scheme 3.15. Dissociate mechanism for the reaction of Cp*Fe(P(OCH$_2$)$_3$CEt)$_2$Ph (**3.3**) with PMe$_3$…………………………………………………………………... 133
Scheme 3.16. Calculated free energies for the reaction of Cp*Fe(P(OCH$_2$)$_3$CEt)$_2$Ph (**3.3**) and Me$_3$NO in THF-d_8. Numbers are free energies (kcal/mol) relative to complex **3.3**. Lowest energy spin states are labeled in the boxes on the top left of structures…………………………………………………... 140
Scheme 3.17. Proposed Pathway for the Reaction of Cp*Fe(P(OCH$_2$)$_3$CEt)$_2$Ph (**3.3**) and AgOTf……………………………………………………………………….. 145
Scheme 3.18. Calculated Free Energies for the Reaction of Cp*Fe(P(OCH$_2$)$_3$CEt)$_2$Ph (**3.3**) and AgOTf in THF-d_8. Numbers are free energies (kcal/mol) relative to complex **3.3**. Lowest energy spin states are labeled in the boxes on the top left of structures…………………………………………………... 145
Scheme 3.19. Nucleophilic migration of R$^{\delta-}$ to M≡O$^{\delta+}$…………………………… 149
Table 3.3. Reaction conditions and yields for reaction of Cp*Fe(P(OCH$_2$)$_3$CEt)$_2$Me (3.5) with various oxidants…………………………… 165
Scheme 4.2. Proposed pathways for partial oxidation of hydrocarbons involving oxygen atom insertion into a M–R bond and 1,2-CH-Addition across a M–OR bond……………………………………………………………………………… 166
Scheme 4.3. Calculated pathway for oxygen atom insertion into Ni–C bond in Hillhouse reaction……………………………………………………………….. 167
Scheme 4.4. O-atom insertion into Cp*M(CO)(NCMe)R via formation of the M=O…………………………………………………………………………… 167
Scheme 4.5. Synthesis of (N$_3$)CoMe (**4.1**)……………………………………… 168
Scheme 5.1. Transitions for the nucleophilicity of the M–C$^{\delta-}$ bond or the electrophilicity of the bound O$^{\delta+}$ in the periodic table……………………………… 183
Scheme 5.2. Summary for the O-atom insertion into middle and late metal–carbonyl bonds…………………………………………………………………… 186
Scheme 5.3. Proposed (^{tBu}N$_4$)FeR$_2$ and (^{tBu}N$_4$)Fe(CH$_3$CN)R(OTf) (^{tBu}N$_4$ = (N,N'-di-tert-butyl-2,11-diaza[3.3](2,6)pyridinophane) complexes for future O-atom insertion reaction and the ^{tBu}N$_4$ ligand stays coordination with Fe center when reacting with oxidants such as H$_2$O$_2$.. 189

LIST OF FIGURES

Figure 1.1. Plot of calculated ΔG_{rxn}, $\Delta G^{\ddagger}$ (free energies, kcal/mol) for the OMBV reaction with four- and six-coordinate $[(bpy)_xM(Me)(OOH)]_n$ systems. For each data point, the metal ion and oxidation state are indicated ($R^2 = 0.77$)…………… 40

Figure 1.2. Plot of calculated M–CH_3 BDFE against OMBV activation barriers in kcal/mol ($R^2 = 0.73$). The metal ion is indicated………………………………….. 40

Figure 1.3. Plot of calculated Mulliken charges on the carbon of the methyl migrating group for four- and six-coordinate Metallo-Criegee intermediates and calculated OMBV barriers (free energies, kcal/mol) ($R^2 = 0.65$). The central metal ion is indicated…………………………………………………………………... 40

Figure 1.4. Plot of calculated Mulliken charges on the carbon of the methyl migrating group of the OMBV transition states and calculated barriers (free energies, kcal/mol) for four- and six-coordinate geometries discussed in the text ($R^2 = 0.60$). The central metal ion is indicated…………………………………… 41

Figure 2.1. A sample of ^1H NMR spectrum for the reaction of $Cp^*W(O)_2(CH_2SiMe_3)$ (**2.1**) and $NaIO_4$ (5 equiv) in 1:1 THF-d_8:D_2O (v:v) at –1.3 °C. Resonance of the intermediate $Cp^*W(O)_2(OCH_2SiMe_3)$ (**2.3**) are assigned as 4.17 (CH_2, s), 2.04 (CH_3, s), –0.05 ($SiMe_3$, s) ppm. The CH_2 group of **2.1** and $TMSCH_2OH$ resonate at 0.43 ppm and 3.16 ppm, respectively…………………… 68

Figure 2.2. Plot of concentration versus time for all species observed during the conversion of $Cp^*W(O)_2(CH_2SiMe_3)$ (**2.1**) and $NaIO_4$ to $TMSCH_2OH$ including complex **2.1** (blue, circles), $Cp^*W(O)_2(OCH_2SiMe_3)$ (**2.3**) (brown, squares), $TMSCH_2OH$ (green, triangles) and the sum of all three species (purple, crosses). Data are from one experiment and were acquired at –1.3 °C in 1:1 THF-d_8:D_2O (v:v) with $NaIO_4$ (5 equiv). Multiple experiments result in similar plots………… 69

Figure 2.3. MS data for the $TMSCH_2OH$ product of the reaction of $Cp^*W(^{16}O)_2(CH_2TMS)$ (**2.1**) and $NaIO_4$………………………………………... 71

Figure 2.4. MS spectrum for the product of reaction of $Cp^*W(^{16}O)_2(CH_2SiMe_3)$ (**2.1**) with $NaI^{18}O_4$ in THF……………………………………………………… 71

Figure 2.5. Plots of observed and fitted data for the decay of $Cp^*W(O)_2(CH_2SiMe_3)$ (**2.1**)…………………………………………………….. 74

Figure 2.6. Plot of observed and fitted data for the concentration variation of $Cp^*W(O)_2(OCH_2SiMe_3)$ (**2.3**)…………………………………………………... 74

Figure 2.7. Plot of observed and fitted data for the growing of Me_3SiCH_2OH (**2.4**)…………………………………………………………………………… 75

Figure 2.8. Plots of all observed and fitted data for the conversion of $Cp^*W(O)_2(CH_2SiMe_3)$ (**2.1**) with 5 equivalent of $NaIO_4$ to Me_3SiCH_2OH (**2.4**) in THF-d_8 at –1.3 °C…………………………………………………………….. 75

Figure 2.9. Plot of k_{obs1} vs. $[IO_4^-]$ for the reaction of $Cp^*W(O)_2(CH_2SiMe_3)$ (**2.1**) with $NaIO_4$ showing a first order dependence on $[IO_4^-]$ (R^2=0.99)……………….. 76

Figure 2.10. Plot of ln(k/T) vs. 1/T for the conversion of $Cp^*W(O)_2(CH_2SiMe_3)$ (**2.1**) and $NaIO_4$ (5 equiv) to $Cp^*W(O)_2(OCH_2SiMe_3)$ (**2.3**) (R^2=0.99)…………… 77

Figure 2.11. DFT calculated transition state for the oxy-insertion step of the overall reaction: $Cp^*W(O)_2(CH_2SiMe_3)$ (**2.1**) + IO_4^- → $Cp^*W(O)_2(OCH_2SiMe_3)$ (**2.3**) + IO_3^-. Bond lengths are given in Å and bond angles in degrees…………… 79

Figure 2.12. First order decay of $Cp^*W(O)_2(CH_2SiMe_3)$ (**2.1**) with $[Bu_4N][IO_4]$ (15 equiv) and 50 equivalents of D_2O in THF-d_8 at 50 °C………………………… 81

Figure 2.13. First order decay of $Cp^*W(O)_2(CH_2SiMe_3)$ (**2.1**) with $[Bu_4N][IO_4]$ (15 equiv) and 100 equivalents of D_2O in THF-d_8 at 50 °C……………………….. 81

Figure 2.14. First order decay of $Cp^*W(O)_2(CH_2SiMe_3)$ (**2.1**) with $[Bu_4N][IO_4]$ (15 equiv) and 200 equivalent of D_2O in THF-d_8 at 50 °C………………………... 82

Figure 2.15. First order decay of $Cp^*W(O)_2(CH_2SiMe_3)$ (**2.1**) with $[Bu_4N][IO_4]$ (15 equiv) and 300 equivalents of D_2O in THF-d_8 at 50 °C……………………….. 82

Figure 2.16. First order decay of $Cp^*W(O)_2(CH_2SiMe_3)$ (**2.1**) with $[Bu_4N][IO_4]$ (15 equiv) and 400 equivalents of D_2O in THF-d_8 at 50 °C……………………… 83

Figure 2.17. First order decay of $Cp^*W(O)_2(CH_2SiMe_3)$ (**2.1**) with $[Bu_4N][IO_4]$ (15 equiv) and 600 equivalents of D_2O in THF-d_8 at 50 °C……………………….. 83

Figure 2.18. First order decay of $Cp^*W(O)_2(CH_2SiMe_3)$ (**2.1**) with $[Bu_4N][IO_4]$ (15 equiv) and 1000 equivalents of D_2O in THF-d_8 at 50 °C…………………… 84

Figure 2.19. Plot of k_{obs} vs. $[D_2O]$ for the reaction of $Cp^*W(O)_2(CH_2SiMe_3)$ (**2.1**) and excess $[Bu_4N][IO_4]$ (15 equiv) in THF-d_8 with various amounts of D_2O showing a second-order dependence on $[D_2O]$ (R^2=0.99)………………………… 85

Figure 2.20. DFT calculated transition state with water for the oxy-insertion step of the overall reaction: $Cp^*W(O)_2(CH_2SiMe_3)$ (**2.1**) + $IO_4^- \rightarrow$ $Cp^*W(O)_2(OCH_2SiMe_3)$ (**2.3**) + IO_3^-. Bond lengths are given in Å and bond angles in degrees……………………………………………………………… 86

Figure 2.21. Plot of k_{obs} vs. $[OH^-]$ for the reaction of $Cp^*W(O)(\eta^2\text{-}O)_2(CH_2SiMe_3)$ (**2.2**) with NaOH showing a first-order dependence on $[OH^-]$ (R^2=0.99)……………………………………………………………………….. 87

Figure 2.22. Plot of ln(k/T) vs. 1/T for the reaction of $Cp^*W(O)(\eta^2\text{-}O)_2(CH_2SiMe_3)$ (**2.2**) with NaOH (5 equiv) (R^2=0.99)…………………………… 88

Figure 2.23. MS data for the $TMSCH_2OH$ product of the reaction of $Cp^*W(O)(\eta^2\text{-}O_2)(CH_2SiMe_3)$ (**2.2**) and NaOH…………………………………… 89

Figure 2.24. MS data for the $TMSCH_2OH$ product of the reaction of $Cp^*W(O)(\eta^2\text{-}O_2)(CH_2SiMe_3)$ (**2.2**) and $Li^{18}OH$………………………………….. 90

Figure 2.25. DFT calculated organometallic Baeyer-Villiger (OMBV) transition state for oxy-insertion of hydroperoxide into W–C bond of $Cp^*W(O)(\eta^2\text{-}O_2)$ (CH_2SiMe_3) (**2.2**). Bond lengths are given in Å and bond angles in degrees……… 92

Figure 2.26. Calculated transition state for oxy-insertion of $Cp^*W(O)(\eta^2\text{-}O_2)$ (CH_2SiMe_3) (**2.2**) with (red) and without (black) added proton. Bond lengths are given in Å…………………………………………………………………….. 96

Figure 3.1. ^{1}H NMR spectrum of $Cp^*Fe(P(OCH_2)_3CEt)_2Cl$ (**3.2**) in THF-d_8. 125

Figure 3.2. ORTEP drawing of $Cp^*Fe(P(OCH_2)_3CEt)_2Ph$ (**3.3**) (50% probability ellipsoids; H atoms omitted). Selected bond lengths (Å): Fe–C1 1.9993(2), Fe–P1 2.0854(4), Fe–P2 2.0996(4). Selected bond angles (°): C1–Fe–P1 92.91(4), C1–Fe–P2 92.73(4), P1–Fe–P2 91.65(2)………………………………………………… 126

Figure 3.3. ^{13}C NMR spectrum of $PhOH{\cdot}OMe_3$ from the reaction of $Cp^*Fe(P(OCH_2)_3CEt)_2Ph$ (**3.3**) with 5 *equiv* of Me_3NO in THF-d_8……………… 127

Figure 3.4. ^{1}H NMR spectrum of $PhOH{\cdot}ONMe_3$ generated from the reaction of $Cp^*Fe(P(OCH_2)_3CEt)_2Ph$ (**3.3**) with 5 equiv of Me_3NO in THF-d_8……………… 128

Figure 3.5. ^{1}H NMR spectrum of $PhOH{\cdot}OMe_3$ from the reaction of PhOH with

excess Me_3NO in THF-d_8…………………………………………………………… 128

Figure 3.6. Mass spectrum for 1,2,3,4-tetramethylfulvene ($C_{10}H_{14}$, MW = 134) from the reaction of $Cp^*Fe(P(OCH_2)_3CEt)_2Ph$ (**3.3**) with excess Me_3NO in THF-d_8…………………………………………………………………………… 129

Figure 3.7. First order decay of $Cp^*Fe(P(OCH_2)_3CEt)_2Ph$ (**3.3**) with 5 equiv. of PMe_3 in THF-d_8 photolyzed at 21 °C with $k_{obs} = 0.049$ min^{-1} = 0.82 ×10^{-3} s^{-1}…… 131

Figure 3.8. First order decay of $Cp^*Fe(P(OCH_2)_3CEt)_2Ph$ (**3.3**) with 10 equiv. of PMe_3 in THF-d_8 photolyzed at 21 °C with $k_{obs} = 0.033$ min^{-1} = 0.55 ×10^{-3} s^{-1}…… 132

Figure 3.9. First order decay of $Cp^*Fe(P(OCH_2)_3CEt)_2Ph$ (**3.3**) with 15 equiv. of PMe_3 in THF-d_8 photolyzed at 21 °C with $k_{obs} = 0.060$ min^{-1} = 1.0 ×10^{-3} s^{-1}……. 132

Figure 3.10. First order decay of $Cp^*Fe(P(OCH_2)_3CEt)_2Ph$ (**3.3**) with 20 equiv. of PMe_3 in THF-d_8 photolyzed at 21 °C with $k_{obs} = 0.061$ min^{-1} = 1.0 ×10^{-3} s^{-1}….. 133

Figure 3.11. Plot of k_{obs} vs. [PMe_3] for the reaction of $Cp^*Fe(P(OCH_2)_3CEt)_2Ph$ (**3.3**) with PMe_3 showing a zero order dependence on [PMe_3]…………………… 134

Figure 3.12. Plot of concentration versus time for the reaction of $Cp^*Fe(P(OCH_2)_3CEt)_2Ph$ (**3.3**) with 6 equiv. of Me_3NO photolyzed at 21 °C in THF-d_8 including complex **3.3** (green, diamonds), Me_3NO (purple, crosses), $O{=}P(OCH_2)_3CEt$ (black, x), 1,2,3,4-tetramethylfulvene (blue, triangles) and $PhOH{\cdot}ONMe_3$ (red, circles)…………………………………………………….. 134

Figure 3.13. Plot of concentration versus time for the starting material and three products observed during the reaction of $Cp^*Fe(P(OCH_2)_3CEt)_2Ph$ (**3.3**) with Me_3NO photolyzed at 21 °C in THF-d_8 including complex **3.3** (green, diamonds), $O{=}P(OCH_2)_3CEt$ (black, x), 1,2,3,4-tetramethylfulvene (blue, triangles) and $PhOH{\cdot}ONMe_3$ (red, circles)…………………………………………………….. 135

Figure 3.14. First order decay of $Cp^*Fe(P(OCH_2)_3CEt)_2Ph$ (**3.3**) with 6 equiv. of Me_3NO in THF-d_8 photolyzed at 21 °C with $k_{obs} = 0.060$ min^{-1} = 1.0 ×10^{-3} s^{-1}….. 136

Figure 3.15. First order growth of $PhOH{\cdot}ONMe_3$ in the reaction of $Cp^*Fe(P(OCH_2)_3CEt)_2Ph$ (**3.3**) with 6 equiv. of Me_3NO in THF-d_8 photolyzed at 21 °C with $k_{obs} = 0.053$ min^{-1} = 0.90 ×10^{-3} s^{-1}………………………………….. 137

Figure 3.16. First order growth of 1,2,3,4-tetramethylfulvene in the reaction of $Cp^*Fe(P(OCH_2)_3CEt)_2Ph$ (**3.3**) with 6 equiv. of Me_3NO in THF-d_8 photolyzed at 21 °C with $k_{obs} = 0.055$ min^{-1} = 0.91 ×10^{-3} s^{-1}………………………………… 137

Figure 3.17. Plot of concentration versus time for the reaction of $P(OCH_2)_3CEt$ with 6 equiv. of Me_3NO at 21 °C in THF-d_8 including $P(OCH_2)_3CEt$ (black, diamonds), $O{=}P(OCH_2)_3CEt$ (red, circles), Me_3NO (blue, triangles)…………….... 138

Figure 3.18. First order decay of $P(OCH_2)_3CEt$ with 6 equiv. of Me_3NO in THF-d_8 photolyzed at 21 °C with $k_{obs} = 0.033$ min^{-1} = 0.55 ×10^{-3} s^{-1}………………….. 138

Figure 3.19. Spin density plot of oxo intermediate, $Cp^*Fe(P(OCH_2)_3CEt)(O)Ph$, [scale: 0.33, contour value: 0.006943]………………………………………….. 141

Figure 3.20. ^{1}H NMR spectrum of 1,2,3,4,5-pentamethly-5-phenyl-cyclopentadiene (Cp*Ph) isolated from the reaction of $Cp^*Fe(P(OCH_2)_3CEt)_2Ph$ (**3.3**) and AgOTf in CD_3CN…………………………………………………….. 143

Figure 3.21. ^{13}C NMR spectrum for 1,2,3, 4,5-pentamethly-5-phenyl-cyclopentadiene (Cp*Ph) isolated from the reaction of $Cp^*Fe(P(OCH_2)_3CEt)_2Ph$ (**3.3**) and AgOTf in CD_3CN…………………………………………………….. 143

Figure 3.22. Mass spectrum for 1,2,3,4,5-pentamethly-5-phenyl-cyclopentadiene

(Cp*Ph) ($C_{14}H_{20}$, MW = 212)………………………………………………………… 144
Figure 3.23. ^{1}H NMR spectrum for Cp*Fe($P(OCH_2)_3CEt)_2Me$ (**3.5**) in CD_3CN…. 148
Figure 3.24. ^{13}C NMR spectrum for Cp*Fe($P(OCH_2)_3CEt)_2Me$ (**3.5**) in CD_3CN… 148
Figure 4.1. ^{1}H NMR spectrum of (N_3)CoMe (**4.1**) in C_6D_6 at room temperature… 169
Figure 4.2. ^{1}H NMR spectrum for the reaction of (N_3)CoMe (**4.1**) and H_2O_2 (~35% aq) in THF-d_8………………………………………………………………… 170
Figure 4.3. ^{1}H NMR spectrum for the reaction of (N_3)CoMe (**4.1**) and excess *m*CPBA in THF-d_8 at room temperature after added 1 µL D_2O………………….. 172
Figure 4.4. ^{1}H NMR spectrum for the reaction of (N_3)CoMe (**4.1**) and excess Me_3NO in THF-d_8 at room temperature…………………………………………… 173
Figure 4.5. ^{1}H NMR spectrum for the reaction of (N_3)CoMe (**4.1**) and excess PyO in THF-d_8 at 90 °C for 20 hours……………………………………………… 174

LIST OF TABLES

Table 2.1. Observed and fitted data for the conversion of Cp*W(O)$_2$(CH$_2$SiMe$_3$) (**2.1**) with 5 equivalent of NaIO$_4$ to Me$_3$SiCH$_2$OH (**2.4**)………………………….. 74

Table 2.2. Reaction conditions and yields for reaction of Cp*W(O)(η^2-O)$_2$(CH$_2$SiMe$_3$) **(2.2)** with Brønsted acid……………………………………….. 93

Table 3.1. Reaction conditions, products and yields for the reactions of Cp*Fe(CO)(NCMe)Ph (**3.1**) with various oxidants……………………………….. 123

Table 3.2. Reaction conditions and yields for Cp*Fe(P(OCH$_2$)$_3$CEt)$_2$Ph (**3.3**) with various oxidants…………………………………………………………… 147

Table 3.3. Reaction conditions and yields for reaction of Cp*Fe(P(OCH$_2$)$_3$CEt)$_2$Me (3.5) with various oxidants…………………………… 150

1 Introduction

1.1 Methane to Methanol (MTM)

1.1.1 Rationale and Direction for Methane to Methanol

The world's energy consumption has increased almost 100% in the past three decades due to the growth of the population and economy. Fossil fuels supply over 86% of the world's energy, and one fourth of that is from natural gas. Natural gas will play a more important role in the energy supply, due to the enormous quantity of shale gas and the development of new technology to use shale gas.[1] For instance, the United States was known to import a large amount of oil for decades; however, the US became a net carbon exporter in 2013. A major factor for this change is the increase in the US's natural gas production by 34% since 2005. Despite access to substantial new reserves of natural gas, its use has been limited by the expense of transportation. Due to its non-polar, light molecular weight structure, natural gas is a low-boiling (–162 °C at 1 atm) gas and its liquefaction requires substantial energy input and expensive infrastructure. For example, a single liquefied natural gas (LNG) ship costs over 300 million dollars.

The infrastructure for moving natural gas in the gas phase is also expensive. For example, China and Russia just came an agreement that China will import natural gas of a total value of 400 billion dollars from Russia in the next 30 years. However, before the Chinese people could use the natural gas from Siberia, a pipeline that costs over $5 billion has to be built.[2] Another example is the abandoned Alaska Pipeline Project, which was planned to spend ~ $40 billion to build a natural gas pipeline (by TransCanada Corp. and ExxonMobil) to access the vast natural gas reserves of Alaska's North Slope.[3]

A solution to the expensive transportation of natural gas is the selective oxidation of methane to a transportable liquid with low cost by using current infrastructure. The examples above demonstrate the attractiveness of this process. The reaction of methane with O_2 to produce methanol is a thermodynamically favorable process ($CH_4 + \frac{1}{2}O_2 \rightarrow CH_3OH$, $\Delta G = -27.6$ kcal/mol) and methanol can be easily transported by current infrastructure. A catalyst that partially converts methane-to-methanol (MTM) will significantly lower the cost of transportation of natural gas. In addition to the much lower cost of transportation of a liquid, large scale conversion of methane to methanol has several other advantages. First, methanol can be used directly as a fuel for vehicles. For example, It takes only ~$300 relative to current vehicles costs to upgrade to the flex fuel vehicles that use M85 (85% methanol/15% unleaded gasoline blend) or M100 (pure methanol). Second, methanol can be converted to gasoline. It is reported that ExxonMobil has developed this technology. Another ways is to convert methanol to dimethyl ether, which is a component in diesel fuel. Also, methanol is a precursor for many chemicals such as ethylene and propylene in the chemical industry. Thus, methanol is a versatile chemical feedstock.

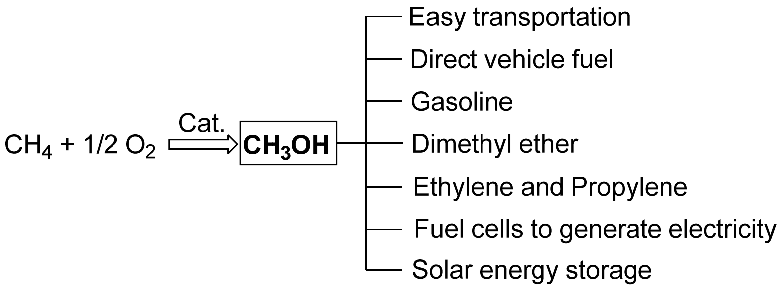

Scheme 1.1. Advantages of partial oxidation of methane-to-methanol (MTM) process.

Although the partial oxidation of methane to methanol is of significant practical interest, it is one of the most challenging processes in chemistry. The difficulty is due to the inert nature of methane, which is a result of its high bond dissociation energy (BDE ~ 105 kcal/mol) and the non-polar C–H bond. As a result, methane is very unreactive. For example, most reactions of methane involving C–H bond hemolysis, which can only occur with high energy species or under forcing conditions, and consequently, the selectivity is typically low. Also, methane rarely undergoes typical electrophilic or nucleophilic substitution reactions due to the non-polar C–H bond, except with the most reactive classes of substrates.[4-6] Furthermore, methane is a very weak ligand for the coordination to metal complexes, which is often an essential step in metal-mediated catalysis. This problem is amplified in the presence of more competitive substrates or solvents. The last issue raises another challenge for the preparation of methanol, which is more polar and a better coordinating ligand than methane and would result in catalyst inhibition or over oxidation to other products.

The current process for converting methane to methanol is an indirect conversion via syn-gas (H_2 + CO), which requires high temperature (~ 900 °C) and pressure and is very energy intensive.[7] The syn-gas process requires a very complex and expensive infrastructure that can cost as much as $10 billion for one plant. The expensive cost of syn-gas plants limits scale-up because many companies cannot afford them, the capital investment requires years for return on investments and they must be built on a large scale. More ideal is the construction of many gas-to-liquids (GTL) plants at natural gas sites, but this is not economically viable with current technologies. For these reasons, a lot of natural gas resources are simple flared as waste. For example, it is estimated that Nigeria loses ~ $3 billion per year to natural gas flares. If this gas is used, it will produce

~33,000 BOE per/day. However, to make use of this wasted natural gas, a GTL plant cost of ~$8.4 billion is required to be built by Chevron/Sasol first.[8]

As a result, a catalyst for the moderate temperature (< 250 °C) and moderate (1-30 atm) pressure conversion of methane to methanol, with a plant that can be easily built for small and middle scale use, has been the focus of intense research.[9-15] Such a catalyst would reduce the capital cost associated with construction of a GTL plant, to an easily transportable liquid. If a MTM process is competitive with the syn-gas process and the production of gasoline, it must be able to: 1) produce millions of tons of liquid per year; 2) not only substantially reduces the expense using current methods, but also be competitive with the overall yield and atom-efficiency of existing process. Several key guidelines are important to consider for a scalable MTM process, including catalyst selectivity, rate and lifetime.[16,17] Our goal is to long lifetime, high selectivity and rate transition metal-mediate catalysts for this GTL process.

1.1.2 Heterogeneous Catalyzed Methane Oxy-functionalization

Heterogeneous catalysts for methane oxy-functionalization have been reported, including oxidative coupling of methane using basic metal oxides,[18,19] partial oxidation by transition metal oxides and zeolite supported iron complexes.[20-22] Most metal oxides catalysts likely function by homolytic C–H bond cleavage of the strong covalent bond of methane (C–H BDE ~105 kcal/mol). Thus, these processes are energy intensive and need high temperature (> 250 °C). Furthermore, methanol has weaker C–H bonds (C–H BDE ~96 kcal/mol) than methane and is hence more reactive. As a result, these catalysts typically function with low yield or relatively poor selectivity due to over oxidation. It is often possible to get high selectivity at low conversion or low selectivity with low yield, but high selectivity (> 90%) at high conversion (> 70%) has not yet been observed. For example, Hutching and co-worker reported direct catalytic conversion of methane to methanol in an aqueous medium by using copper-promoted Fe-ZSM-5.[22] The proposed mechanism involves a high valent Fe=O complex supported in ZSM-5 (Scheme 1.2). The best result is 10% conversion of methane with 96% selectivity to partially oxygenated products (CH_3OH, CH_3OOH, HCOOH, with only a 8% selectivity for MeOH) at 550 °C for 3h.[22] As a typical heterogeneous catalyzed hydrocarbons functionalization reaction, the reaction temperature is high and the selectivity of MeOH and total yield of MeOH is typically low. High selective oxidation of hydrocarbons with high conversion has only been observed for long chain alkanes but not methane. [23-28] Despite these chievements, extension of similar strategies to the selective partial oxidation of methane to methanol is still a big challenge.

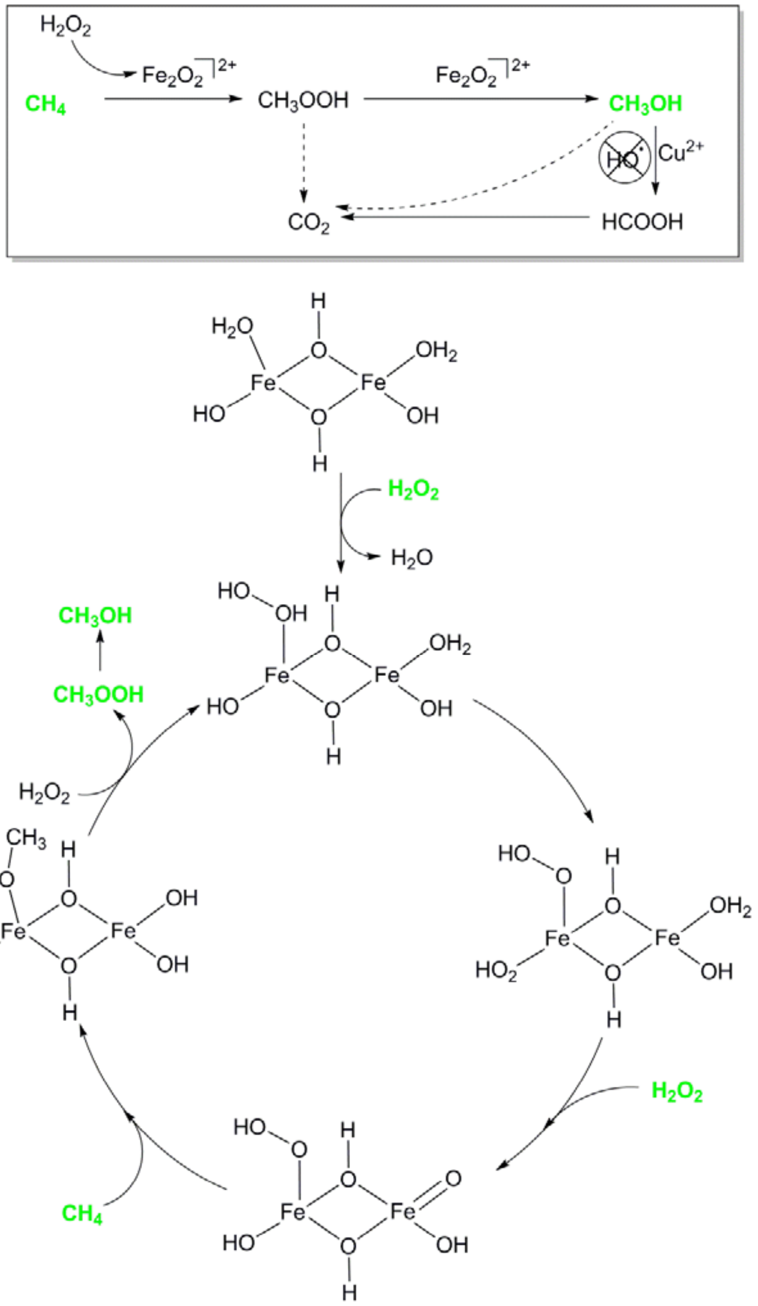

Scheme 1.2. Catalytic cycle for the oxidation of CH_4 to CH_3OOH using H_2O_2, catalyzed by a binuclear Fe species in ZSM-5. The overall charge in each case is formally +2 as thespecies acts as an extra-framework cation within the zeolite.

While traditional heterogeneous catalysts for partial oxidation of methane to methanol suffer from poor selectivity, a potential promising strategy is combine the single site homogenous catalysts on heterogeneous frameworks which might achieve both high conversion and selectivity. A few examples using these strategy have been reported. For example, a bipyridineylplatium-polyoxometalate hybrid complex supported on silica, $[Pt(mebpm)Cl_2][H_4PV_2Mo_2O_{40}]/SiO_2$, which catalyzes the aerobic oxidation of methane to methanol in water under mild reaction conditions (50-60 °C, 1-2 bar O_2) was reported by Neumann and co-workers in 2004 (Scheme 1.3).[29] However, this reaction still suffers from poor selectivity and low conversion for methanol. It produces nearly as much $CH_2{=}O$ as MeOH and also yield the over oxidized product $CH_3CH{=}O$ as well, with only ~1% methane conversion reported (~ 33 turnover numbers).

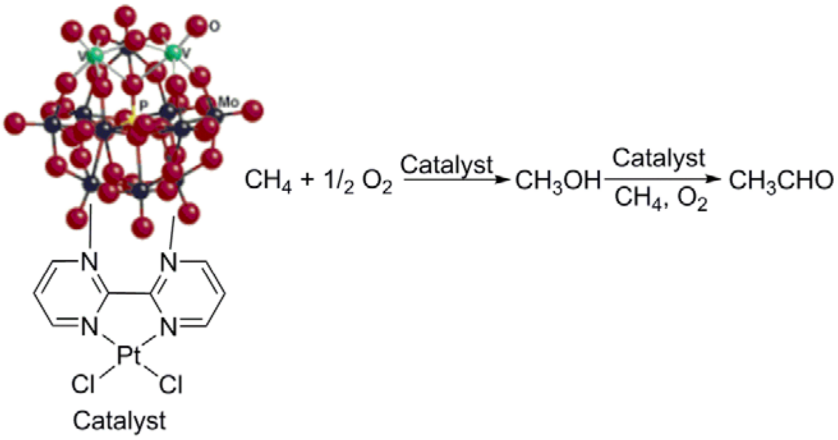

Scheme 1.3. Selective oxidation of methane to methanol by bipyrimidinylplatinum polyoxometalate hybrid compound catalyst.

Another new type of solid catalyst for direct, low-temperature oxidation of methane to methanol was reported by Schuth and co-workers in 2009 (Scheme 1.4).[30] This catalyst works similar to the Periana bipyridine catalyst (see below) with high selectivity and stability over five recycling steps. While the strategy is promising, the same drawbacks as the analogous homogeneous catalysts (see below) need to be overcome to achieve a more practical use.

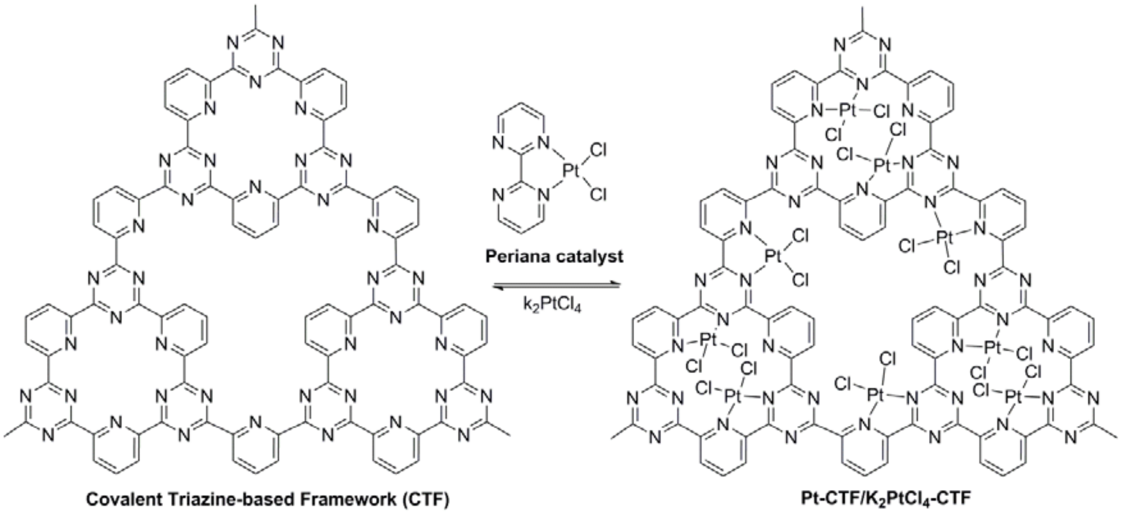

Scheme 1.4. Structure of supported Periana catalyst on covalent triazine-based framework (CTF).

1.1.3 Methane Functionalization by Homogeneous Transition Metal-Mediated Catalysts-The Shilov and Related systems

Although heterogeneous catalysts often have long lifetime and reactivity, it is often difficult to elucidate the nature of the active catalytic site for heterogeneous catalysts and, hence, it is often difficult to tune the selectivity. To the contrast, the molecular homogenous catalysts are often more tunable than heterogeneous catalysts and thus often achieve high selectivity. Thus, we believe that the use of homogeneous transition metal catalyst has the potential to selectively partial oxidation hydrocarbons in high selectivity.

Selective functionalization of hydrocarbons using transition metal catalysts usually requires two steps, C–H bond activation and C–X (X = O, Cl *et.al.*) bond formation. Challenges present for both steps. The challenge for C–H bond activation is that it often requires the coordination of C–H bond to the metal as the first step, which is difficult as C–H bond coordination is usually thermodynamically unfavorable. Furthermore, there are often better coordinating ligands than methane in the reaction mixture, for example, Cl^-, HSO_4^-, H_2O, TFA^- (TFA = trifluoroacetate) are usually competitive with methane for coordination to the metals. In addition, methanol has better coordination to electrophilic metal centers than methane, which raises a potential problem that once methanol is produced it will inhibit the catalyst. Finally, the development of catalysts that prefer to react with methane over methanol is a big challenge.

Challenges for C–X bond formation also exist. One strategy to form C–X bond is via reductive functionalization of a M–R bond, which often requires an electrophilic alkyl and high oxidation state metal center. However, high oxidation state metals with few d electrons are often not favorable for C–H bond activation. A catalytic cycle with a solution for these conflicts involves three steps: 1) a low oxidation state metal catalyst serves to activate the C–H bond of hydrocarbons to form the metal–hydrocarbyl (M–R); 2) oxidation of the metal center to a higher oxidation state (generally via a net 2 e^- process); 3) reductive functionalization of the M–R bond with X^- to form the C–X bond and generate the functionalized product (Scheme 1.5).

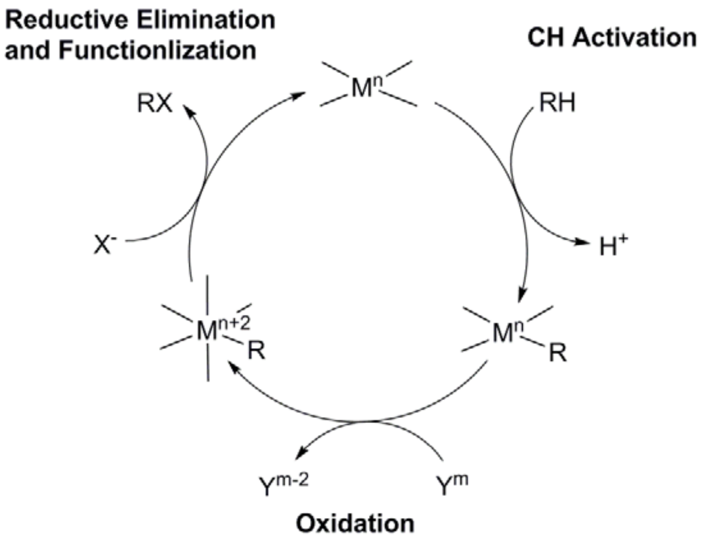

Scheme 1.5. General catalytic cycle for selective functionalization of hydrocarbons (X = OH, Cl).

The C–H activation in the first step usually occur via a classic σ-bond metathesis and electro-rich d^6 or d^8 late transition metal complexes are often more active for this step. For the next oxidation step, it cannot either be too thermodynamically favorable that reductive elimination would not occur making the cycle irreversible, or be too thermodynamically unfavorable that making it too difficult to find a suitable oxidant to approach the high oxidation states of the catalyst. Ideally, the oxidant can be recycled from air to lower the cost of the whole conversion. Too expensive oxidants will definitely limit the practical (commercial) utilization of this cycle. The third reductive functionalization step is proposed to involve nucleophilic addition of X^- (*i.e.* H_2O, Cl^-) to an electrophilic metal–alkyl ligand. Such requirements limit the metal-mediated complex catalyst for this approach. The low oxidation state of the metal complex should be electro-rich and active enough for the C–H activation of RH, however, after the oxidation state, the high oxidation of the metal center is required to be electrophilic enough for the nucleophilic attack of the X^- to have reductive elimination. For example, the early transition metal complexes are too thermodynamically favorable to oxidize to the high oxidation step that the reductive elimination will not occur. The middle transition metal complexes will also suffer from this problem. Moreover, the oxidation of the middle transition metals are usually more complicated (lose more than 2 e^{-}) to achieve their highest oxidation states which may cause decomposition via losing the coordinated ligands. Only some of the late transition or main group (*i.e.* Tl) metal complexes match the requirements of this cycle and are experimentally proved to be catalytic active (see below).

In 1969, Shilov and co-workers reported a catalyst using the cycle in Scheme 1.5 for partial oxidation of alkanes to alcohols and chlorinated products by using an aqueous solution of Pt^{II} salt with Pt^{IV} as the oxidant.[9] The Pt^{II} complex initiates alkane C–H activation to generate a Pt^{II}–alkyl intermediate, which is oxidized to Pt^{IV}–alkyl by $[PtCl_6]^{2-}$. Subsequent nucleophilic attack of water or chloride at the Pt^{IV}–CH_3 bond releases the functionalized product CH_3X (X = OH or Cl) (Scheme 16). However, the rate of the conversion is very slow. The use of Pt^{IV} as a stoichiometric oxidant also limits the practical application of this system. The oxidation step is a real issue, and development of processes with oxidants other than Pt^{IV} has been challenging.

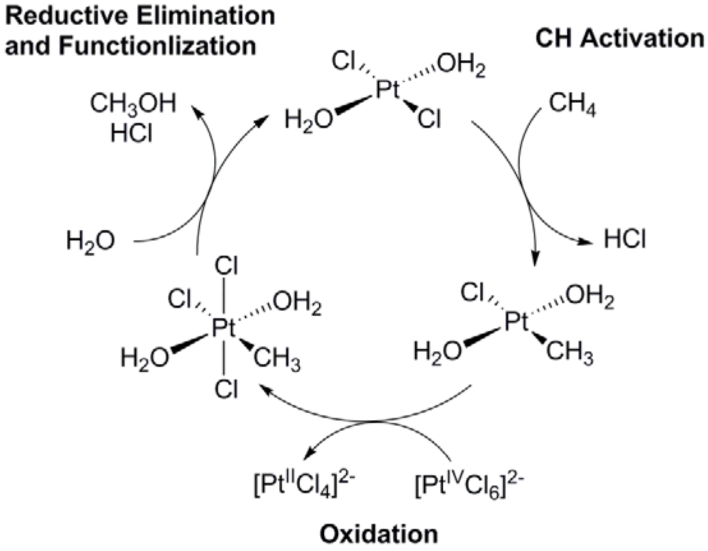

Scheme 1.6. Proposed catalytic cycle for methane functionalization by Shilov system.

Periana and co-workers improved the Shilov system by using concentrated sulfuric acid (oleum) as the solvent and as a stoichiometric oxidant with SO_2 as the reductive product.[11] The reaction of methane (3400 kPa) in 102% sulfuric acid catalyzed by (bpym)$PtCl_2$ (bpym = 2,2'-bipyrimidine) produces methyl bisulfate (which can be hydrolyzed to methanol) in greater than 70% yield based on methane at 220 °C for 2.5 h. The proposed mechanism is similar to the Shilov system by using SO_4^{2-} or SO_3 instead of $[PtCl_6]^{2-}$ in the oxidation step (Scheme 1.7). Another important feature of this system is that the oxidation of the methyl bisulfate product is at least 100 times slower than methane under the catalytic conditions as the σ-bond metathesis C–H bond activation prefer the stronger C–H bond of CH_4.[11,31] This feature prohibits the over oxidation of the product. The bisulfate plays the role as a protecting[14] group to prevent the over oxidation of the functionalized CH_3– group. The primary limitation of this system is that the catalysis is inhibited after > 1 M of methyl bisulfate is produced. Hence it is required to scale up higher concentration of the functionalized product in sulfuric acid. This catalytic cycle has been extended to other late metal systems. For example, Hg^{II},[10] Tl^{III},[32] Pd^{II} and Au^{I}[14] based catalysts have been reported to catalyze the partial oxidation of methane to methyl bisulfate in sulfuric acid.

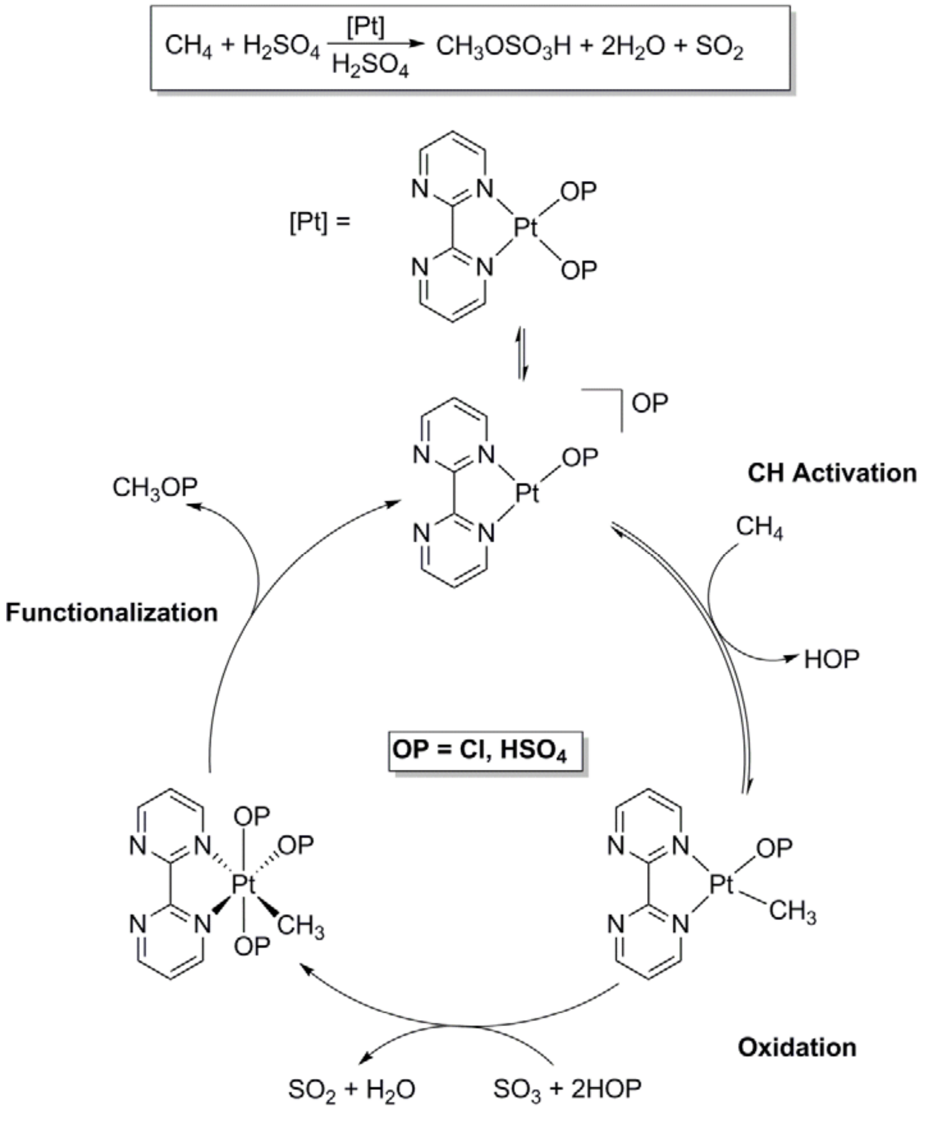

Scheme 1.7. Selective oxidation of CH_4 using (bpmy)Pt(Cl)$_2$ in concentrated sulfuric acid (OP = Cl, HSO_4).

1.1.4 Other Approaches to Oxy-functionalization of Hydrocarbons

The Shilov-type and related systems for selective functionalization of hydrocarbons generally proceeds by initial CH activation, oxidation of the catalyst and C–X bond formation via reductive functionalization. These systems require two oxidation states for the catalyst, the lower oxidation state for C–H bond activation and higher oxidation state for C–X bond formation. As discussed above, the challenging oxidation step usually limits the application of this type of catalyst. For the later developed Shilov-type catalysts, many efforts and improvements have been focused on searching for cheaper alternative oxidants to Pt^{IV}, but no viable process has been achieved. The “two functions on two different oxidation states” in a Shilov-type system is a stringent requirement for the electronic property of the metal center. As analyzed above, only some of the late transition or main group (*i.e.* Tl) metal complexes match the requirements of this cycle and are experimentally proved to be catalytic active (see above). Thus, to develop a new catalytic cycle for the selective oxidation of hydrocarbons without the stringent oxidation step is attractive and has been one of our goals.

An alternate strategy is to design a catalyst that achieves C–H activation and C–X bond formation at the same oxidation state. Two possible catalytic pathways are shown in scheme 1.8. Pathway A involves C–H bond activation via 1,2-addition across the M=O bond to generate M(R)(OH), followed by the C–O reductive elimination to form the functionalized alcohol product and M, which is oxidized by YO to regenerate the M=O species. Ideally, the in site oxidant YO can be regenerated by O_2. The CH activation via 1,2-addition across the M=O bond in the first step is an even-electron process that does not change the formal oxidation state of the metal center.[33-41] Furthermore, 1,2-CH-addition across the M=O bond initiates from the coordination of the C–H bond to the metal center followed by a metal-mediated C–H bond cleavage. It is expected to selectively activate stronger C–H bonds over weaker C–H bonds like other metal-mediated C–H activation reactions.[42,43] However, to our knowledge, C–H bond activation via 1,2-addition across the M=O bond has not been observed. Only examples of the analogous C–H activation by isoelectronic d^0 metal-imido complex have been reported.[44-55]

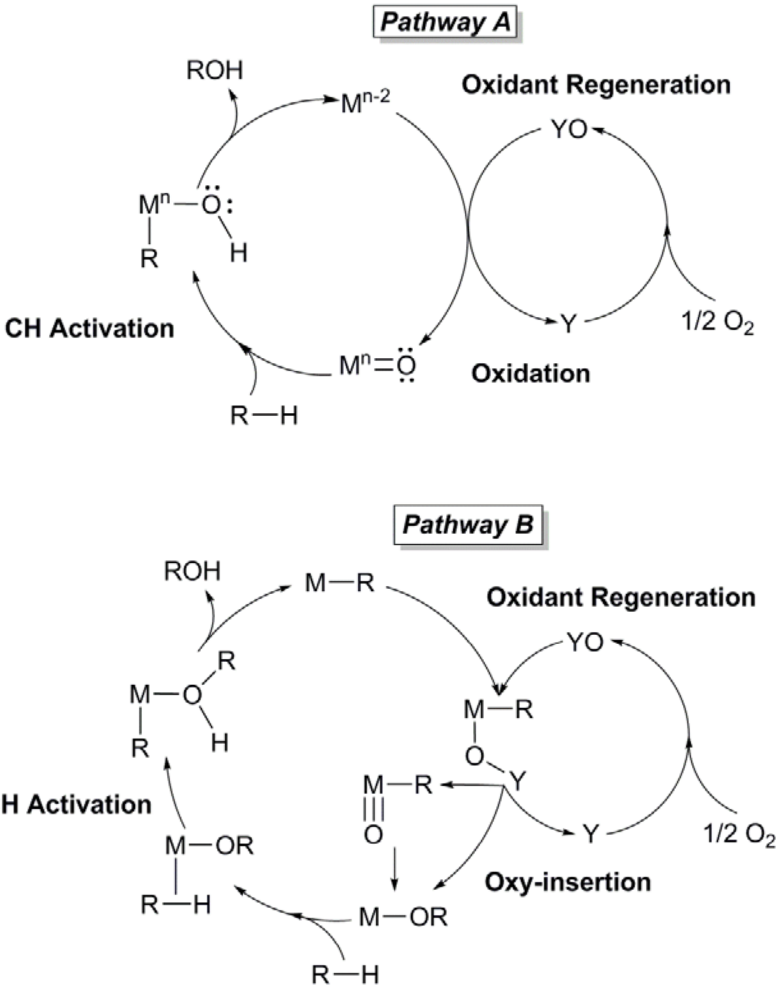

Scheme 1.8. Two possible pathways for oxidation of hydrocarbons (RH) involving C–H activation via 1,2-addition across metal-heteroatom bonds.

Pathway B in Scheme 1.8 involves C–H bond activation by 1,2-addition across a metal-alkoxide bond (M–OR) to generate the functionalized alcohol and M–R, a net oxygen atom insertion into the M–R bond from the oxygen donor YO to reform the M–OR completes the catalytic cycle.[43,56,57] For both reactions, Recycling of YO from Y + O_2 results in the net reaction: RH + ½ O_2 → ROH. C–H bond activation by 1,2-addition across a metal-alkoxide bond is also a metal-mediated process and expected to selectively activate stronger C–H bonds. Examples of C–H activation by M–OR bonds have been reported (see below).[43,58-62] For the net oxygen atom insertion into the M–R bond to form M–OR step, two possible pathways are shown (Pathway B in Scheme 1.8). One pathway is similar to the classic Baeyer-Villiger organic reaction (Scheme 1.9), involving the migration of the hydrocarbyl ligand (R) to the coordinated O atom of YO to form M–OR with the release of Y group.[57] Examples of this pathway have been reported (see below). The other pathway involves the formation of a metal oxo intermediate M(=O)(R), followed by migration of the R group to the oxo to generate M–OR. Examples of the second pathway have also been reported (see below).[63,64]

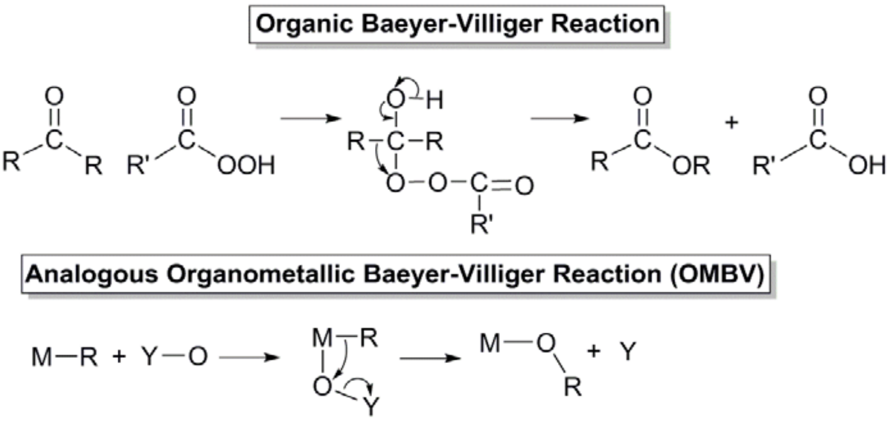

Scheme 1.9. Generic mechanisms for the organic Baeyer-Villiger reaction and the analogous organometallic Baeyer-Villiger reaction (OMBV).

The OMBV O-insertion into M–R bond reaction provides a new strategy for the C–O bond formation, which enhances the feasibility of catalytic selective oxidation of hydrocarbons by combining C–H activation/C–O bond formation via Pathway B in Scheme 1.8. The C–O bond formation by OMBV reaction and C–X bond formation via reductive functionalization in Shilov-type system have different requirements for the catalysts (Scheme 1.10). C–X bond formation via reductive functionalization proceeds through the nucleophilic attack of X^-, which required an electrophilic $R^{\delta+}$ group. In order to have this $R^{\delta+}$ group, the metal center must be at high oxidation state and very electro-negative. Such requirements do not only limit the catalyst to a few late 2nd row or 3rd row transition metal or special main (Tl) metal complexes (see above), but also require strong oxidants for the oxidation step. To the contrast, in the OMBV reaction, studies of the mechanism shown that the migration of the R group is more like a nucleophilic attack of the coordinate O-atom of YO by the nucleophilic $R^{\delta-}$ group.[57,65] As a result, the catalyst does not need an electro-negative metal center to form an electrophilic $R^{\delta+}$ group as in the Shilov-type reaction. Thus, the 1st row transition metals and middle transition metals will also have a chance. In addition, there is no oxidation state change for the metal center, which will subsequently not suffer from the same oxidation problem in the Shilov-type reaction.

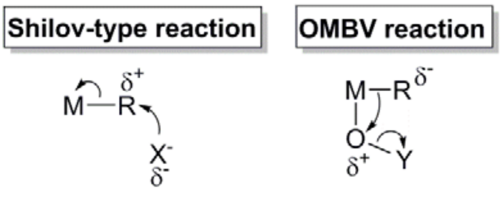

Scheme 1.10. Electronic properties for the C–X bond formation in the Shilov-type systems and C–O bond formation via organometallic Baeyer-Villiger reaction (OMBV).

1.2 C–H Activation by Metal–alkoxide Bonds (M–OR)

Combination of C–H activation by M–OR and C–O bond formation by net O-atom insertion (Pathway B in Scheme 1.8.) in a catalyst creates the opportunity to the oxy-functionalization of hydrocarbons (RH). Our group is one of the pioneers to study C–H activation by M–OR and initiators of the catalytic cycle of Pathway B in Scheme 1.8.

Based on the previous work on H_2 and CH activation by metal-hetero-atom complexes,[66,67] our group reported C–H activation of benzene by $TpRu(PMe_3)_2OH$ complex in 2005.[58] Heating $TpRu(PMe_3)_2OH$ in C_6D_6 at 80 °C results in H/D exchange between hydroxide and C_6D_6. The proposed mechanism involves the dissociation of one PMe_3 ligand, coordination of C_6D_6 to Ru and C–H activation of benzene via σ-bond metathesis to form the Ru phenyl complex. A replacement of the coordinated water by PMe_3 generates the final C–H activation product (Scheme 1.11). By using PH_3 for PMe_3 ligand, DFT calculations show a $\Delta G = +9.1$ kcal/mol for this reaction, which is thermodynamically unfavorable. Kinetic studies revealed that H/D exchange at the hydroxide ligand in C_6D_6 is first order in Ru complex with $k_{\mathrm{obs}} = 8.0(2) \times 10^{-5}\ \mathrm{s}^{-1}$ (80 °C) and $\Delta G^{\ddagger}_{\mathrm{obs}} = +21.4$ kcal/mol, corresponding to the DFT calculated $\Delta G^{\ddagger}_{\mathrm{cal}} = +21.2$ kcal/mol for the reaction.

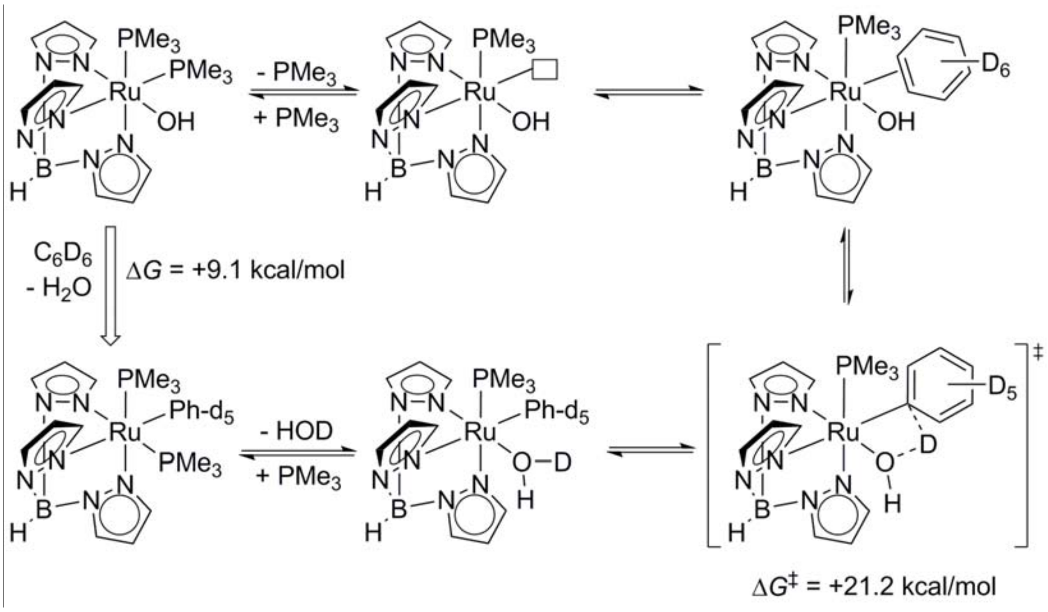

Scheme 1.11. Proposed mechanism and calculated results (PH_3 for PMe_3) for C–H activation of benzene by $TpRu(PMe_3)_2OH$.

Reaction of $TpRu(PMe_3)_2OH$ with toluene-*d*$_8$ at 80 °C also results in H/D exchange (Scheme 1.12).[58] The kinetic selectivity (after statistical correction) for H/D exchange of $TpRu(PMe_3)_2OH$ in toluene-*d*$_8$ is para:meta:ortho:methyl = 4.4:3.9:2.5:1.0. The selectivity for para and meta positions in preference to the ortho and methyl positions is consistent with a metal-mediated process and suggests that the H/D exchange does not likely involve a hydrogen atom abstraction pathway.

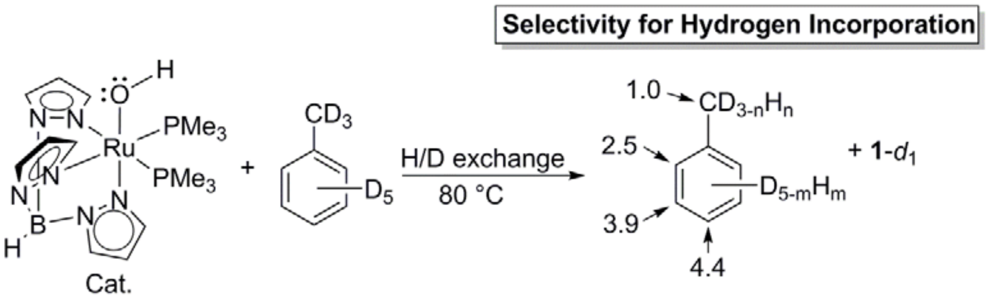

Scheme 1.12. Statistically corrected results for the H/D exchange reaction of $TpRu(PMe_3)_2OH$ in toluene-*d*$_8$.

Periana, Goddard and co-workers reported C–H bond activation by Ir^{III}–OMe complex at the same time in 2005.[60,68,69] (κ^2-*O*,*O*-acac)$_2$Ir(HOMe)(OMe) (acac = acetylacetonate) reacts with C_6H_6 in the presence of pyridine to produce (κ^2-*O*,*O*-acac)$_2$Ir(Py)(Ph) (Py = pyridine) and methanol in 75% yield when heating in benzene at 160 °C after 10 min. When (κ^2-*O*,*O*-acac)$_2$Ir(Py)(OMe) is used, > 95% yield of (κ^2-*O*,*O*-acac)$_2$Ir(Py)(Ph) and methanol are formed at 180 °C after 4 h. A σ-bond metathesis pathway is proposed for this C–H bond activation reaction (Scheme 1.13). After the dissociation of the MeOH or Py ligand, a rearrangement of the acac ligand places the open coordination site *cis* to the –OMe ligand. Following benzene coordination, C–H addition cross the Ir–OMe bond and re-coordination of the Py ligand forms the final product. Computational studies calculated a $\Delta G^‡ = +23.4$ kcal/mol for the C–H bond activation step and a $\Delta G = -17.1$ kcal/mol for the overall reaction,[60] which is unlike the thermodynamically unfavorable Ru–Ph bond formation in the TpRu system introduced above.

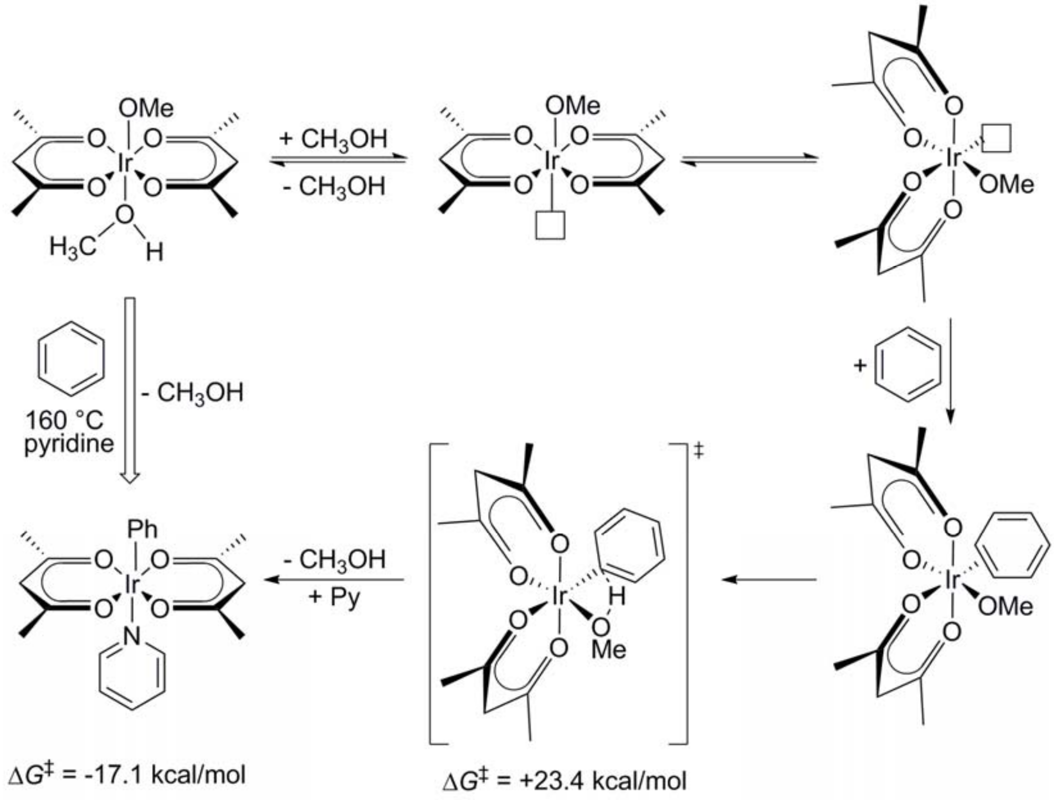

Scheme 1.13. proposed mechanism for C–H activation by (κ^2-*O,O*-acac)$_2$Ir(HOMe)(OMe) (acac = acetylacetonate).

In 2007, Goldberg and co-workers reported C–H activation of arenes by (PNP)Rh^{I} (PNP = 2,6-bis[(di-*tert*-butylphosphino)methyl]pyridine) hydroxide, trifluoroethoxide and phenoxide complexes.[61,70] The proposed mechanism is different from the mechanism of Ru^{II} and Ir^{III} complexes discussed above. Mechanistic studies support a pathway that involves the dissociation of the OR$^-$ group by either associative or dissociative substitution as the first step, followed by the formation of a cationic Rh^{I} solvent (which is water) complex. Displacement of H_2O by arenes and then C–H oxidative addition and deprotonation of the Rh^{III}–H by free RO$^-$ forms the products (Scheme 1.14).

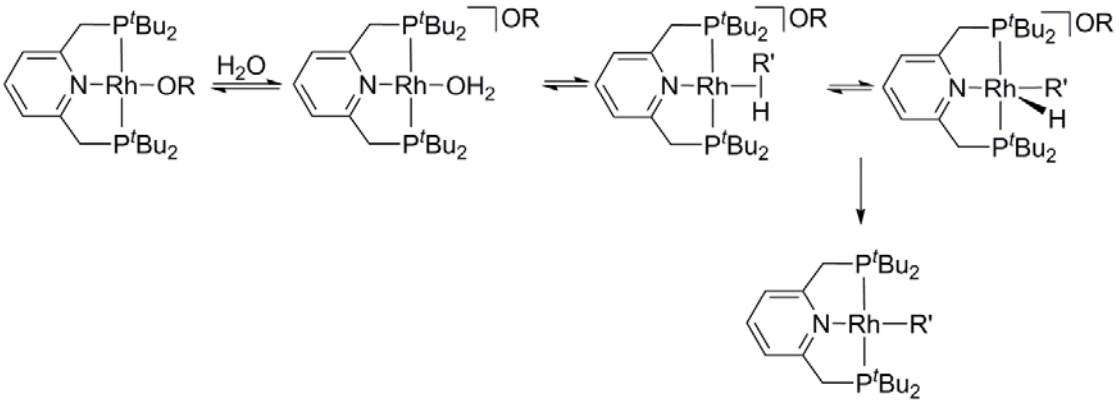

Scheme 1.14. Proposed mechanism for C–H activation of arenes by (PNP)Ph(OR).

Another example of C–H activation of allylic C–H bonds by a neutral hydroxide-bridged rhodium dimer [(COD)Rh(μ_2-OH)]$_2$ (COD = 1,5-cyclooctadiene) was reported by Bercaw, Labinger and co-workers in 2009 (Scheme 1.15).[62] The air- and water-tolerant [(COD)Rh(μ_2-OH)]$_2$ cleanly activates the aliphatic C–H bond of indene to generate [(COD)Rh(η^3-indenyl)]. The proposed mechanism involves direct coordination of indene to the dimer followed by rate-determining C–H bond cleavage, in contrast to the previously reported analogous reactions of [(diimine)M(μ^2-OH)]$_2^{2+}$(M = Pd, Pt),[71,72] for which the dimer must be cleaved before rate-determining displacement of solvent by indene. The detailed mechanism of the C–H bond cleavage was not clearly demonstrated. The authors suggested either an σ-bond metathesis pathway similar to the Ru^{II}[58] and Ir^{III} [60,68,69]systems or an oxidative addition pathway like the Rh^{I} system. It was noted that the mechanism similar to Rh^{I} is not likely as the dissociation of a hydroxide ligand from the dimer would not be easy.

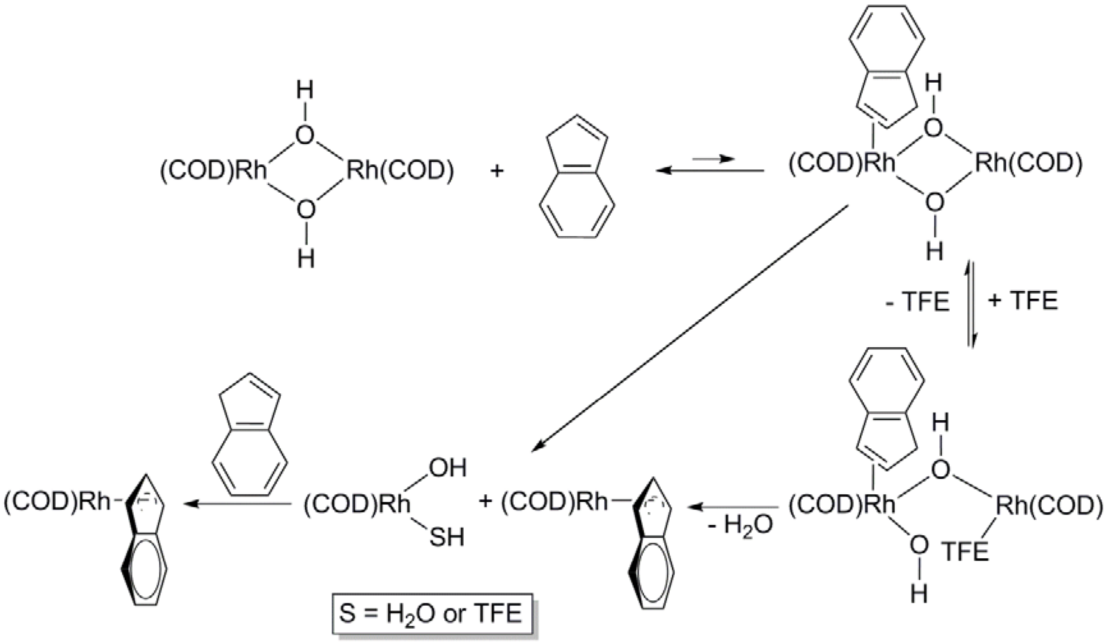

Scheme 1.15. Proposed mechanism for C–H activation of indene by [(COD)Rh(μ-OH)]$_2$.

To summarize, all these reported examples of C–H activation by M–OR involve late d^6 or d^8 metal-hetero atom bonds. We suggested in the previously discussed intermolecular C–H activation by TpRu(PMe$_3$)$_2$X, "*the possibility that C–H activation events mediated by non-dative, heteroatom-based ligands coordinated to the late transition metals in low oxidation states possess inherently lower activation barriers than similar reactions with metal–alkyl or –aryl bonds*".[43] The electron-rich d^6 or d^8 metal center can provide back π-bonding to the hetero-atom and might facilitate C–H bond activation. This character suggested that late d^6 or d^8 transition metal complexes might be a good choice for the catalyst design for the selective oxidation of hydrocarbons via Pathway B in Scheme 1.8, if O-atom insertion into these M–R bonds to from M–OR bonds is also feasible.

1.3 C–O bond Formation by Oxygen Atom Insertion

While C–H activation of the RH by M–OR have been reported, the other key step in Pathway B in Scheme 1.8, the C–O bond formation via net O-atom insertion into M–R bonds has also been reported. Various mechanisms and oxygen donors are involved in these O-atom insertion reactions. Ideally, the O-atom insertion step will not proceed via radical pathway for a high selectivity and the oxygen donor YO can be regenerated by O_2.

1.3.1 Oxygen Atom Insertion by Radical Pathway

Some early transition metal complexes, such as Group IV complexes, initiate O atom insertion into M–R bonds; however, these reactions commonly proceed by radical pathways.[73-75] For example, Brindley and co-workers reported Cp_2ZrR_2 reacts approximately 1 equivalent of oxygen to form the corresponding dialkoxides, $Cp_2Zr(OR)_2$ in high yield in toluene and at temperatures in the range 30-60 °C.[74,76] A radical process was proposed for this O atom insertion reaction (Scheme 1.16). And some other O-atom insertion reactions via radical pathways have been observed to Zr and Hf complexes.[73-76] Similar reactions occur to some main group and Group (VI) metal complexes.[73,76-86] For example, Bercaw and co-workers reported $(Cp^*)_2W{=}O$ reacted with O_2 to generate the O-atom insertion into Cp*–W product (Scheme 1.17).[83] To be generally useful for selective oxidations at high conversion, ideally, the C–O bond forming step should proceed without the formation of radical intermediates.

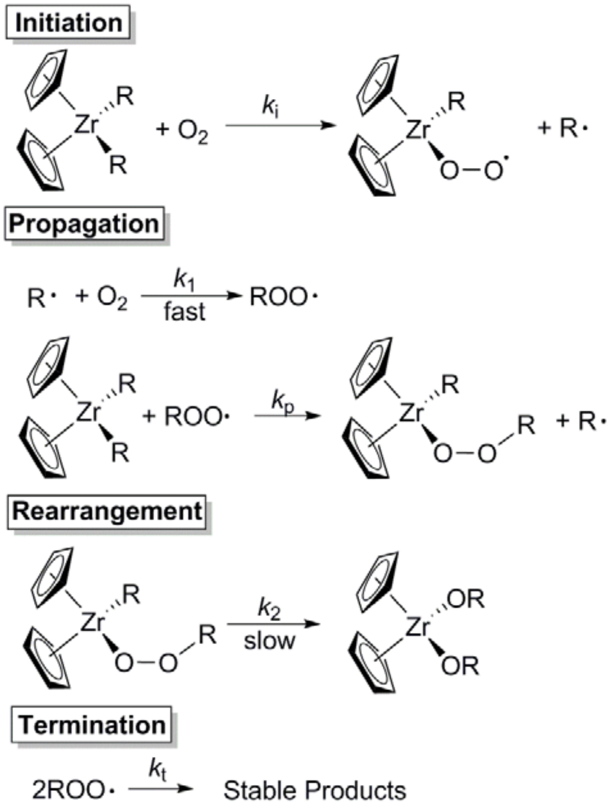

Scheme 1.16. Proposed mechanism for O-atom insertion into Zr–R bond via radical pathway.

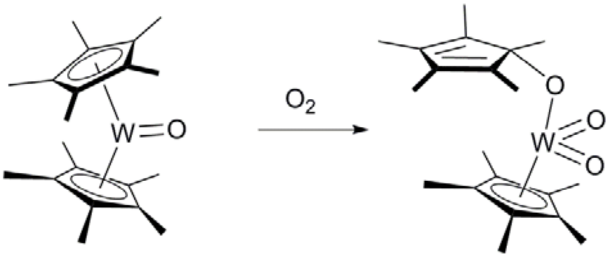

Scheme 1.17. The reaction of $(Cp^*)_2W{=}O$ with O_2.

1.3.2 Oxygen Atom Insertion by Non-radical Pathways

1.3.2.1 Oxygen Atom Insertion by Migration of R to M(η^2-O2)

To our knowledge, the first well-defined oxygen atom insertion into metal–carbon bonds came from a 1988 publication by Bercaw and co-workers that focused on O atom insertion into Ta^V hydrocarbyl bonds.[87] This oxygen atom insertion into Ta–C bond is proposed to be catalyzed by electrophiles (*e.g.*, proton) via coordinating one oxygen atom of the coordinated η^2-O_2 of $(Cp^*)_2Ta(\eta^2\text{-}O_2)R$, which increases the electrophilicity of oxygen atom and facilitates the transfer of the R group to the other oxygen atom to form the oxy-insertion product $(Cp^*)_2Ta(O)OR$ (Scheme 1.18).[87]

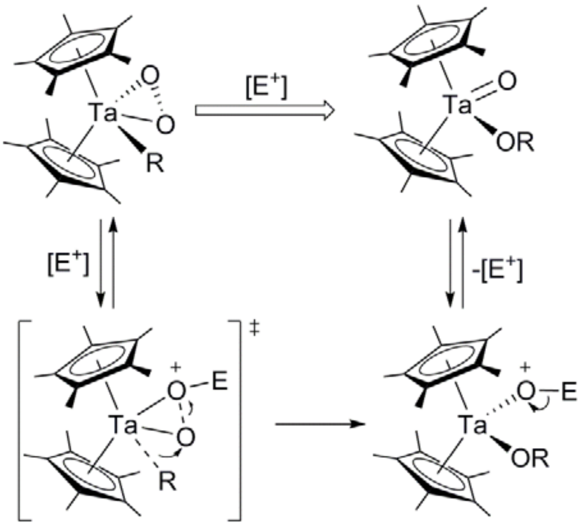

Scheme 1.18. Proposed mechanism for O-atom insertion into Ta–C bond catalyzed by electrophiles.

Theopold and co-workers reported O_2 insertion into Cr–Ar bond to form the paramagnetic product $Tp^{tBu,Me}Cr^{IV}(O)(OPh)$ ($Tp^{tBu,Me}$ = hydrotris(3-*tert*-butyl-5-methylpyrazolyl)borate). The proposed mechanism involves the formation of the η^2-O_2 peroxo intermediate $Tp^{tBu,Me}Cr^{IV}(\eta^2\text{-}O_2)Ph$ followed by the migration of phenyl group to the η^2-O_2 peroxo ligand (Scheme 1.19).[88] To determine the mechanism of this O atom insertion reaction, an equimolar solution of $Tp^{tBu,Me}Cr(C_6D_5)$ and $Tp^{tBu}Cr(C_6H_5)$ was allowed to react with O_2 for a crossover reaction. ^2H NMR analysis of the product mixture showed the presence of $Tp^{tBu,Me}Cr(O)(OC_6D_5)$ as the only major deuterated product. If the reaction proceeds via a intermolecular radical pathway, $Tp^{tBu}Cr(O)(OC_6D_5)$

will also be observed. This crossover reaction supports an intramolecular fashion for the O-atom insertion instead of a radical process.

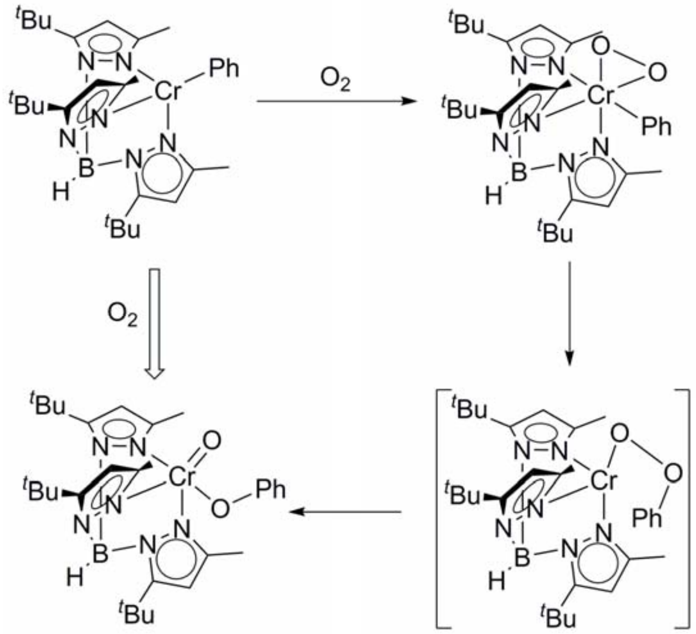

Scheme 1.19. Proposed mechanism for O-atom insertion into Cr–Ph bond.

1.3.2.2 Oxygen Atom Insertion into M–R bonds by Migration of R to M=O

Very few examples of well-defined alkyl or aryl migration to oxo ligands to form M–OR products have been reported. Brown and Mayer reported high valent Re^{VII}–oxo complexes that undergo insertion of an oxo ligand, probably best considered as an electrophilic oxene type ligand, into Re–Ph bonds under photolytic and thermal conditions.[63,64,89] In 1994, they first reported the C–H activation by Re^{V} complex TpRe(O)(Cl)I under photolysis to form TpRe(O)(Cl)Ph, which was followed by a photolytic phenyl-to-oxo migration to produce the O-atom insertion product TpRe(OPh)(Cl)L (L = Py, MeCN, Me_3PO) in the presence of L (Scheme 1.20).

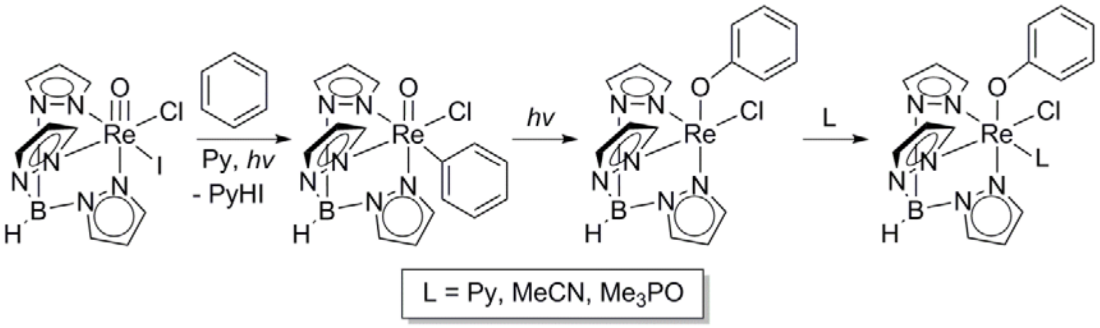

Scheme 1.20. O-atom insertion into Re–Ar bonds by migration of Ar to Re^V=O.

Brown and Mayer later synthesized the Re^{VII}-dioxo-aryl complex $[TpRe(O)_2](Ph)[OTf]$ from the reaction of the Re^V-oxo and pyridine-*N*-oxide at low temperature.[64] Phenyl-to-oxo migration to generate a Re^{VII}-phenoxide complex was observed from this Re^{VII}-dioxo-phenyl complex at room temperature. When using Me_2SO, the adduct $[TpRe(O)(OSMe_2)Ph][OTf]$ is generated and in a rapid equilibrium with the dioxo complex via dissociation of Me_2S. Phenyl-to-oxo migration was observed is this case to produce the phenoxide complex $[TpRe(O)(OSMe_2)(OPh)][OTf]$ (Scheme 1.21).[64] It was proposed that the strong oxo-to-Re π-donation enhances the electrophilicity of the oxo ligand, which facilitates the nucleophilic attack of the $R^{\delta-}$ group to the $M{\equiv}O^{\delta+}$ ligand to produce the phenyl-to-oxo migration product (Scheme 1.22). This $R^{\delta-}$ to $M{\equiv}O^{\delta+}$ migration is similar as the $R^{\delta-}$ to $M–O^{\delta+}–Y$ migration in the OMBV reaction, which are different from the nucleophilic attack of X^- to the $M–R^{\delta+}$ in the Shilov-type reaction (see above, Scheme 1.10).

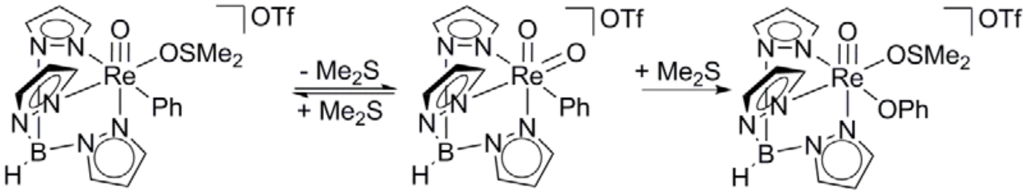

Scheme 1.21. O atom insertion into Re–Ar bonds by migration of Ar to Re=O.

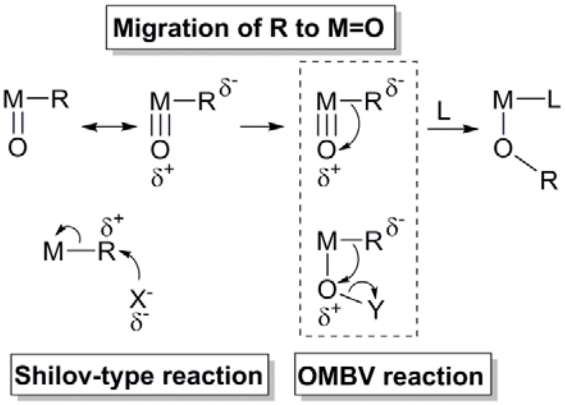

Scheme 1.22. Comparison of the migrations in the R to M=O, Organometallic Baeyer-Villiger (OMBV) reaction and Shilov-type reaction.

Hillhouse and co-workers reported examples of oxygen atom insertion into Ni–R bonds to form Ni–OR by using N_2O as the oxygen donor. N_2O reacts (1 atm, 55 °C, 48 h) with benzene solutions of the metallacyclopentane complex (bipy)Ni$(CH_2)_4$ **(**bipy = 2,2'-bipyridine) to effect a formal O-atom insertion into a Ni–C bond with elimination of dinitrogen, affording purple (bipy)Ni-(OC_4H_8) in 55% isolated yield (Scheme 1.23). [90-92]

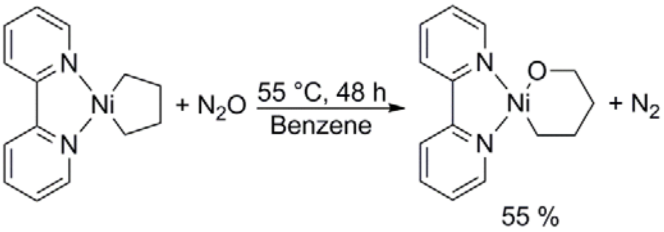

Scheme 1.23. Oxygen atom insertion into Ni–C bond in the Hillhouse system.

Recently, Cundari and co-workers studied the Hillhouse system computationally by performing DFT calculations on (bpy)Ni(cyclo-$(CH_2)_4$) to investigate the mechanism for O-atom insertion (Scheme 1.24).[93] The calculations suggest that the reaction proceeds through a Ni–oxyl intermediate followed by migration of alkyl ligand to form an alkoxide. The calculated electronic structure of the oxo complex is best thought of as a Ni^{III}–oxyl (*i.e.*, O^-). Formation of the Ni^{III}–oxyl was proposed to be the rate-determining step with a calculated activation barrier of 29.4 kcal/mol. When pyridine-*N*-oxide is calculated as the oxidant rather than N_2O for O-atom insetion into(bpy)Ni(cyclo-$(CH_2)_4$), a much higher activation barrier (> 50 kcal/mol) is calculated for the generation of the Ni-oxo intermediate. The release of N_2 from N_2O is considered as a thermodynamic driving force.

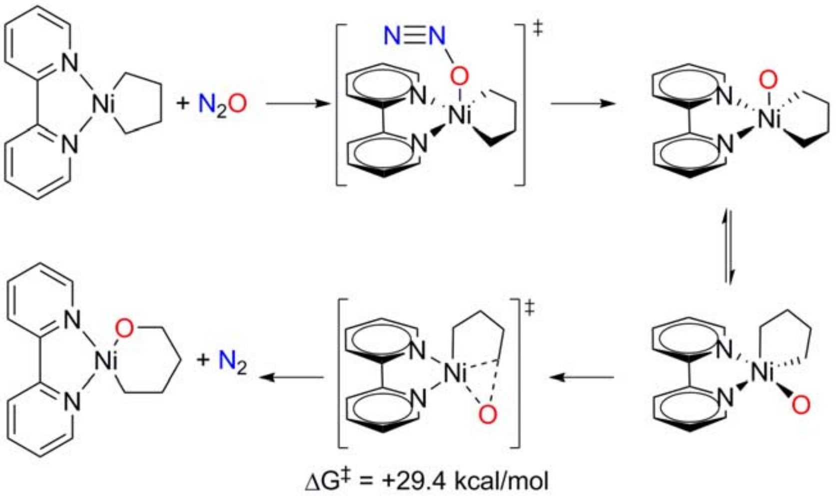

Scheme 1.24. Calculated pathway for oxygen atom insertion into Ni–C bond.

O-atom insertion into Pd–Ar bond has also been reported. In 1993, Van Koten and co-workers reported a [2-((dimethylamino)methyl)-3-naphthyllpalladium complex reacted with tBuOOH to generated the Pd–alkoxide dimer as the product (Scheme 1.25).[94,95] The proposed mechanism involves formation of a square pyramidal Pd^{IV}=O intermediate. Migration of the Ar to Pd^{IV}=O generate the O-atom insertion product.

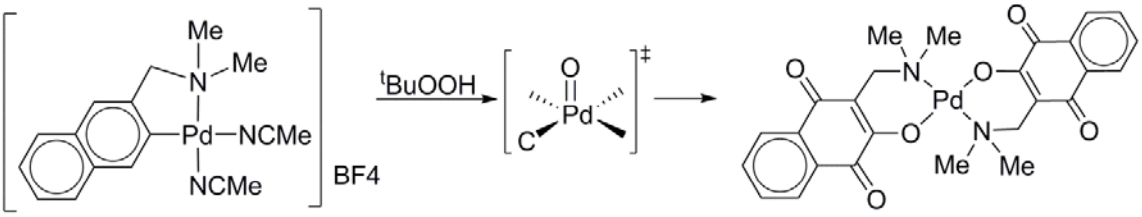

Scheme 1.25. O-atom insertion form [2-((dimethylamino)methyl)-3-naphthyllpalladium complex and tBuOOH via formation of P^{IV}=O intermediate.

Later, and co-workers reported another example of O atom insertion into Pd–Ar bond and proposed a similar mechanism to Hillhouse nickel system involving the formation of a $Pd^{IV}=O$ intermediate (Scheme 1.26).[96,97] But no experimental data was presented to support this proposal.

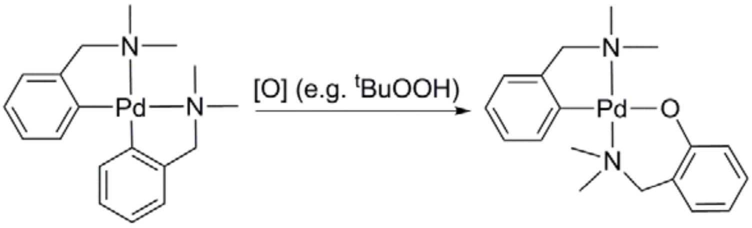

Scheme 1.26. O-atom insertion into Pd–Ar bond.

1.3.2.3 Oxygen Atom Insertion by Migration of R to M–OY

Methyltrioxorhenium (MTO) is observed to react with oxidants in aqueous solution to produce methanol under various conditions, and the kinetics were studied by Espenson and co-workers.[98] Methanol was generated in both acidic and basic solution, and the rates are highly pH dependent. In aqueous solution, MTO reacts with H_2O_2 to produce the η^2-peroxo complex $ReO_2(\eta^2\text{-}O_2)Me$ (**A**) and $ReO(\eta^2\text{-}O_2)_2Me$ (**B**):H_2O (Scheme 2.3). The equilibrium constants for their formation are $k_1 = 16.1(2)$ L·mol^{-1} and $k_2 = 1.32(2) \times 10^2$ L·mol^{-1} at pH = 0, $\mu = 2.0$ M, and 25 °C. Slow decomposition of A and B(H_2O) generates MeOH. In contrast, MeOH release is facilitated in basic solution in two pathways (Scheme 1.27).[98] Methanol is released by either the attack of hydroperoxide anion to MTO or the attack of hydroxide anion to complex **B**, with $k_A = 6.2(3) \times 10^9$ and $k_{MTO} = 4.1(2) \times 10^8$ L·mol^{-1}·s^{-1} at $\mu = 0.01$ M and 25 °C.

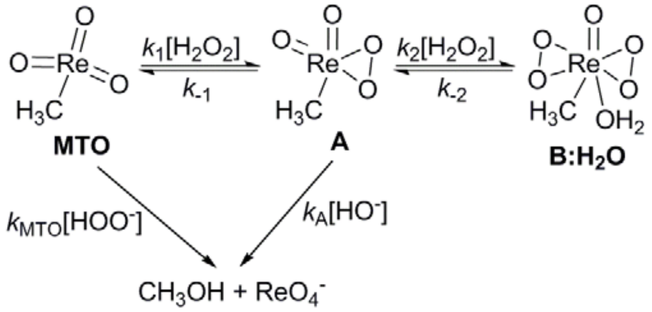

Scheme 1.27. The kinetics of the reaction of MTO and H_2O_2 to release MeOH in aqueous solution.

Periana, Goddard and co-workers extended the MTO reaction and reported facile conversion of Re–Me bond of MTO to a Re–OMe bond upon treatment of various oxidants (H_2O_2, PyO, PhIO and IO_4^-).[57] They studied the mechanism of these reactions experimentally and computationally and pointed out that the O-atom insertion in MTO does not likely occur by the migration of the methyl ligand to the oxo ligand of MTO. For example, reaction of $Re^{16}O_3Me$ with ^{18}O labeled oxidant ($I^{18}O_4^-$) produced only $Me^{18}OH$. An organometallic Baeyer-Villiger (OMBV) pathway, which is similar to the classic Baeyer-Villiger organic reaction (see Scheme 1.9), involving the migration of the methyl ligand to the coordinated O atom of the oxidants to the MTO was proposed (Scheme 1.28).[57] This result demonstrates O-atom insertion into a M–R bond without formation of a metal–oxo species or M((η^2-O_2) Species, and provide a new pathway to form C–O bonds.

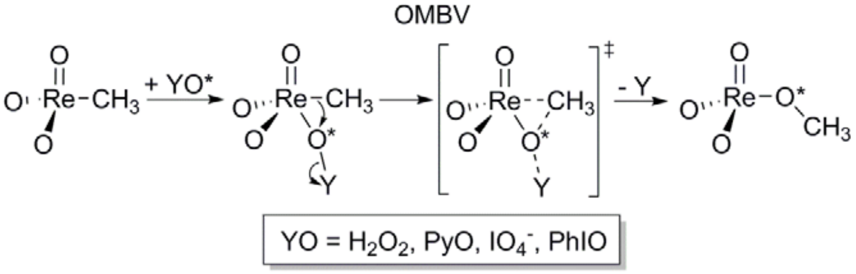

Scheme 1.28. Proposed mechanism for the O-atom insertion into MTO with various oxidants.

Two possible pathways for the O-atom insertion reaction of MTO and IO_4^- were studied computationally, the OMBV pathway and η^2-peroxo pathways.[57] The η^2-peroxo pathway involves the formation of a η^2-peroxo complex as the intermediate. Calculations show a much lower energy barrier for the OMBV pathway (17 kcal/mol) than the η^2-peroxo pathway (25 kcal/mol) (Scheme 1.29). The 17 kcal/mol activation barrier is remarkably low for a M–R to M–OR transformation and is consistent with the observed facile O-atom insertion reaction of MTO and IO_4^- at room temperature.

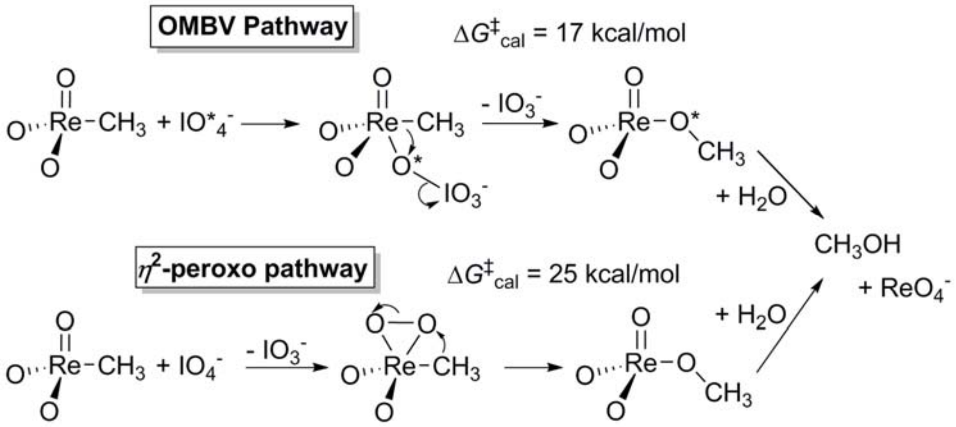

Scheme 1.29. Two possible pathways for the reaction of MTO with IO_4^- to produce MeOH.

Extension of this O-atom insertion reaction to the Re–aryl complexes also results in the formation of the O-atom insertion products. The original synthesis of a phenyl variant of aryltrioxorhenium $ArReO_3$ (Ar = phenyl) for O-atom insertion did not succeed as it easily decomposed to release biphenyl. However, The 2,4,6-trimethyl substituted $ArReO_3$ (Ar = mesityl) was synthesized and reacted with O-atom donors to produce the corresponding phenol in almost quantitative yield (Scheme 1.30).[65] As observed with the MTO system, ^{18}O-labeling studies show that the inserted O-atom originates from the oxidant rather than an oxo ligand. Computational studies reveal an activation barrier of 10.7 kcal/mol for the O-atom insertion reaction of $ArReO_3$ with H_2O_2 via the OMBV pathway, which is much lower than the reaction of MTO with H_2O_2. These results suggest a parallel to the BV reactions observed in organic chemistry, where conversion of aryl ketones to the corresponding esters by treatment with O-atom donors such as H_2O_2 are more facile than with alkyl ketones.[99] This is typically explained by the more electro-rich and nucleophilic aryl group than alkyl group and the greater stabilization of charge by delocalizationin the transition state that is possible in aryl versus alkyl migration. The faster migration of more necleophilic Ar group than the Me group to the Re–OY ligand is consistent with the $R^{\delta-}$ to $M–O^{\delta+}–Y$ migration analysis (see Scheme 1.10).

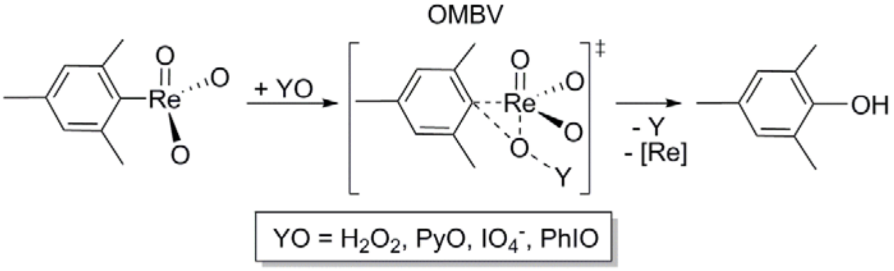

Scheme 1.30. O-atom insertion into $ArReO_3$ and related complex via organometallic Baeyer-Villiger (OMBV) pathway.

Although O-atom insertion into M–R bonds of MTO and related complexes has been observed, theoretical studies have indicated that the activation barrier for this pathway can be high, especially for late-transition-metal complexes (see below).[100] Thus, the implementation of a combined C−H activation/oxygen insertion strategy for catalytic hydrocarbon oxidation depends on uncovering methods for lowering the activation barrier for oxygen insertion into metal−hydrocarbyl bonds. This work led us to consider catalysts that would facilitate an organometallic BV reaction. Mark Pouy who worked in our group demonstrated that methanol release from O-atom insertion into MTO by H_2O_2 could be facilitated by flavins.[101] Flavins catalyzed the reaction involving H_2O_2 by reacting with H_2O_2 to generate the hydroperoxo flavins, which has better oxidation performance than H_2O_2 (Scheme 1.31). Experimental data show that the production of methanol can be accelerated up to 600 times when flavins are used as the catalyst at pH = 3.4 at room temperature. Computational studies by the Cundari group show that the catalyzed reaction has a much lower energy barrier with $\Delta\Delta G^{\ddagger} = 4.8$ kcal/mol (Scheme 1.32).[101] This flavins chemistry is the first example of catalyzed oxygen atom insertion into M−R bonds and is a step forward in catalytic hydrocarbon oxidation by combined C−H activation/oxygen insertion.

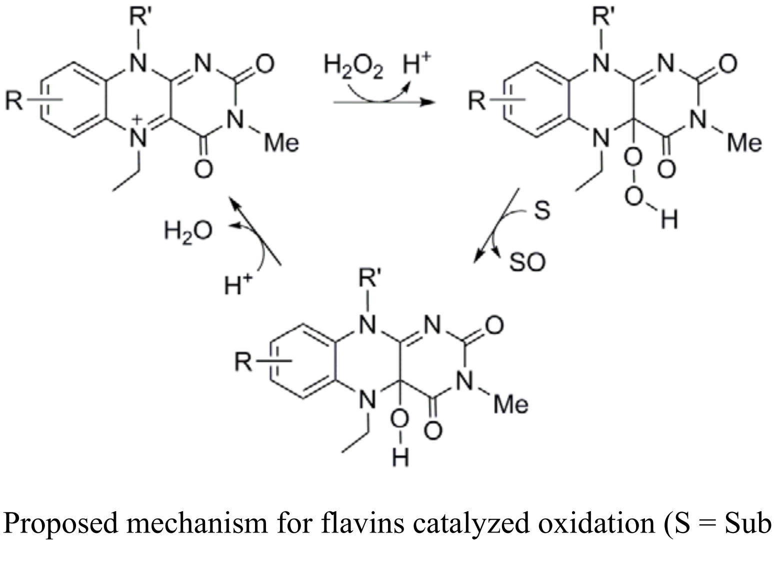

Scheme 1.31. Proposed mechanism for flavins catalyzed oxidation (S = Substrate).

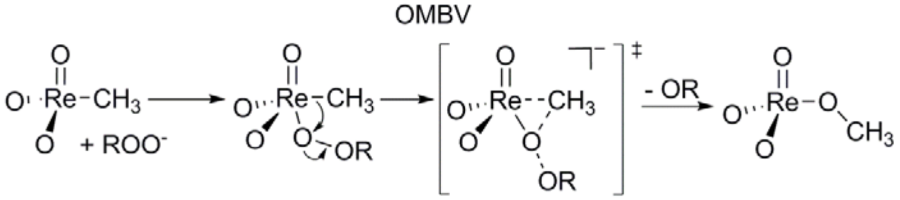

Scheme 1.32. Reaction of MTO with flavins peroxide and hydroperoxide anions via a BV transition state (R = flavins or H; $\Delta\Delta G^{\ddagger}$ = 4.8 kcal/mol).

1.3.2.4 Computational Study of Oxygen Atom Insertion into Late Transition Metal–alkyl Complexes

The Cundari and Gunnoe groups studied the feasibility of extension of the O-atom insertion into metal–carbon bonds via OMBV pathway to late transition metals (group VII to group X) complexes computationally.[100] This study was designed to assess the impact of metal identity on OMBV O-atom insertion reactions. As some late d^6 or d^8 transition metal M–OR complexes have been reported to activate C–H bond of RH via 1,2-addition (see above), we focused our studies on the d^6 or d^8 late transition metals (group VII-X) complexes. The reaction $[(bpy)_xM(Me)(OOH)]_n \rightarrow [(bpy)_xM(OMe)(OH)]_n$ (x = 1 or 2; bpy = 2,2'-bipyridyl; n is varied to maintain the d-electron count at d^6 or d^8) is set up as the model reaction. Six d^8 square planar complexes (M = Pt^{II}, Pd^{II}, Ni^{II}, Ir^{I}, Rh^{I}, and Co^{I}) and eight d^6 octahedral systems (M = Ir^{III}, Rh^{III}, Co^{III}, Fe^{II} Ru^{II}, Os^{II}, Mn^{I}, and Tc^{I}) were studied (Scheme 1.33).[100]

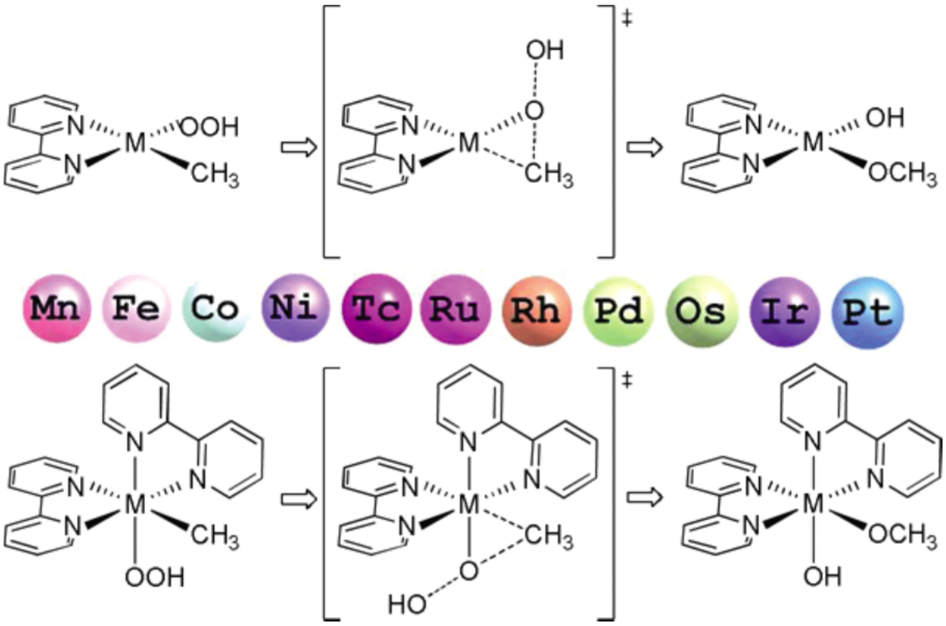

Scheme 1.33. The model reaction and metals that are studied computationally for the OMBV O-atom insertion reactions.

Using density functional theory (DFT) calculations, the structures and energies of ground-state and transition-state species of all the metals in Scheme 1.33 were calculated. Clear trends in calculated $\Delta G^{\ddagger}$'s for the O-atom insertions via OMBV pathway were elucidated. The OMBV insertions are favored by lower coordination numbers (x = 1 versus x = 2 for $[(\mathrm{bpy})_x\mathrm{M(Me)(OOH)}]_n$), earlier transition metals, and 1st row (3d) transition metals (Figure 1.1). Further studies indicate that the OMBV insertion barriers are linearly related to the M–CH$_3$ bond dissociation free energies (BDFE) (Figure 1.2) and calculated charges on the carbon of the methyl migrating group in the OMBV transition states and intermediates (Figures 1.3 and 1.4). These results are consistent with the R$^{\delta-}$ to M–O$^{\delta+}$–Y migration analysis for the OMBV reactions (see Scheme 1.8). The late 2nd row or 3rd row transition metals are more electro-negative than the 1st row transition metals and are more likely to generate a nucleophilic R$^{\delta+}$, which is more favorable in the reductive elimination reaction in the Shilov-type system but not in the OMBV reaction.

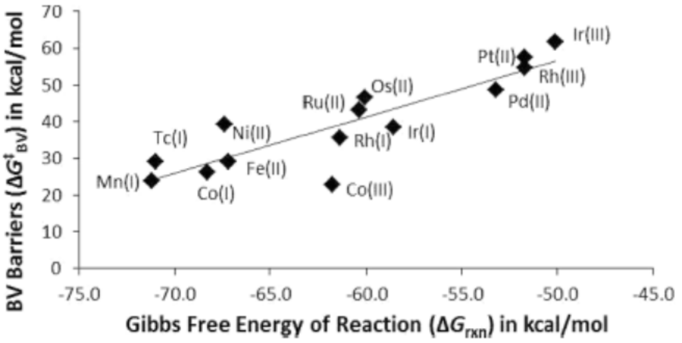

Figure 1.1. Plot of calculated ΔG_{rxn}, $\Delta G^{\ddagger}$ (free energies, kcal/mol) for the OMBV reaction with four- and six-coordinate $[(bpy)_xM(Me)(OOH)]_n$ systems. For each data point, the metal ion and oxidation state are indicated ($R^2 = 0.77$).

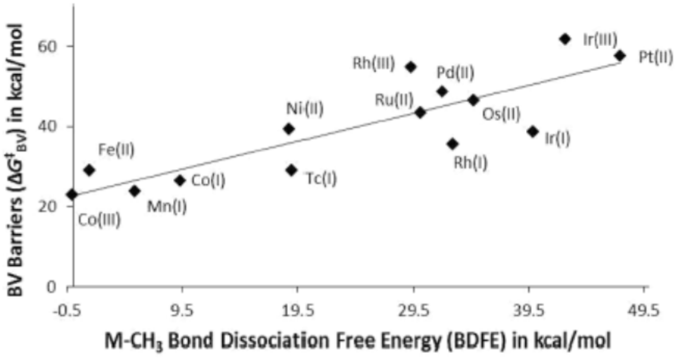

Figure 1.2. Plot of calculated $M-CH_3$ BDFE against OMBV activation barriers in kcal/mol ($R^2 = 0.73$). The metal ion is indicated.

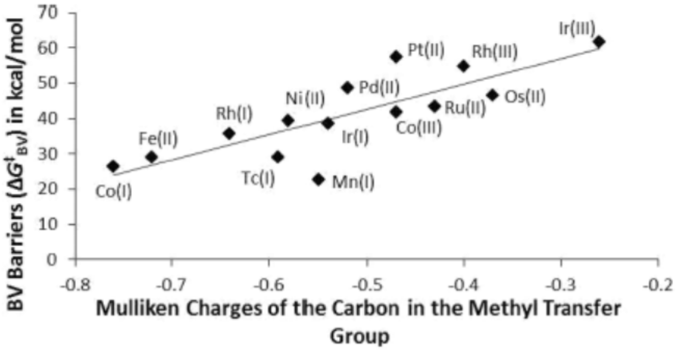

Figure 1.3. Plot of calculated Mulliken charges on the carbon of the methyl migrating group for four- and six-coordinate Metallo-Criegee intermediates and calculated OMBV barriers (free energies, kcal/mol) ($R^2 = 0.65$). The central metal ion is indicated.

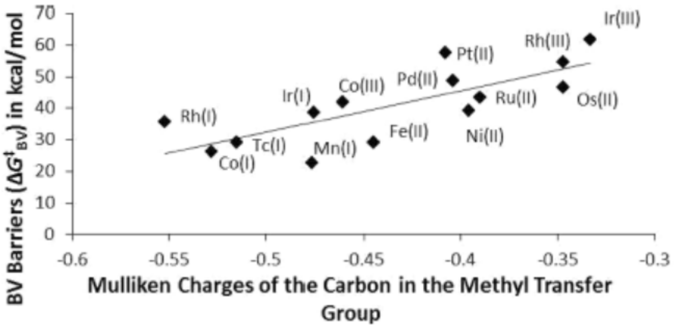

Figure 1.4. Plot of calculated Mulliken charges on the carbon of the methyl migrating group of the OMBV transition states and calculated barriers (free energies, kcal/mol) for four- and six-coordinate geometries discussed in the text ($R^2 = 0.60$). The central metal ion is indicated.

1.3.3 Previous Work by Gunnoe Group

Demonstration of the OMBV reaction with Re^{VII} as well as net oxygen atom insertion into Ni^{II} and Pd^{II}–R bonds led us to attempt to extend O-atom insertion reactions to other late transition metal system. Although Re^{VII} undergo the O-atom insertion reaction, its high oxidation state and zero d-electron count makes C–H activation unlikely. Thus, extension of the O-atom insertion studies to metal centers known to facilitate C–H activation is necessary for the development of catalysts for hydrocarbon functionalization.

As discussed above, metal–alkyls that are $\text{M–C}^{\delta+}$ polarized prefer reductive functionalization with X^- nucleophilies, but $\text{M–C}^{\delta-}$ polarized systems do not. Metal–alkyls that are $\text{M–C}^{\delta-}$ polarized likely undergo migration of $R^{\delta-}$ to the electrophilic $\text{M–O}^{\delta+}\text{–Y}$ in OMBV reactions or to the electrophilic $\text{M≡O}^{\delta+}$ in the R to M=O reactions. Late 2nd row or 3rd row transition metals are more likely to generate a nucleophilic $R^{\delta+}$ but also seems to generate more nucleophilic $O^{\delta+}$. Which plays a more important role, the nucleophilicity of the $\text{M–C}^{\delta-}$ bond or the electrophilicity of the bound $O^{\delta+}$? It is difficult to answer as relatively little is known about the O-atom insertion reactions with only few examples were demonstrated (Scheme 1.34). Moreover, can we extend the OMBV reaction to a series of M–R complexes with different electronic configurations and geometries and other oxidants? If more OMBV reaction are discovered, Is there any transition series between early transition metals with generally more nucleophilic –R$^{\delta-}$ groups and later transition metals with generally less nucleophilic –R group but more electrophilic O$^{\delta+}$ group that is likely to facilitate the O-atom insertion reaction? More researches are required to elucidate these questions.

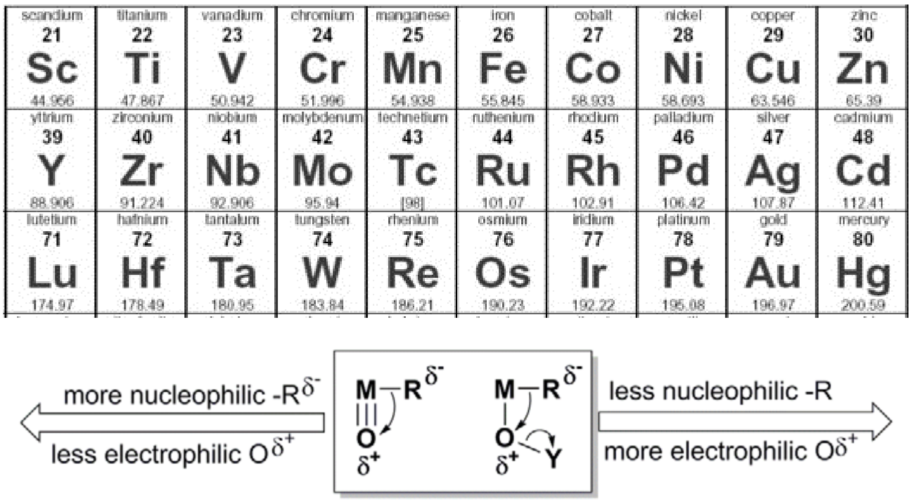

scandium 21 Sc 44.956	titanium 22 Ti 47.867	vanadium 23 V 50.942	chromium 24 Cr 51.996	manganese 25 Mn 54.938	iron 26 Fe 55.845	cobalt 27 Co 58.933	nickel 28 Ni 58.693	copper 29 Cu 63.546	zinc 30 Zn 65.39
yttrium 39 Y 88.906	zirconium 40 Zr 91.224	niobium 41 Nb 92.906	molybdenum 42 Mo 95.94	technetium 43 Tc [98]	ruthenium 44 Ru 101.07	rhodium 45 Rh 102.91	palladium 46 Pd 106.42	silver 47 Ag 107.87	cadmium 48 Cd 112.41
lutetium 71 Lu 174.97	hafnium 72 Hf 178.49	tantalum 73 Ta 180.95	tungsten 74 W 183.84	rhenium 75 Re 186.21	osmium 76 Os 190.23	iridium 77 Ir 192.22	platinum 78 Pt 195.08	gold 79 Au 196.97	mercury 80 Hg 200.59

Scheme 1.34. Transitions for the nucleophilicity of the M–C$^{\delta-}$ bond or the electrophilicity of the bound O$^{\delta+}$ in the periodic table.

Several complexes have been reported to facilitate the 1,2-addition of C–H bonds across metal–heteroatom bonds, as discussed above. Thus, with the first step of catalytic cycle shown in Scheme 1.8 under investigation in the Gunnoe group with metals such as Pt^{II} and Rh^{III}, the complementary O-atom insertion studies were begun with Pt^{II}–R and Rh^{III}–R complexes (R = Me or Ph).[102] In addition, Pt^{II} and Rh^{III} complexes might be sufficiently electrophilic to enhance the electrophilicity of the coordinated oxygen of the oxidant. Joanna Webb in our group initiated O-atom insertion into Pt^{II} and Rh^{III}–C bonds studies.

The labile nature of the THF ligand in the previously reported complex $[(^{t}bpy)Pt(Ph)(THF)][BAr'_4]$ [^{t}bpy = 4,4'-di-tert-butyl-2,2'-bipyridine; Ar' = 3,5-$(CF_3)_2C_6H_3$] allows access to an open site for possible oxidant coordination. Initial reactions of $[(^{t}bpy)Pt(Ph)(THF)][BAr'_4]$ with a variety of oxidants, including $^{t}BuOOH$, $^{t}Bu_4NIO_4$ and N_2O in 1,2-dichlorobenzene-d_4 (*o*-DCB) and PhIO, H_2O_2 and $NaIO_4$ in D_2O/THF-d_8 resulted in decomposition to intractable products. No indication of O-atom insertion into the Pt–Ph bond (*e.g.*, formation of PhOH) was obtained.[103]

The reaction of $[(^{t}bpy)Pt(Ph)(THF)][BAr'_4]$ with some other oxidants including DMSO, $ONMe_3$ and pyridine-*N*-oxide formed the coordinated YO products $[(^{t}bpy)Pt(Ph)(YO)][BAr'_4]$ (Scheme 1.35).[103] The product from DMSO coordination was characterized to have an *S*-bound DMSO ligand. Thermolysis of the *S*-bound complex $[(^{t}bpy)Pt(Ph)(DMSO)][BAr'_4]$ in 1,2-dichlorobenzene-d_4 resulted in no reaction or indication of oxy-insertion after 48 hours at 120 °C and an additional 24 hours at 170 °C. Thermolysis of $[(^{t}bpy)Pt(Ph)(ONMe_3)][BAr'_4]$ and $[(^{t}bpy)Pt(Ph)(PyO)][BAr'_4]$ resulted in decomposition at 100 °C with no evidence of phenol production upon addition of acid. $[(^{t}bpy)Pt(Ph)(PyO)][BAr'_4]$ decomposed to generate free pyridine, which coordinates to the Pt center to yield $[(^{t}bpy)Pt(Ph)(pyridine)][BAr'_4]$.

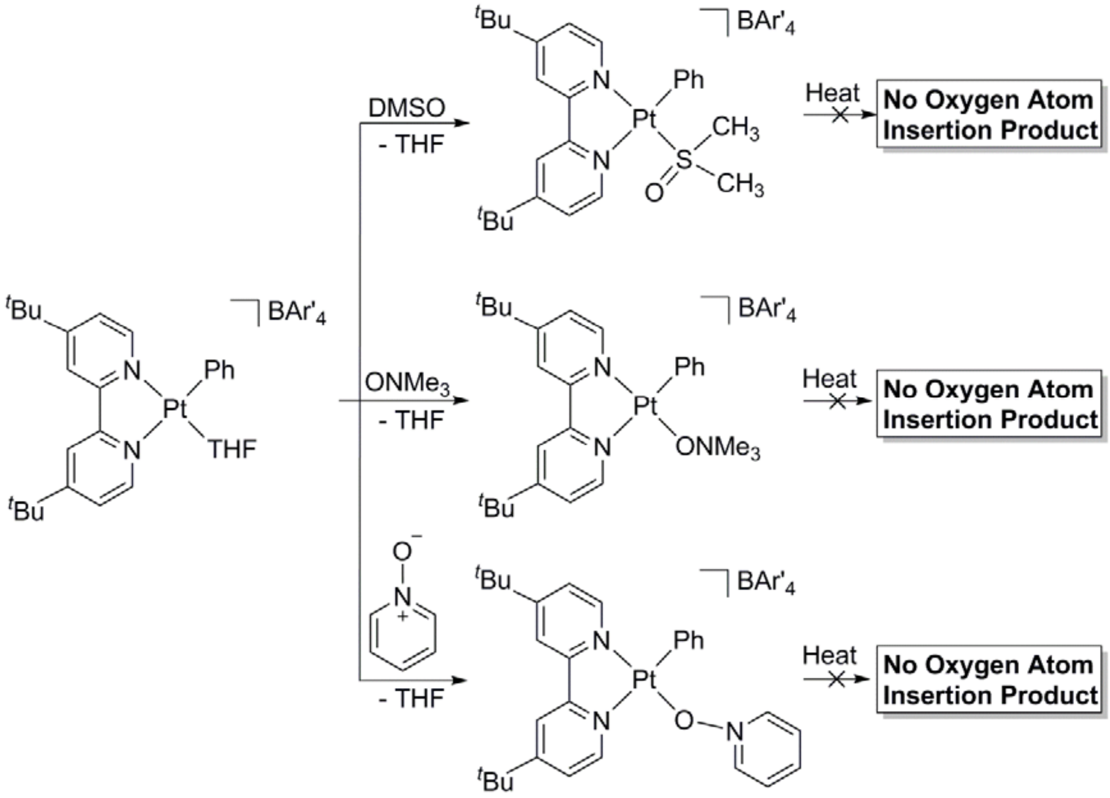

Scheme 1.35. Reaction of [(^{t}bpy)Pt(Ph)(THF)][BAr’$_4$] with YO (YO = $Me_2S=O$, $ONMe_3$ or PyO) to form coordinated YO products [(^{t}bpy)Pt(Ph)(YO)][BAr’$_4$] without the generation of the O-atom insertion products upon heating.

With no successful O-atom insertion into Pt–Ph bond, [(^{t}bpy)$_2$Rh(Me)(OTf)][BAr’$_4$] was synthesized to probe for O-atom insertion into Rh–C bond (Scheme 1.36).[103] The reaction of previously reported [(^{t}bpy)$_2$Rh(Cl)$_2$](Cl) with one equivalent of NaBAr’$_4$ at room temperature yields [(^{t}bpy)$_2$Rh(Cl)$_2$][BAr’$_4$], which is methylated by two equivalent of Me_2Mg to produce [(^{t}bpy)$_2$Rh(Me)$_2$][BAr’$_4$] in the next step. Protonation of [(^{t}bpy)$_2$Rh(Me)$_2$][BAr’$_4$] with one equivalent of HOTf provides the corresponding mono-methyl complex [(^{t}bpy)$_2$Rh(Me)(OTf)][BAr’$_4$] with ~90% of the major targeted *cis*- isomer with ~10% of the *trans* isomer. Separation of the isomers was not attempted as the minor isomer did not affect subsequent reactions.

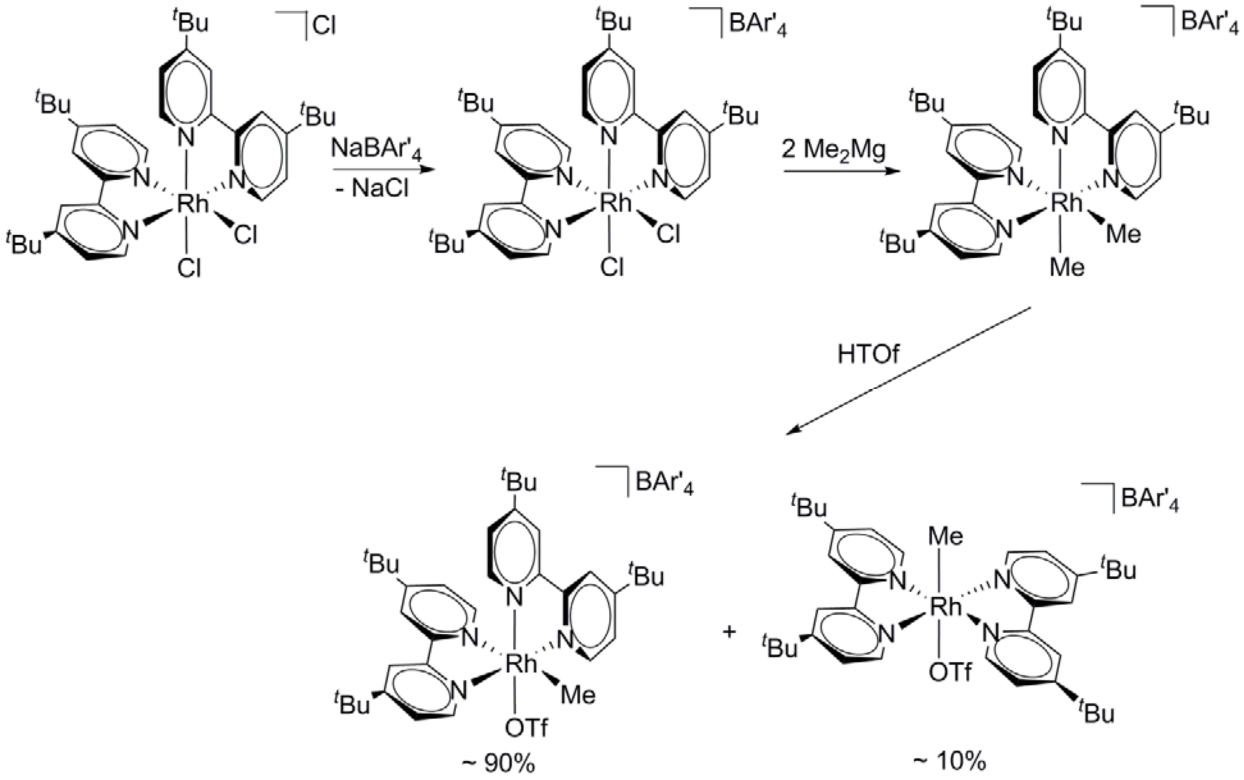

Scheme 1.36. Synthesis of [(^{t}bpy)$_2$Rh(Me)(OTf)][BAr'$_4$].

The labile nature of the triflate ligand of [(^{t}bpy)$_2$Rh(Me)(OTf)][BAr'$_4$] was demonstrated by heating (90 °C) [(^{t}bpy)$_2$Rh(Me)(OTf)][BAr'$_4$] in the presence of water to produce [(^{t}bpy)$_2$Rh(Me)(H_2O)][BAr'$_4$].[103] Due to the ability of the triflate ligand to dissociate to form an open coordination site, [(^{t}bpy)$_2$Rh(Me)(OTf)][BAr'$_4$] was treated with a series of oxidants including PyO, ONMe$_3$, ^{t}BuOOH, Bu$_4$NIO$_4$, N_2O, OPPh$_3$, MesIO (mes = mesityl), *m*-CPBA (meta-chloroperoxybenzoic acid), OsO$_4$, WO$_3$, PhIO, H_2O_2 and NaIO$_4$. Oxy-insertion should give a Rh^{III}–OMe complex or free MeOH. For ^{t}BuOOH, Bu$_4$NIO$_4$, NaIO$_4$, N_2O, OPPh$_3$, 2,6-dichloro-PyO, 4-nitro-PyO, MesIO, *m*-CPBA, OsO$_4$, WO$_3$, PhIO, H_2O_2, no O-atom insertion reactivity was observed upon heating at 180 °C by ^{1}H NMR spectroscopy. In all cases, decomposition resulted after several days of heating at 180 °C. For ^{t}BuOOH, a base (*i.e.*, 2,6-lutidine or LDA (LDA =

lithium diisopropylamide)) was added to produce the $^tBuOO^-$ ion in situ in order to access a coordinated *tert*-butylhydroperoxide complex. However, in all cases, no O-atom insertion products were observed by ^1H NMR spectroscopy. Decomposition occurs after heating at 180 °C for 24 hours.[103]

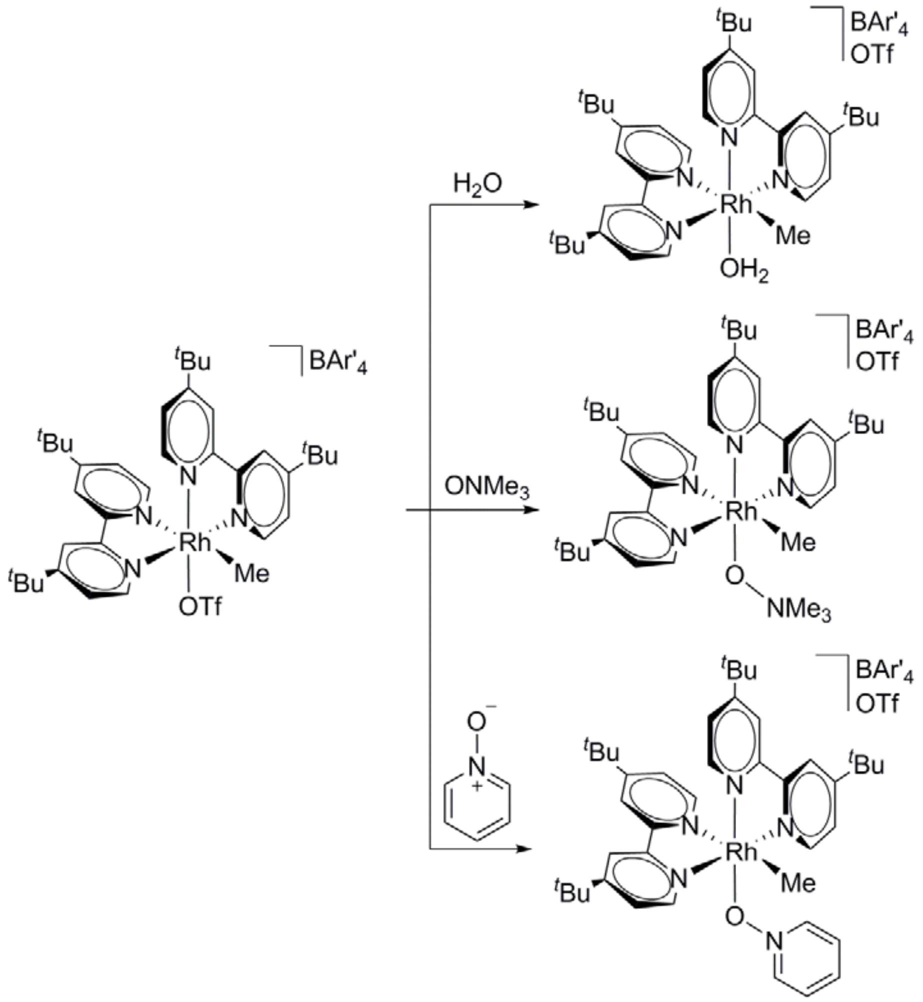

Scheme 1.37. Reactions of $[(^tbpy)_2Rh(Me)(OTf)][BAr'_4]$ with H_2O, $ONMe_3$ and PyO (80 °C) to form the coordinated products.

Similar to the reactions of $[(^tbpy)Pt(Ph)(THF)][BAr'_4]$ with $ONMe_3$ and PyO, the reactions of $[(^tbpy)_2Rh(Me)(OTf)][BAr'_4]$ with $ONMe_3$ and PyO (80 °C) form $[(^tbpy)_2Rh(Me)(ONMe_3)][BAr'_4][OTf]$ and $[(^tbpy)_2Rh(Me)(PyO)][BAr'_4][OTf]$ (Scheme

1.37).[103] Heating [(^{t}bpy)$_2$Rh(Me)(ONMe$_3$)][BAr'$_4$][OTf] in 1,2-dicholorobenzene at 160 °C for 24 hours results in a mixture of products including starting material, [(^{t}bpy)$_2$Rh(Me)(OTf)][BAr'$_4$], and presumably a NMe$_3$ coordinated complex resulting from the decomposition of ONMe$_3$. The addition of one equivalent of pyridine to the product mixture results in full conversion to [(^{t}bpy)$_2$Rh(Me)(Py)][BAr'$_4$] (Scheme 1.38).[103]

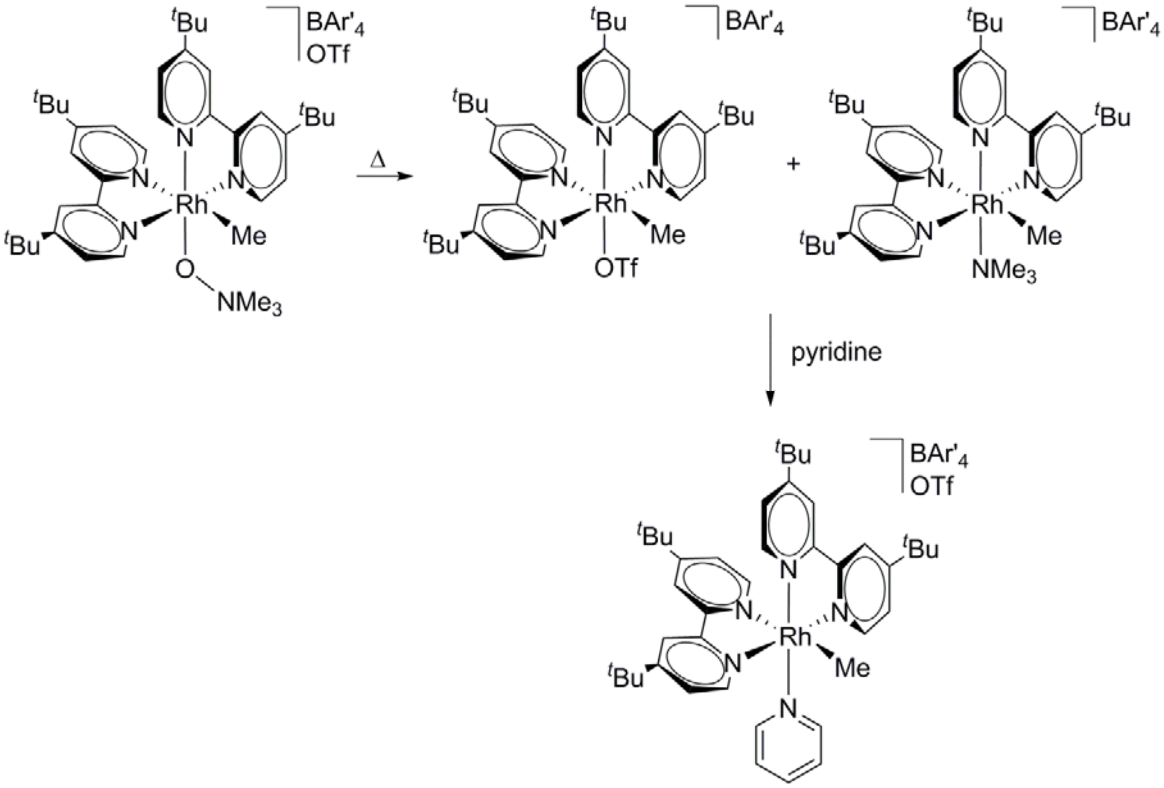

Scheme 1.38. Reactivity of [(^{t}bpy)$_2$Rh(Me)(ONMe$_3$)][BAr'$_4$][OTf] at 160 °C.

Thermolysis of [(^{t}bpy)$_2$Rh(Me)(PyO)][BAr'$_4$][OTf] in 1,2-dicholorobenzene results in decomposition of the PyO ligand after 48 hours to form the dicationic coordinated pyridine complex [(^{t}bpy)$_2$Rh(Me)(Py)][BAr'$_4$][OTf]. Photolysis of [(^{t}bpy)$_2$Rh(Me)(PyO)][BAr'$_4$][OTf] and [(^{t}bpy)$_2$Rh(Me)(PyO)][BAr'$_4$][OTf] in CDCl$_3$ and CD$_2$Cl$_2$ resulted in clean conversion to [(^{t}bpy)$_2$Rh(Me)(Cl)][BAr'$_4$], which was probably from the reaction of the starting materials with the solvents (Scheme 1.39).[103] Decomposition resulted when photolysis of the starting materials in some other solvents such as DMSO-d_6.

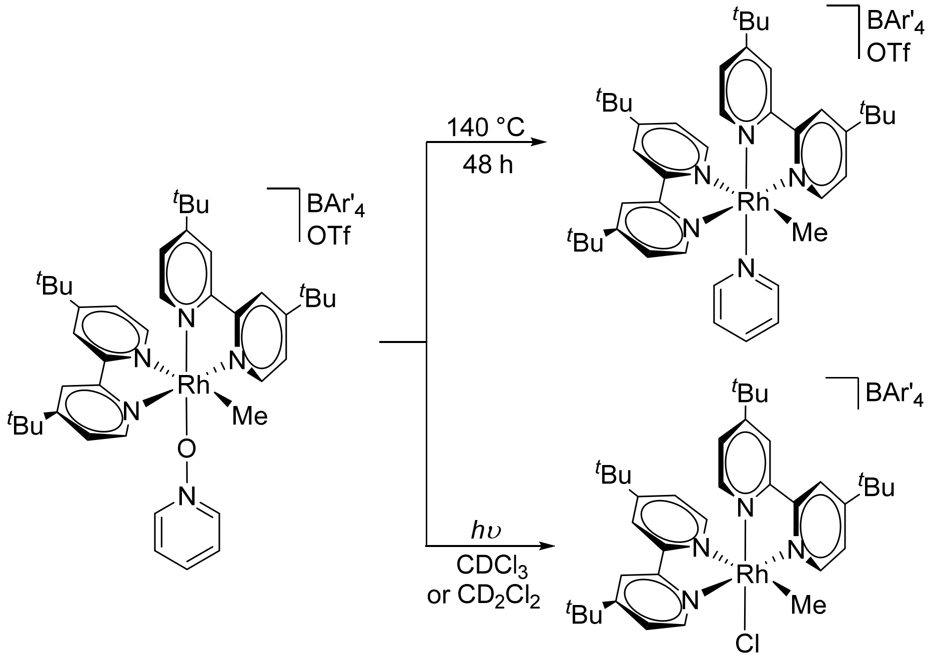

Scheme 1.39. Reactivity of [(^{t}bpy)$_2$Rh(Me)(PyO)][BAr'$_4$][OTf] under thermolysis and photolysis.

To sum, the attempt of O-atom insertion into Pt^{II} and Rh^{III}–C bonds resulted in no success. As discussed above, "which plays a more important role, the *nucleophilicity of the M–C$^{\delta}$ bond or the electrophilicity of the bound O$^{\delta+}$?* However, given the no O-atom insertion reaction for the Pt^{II} and Rh^{III}–R complexes with various oxidants, it more likely that *the nucleophilicity of the M–C$^{\delta-}$ bond plays a more important role than the electrophilicity of the bound O$^{\delta+}$ does* in the OMBV or R to M=O reactions, particularly if the attempt of O-atom insertion into early transition metals with generally more nucleophilic –R$^{\delta-}$ groups succeeds.

1.4. Summary and Directions

To our knowledge, C–H bond activation via 1,2-addition across M=O bond, a key step in pathway A, has never been reported. In contrast, C–H bond activation by 1,2-addition across a metal-alkoxide bond (M–OR) and net oxygen atom insertion into the M–R bond to form M–OR bond, both steps in pathway B, have been reported. Herein, we will focus on development of catalysts based on pathway B. However, only limited examples of C–O bond formation by a net oxygen atom insertion in the M–R bond have been reported and studied. Scheme 1.40 summarizes the O-atom insertion reactions into the transition M–R bonds including O-insertion into Group (IV) metal complex via radical pathway, migration of R to $Ta^{V}(\eta^2\text{-}O_2)$ in Group (V), migration of R to Re^{VII}-oxo and OMBV reaction of Re^{VII}–Me in group (VII), and O-atom insertion reactions for Ni^{II} and Pd^{II} in Group (X). However, in the O-atom insertion into Ta^{V}–R bond paper in 1988, Bercaw and co-workers stated, "The detail of the actual oxygen-transfer step in controlled metal-mediated oxidations are still poorly understood … examples of clean carbon-oxygen bond formation for well-characterized compounds are rarer still."[87] Despite a few new examples, we believe that this statement remains true over 20 years later.

An increased understanding of factors that control oxygen atom insertion to form C–O bond could make it possible to create a catalytic cycle that is capable of bridging CH activation by M–OR and C–O bond formation by net O-atom insertion. We have the following questions to answer: *Which plays a more important role, the nucleophilicity of the M–*$C^{\delta-}$ *bond or the electrophilicity of the bound* $O^{\delta+}$*? Can we extend the OMBV reaction to a series of M–R complexes with different electronic configurations and* *geometries and other oxidants? If more OMBV reaction are discovered, Is there any transition series between early transition metals with generally more nucleophilic –R*$^{\delta-}$ *groups and later transition metals with generally less nucleophilic –R group but more electrophilic O*$^{\delta+}$ *group that is likely to facilitate the O-atom insertion reaction?*

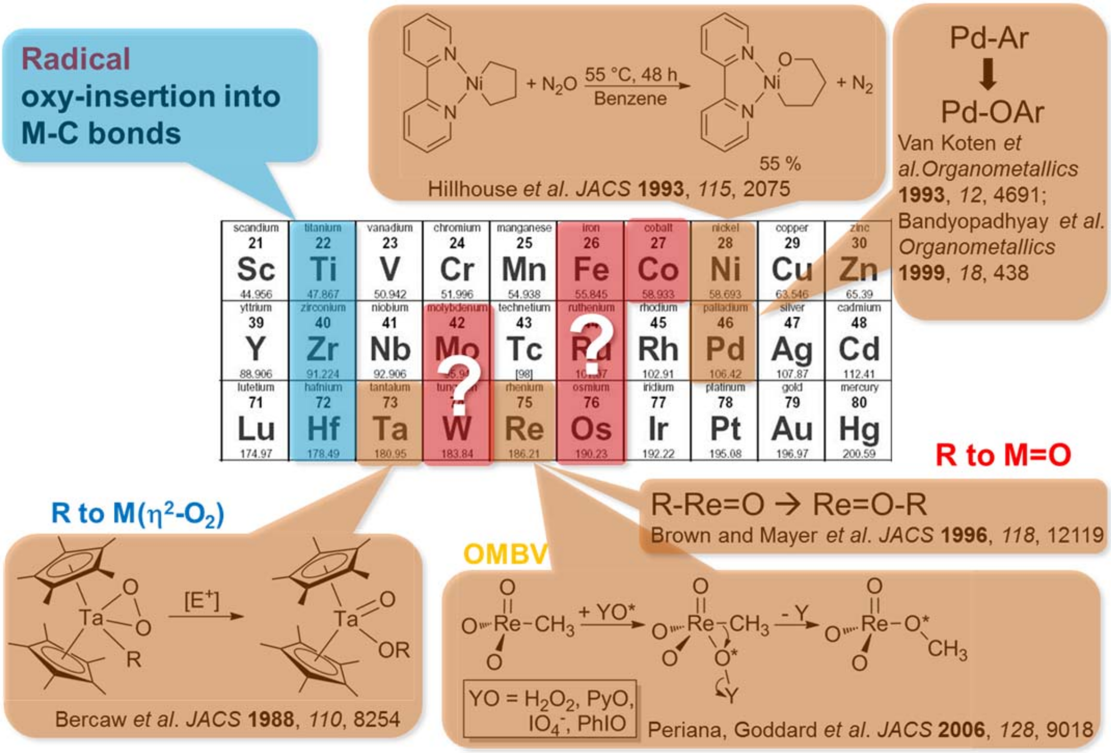

Scheme 1.40. Summary of the O-atom insertion reactions into transition M–R bonds.

With no success of the attempt of O-atom insertion into Pt^{II} and Rh^{III}–C bonds, we focused our studies on the early transition metals and 1st row late transition metals with generally more nucleophilic –R$^{\delta-}$ groups. Thus, one of our goals is to discover more O-atom insertion reactions into transition M–R bonds, especially W (between Ta and Re), Fe and Co–R complexes (1st row late transition metals). Moreover, to uncover the mechanisms of these O-atom insertion reactions and demonstrate the principles of the C–O bond formations via O-atom insertions; to provide direction for the development of catalyst for selective oxidation of hydrocarbons via combination of C–H activation/C–O bond formation. Herein, this thesis is focused on studies of new C–O bond reactions via O-atom insertion into transition M–R bonds including mechanism studies experimentally and computationally. Chapter Two is focused on the O-atom insertion into W–R bonds via variable pathways. Chapter Three is focused on the O-atom insertion into Fe^{II} complex. Chapter Four is focused on MeOH release from a Co^{I}–Me complex. Chapter Five summarizes these reactions and outlooks the future work of C–O bond formation via O-atom insertion into M–R bonds.

1.5 References

(1) Conley, B. L.; Tenn, W. J.; Young, K. J. H.; Ganesh, S.; Meier, S.; Ziatdinov, V.; Mironov, O.; Oxgaard, J.; Gonzales, J.; Goddard, W. A.; Periana, R. A. In *Activation of Small Molecules*; Wiley-VCH Verlag GmbH & Co. KGaA: 2006, p 235.

(2) Russia, China Add to $400 Billion Gas Deal With Accord http://www.bloomberg.com/news/2014-11-10/russia-china-add-to-400-billion-gas-deal-with-accord.html. In 2014.

(3) TransCanada, THe Alaska Pipeline Project http://www.transcanada.com/natural-gas-pipelines-projects.html. In 2012

(4) Olah, G. A.; Schlosberg, R. H. *J. Am. Chem. Soc.* **1968**, *90*, 2726.

(5) Olah, G. A.; Klopman, G.; Schlosberg, R. H. *J. Am. Chem. Soc.* **1969**, *91*, 3261.

(6) Olah, G. A.; Halpern, Y.; Shen, J.; Mo, Y. K. *J. Am. Chem. Soc.* **1971**, *93*, 1251.

(7) George A. Olah, A. M. *Hydrocarbon Chemistry*; 2nd ed.; John Wiley & Sons, 2003.

(8) Cost of delayed Chevron Nigeria plant now $8.4 bln. in Reuters news, 2011

(9) Shilov, A. E.; Shul'pin, G. B. *Chem. Rev.* **1997**, *97*, 2879.

(10) Periana, R. A.; Taube, D. J.; Evitt, E. R.; Löffler, D. G.; Wentrcek, P. R.; Voss, G.; Masuda, T. *Science* **1993**, *259*, 340.

(11) Periana, R. A.; Taube, D. J.; Gamble, S.; Taube, H.; Satoh, T.; Fujii, H. *Science* **1998**, *280*, 560.

(12) Lin, M.; Hogan, T. E.; Sen, A. *J. Am. Chem. Soc.* **1996**, *118*, 4574.

(13) Lin, M.; Hogan, T.; Sen, A. *J. Am. Chem. Soc.* **1997**, *119*, 6048.

(14) Jones, C. J.; Taube, D.; Ziatdinov, V. R.; Periana, R. A.; Nielsen, R. J.; Oxgaard, J.; Goddard, W. A. *Angew. Chem. Int. Ed.* **2004**, *43*, 4626.

(15) Muehlhofer, M.; Strassner, T.; Herrmann, W. A. *Angew. Chem. Int. Ed.* **2002**, *41*, 1745.

(16) Conley, B. L.; Tenn Iii, W. J.; Young, K. J. H.; Ganesh, S. K.; Meier, S. K.; Ziatdinov, V. R.; Mironov, O.; Oxgaard, J.; Gonzales, J.; Goddard III, W. A.; Periana, R. A. *J. Mol. Catal. A: Chem.* **2006**, *251*, 8.

(17) Stahl, S. S.; Labinger, J. A.; Bercaw, J. E. *Angew. Chem. Int. Ed.* **1998**, *37*, 2180.

(18) Forlani, O.; Rossini, S. *Mater. Chem. Phys.* **1992**, *31*, 155.

(19) Maitra, A. M. *Applied Catalysis A: General* **1993**, *104*, 11.

(20) Krylov, O. V. *Catal. Today* **1993**, *18*, 209.

(21) Raja, R.; Ratnasamy, P. *Applied Catalysis A: General* **1997**, *158*, L7.

(22) Hammond, C.; Forde, M. M.; Ab Rahim, M. H.; Thetford, A.; He, Q.; Jenkins, R. L.; Dimitratos, N.; Lopez-Sanchez, J. A.; Dummer, N. F.; Murphy, D. M.; Carley, A. F.; Taylor, S. H.; Willock, D. J.; Stangland, E. E.; Kang, J.; Hagen, H.; Kiely, C. J.; Hutchings, G. J. *Angew. Chem. Int. Ed.* **2012**, *51*, 5129.

(23) Ushikubo, T. O., K; Umezawa, T; Kiyono, K; Sawaki, I. 1993; Vol. EP529853.

(24) Ushikubo, T. N., H; Koyasu, Y; Wajiki, S. 1994; Vol. Ep 608838.

(25) Glaeser, L. C. B., F. Jr.; Toft, M. A. 1989; Vol. US 4877764.

(26) Lyons, J. E. E., P. E., Jr.; Karmakar, S.; Shaikh. S. N. 1998.

(27) Michalakos, P. M.; Birkeland, K.; Kung, H. H. *J. Catal.* **1996**, *158*, 349.

(28) Mizuno, N.; Ishige, H.; Seki, Y.; Misono, M.; Suh, D.-J.; Han, W.; Kudo, T. *Chem. Commun.* **1997**, 1295.

(29) Bar-Nahum, I.; Khenkin, A. M.; Neumann, R. *J. Am. Chem. Soc.* **2004**, *126*, 10236.

(30) Palkovits, R.; Antonietti, M.; Kuhn, P.; Thomas, A.; Schüth, F. *Angew. Chem. Int. Ed.* **2009**, *48*, 6909.

(31) Ahlquist, M.; Nielsen, R. J.; Periana, R. A.; Goddard III, W. A. *J. Am. Chem. Soc.* **2009**, *131*, 17110.

(32) Hashiguchi, B. G.; Konnick, M. M.; Bischof, S. M.; Gustafson, S. J.; Devarajan, D.; Gunsalus, N.; Ess, D. H.; Periana, R. A. *Science* **2014**, *343*, 1232.

(33) Jonas, R. T.; Stack, T. D. P. *J. Am. Chem. Soc.* **1997**, *119*, 8566.

(34) Samuelsson, B.; Dahlen, S.; Lindgren, J.; Rouzer, C.; Serhan, C. *Science* **1987**, *237*, 1171.

(35) Mayer, J. M. *Acc. Chem. Res.* **1998**, *31*, 441.

(36) Feng, Y.; Gunnoe, T. B.; Grimes, T. V.; Cundari, T. R. *Organometallics* **2006**, *25*, 5456.

(37) Bryant, J. R.; Taves, J. E.; Mayer, J. M. *Inorg. Chem.* **2002**, *41*, 2769.

(38) Larsen, A. S.; Wang, K.; Lockwood, M. A.; Rice, G. L.; Won, T.-J.; Lovell, S.; Sadílek, M.; Tureček, F.; Mayer, J. M. *J. Am. Chem. Soc.* **2002**, *124*, 10112.

(39) Goldsmith, C. R.; Jonas, R. T.; Stack, T. D. P. *J. Am. Chem. Soc.* **2001**, *124*, 83.

(40) Que, L.; Ho, R. Y. N. *Chem. Rev.* **1996**, *96*, 2607.

(41) Chen, M. S.; White, M. C. *Science* **2007**, *318*, 783.

(42) Northcutt, T. O.; Wick, D. D.; Vetter, A. J.; Jones, W. D. *J. Am. Chem. Soc.* **2001**, *123*, 7257.

(43) Feng, Y.; Lail, M.; Foley, N. A.; Gunnoe, T. B.; Barakat, K. A.; Cundari, T. R.; Petersen, J. L. *J. Am. Chem. Soc.* **2006**, *128*, 7982.

(44) Walsh, P. J.; Hollander, F. J.; Bergman, R. G. *J. Am. Chem. Soc.* **1988**, *110*, 8729.

(45) Hoyt, H. M.; Michael, F. E.; Bergman, R. G. *J. Am. Chem. Soc.* **2004**, *126*, 1018.

(46) Cummins, C. C.; Baxter, S. M.; Wolczanski, P. T. *J. Am. Chem. Soc.* **1988**, *110*, 8731.

(47) Schaller, C. P.; Wolczanski, P. T. *Inorg. Chem.* **1993**, *32*, 131.

(48) Bennett, J. L.; Wolczanski, P. T. *J. Am. Chem. Soc.* **1994**, *116*, 2179.

(49) Schaller, C. P.; Bonanno, J. B.; Wolczanski, P. T. *J. Am. Chem. Soc.* **1994**, *116*, 4133.

(50) Schaller, C. P.; Cummins, C. C.; Wolczanski, P. T. *J. Am. Chem. Soc.* **1996**, *118*, 591.

(51) Bennett, J. L.; Wolczanski, P. T. *J. Am. Chem. Soc.* **1997**, *119*, 10696.

(52) Schafer, D. F.; Wolczanski, P. T. *J. Am. Chem. Soc.* **1998**, *120*, 4881.

(53) Slaughter, L. M.; Wolczanski, P. T.; Klinckman, T. R.; Cundari, T. R. *J. Am. Chem. Soc.* **2000**, *122*, 7953.

(54) Cundari, T. R.; Klinckman, T. R.; Wolczanski, P. T. *J. Am. Chem. Soc.* **2002**, *124*, 1481.

(55) de With, J.; Horton, A. D. *Angew. Chem. Int. Ed. Engl.* **1993**, *32*, 903.

(56) Webb, J. R.; Bolaño, T.; Gunnoe, T. B. *ChemSusChem* **2011**, *4*, 37.

(57) Conley, B. L.; Ganesh, S. K.; Gonzales, J. M.; Tenn, W. J.; Young, K. J. H.; Oxgaard, J.; Goddard, W. A.; Periana, R. A. *J. Am. Chem. Soc.* **2006**, *128*, 9018.

(58) Feng, Y.; Lail, M.; Barakat, K. A.; Cundari, T. R.; Gunnoe, T. B.; Petersen, J. L. *J. Am. Chem. Soc.* **2005**, *127*, 14174.

(59) Cundari, T. R.; Grimes, T. V.; Gunnoe, T. B. *J. Am. Chem. Soc.* **2007**, *129*, 13172.

(60) Tenn, W. J.; Young, K. J. H.; Bhalla, G.; Oxgaard, J.; Goddard, W. A.; Periana, R. A. *J. Am. Chem. Soc.* **2005**, *127*, 14172.

(61) Kloek, S. M.; Heinekey, D. M.; Goldberg, K. I. *Angew. Chem. Int. Ed.* **2007**, *46*, 4736.

(62) Bercaw, J. E.; Hazari, N.; Labinger, J. A. *Organometallics* **2009**, *28*, 5489.

(63) Brown, S. N.; Mayer, J. M. *J. Am. Chem. Soc.* **1994**, *116*, 2219.

(64) Brown, S. N.; Mayer, J. M. *J. Am. Chem. Soc.* **1996**, *118*, 12119.

(65) Bischof, S. M.; Cheng, M.-J.; Nielsen, R. J.; Gunnoe, T. B.; Goddard, W. A.; Periana, R. A. *Organometallics* **2011**, *30*, 2079.

(66) Conner, D.; Jayaprakash, K. N.; Gunnoe, T. B.; Boyle, P. D. *Inorg. Chem.* **2002**, *41*, 3042.

(67) Conner, D.; Jayaprakash, K. N.; Wells, M. B.; Manzer, S.; Gunnoe, T. B.; Boyle, P. D. *Inorg. Chem.* **2003**, *42*, 4759.

(68) Tenn, W. J.; Young, K. J. H.; Oxgaard, J.; Nielsen, R. J.; Goddard, W. A.; Periana, R. A. *Organometallics* **2006**, *25*, 5173.

(69) Oxgaard, J.; Tenn, W. J.; Nielsen, R. J.; Periana, R. A.; Goddard, W. A. *Organometallics* **2007**, *26*, 1565.

(70) Hanson, S. K.; Heinekey, D. M.; Goldberg, K. I. *Organometallics* **2008**, *27*, 1454.

(71) Williams, T. J.; Caffyn, A. J. M.; Hazari, N.; Oblad, P. F.; Labinger, J. A.; Bercaw, J. E. *J. Am. Chem. Soc.* **2008**, *130*, 2418.

(72) Bercaw, J. E.; Hazari, N.; Labinger, J. A.; Oblad, P. F. *Angew. Chem. Int. Ed.* **2008**, *47*, 9941.

(73) Blackburn, T. F.; Labinger, J. A.; Schwartz, J. *Tetrahedron Lett.* **1975**, *16*, 3041.

(74) Brindley, P. B.; Scotton, M. J. *J. Chem. Soc., Perkin Trans. 2* **1981**, 419.

(75) Lubben, T. V.; Wolczanski, P. T. *J. Am. Chem. Soc.* **1987**, *109*, 424.

(76) Brindley, P. B.; Hodgson, J. C. *J. Organomet. Chem.* **1974**, *65*, 57.

(77) Walling, C.; Cioffari, A. *J. Am. Chem. Soc.* **1970**, *92*, 6609.

(78) Garst, J. F.; Smith, C. D.; Farrar, A. C. *J. Am. Chem. Soc.* **1972**, *94*, 7707.

(79) Panek, E. J.; Whitesides, G. M. *J. Am. Chem. Soc.* **1972**, *94*, 8768.

(80) Alexandrov, Y. A.; Lebedev, S. A.; Kuznetsova, N. V.; Razuvaev, G. A. *J. Organomet. Chem.* **1979**, *177*, 91.

(81) Ryan, D. A.; Espenson, J. H. *J. Am. Chem. Soc.* **1982**, *104*, 704.

(82) Arasasingham, R. D.; Balch, A. L.; Cornman, C. R.; Latos-Grazynski, L. *J. Am. Chem. Soc.* **1989**, *111*, 4357.

(83) Parkin, G.; Bercaw, J. E. *J. Am. Chem. Soc.* **1989**, *111*, 391.

(84) Atkinson, J. M.; Brindley, P. B. *J. Organomet. Chem.* **1991**, *411*, 139.

(85) Möller, M.; Husemann, M.; Boche, G. *J. Organomet. Chem.* **2001**, *624*, 47.

(86) Chen, T.; Zhang, X.-H.; Wang, C.; Chen, S.; Wu, Z.; Li, L.; Sorasaenee, K. R.; Diminnie, J. B.; Pan, H.; Guzei, I. A.; Rheingold, A. L.; Wu, Y.-D.; Xue, Z.-L. *Organometallics* **2005**, *24*, 1214.

(87) Van Asselt, A.; Trimmer, M. S.; Henling, L. M.; Bercaw, J. E. *J. Am. Chem. Soc.* **1988**, *110*, 8254.

(88) Hess, A.; Hörz, M. R.; Liable-Sands, L. M.; Lindner, D. C.; Rheingold, A. L.; Theopold, K. H. *Angew. Chem. Int. Ed.* **1999**, *38*, 166.

(89) Brown, S. N.; Mayer, J. M. *Organometallics* **1995**, *14*, 2951.

(90) Matsunaga, P. T.; Hillhouse, G. L.; Rheingold, A. L. *J. Am. Chem. Soc.* **1993**, *115*, 2075.

(91) Koo, K.; Hillhouse, G. L.; Rheingold, A. L. *Organometallics* **1995**, *14*, 456.

(92) Matsunaga, P. T.; Mavropoulos, J. C.; Hillhouse, G. L. *Polyhedron* **1995**, *14*, 175.

(93) Figg, T. M.; Cundari, T. R. *Organometallics* **2012**, *31*, 4998.

(94) Alsters, P. L.; Boersma, J.; van Koten, G. *Organometallics* **1993**, *12*, 1629.

(95) Alsters, P. L.; Teunissen, H. T.; Boersma, J.; Spek, A. L.; van Koten, G. *Organometallics* **1993**, *12*, 4691.

(96) Kamaraj, K.; Bandyopadhyay, D. *Organometallics* **1999**, *18*, 438.

(97) Wadhwani, P.; Bandyopadhyay, D. *Organometallics* **2000**, *19*, 4435.

(98) Abu-Omar, M. M.; Hansen, P. J.; Espenson, J. H. *J. Am. Chem. Soc.* **1996**, *118*, 4966.

(99) Smith, M. B.; J. March. March's Advanced Organic Chemistry, 6th ed.; John Wiley Sons, Inc.: Hoboken, NJ, 2007; p 1619.

(100) Figg, T. M.; Webb, J. R.; Cundari, T. R.; Gunnoe, T. B. J. *Am. Chem. Soc.* 2**011,** 1*34,* 2332.

(101) Pouy, M. J.; Milczek, E. M.; Figg, T. M.; Otten, B. M.; Prince, B. M.; Gunnoe, T. B.; Cundari, T. R.; Groves, J. T. J. *Am. Chem. Soc.* 2**012,** 1*34,* 12920.

(102) Webb, J. R.; Munro-Leighton, C.; Pierpont, A. W.; Gurkin, J. T.; Gunnoe, T. B.; Cundari, T. R.; Sabat, M.; Petersen, J. L.; Boyle, P. D. I*norg. Chem.* 2**011,** 5*0,* 4195.

(103) Webb, J. R.; Figg, T. M.; Otten, B. M.; Cundari, T. R.; Gunnoe, T. B.; Sabat, M. *Eur. J. Inorg. Chem.* 2**013,** 2*013,* 4515.

2 Variable Pathways for Oxygen Atom Insertion into Metal–Carbon Bonds: The Case of $Cp^*W(O)_2(CH_2SiMe_3)$

2.1 Rationale for Study of Oxygen Atom Insertion into W–C bonds

Hydrocarbon oxidation is a fundamentally important process for the petrochemical industry.[1-3] The development of new catalysts for the selective oxidation of hydrocarbons, especially alkanes, has the potential to enhance the efficiency of production of chemicals and fuels.[4-11] However, the selective functionalization (e.g., direct partial oxidation) of alkanes is among the most challenging catalytic processes.

As discussed in Chapter One, transition metal catalysts for the partial oxidation of alkanes to form alcohols must be able to perform two key steps: C–H bond activation and C–O bond formation. The Pt-based Shilov system, developed in 1960's, was among the first homogenous catalysts to successfully activate alkanes to form alcohols or alcohol precursors. It has been proposed that C–H bond activation occurs at Pt^{II} followed by C–X (X = OH or Cl) bond formation at Pt^{IV}–alkyl by reductive (i.e., reduction of Pt^{IV} to Pt^{II}) nucleophilic addition to an electrophilic Pt^{IV}–alkyl ligand.[12,13] The use of expensive Pt^{IV} as a stoichiometric oxidant to convert Pt^{II}–alkyl to Pt^{IV}–alkyl limits the utility of this catalyst (Scheme 2.1).[12-14]

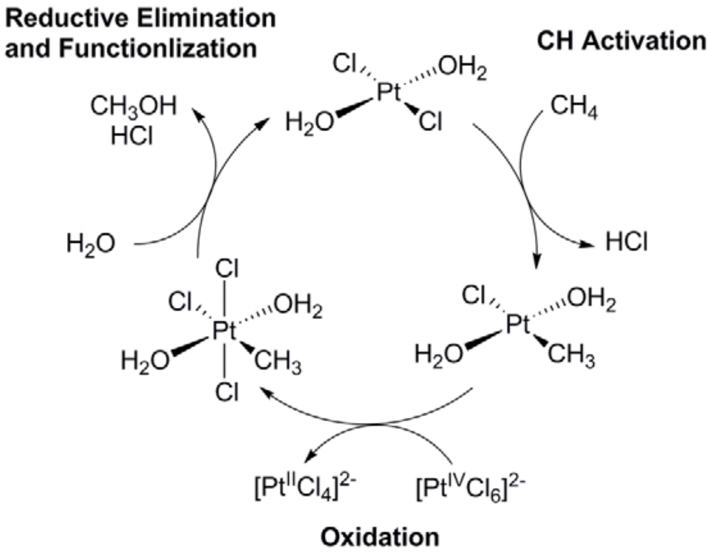

Scheme 2.1. Proposed catalytic cycle for methane functionalization by Shilov system.

While C–X (X = OH or Cl) bond formation in the Shilov-type catalysts has been proposed to involve nucleophilic addition of water or halide to an electrophilic Pt^{IV}–alkyl ligand,[12] an alternative strategy for metal-mediated C–O bond formation involves net oxygen atom insertion into metal–alkyl bonds. For example, one possible catalytic cycle incorporates oxygen atom insertion into a M–R bond followed by C–H activation via net 1,2-addition across a M–OR bond to convert alkane to alcohol.[10,15-18] Scheme 2.2 shows two distinct pathways for oxygen atom insertion into M–R bonds from the reaction of a M–R moiety with an oxygen atom delivery reagent (YO). One pathway involves a migration of the ligand R to a metal-oxo intermediate. The second pathway incorporates direct oxy-insertion from M(OY)(R) without the formation of a metal-oxo intermediate. To be generally useful for selective oxidations at high conversion, ideally, the C–O bond forming step should proceed without the formation of free radicals for high selectivity.

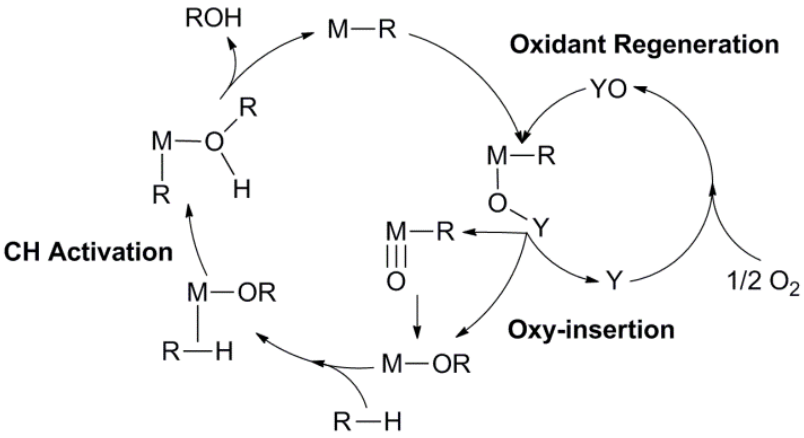

Scheme 2.2. Proposed pathways for partial oxidation of hydrocarbon involving oxygen atom insertion into a M–R bond and 1,2-CH-additon across a M–OR bond.

As introduced in Chapter One, the 1,2-addition of C–H bonds across M–NHR and M–OR bonds is known. In 2003, our group studied and reported intramolecular C–H activation by Tp–Ru^{II} (Tp = hydridotris(pyrazolyl)borate) amido complex and commented on the potential utility of this transformation in catalytic transformations.[19] Then, in 2005 we reported intermolecular benzene C–H activation by Ru^{II} hydroxide and anilide complexes.[17,20] Related chemistry includes an Ir^{III} complex and Ru^{II} complexes by Periana, Goddard *et al.*,[16,21] a Rh^{I} complex reported by Heinekey, Goldberg *et al.*,[22] and a Rh^{I} complex reported by Bercaw, Labinger *et al.*[23]

While insertions of oxygen atoms into M–C bonds are known, examples that occur by non-radical routes are rare. In a 1988 publication that focused on oxygen atom insertion into Ta(V) hydrocarbyl bonds (Scheme 2.3), Bercaw *et al.* stated, "The details of the actual oxygen-transfer step in controlled metal-mediated oxidations are still poorly understood … examples of clean carbon-oxygen bond formation for well-characterized compounds are rarer still."[24] Despite a few recent examples,[15,25-30] we believe that this statement remains accurate.

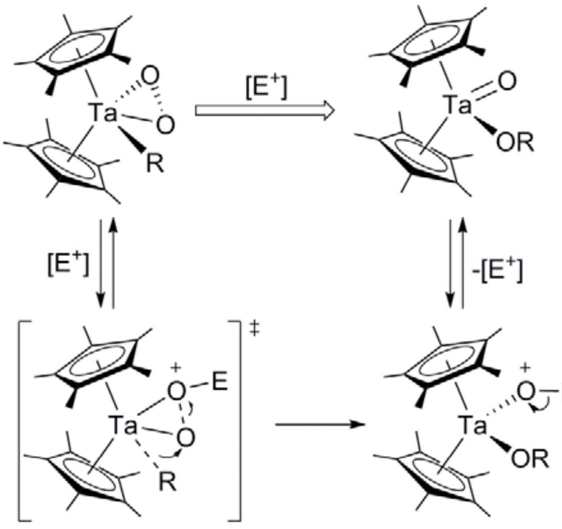

Scheme 2.3. Proposed mechanism for O-atom insertion into Ta–C bond catalyzed by electrophiles.

As discussed in Chapter One, some early transition metal complexes, such as Group IV complexes, initiate oxygen atom insertion into M–R bonds; however, these reactions commonly proceed by radical pathways.[31,32] Brown and Mayer reported oxy-insertion into M–Ar (Ar = aryl) bonds with Re^{VII} via the migration of the Ar group to an oxo ligand.[27,29] Two mechanisms were reported. They first reported the C–H activation by Re^{V} complex TpRe(O)(Cl)I under photolysis to form TpRe(O)(Cl)Ph, which was followed by a photolytic phenyl-to-oxo migration to produce the O-atom insertion product TpRe(OPh)(Cl)L (L = Py, MeCN, Me_3PO) in the presence of L. Then a similar migration of aryl ligand to Re^{VII}–oxo reaction was reported under thermal condition. Similar mechanisms that involve the formation of metal-oxo have also been proposed for the oxygen atom insertion of Pd complexes, but mechanistic studies have not been disclosed.[26,33] Hillhouse *et al.* have reported net oxygen insertion into a series of Ni^{II}–R bonds and a Hf–Ph bond upon reaction with N_2O.[28,34] Espenson *et al.* reported that methyltrioxorhenium (MTO) reacts with oxidants to release methanol.[35] Methanol was generated in both acidic and basic solution, and the rates are highly pH dependent. In aqueous solution, MTO reacts with H_2O_2 to produce the η^2-peroxo complex $ReO_2(\eta^2$-$O_2)Me$ (**A**) and $ReO(\eta^2$-$O_2)_2Me$ (**B**):H_2O (Scheme 2.4). The equilibrium constants for their formation are $k_1 = 16.1(2)$ L·mol^{-1} and $k_2 = 1.32(2) \times 10^2$ L·mol^{-1} at pH = 0, $\mu = 2.0$ M, and 25 °C. Slow decomposition of A and B(H_2O) generates MeOH. In contrast, MeOH release is facilitated in basic solution in two pathways (Scheme 2.4). Methanol is released by either the attack of hydroperoxide anion to MTO or the attack of hydroxide anion to complex **B**, with $k_A = 6.2(3) \times 10^9$ and $k_{MTO} = 4.1(2) \times 10^8$ L·mol^{-1}·s^{-1} at μ = 0.01 M and 25 °C.

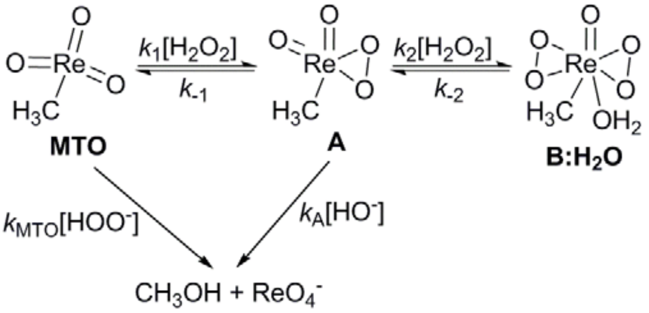

Scheme 2.4. The kinetics of the reaction of MTO and H_2O_2 to release MeOH in aqueous solution.

Periana, Goddard and co-workers extended the MTO reaction and reported facile conversion of Re–Me bond of MTO to a Re–OMe bond upon treatment of various oxidants (H_2O_2, PyO, PhIO and IO_4^-). They studied the mechanism of these reactions experimentally and computationally and pointed out that the O-atom insertion in MTO does not likely occur by the migration of the methyl ligand to the oxo ligand of MTO. For example, reaction of $Re^{16}O_3Me$ with ^{18}O labeled oxidant ($I^{18}O_4^-$) produced only $Me^{18}OH$. An organometallic Baeyer-Villiger (OMBV) pathway, which is similar to the classic Baeyer-Villiger organic reaction (Scheme 2.5), involving the migration of the methyl ligand to the coordinated O atom of the oxidants to the MTO was proposed (Scheme 2.6). This result demonstrates O-atom insertion into a M–R bond without formation of a metal–oxo species, which is often thermodynamically too stable for transition metal oxo complexes to have migration of R group to the oxo ligand. This organometallic version of the Baeyer-Villiger (BV) reaction demonstrated a new pathway to form C–O bonds.

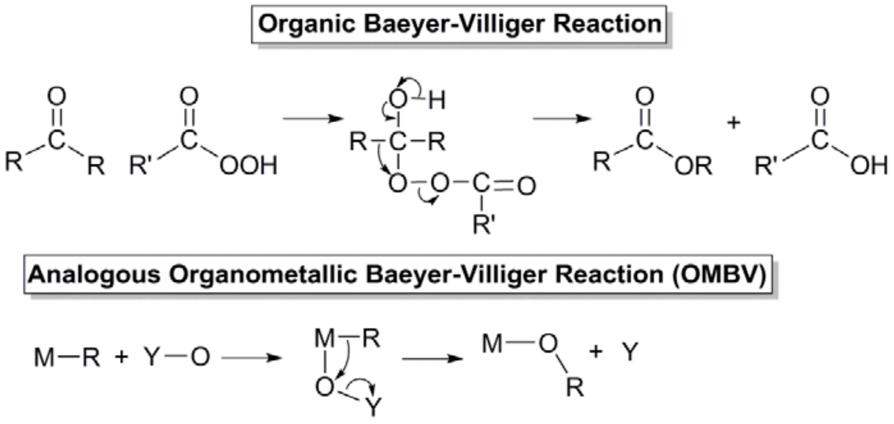

Scheme 2.5. Generic mechanisms for the organic Baeyer-Villiger reaction and the analogous organometallic Baeyer-Villiger reaction (OMBV).

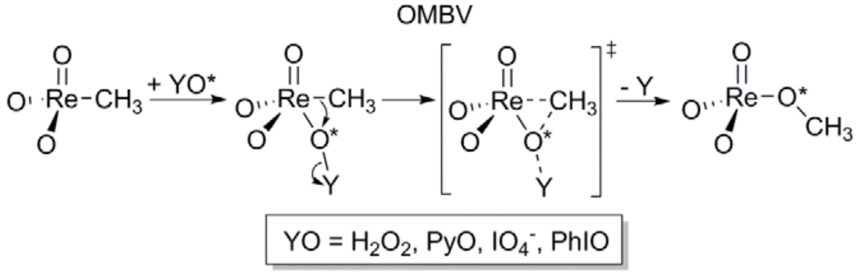

Scheme 2.6. Proposed mechanism for the O-atom insertion into MTO with various oxidants.

Two possible pathways for the O-atom insertion reaction of MTO and IO_4^- were studied computationally, the OMBV pathway and η^2-peroxo pathways. The η^2-peroxo pathway involves the formation of a η^2-peroxo complex as the intermediate. Calculations show a much lower energy barrier for the OMBV pathway (17 kcal/mol) than the η^2-peroxo pathway (25 kcal/mol) (Scheme 2.7). The 17 kcal/mol activation barrier is remarkably low for a M–R to M–OR transformation and is consistent with the observed facile O-atom insertion reaction of MTO and IO_4^- at room temperature. Similar O-atom insertion reaction was observed with $ArReO_3$ (Ar = mesityl) with oxidants. These OMBV reactions provide a totally new strategy for C–O bond formation from O-atom insertion into M–R bond.

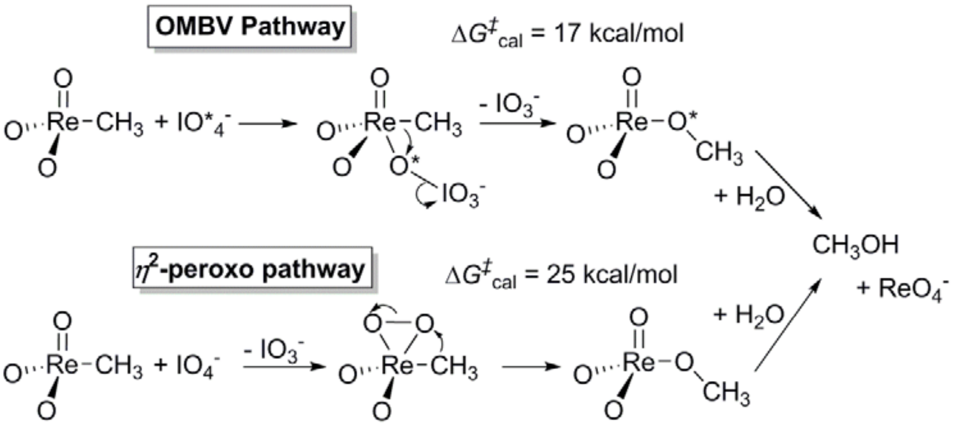

Scheme 2.7. Two possible pathways for the reaction of MTO with IO_4^- to produce MeOH.

Given the importance of metal-mediated C–O bond formation, we have been interested in understanding mechanisms and strategies to facilitate these transformations. However, to our knowledge, detailed studies of reactions that give clean oxygen atom insertion into metal-hydrocarbyl bonds are limited to the studies of Re^{VII} complexes.[15,27,29,35,36]

As discussed above, metal–alkyls that are M–$C^{\delta+}$ polarized likely undergo reductive functionalization with X^- nucleophilies, but M–$C^{\delta-}$ polarized systems do not. Metal–alkyls that are M–$C^{\delta-}$ polarized likely undergo migration of $R^{\delta-}$ to the electrophilic M–$O^{\delta+}$–Y in OMBV reactions. Late 2nd row or 3rd row transition metals are more likely to generate a nucleophilic $R^{\delta+}$ but also more nucleophilic $O^{\delta+}$. It is unclear whether the nucleophilicity of the $M–C^{\delta-}$ bond or the electrophilicity of the bound $O^{\delta+}$ plays a more important role. For the OMBV reaction, can it be extended to a range oxidants and M–R complexes with other geometries and electronic configurations? One of our goals is to discover more OMBV type O-atom insertion reactions and demonstrate the relative importance of the two factors discussed above.

With no success of the attempt to extended the OMBV reaction to the late transition Ru^{III}– and Pt^{II}–R complexes,[18] We sought to focus our search on the middle transition metal–alkyl that are more $M–C^{\delta-}$ polarized for the OMBV type O-atom insertion reactions. Herein, this chapter will present our studies of extension of the OMBV reaction to the W complexes. We initiated the O-atom insertion into W–C bond by noticing that complex $Cp^*W(O)_2(CH_2SiMe_3)$ (**2.1**) reacted with H_2O_2 to produce $Cp^*W(O)(\eta^2\text{-}O_2)(CH_2SiMe_3)$ (**2.2**), which is similar to the reaction of $MeReO_3$ with H_2O_2 to produce $MeRe(\eta^2\text{-}O_2)O_2$ (Scheme 2.4). Analogously, will complex **2.2** react with OH^- to produce $SiMe_3CH_2OH$ just like $MeRe(\eta^2\text{-}O_2)O_2$ reacts with OH^- to give MeOH? Will complex **2.1** react with oxidant (i.e. IO_4^- and H_2O_2) to generate $SiMe_3CH_2OH$ like MTO reacts with oxidants to release MeOH? If yes, will these alcohol produced reaction proceed through the OMBV type pathway? We will answer all these questions in this chapter. Herein, we present studies of oxygen atom insertion into the W–CH_2SiMe_3 bond of $Cp^*W(O)_2(CH_2SiMe_3)$ (**2.1**) and $Cp^*W(O)(\eta^2\text{-}O_2)(CH_2SiMe_3)$ (**2.2**). Complex **2.1** and **2.2** have been previously prepared and studied by Legzdins *et al.*[36] The major contents of this chapter are from our research article published in *J. Am. Chem. Soc.*[37] Kurtis M. Carsch, Cody Freitag and Professor Thomas Cundari are from University of North Texas and did the computational study in this chapter.

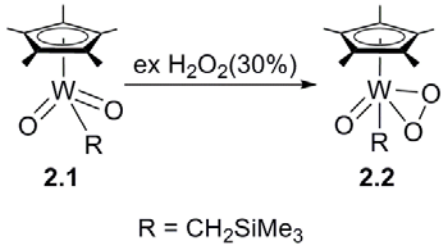

Scheme 2.8. $Cp^*W(O)_2(CH_2SiMe_3)$ (**2.1**) reacts with H_2O_2 (30%) to generate $Cp^*W(O)(\eta^2\text{-}O_2)(CH_2SiMe_3)$ (**2.2**).

2.2 Results and Discussion

2.2.1 Reaction of $Cp^*W(O)_2(CH_2SiMe_3)$ (2.1) with $NaIO_4$.

The reaction of $Cp^*W(O)_2(CH_2SiMe_3)$ (**2.1**) with H_2O_2 has been reported to yield the η^2-peroxo complex $Cp^*W(O)(\eta^2\text{-}O_2)(CH_2SiMe_3)$ (**2.2**);[36] however, the reaction of **2.1** with 1 equivalent of $NaIO_4$ in 1:1 THF-d_8:D_2O or 1:1 1,4-dioxane-d_8:D_2O (v:v) does not produce complex **2.2**. Rather, $TMSCH_2OH$ (TMS = $SiMe_3$, trimethylsilyl) is formed without observation of **2.2** as an intermediate. The reaction is complete within two hours at room temperature and produces $TMSCH_2OH$ in almost 100% yield by ^1H NMR spectroscopy (eq 2.1).

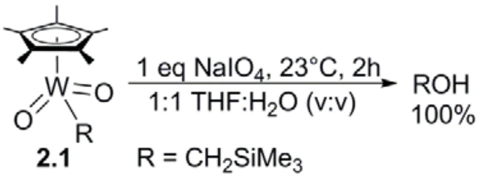

(2.1)

To determine the pathway for the conversion of **2.1** and $NaIO_4$ to $TMSCH_2OH$, we first considered the possibility that the η^2-peroxo complex $Cp^*W(O)(\eta^2\text{-}O_2)(CH_2SiMe_3)$ (**2.2**) is formed as an intermediate, followed by oxy-insertion into the W–

C bond and subsequent protonolysis to give free TMSCH$_2$OH. Complex **2.2** was prepared and then reacted with NaIO$_4$ under the same conditions as the alcohol release from **2.1** and NaIO$_4$, and no alcohol was observed by ^{1}H NMR spectroscopy (Scheme 2.9). Furthermore, **2.2** does not react with NaIO$_3$ or D$_2$O to produce TMSCH$_2$OH under the same conditions. Thus, the evidence suggests that the formation of TMSCH$_2$OH from **2.1** and NaIO$_4$ does not likely proceed via complex **2.2**.

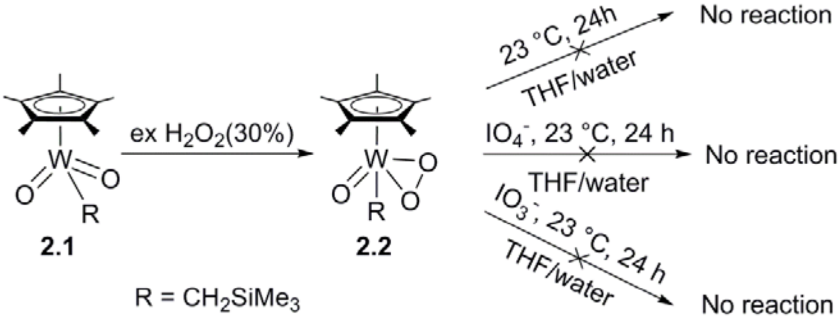

Scheme 2.9. Reactions of Cp*W(O)(η^2-O$_2$)(CH$_2$SiMe$_3$) (**2.2**) with oxidants or water do not result in O-atom insertion into W–R bond.

The reaction of **2.1** and NaIO$_4$ (5 equiv) in 1:1 THF-d_8:D$_2$O (v:v) was monitored at –1.3 °C in by ^{1}H NMR spectroscopy. During the conversion, the disappearance of **2.1**, the emergence of an intermediate and the appearance of TMSCH$_2$OH were observed at –1.3 °C, the formation of TMSCH$_2$OH occurs in approximately 100% yield with $t_{1/2}$ ~40 min. On the basis of ^{1}H NMR spectroscopy, the intermediate is proposed to be the tungsten alkoxide complex Cp*W(O)$_2$(OCH$_2$SiMe$_3$) (**2.3**); but, we were not able to isolate **2.3** even at low temperature that the solvent is almost frozen. Complex **2.3** was protonated to produce TMSCH$_2$OH immediately. The ^{1}H NMR resonances of the intermediate **2.3** are assigned as 4.17 (CH$_2$, s), 2.04 (CH$_3$, s), –0.05 (SiMe$_3$, s) ppm (Figure 2.1). We sought examples of M–OR singlet to complex **2.3** in order to compare chemical shifts in ^{1}H NMR. Mo(O)$_2$(OEt)$_2$ exhibits a resonance due to the OCH_2Me at

4.65 ppm,[38] and the similar complex (bpy)Mo(O)$_2$(OEt)$_2$ (bpy = 2,2'-bipyridine) exhibits a methylene resonance at 3.86 ppm.[39] These two M–OR shifts are close to the singlet of of the CH$_2$ group of intermediate **2.3**, which sopports **2.3** was proposed as a M–OR complex. In contrast, the CH$_2$ group of **2.1** and **2.2** resonate at 0.43 ppm and 3.16 ppm, respectively. In addition to NaIO$_4$, complex **2.1** reacts with iodosobenzene (PhI=O) in 1,4-dioxane at room temperature to produce **2.3** in ~20% yield in 20 min by ^{1}H NMR spectroscopy (eq 2.2); however, at prolonged reaction times an intractable mixture of products is formed.

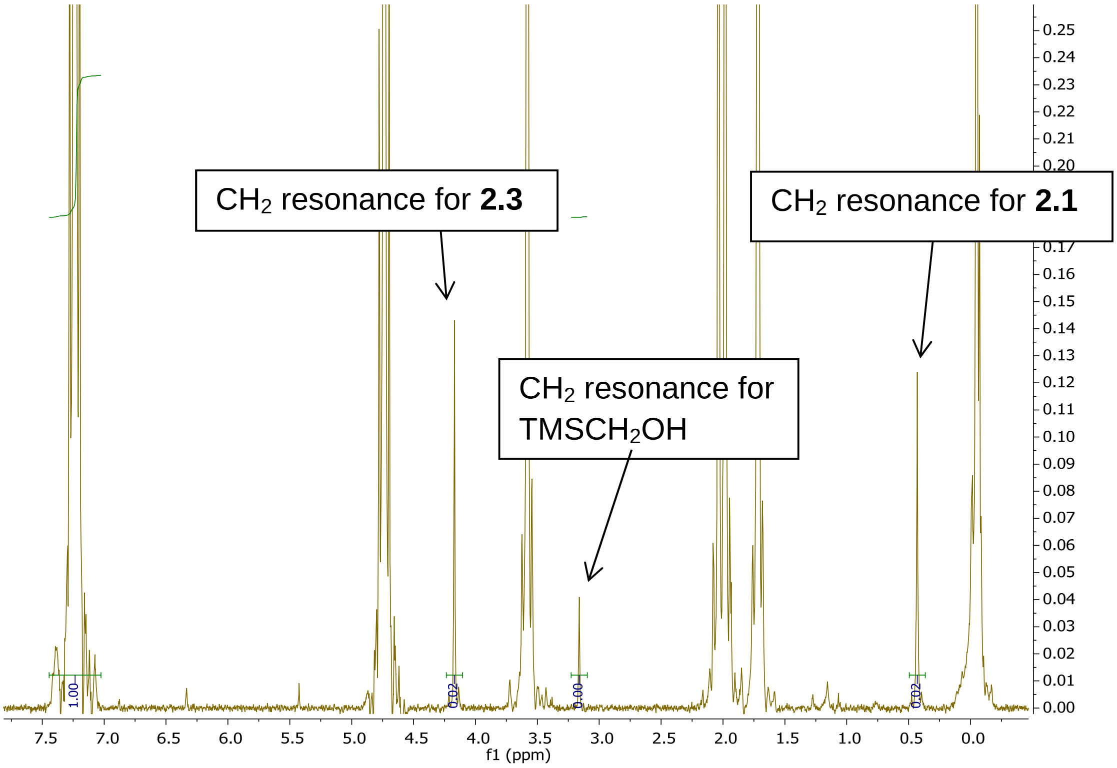

Figure 2.1. A sample of ^{1}H NMR spectrum for the reaction of Cp*W(O)$_2$(CH$_2$SiMe$_3$) (**2.1**) and NaIO$_4$ (5 equiv) in 1:1 THF-d_8:D$_2$O (v:v) at –1.3 °C. Resonance of the intermediate Cp*W(O)$_2$(OCH$_2$SiMe$_3$) (**2.3**) are assigned as 4.17 (CH$_2$, s), 2.04 (CH$_3$, s), –0.05 (SiMe$_3$, s) ppm. The CH$_2$ group of **2.1** and TMSCH$_2$OH resonate at 0.43 ppm and 3.16 ppm, respectively.

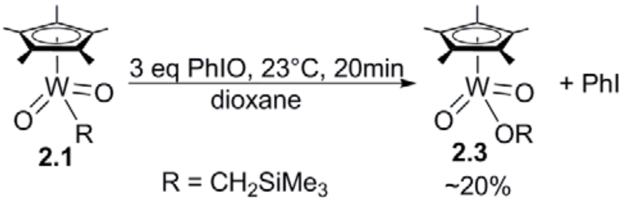

(2.2)

Figure 2.2 depicts the concentration versus time plot for all species observed in the conversion of **2.1** and $NaIO_4$ to $TMSCH_2OH$, based on the integrations of the methylene resonances of **2.1**, the $TMSCH_2OH$ product, and complex **2.3**. The sum of concentrations of these three species (purple crosses, Figure 2.2) remains constant over the course of the reaction.

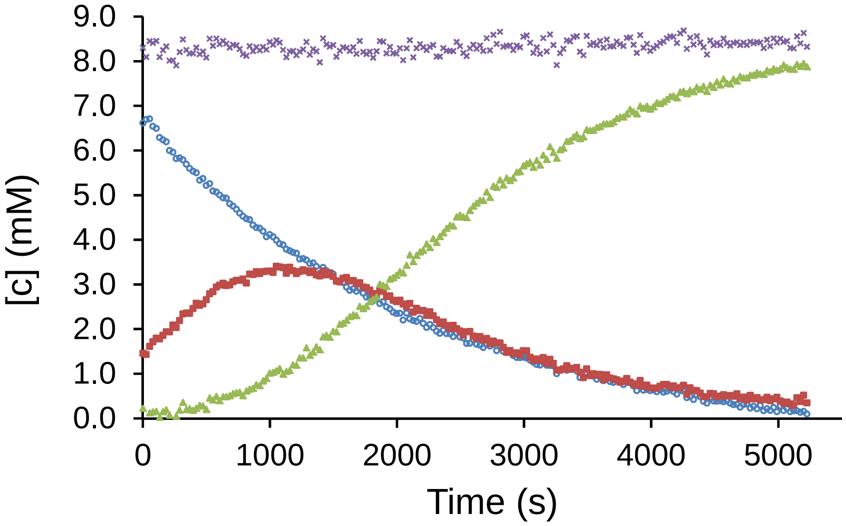

Figure 2.2. Plot of concentration versus time for all species observed during the conversion of $Cp^*W(O)_2(CH_2SiMe_3)$ (**2.1**) and $NaIO_4$ to $TMSCH_2OH$ including complex **2.1** (blue, circles), $Cp^*W(O)_2(OCH_2SiMe_3)$ (**2.3**) (brown, squares), $TMSCH_2OH$ (green, triangles) and the sum of all three species (purple, crosses). Data are from one experiment and were acquired at –1.3 °C in 1:1 THF-d_8:D_2O (v:v) with $NaIO_4$ (5 equiv). Multiple experiments result in similar plots.

Scheme 2.10 depicts a proposed organometallic Baeyer-Villiger (OMBV) pathway for the formation of $TMSCH_2OH$ from the reaction of **2.1** with $NaIO_4$. Periodate coordinates to complex **2.1**, followed by concerted migration of the alkyl ligand to the coordinated oxygen atom of IO_4^- and loss of IO_3^-. Protonation of complex **2.3** generates the alcohol product. Assuming that the oxygen atoms of coordinated IO_4^- do not exchange with the oxo ligands of the putative adduct $[Cp^*W(O)_2(OIO_3)(R)]^-$, in the proposed pathway the oxygen atom in the $TMSCH_2OH$ product should be derived from the oxygen donor (*i.e.*, IO_4^-) and not from the oxo ligand of complex **2.1**. As a result, most of the alcohol product should be $TMSCH_2{}^{18}OH$ (MW = 106) other than $TMSCH_2{}^{16}OH$ (MW = 104). Figures 2.4 shows the GC/MS analysis of the reaction of $Cp^*W({}^{16}O)_2(CH_2SiMe_3)$ with $NaI^{18}O_4$ and only $TMSCH_2{}^{18}OH$ is formed (compare to the analysis of the reaction of $Cp^*W({}^{16}O)_2(CH_2SiMe_3)$ with $NaI^{16}O_4$ and only $TMSCH_2{}^{16}OH$ is formed in Figure 2.3), which is consistent with the proposed OMBV pathway.

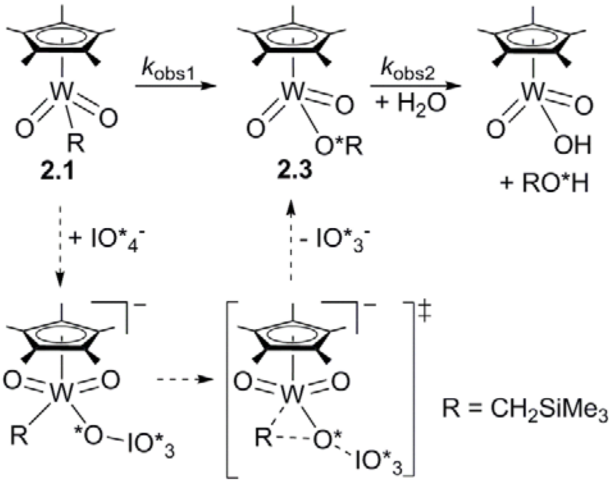

Scheme 2.10. Proposed mechanism for the formation of $TMSCH_2OH$ from the reaction of $Cp^*W(O)_2(CH_2SiMe_3)$ (**2.1**) and $NaIO_4$ in 1:1 THF-d_8:D_2O (v:v).

$$Cp^*W(O)_2(CH_2TMS) + NaIO_4 \rightarrow TMSCH_2OH$$

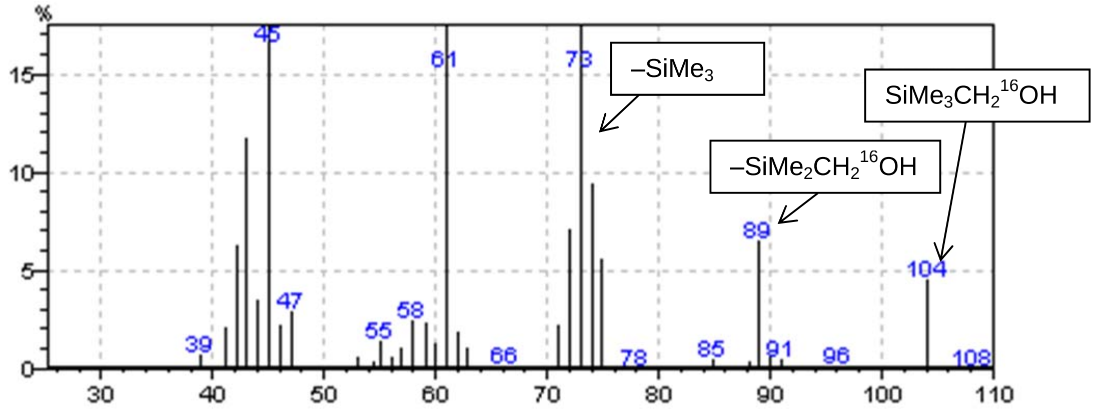

Figure 2.3. MS data for the $TMSCH_2OH$ product of the reaction of $Cp^*W(^{16}O)_2(CH_2TMS)$ (**2.1**) and $NaIO_4$.

$$Cp^*W(O)_2(CH_2TMS) + NaI^{18}O_4 \rightarrow TMSCH_2{}^{18}OH$$

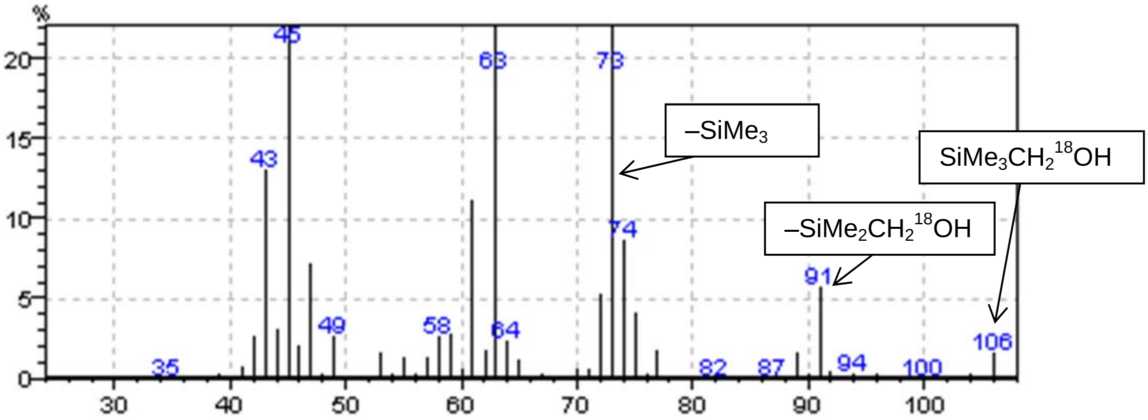

Figure 2.4. MS spectrum for the product of reaction of $Cp^*W(^{16}O)_2(CH_2SiMe_3)$ (**2.1**) with $NaI^{18}O_4$ in THF.

Using kinetic simulation (Kinetica98 software;[40] see Experimental Section), The conversion of **2.1** and $NaIO_4$ to **2.3** and the transformation of **2.3** to **2.4** were kinetically simulated. The procedure and Sample Kinetics Simulation for the reaction of $Cp^*W(O)_2(CH_2SiMe_3)$ (**2.1**) with 5 equivalent of $NaIO_4$ in 1:1 THF-d_8:D_2O (v:v) at –1.3 °C is shown below.

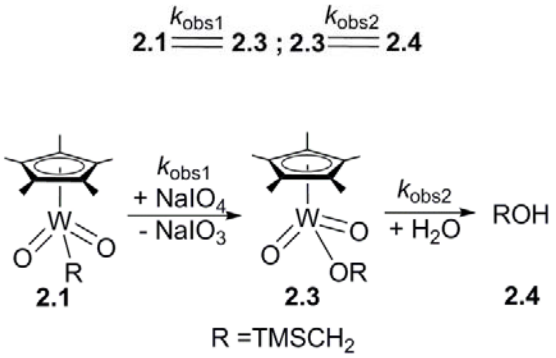

Scheme 2.11. Reactions monitored in the kinetic simulation.

The mechanism in Scheme 2.11 was simulated. The results of one sample experimental data sets and kinetic simulations are given below.

Table 2.1. Observed and fitted data for the conversion of Cp*W(O)$_2$(CH$_2$SiMe$_3$) (**2.1**) with 5 equivalent of NaIO$_4$ to Me$_3$SiCH$_2$OH (**2.4**).

Time (s)	**2.1 (obs)**	**2.1 (cal)**	**2.3 (obs)**	**2.3 (cal)**	**2.4 (obs)**	**2.4 (cal)**
0	1.0000	1.0000	0.0000	1.20E-31	0.0000	1.20E-31
240	0.8026	0.8153	0.1773	0.1635	0.0201	0.0212
480	0.6802	0.6647	0.2915	0.2618	0.0283	0.0734
720	0.5506	0.5419	0.3991	0.3146	0.0503	0.1435
960	0.4714	0.4418	0.4435	0.3359	0.0851	0.2222
1200	0.3967	0.3602	0.4489	0.3364	0.1544	0.3034
1440	0.3352	0.2937	0.4249	0.3234	0.2399	0.3830
1680	0.2631	0.2395	0.3663	0.3022	0.3706	0.4583
1920	0.2171	0.1952	0.2999	0.2768	0.4830	0.5280
2160	0.1859	0.1592	0.2238	0.2495	0.5904	0.5913
2400	0.1517	0.1298	0.1688	0.2222	0.6795	0.6480
2640	0.1253	0.1058	0.1294	0.1959	0.7454	0.6983
2880	0.1059	0.0863	0.0889	0.1713	0.8052	0.7424

3120	0.0902	0.0703	0.0796	0.1488	0.8302	0.7808
3360	0.0729	0.0573	0.0564	0.1285	0.8706	0.8142
3600	0.0674	0.0468	0.0419	0.1104	0.8907	0.8428
3840	0.0553	0.0381	0.0361	0.0945	0.9085	0.8674
4080	0.0436	0.0311	0.0286	0.0805	0.9279	0.8884
4320	0.0299	0.0253	0.0249	0.0684	0.9452	0.9063
4560	0.0274	0.0207	0.0202	0.0579	0.9524	0.9215
4800	0.0213	0.0168	0.0195	0.0489	0.9592	0.9343
5040	0.0260	0.0137	0.0163	0.0412	0.9577	0.9451
5280	0.0140	0.0112	0.0013	0.0346	0.9847	0.9542

The fitted rate constants are list below:

Fitted Rate Constants			
k_{obs1}=	8.51E-04	k_{obs2}=	1.00E-03
sd_1 =	1.00E-07	sd_2=	7.57E-08

Individual plots of all observed and fitted data for the conversion of $Cp^*W(O)_2(CH_2SiMe_3)$ (**2.1**) with 5 equivalent of $NaIO_4$ to Me_3SiCH_2OH (**2.4**) in THF-d_8 at 50 °C are listed below (Figure 2.5-2.7):

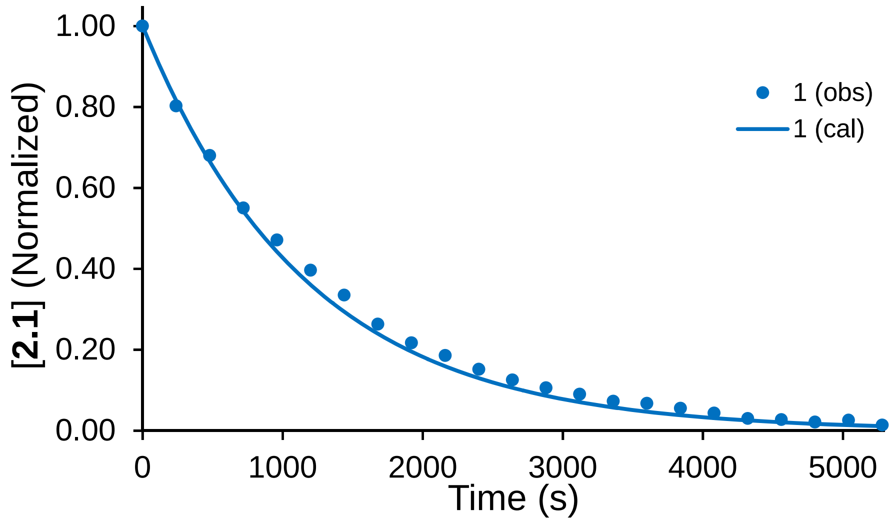

Figure 2.5. Plots of observed and fitted data for the decay of Cp*W(O)$_2$(CH$_2$SiMe$_3$) (**2.1**).

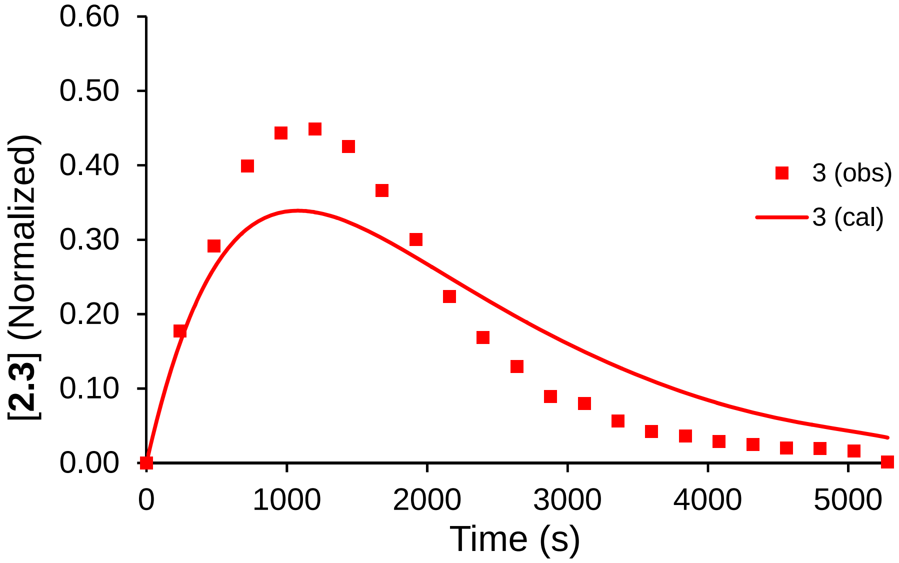

Figure 2.6. Plot of observed and fitted data for the concentration variation of Cp*W(O)$_2$(OCH$_2$SiMe$_3$) (**2.3**).

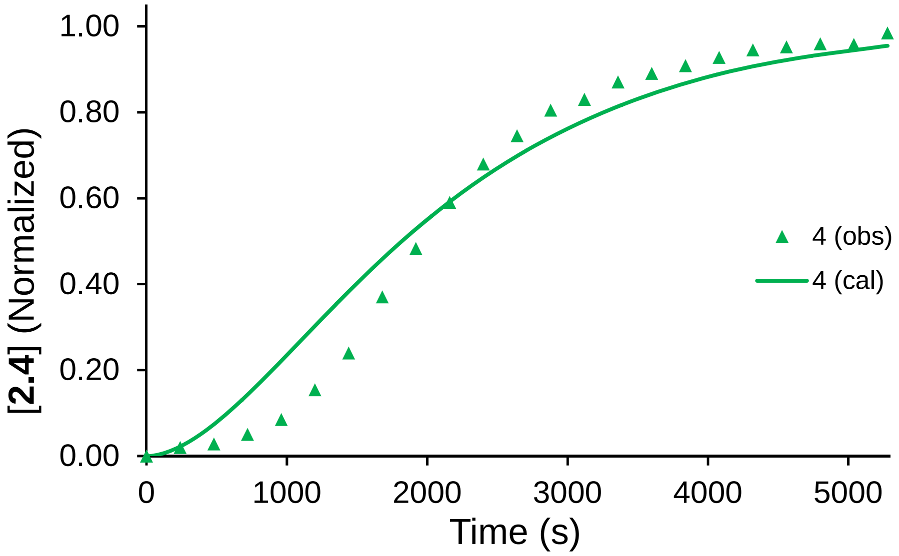

Figure 2.7. Plot of observed and fitted data for the growing of Me_3SiCH_2OH (**2.4**).

The individual plots are combined, and a fitted data plot for the conversion of **2.1** with 5 equivalent of $NaIO_4$ to Me_3SiCH_2OH in THF-d_8 at 50 °C is given below (Figure 2.8):

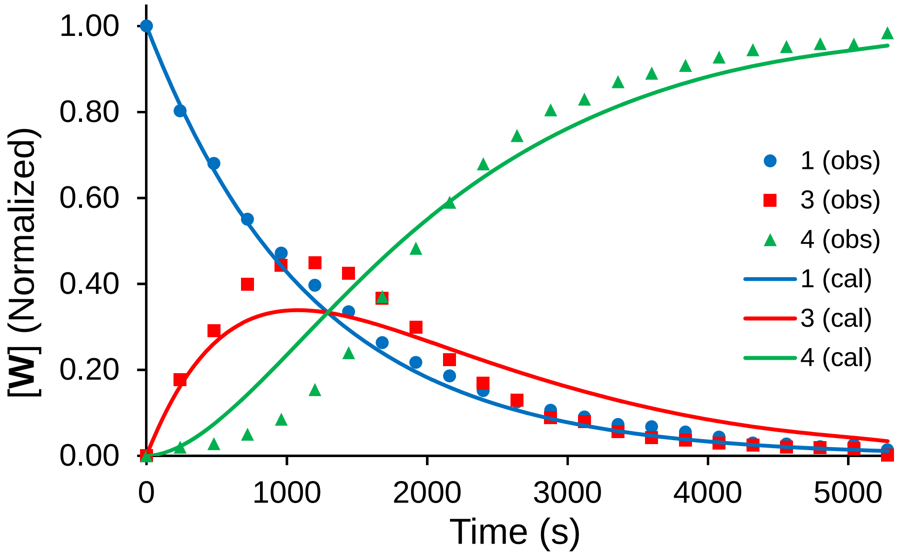

Figure 2.8. Plots of all observed and fitted data for the conversion of $Cp^*W(O)_2(CH_2SiMe_3)$ (**2.1**) with 5 equivalent of $NaIO_4$ to Me_3SiCH_2OH (**2.4**) in THF-d_8 at –1.3 °C.

The rate constants for the formation of **2.3** (k_{obs1} = 8.5(5) × 10^{-4} s^{-1}, corresponding to a $\Delta G^{\ddagger}$ = 19.7(1) kcal·mol^{-1}) and the conversion of **2.3** to $TMSCH_2OH$ (k_{obs2} = 1.0(1) × 10^{-3} s^{-1}, corresponding to a $\Delta G^{\ddagger}$ = 19.6(1) kcal·mol^{-1}) were determined.

Under pseudo-first-order conditions (*i.e.*, excess IO_4^-), complex **2.1** was treated with a series of concentrations of $NaIO_4$ in 1:1 THF-d_8:D_2O (v:v) at –1.3 °C, and a rate constant k_{obs1} for the disappearance of complex **2.1** was determined for each reaction. A plot of k_{obs1} as a function of $[IO_4^-]$ shows a first-order dependence on $[IO_4^-]$ (Figure 2.8). Thus, the experimentally derived rate law for the conversion of **2.1** and IO_4^- to **2.3** is Rate = k_1[**2.1**]$[IO_4^-]$, and the slope of the plot in Figure 2.9 gives k_1 = 1.9(3) × 10^{-2}·M^{-1}·s^{-1} which corresponds to a $\Delta G^{\ddagger}$ = 18.0(1) kcal·mol^{-1} at –1.3 °C.

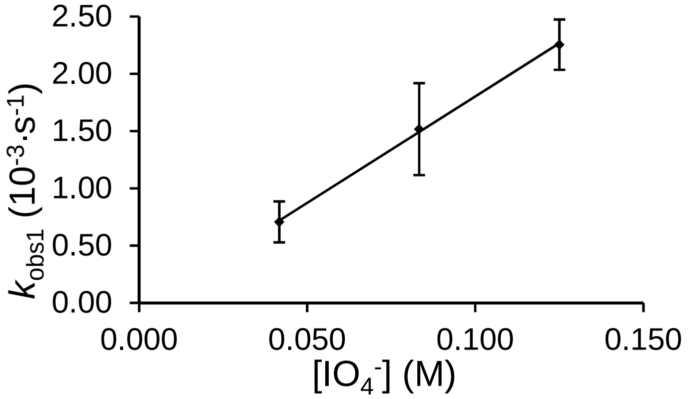

Figure 2.9. Plot of k_{obs1} vs. $[IO_4^-]$ for the reaction of $Cp^*W(O)_2(CH_2SiMe_3)$ (**2.1**) with $NaIO_4$ showing a first order dependence on $[IO_4^-]$ (R^2=0.99).

The conversion of **2.1** and $NaIO_4$ to **2.3** was monitored by ^1H NMR spectroscopy at –1.3, 10.7, 22.7 and 34.7 °C. An Eyring plot using k_1 (determined from the rate of disappearance of **2.1** divided by the $[IO_4^-]$ (Figure 2.10) was used to calculate $\Delta H^{\ddagger}$ = 8.5(2) kcal·mol^{-1} and $\Delta S^{\ddagger}$ = –35.2(7) cal·mol^{-1}·K^{-1} for the conversion of **2.1** to **2.3**. The relatively large $|\Delta S^{\ddagger}|$ for a bimolecular reaction indicates the possibility of substantial solvent ordering in the transition state.

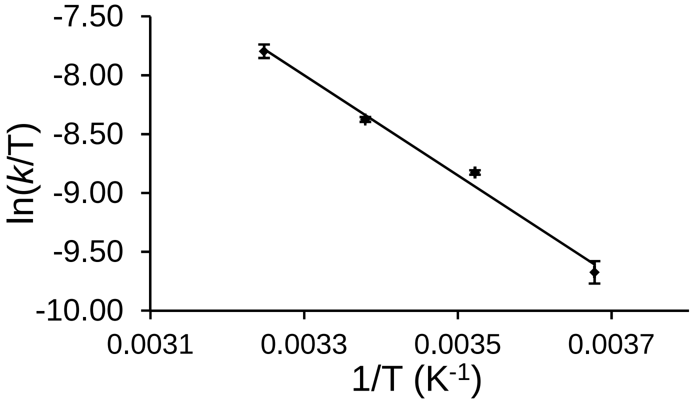

Figure 2.10. Plot of ln(*k*/T) vs. 1/T for the conversion of $Cp^*W(O)_2(CH_2SiMe_3)$ (**2.1**) and $NaIO_4$ (5 equiv) to $Cp^*W(O)_2(OCH_2SiMe_3)$ (**2.3**) ($R^2=0.99$).

Density functional theory (DFT) calculations were carried out (Cundari Group, University of North Texas) to probe the mechanism for the reaction of **2.1** with IO_4^- to form $TMSCH_2OH$. Scheme 2.12 shows the energetics for the lowest energy pathway for **2.1** + IO_4^- → ROH that was calculated. The calculated free energy in 1,4-dioxane and water (1,4-dioxane/water) are given in Scheme 2.12. In the following text, we use the calculated numbers in 1,4-dioxane.

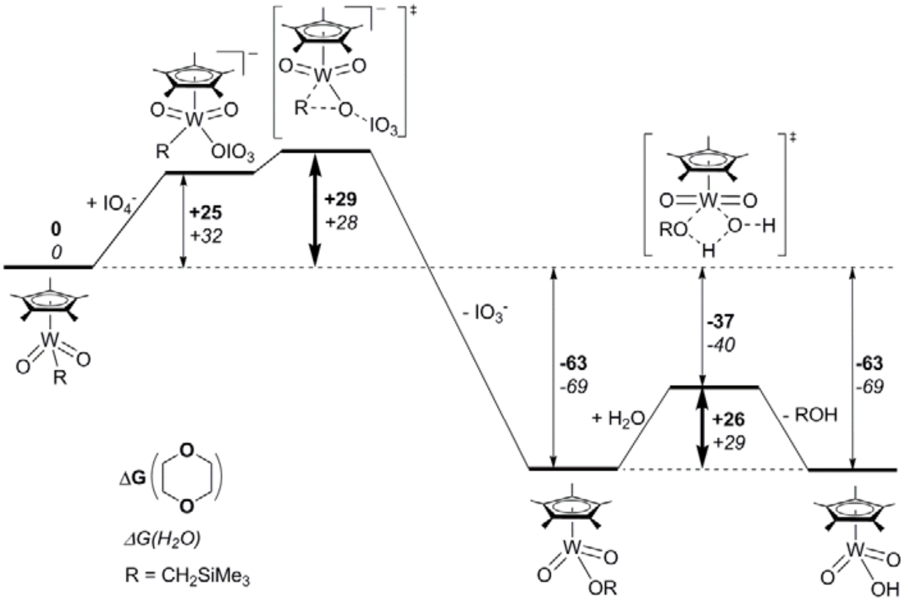

Scheme 2.12. Calculated free energy for the production of $TMSCH_2OH$ in the reaction of $Cp^*W(O)_2(CH_2SiMe_3)$ (**2.1**) with periodate. Numbers are free energies (kcal/mol) for 1,4-dioxane (top, bold) and water (bottom, italics), and are relative to complex **2.1** and IO_4^-.

Through a combination of entropy and solvation effects (free IO_4^- is more heavily solvated than when coordinated to **2.1**), the formation of the adduct **2.1**•OIO_3^- is computed to be endergonic by ≥25 kcal/mol in both solvents relative to separated **2.1** and periodate. Presumably the inclusion of counterion effects would reduce the endergonicity of the reaction to form an anionic adduct, and thus also the corresponding overall activation barrier of the formation of complex **2.3**. Periodate has been implicated in electron transfer reactions as well as two-electron oxygen atom transfer (OAT) chemistry.[41] To model the possibility of one electron chemistry, we investigated the thermodynamics of the electron transfer reaction: **2.1** + $[IO_4]^-$ → **2.1**$^{\bullet-}$ + $[IO_4]^{\bullet}$. This reaction is decidedly endergonic in 1,4-dioxane (ΔG_{calc} = +120 kcal/mol) and water (ΔG_{calc} = +122 kcal/mol).

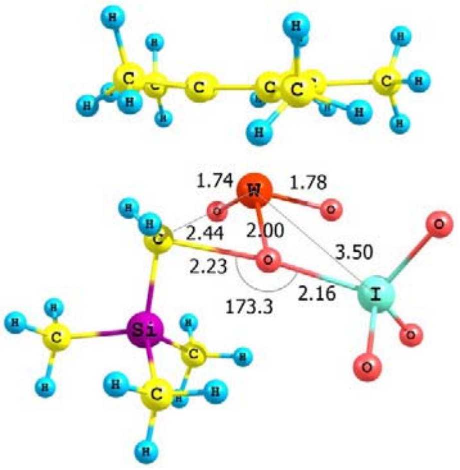

Figure 2.11. DFT calculated transition state for the oxy-insertion step of the overall reaction: $Cp^*W(O)_2(CH_2SiMe_3)$ (**2.1**) + IO_4^- → $Cp^*W(O)_2(OCH_2SiMe_3)$ (**2.3**) + IO_3^-. Bond lengths are given in Å and bond angles in degrees.

The DFT calculations support the hypotheses that oxygen atom insertion into the W–CH_2TMS bond upon reacting with IO_4^- occurs by an OMBV pathway. The calculated energy barrier for oxy-insertion from **2.1**•OIO_3^- is 28 kcal/mol (PCM water). Part of the difference between the computed and experimental barriers (18 kcal/mol vs 29 kcal/mol) is, as delineated below, due to the neglect of explicit solvation of the periodate oxidant and particularly its iodate leaving group. Multiple attempts to isolate alternative transition states (TSs) (*e.g.*, a TS for formation of a peroxo leading to **2.2**, a [3+2] addition of periodate, etc.) either led to already found stationary points or the OMBV transition state depicted in Figure 2.11. The formation of **2.3** is calculated to be favorable, which is consistent with the observation of putative **2.3** as an intermediate in the overall reaction. The calculated I–O bond distance in the transition state for oxygen atom insertion is 2.16 Å, which is much shorter than the 2.399 Å reported for the corresponding TS for MTO, implying an earlier TS for the Cp*W complex. The latter assertion is also supported by the calculated C–O distances for the carbon-oxygen bond being formed in the Baeyer-Villiger TS: 2.23 Å (for Cp*W complex) compared to 2.067 Å (MTO) transition state.[15]

The reaction of complex **2.1** with $[Bu_4N][IO_4]$ (Bu = *n*-butyl) (3 equiv) in rigorously dried THF-d_8 results in no reaction even upon heating at 80 °C for 24 hours, while the same starting material produced the intermediate **2.3** and ultimately $TMSCH_2OH$ in 1:1 THF-d_8:D_2O (v:v) at room temperature in hours. The failure of **2.1** and IO_4^- to produce free alcohol in the absence of water is perhaps not surprising since the conversion of **2.3** to free alcohol requires a proton source. However, the lack of formation of **2.3** for the reaction of **2.1** and IO_4^- in the absence of water is less readily rationalized, especially since calculations show that the formation of **2.3** is thermodynamically favorable from **2.1** and IO_4^-. Water apparently facilitates the oxy-insertion reaction. Possible roles for water in the conversion of **2.1** and IO_4^- to **2.3** include: (1) as a solvent, water helps the ionization of the IO_4^- anion for metal coordination. (2) As an electron donor, water can coordinate the metal center resulting in a more electron-rich metal center and more nucleophilic $–CH_2TMS$ ligand, which is analogous to the role of pyridine in the conversion of MTO and pyridine-*N*-oxide to the oxy-insertion product.[15,42] (3) Water interacts with coordinated IO_4^- to facilitate the dissociation of IO_3^-.

Under pseudo-first-order conditions, the reaction of **2.1** and excess $[Bu_4N][IO_4]$ (15 equiv) with various amounts of D_2O in THF-d_8 was monitored at 50 °C by ^1H NMR spectroscopy. Kinetic plots reveal a first-order decay of **2.1** for each concentration of D_2O. Sample kinetics plots of the rate dependence on water are shown below (Figures 2.12-2.18):

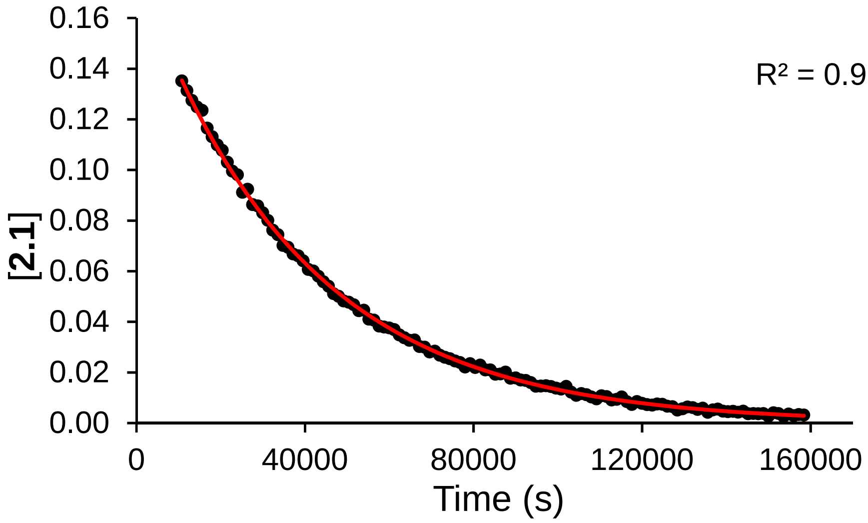

Figure 2.12. First order decay of Cp*W(O)$_2$(CH$_2$SiMe$_3$) (**2.1**) with [Bu$_4$N][IO$_4$] (15 equiv) and 50 equivalents of D$_2$O in THF-*d*$_8$ at 50 °C.

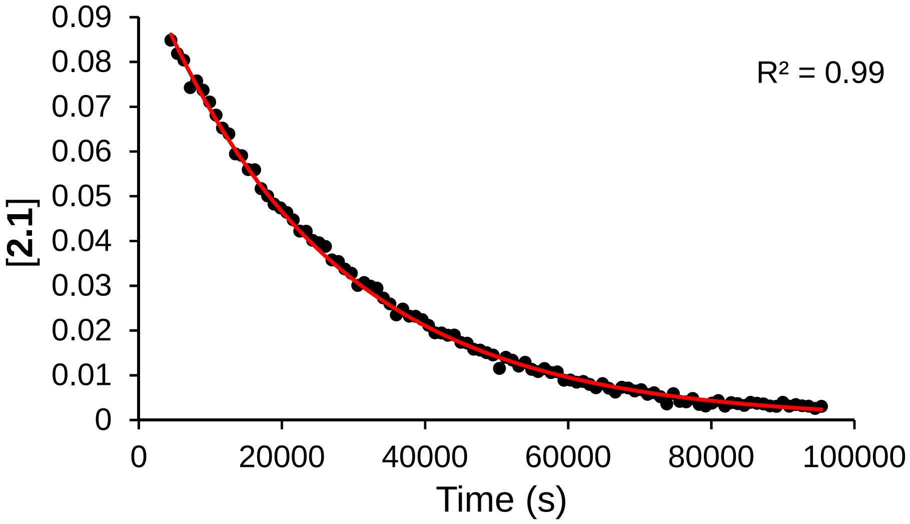

Figure 2.13. First order decay of Cp*W(O)$_2$(CH$_2$SiMe$_3$) (**2.1**) with [Bu$_4$N][IO$_4$] (15 equiv) and 100 equivalents of D$_2$O in THF-*d*$_8$ at 50 °C.

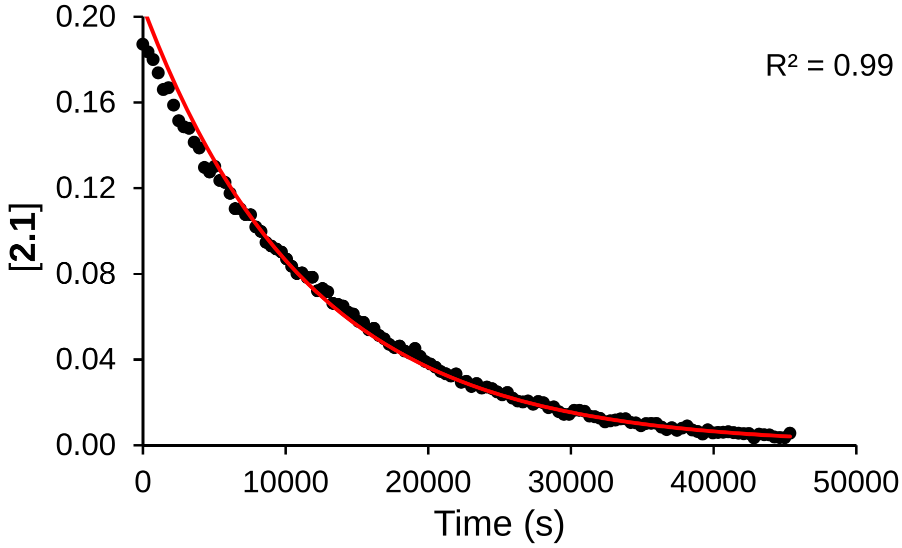

Figure 2.14. First order decay of Cp*W(O)$_2$(CH$_2$SiMe$_3$) (**2.1**) with [Bu$_4$N][IO$_4$] (15 equiv) and 200 equivalent of D$_2$O in THF-*d*$_8$ at 50 °C.

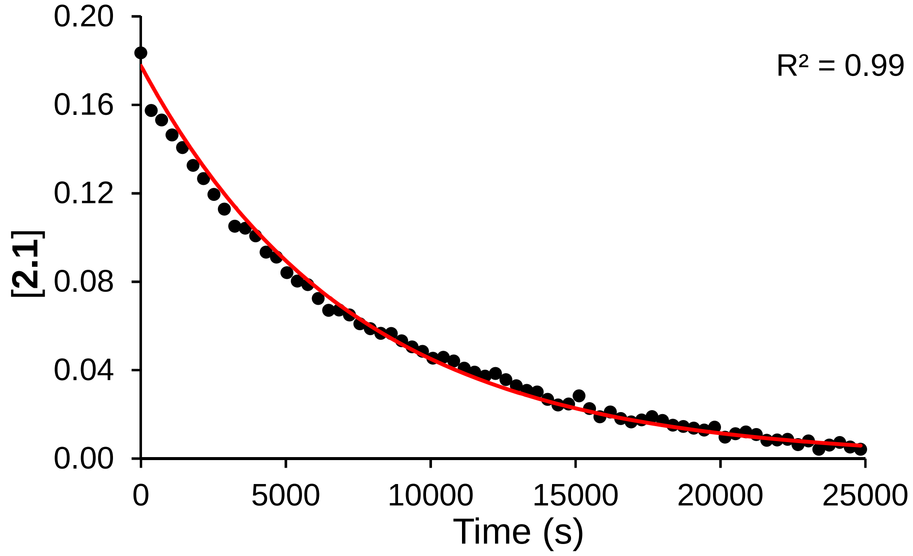

Figure 2.15. First order decay of Cp*W(O)$_2$(CH$_2$SiMe$_3$) (**2.1**) with [Bu$_4$N][IO$_4$] (15 equiv) and 300 equivalents of D$_2$O in THF-*d*$_8$ at 50 °C.

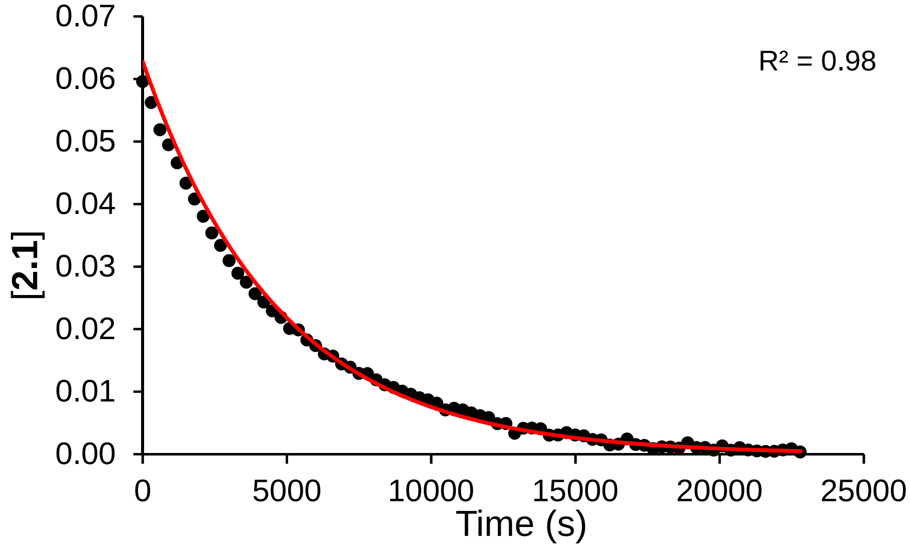

Figure 2.16. First order decay of Cp*W(O)$_2$(CH$_2$SiMe$_3$) (**2.1**) with [Bu$_4$N][IO$_4$] (15 equiv) and 400 equivalents of D$_2$O in THF-*d*$_8$ at 50 °C.

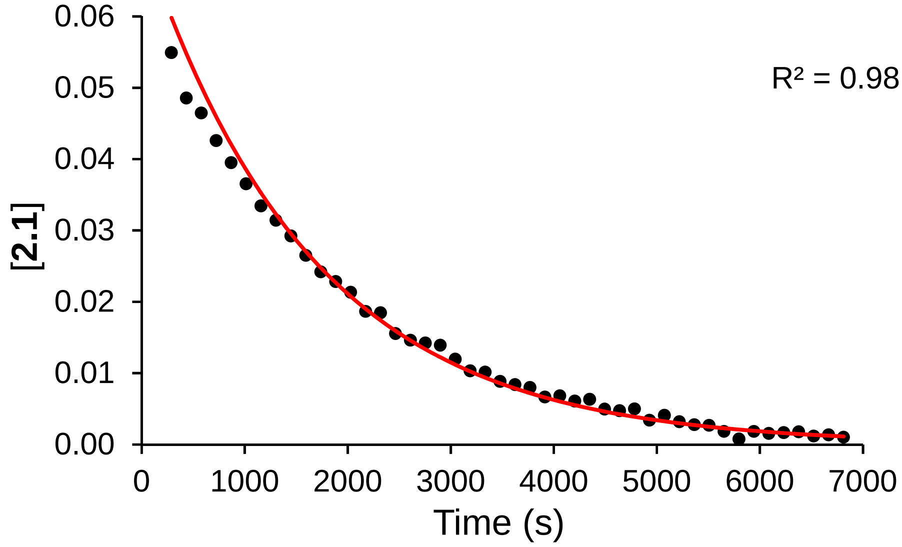

Figure 2.17. First order decay of Cp*W(O)$_2$(CH$_2$SiMe$_3$) (**2.1**) with [Bu$_4$N][IO$_4$] (15 equiv) and 600 equivalents of D$_2$O in THF-*d*$_8$ at 50 °C.

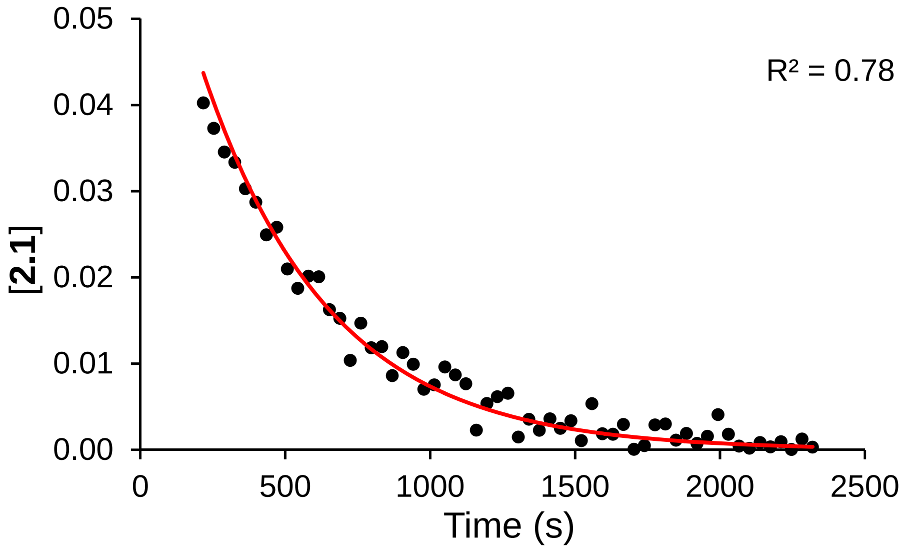

Figure 2.18. First order decay of Cp*$W(O)_2(CH_2SiMe_3)$ (**2.1**) with $[Bu_4N][IO_4]$ (15 equiv) and 1000 equivalents of D_2O in THF-d_8 at 50 °C.

A plot of k_{obs} (divided by the $[IO_4^-]$) as a function of $[D_2O]$ shows that the decay of **2.1** with $[Bu_4N][IO_4]$ has a second-order dependence on $[D_2O]$ (Figure 2.19). Thus, the overall rate law for the conversion of **2.1** and IO_4^- to $TMSCH_2OH$ is Rate = k[**2.1**]$[IO_4^-][D_2O]^2$. A fit of the plot in Figure 2.18 gives $k = 5.8(2)\times10^{-5}\cdot M^{-3}\cdot s^{-1}$ after dividing by $[IO_4^-]$, which corresponds to a $\Delta G^{\ddagger} = 25.2(1)$ kcal·mol^{-1} at 50 °C. The participation of water in the reaction is consistent with the relatively large $|\Delta S^{\ddagger}|$ (see above, $\Delta S^{\ddagger} = –35.2(7)$ cal·mol^{-1}·K^{-1}).

The role of water in the reaction of **2.1** and periodate was investigated computationally. Attempts to model a four-legged piano stool complex with inner-coordination sphere water, Cp*$W(O)_2(OH_2)R$, led instead to an outer-coordination sphere aqua complex in which water is hydrogen bonded to an oxo ligand.

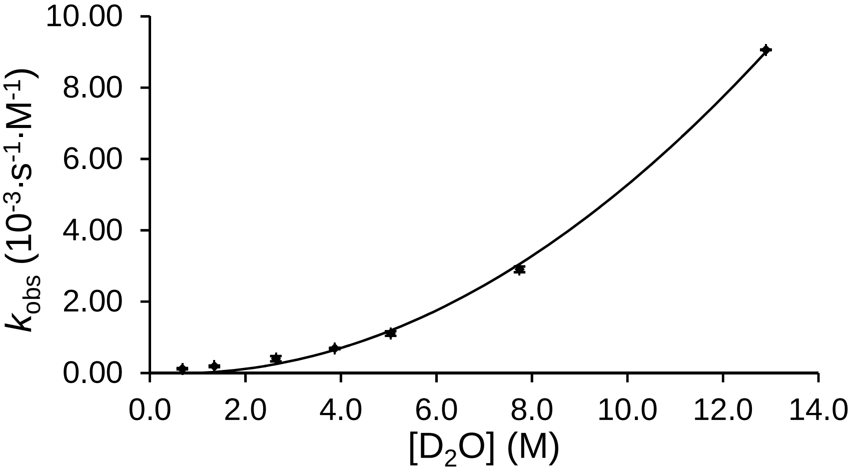

Figure 2.19. Plot of k_{obs} vs. [D_2O] for the reaction of Cp*W(O)$_2$(CH$_2$SiMe$_3$) (**2.1**) and excess [Bu_4N][IO_4] (15 equiv) in THF-d_8 with various amounts of D_2O showing a second-order dependence on [D_2O] (R^2=0.99).

The possibility that water enhances the oxidizing potential of IO_4^- was probed computationally in several ways. The calculation of the oxygen atom transfer (OAT) free energy for $IO_4^- \rightarrow IO_3^- + \frac{1}{2} O_2$ is exergonic by –17 kcal/mol in the gas phase. Inclusion of continuum solvent effects (CPCM, water solvent) increases the exergonicity of this reaction to –26 kcal/mol. The calculations indicate that the increased driving force results from more favorable solvation of the smaller iodate ion in relation to periodate. Thus, the calculations predict that water should enhance the thermodynamics of oxygen atom transfer from IO_4^-, but the extent to which this would enhance the oxy-insertion kinetics is uncertain.

Explicit solvation effects on periodate-mediated OMBV reactions were modeled. Hydrogen-bonding a water molecule to each oxo of the iodate leaving group in the OMBV transition state results in a reduction of the calculated energy barrier from 28 (Scheme 2.10) to 24 kcal/mol, which is closer to the experimental value of 18 kcal/mol (see above). Bond lengths within the active site of the OMBV transition state (Figure

2.20) are little changed upon hydrogen-bonding with three water molecules. What is more noticeable is the shortening of the O–H–O hydrogen bonds by 0.05 Å from 2.00 Å ($[IO_4(OH_2)_3]^-$) to 1.95 Å in the oxy-insertion transition state. In conjunction with the implicit solvation results above, these data lend credence to the proposal that preferential solvation of the iodate leaving group enhances oxy-insertion of periodate into the W–C bond of **2.1** both kinetically and thermodynamically, effectively making the iodate a better leaving group and the periodate a more potent oxidant, both thermodynamically and kinetically.

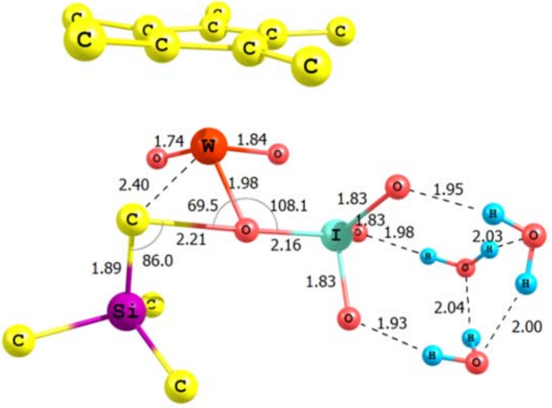

Figure 2.20. DFT calculated transition state with water for the oxy-insertion step of the overall reaction: $Cp^*W(O)_2(CH_2SiMe_3)$ (**2.1**) + IO_4^- → $Cp^*W(O)_2(OCH_2SiMe_3)$ (**2.3**) + IO_3^-. Bond lengths are given in Å and bond angles in degrees.

2.2.2 Reaction of $Cp^*W(O)(\eta^2\text{-}O_2)(CH_2SiMe_3)$ (2.2) with NaOH

As discussed at the beginning of this chapter, the reaction of $MeReO_3$ with H_2O_2 to produce $MeRe(\eta^2\text{-}O_2)O_2$ which can react with OH^- to give MeOH. Will complex **2.2** react with OH^- to produce $SiMe_3CH_2OH$? We observed that complex **2.2** reacted with NaOH to produce $TMSCH_2OH$ in 1:1 THF-d_8:D_2O or 1,4-dioxane-d_8:D_2O (v:v). The reaction produces $TMSCH_2OH$ in quantitative yield (^{1}H NMR) after 3 hours at room temperature (eq 2.3).

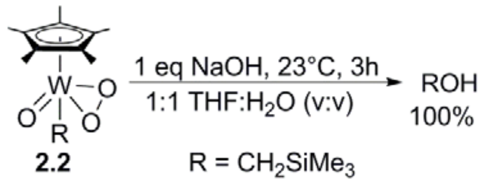

(2.3)

Under pseudo first-order conditions, the reaction of **2.2** with NaOH in 1:1 THF-d_8:D_2O (v:v) was monitored at 10.7 °C by ^{1}H NMR spectroscopy. Kinetic plots reveal a first-order decay of **2.2**, and a plot of k_{obs} as a function of $[HO^-]$ shows that the reaction of **2.2** with NaOH has a first-order dependence on $[OH^-]$ (Figure 2.21). The slope of the plot in Figure 2.21 gives $k = 1.30(6) \times 10^{-2}\cdot M^{-1}\cdot s^{-1}$, which corresponds to a $\Delta G^\ddagger = 19.1(1)$ kcal·mol^{-1} at 10.7 °C.

The rate of the reaction between **2.2** and NaOH was monitored by ^{1}H NMR spectroscopy at –1.3, 10.7, 22.7 and 34.7 °C. An Eyring plot (using k values that were corrected for $[HO^-]$, Figure 2.22) was used to calculate a $\Delta H^\ddagger = 13.6(4)$ kcal·mol^{-1} and a $\Delta S^\ddagger = -20(1)$ cal·mol^{-1}·K^{-1}.

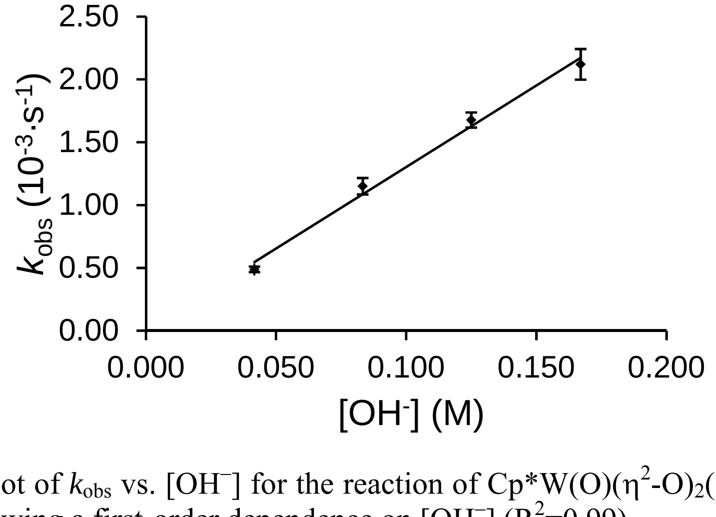

Figure 2.21. Plot of k_{obs} vs. $[OH^-]$ for the reaction of Cp*W(O)(η^2-O)$_2$(CH_2SiMe_3) (**2.2**) with NaOH showing a first-order dependence on $[OH^-]$ (R^2=0.99).

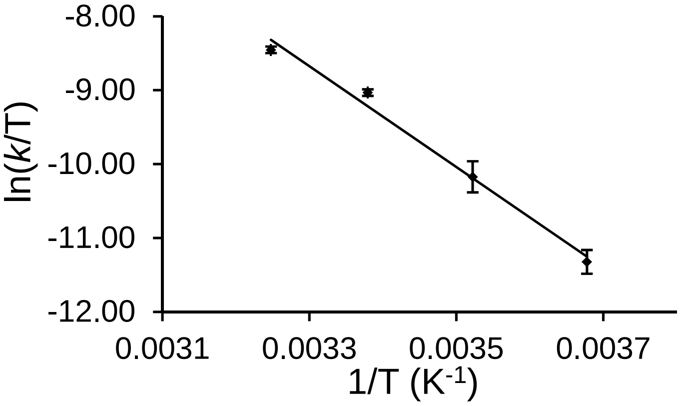

Figure 2.22. Plot of ln(*k*/T) vs. 1/T for the reaction of Cp*W(O)(η^2-O)$_2$(CH$_2$SiMe$_3$) (**2.2**) with NaOH (5 equiv) (R^2=0.99).

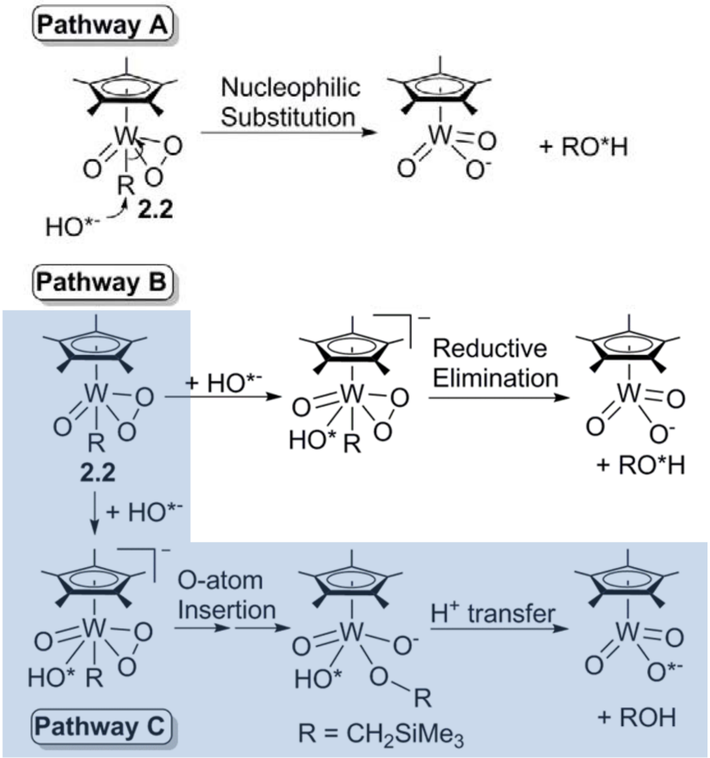

Scheme 2.13. Possible pathways for alcohol release from the reaction of Cp*W(O)(η^2-O$_2$)(CH$_2$SiMe$_3$) (**2.2**) with NaOH in 1:1 THF-d_8:D$_2$O (v:v). Mechanism studies are consistent with Pathway C.

Three possible pathways for the reaction of complex **2.2** with NaOH are shown in Scheme 2.13. In Pathway A, the hydroxide undergoes direct nucleophilic addition to the

TMSCH$_2$ ligand. For this pathway, the oxygen atom in the alcohol would originate from hydroxide. Pathway B involves hydroxide ligand coordination to W followed by C–O bond reductive elimination of the TMSCH$_2$OH. In Pathway B, the oxygen atom of the alcohol would also originate from hydroxide. Pathway C involves hydroxide ligand coordination to W, which would facilitate transfer of the –CH$_2$TMS ligand to an η^2-peroxo oxygen atom. Protonation with water generates alcohol. The oxygen atom of the alcohol in Pathway C originates from complex **2.2**. MeLi was reacted with ^{18}O labeled water to generate the ^{18}O labeled Li^{18}OH in H$_2$^{18}O. The alcohol product from the reaction of **2.2** with Li^{18}OH was then analyzed by GC-MS. Only TMSCH$_2$^{16}OH (MW = 104) was observed in the MS, no TMSCH$_2$^{18}OH (MW = 106) was detected (Figures 2.24, compare to the MS data of the reaction of **2.2** with Na^{16}OH, the same produce was produced), This result is consistent with Pathway C and inconsistent with Pathways A and B in Scheme 2.8.

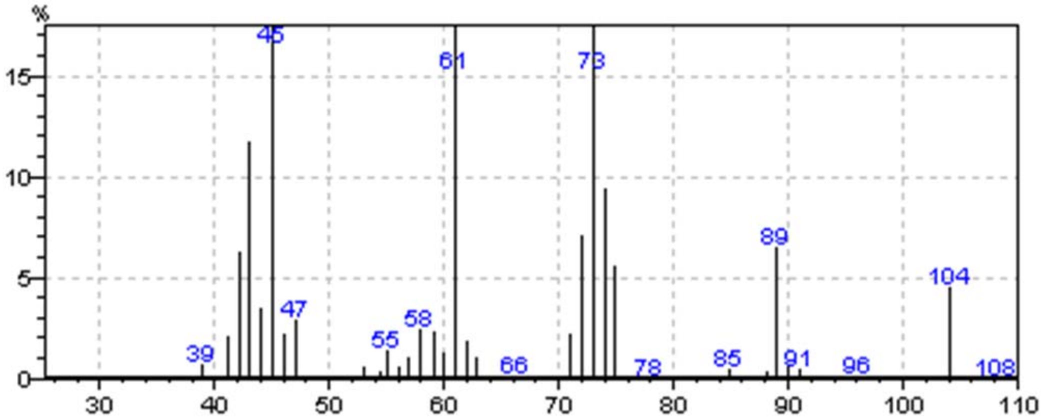

Figure 2.23. MS data for the TMSCH$_2$OH product of the reaction of Cp*W(O)(η^2-O$_2$)(CH$_2$SiMe$_3$) (**2.2**) and NaOH.

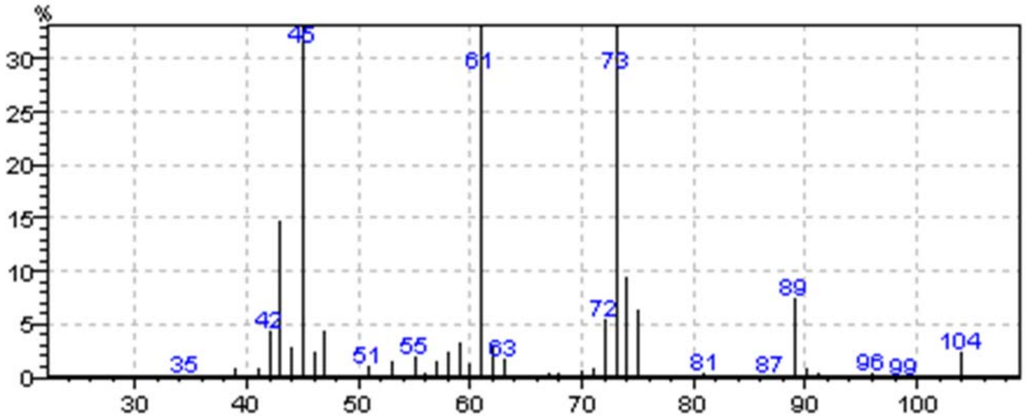

Figure 2.24. MS data for the TMSCH$_2$OH product of the reaction of Cp*W(O)(η^2-O$_2$)(CH$_2$SiMe$_3$) (**2.2**) and Li^{18}OH.

The role of hydroxide for the conversion of **2.2** to TMSCH$_2$OH was probed computationally. Several mechanisms were investigated (Scheme 2.14). The very large calculated free energy barriers (≥ 67 kcal/mol) led us to discount nucleophilic substitution (Pathway A) and reductive elimination (Pathway B). The calculations suggest that the hydroxide coordination assisted alkyl migration to an oxygen atom of the η^2-peroxo ligand (34 and 35 kcal/mol in 1,4-dioxane and water) has almost the same energy barrier as the non-assisted alkyl migration (35 and 32 kcal/mol in 1,4-dioxane and water) (see Scheme 2.12 below). What emerged as the most reasonable pathway was a H-atom transfer pathway in which hydroxide coordinates to **2.2**, followed by proton transfer ($\Delta G^\ddagger$ = 25 and 24 kcal/mol in 1,4-dioxane and water, respectively) to yield a hydroperoxide intermediate, [(κ^1-Cp*)W(O)$_2$(R)(OOH)]$^-$ (Scheme 2.9). The OMBV transition state from the latter is calculated to be 24 and 23 kcal/mol in 1,4-dioxane and water above the starting complex **2.2**, in reasonable agreement with the experimental measurement. After oxy-insertion, hydroxide loss (to yield **2.3** + OH$^-$) or proton transfer (to yield

$[Cp^*W(O)_3]^-$ + ROH) was calculated to be facile ($\Delta G^\ddagger$ = 12 and 11 kcal/mol in 1,4-dioxane and water, respectively).

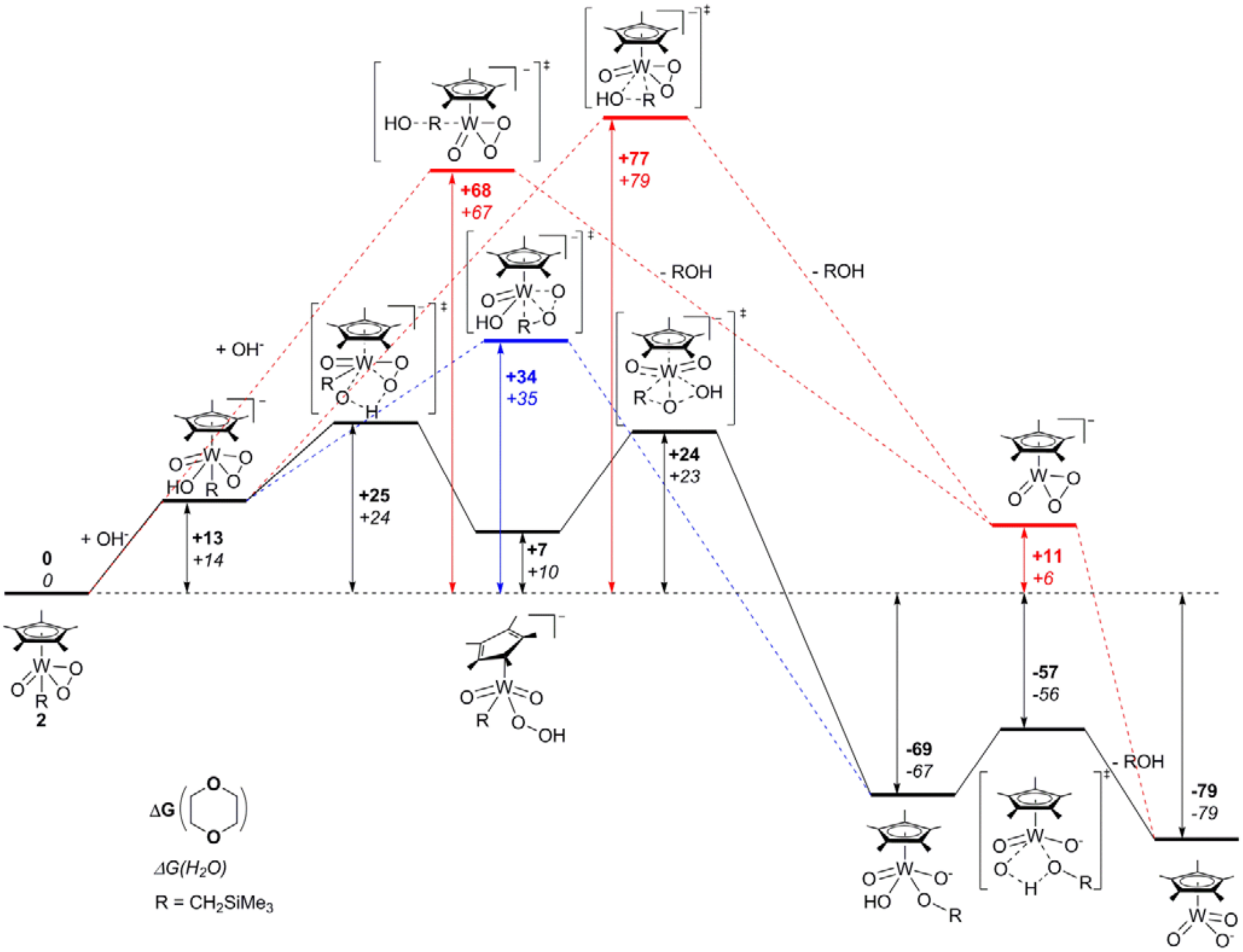

Scheme 2.14. Calculated free energy for the reaction of $Cp^*W(O)(\eta^2\text{-}O_2)$ (CH_2SiMe_3) (**2.2**) with OH^-. Numbers are free energies (kcal/mol) for 1,4-dioxane (top, bold) and water (bottom, italics), and are relative to complex **2.2** (Cp^* = κ^1-Cp^*).

The calculated transition state for oxy-insertion from $[(\kappa^1\text{-}Cp^*)W(O)_2(R)(OOH)]^-$ (Figure 2.25) is structurally similar to the corresponding transition state involving oxygen atom insertion from periodate (Figure 2.11). The C–O bond being formed is longer (2.23 Å vs. 2.10 Å) and the W–C bond being broken is shorter (2.44 Å vs. 2.61 Å) for the periodate transition state, implying an earlier transition state for the OMBV oxy-insertion with periodate in relation to the hydroperoxide congener. The tremendous kinetic and thermodynamic free energy preference for the OMBV pathway in relation to the pathways that lead to reduced W^{IV} intermediates (nucleophilic substitution and reductive elimination, Scheme 2.13) is interesting in connection with the single-electron transfer reaction modeled above and supports the notion of the important role of metal d orbital occupation in oxy-insertion, and further that movement away from d^0 motifs will disfavor the OMBV pathway. Thus, while functionalization of alkyl ligands through processes that formally reduce the metal center can be facile for late transition metal complexes, similar reactions with middle transition metals may have inherently and prohibitively high activation barriers.

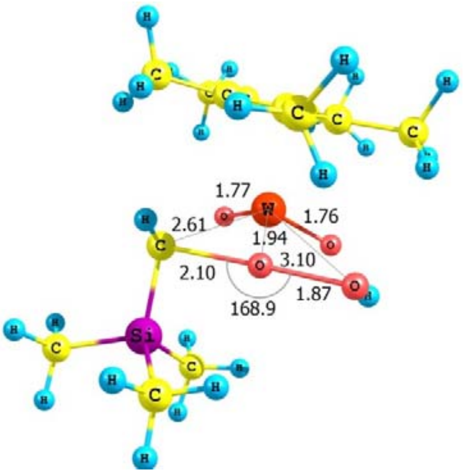

Figure 2.25. DFT calculated organometallic Baeyer-Villiger (OMBV) transition state for oxy-insertion of hydroperoxide into W–C bond of Cp*W(O)(η^2-O_2) (CH_2SiMe_3) (**2.2**). Bond lengths are given in Å and bond angles in degrees.

2.2.3 Reaction of Cp*W(O)(η^2-O_2)(CH_2SiMe_3) (2.2) with Brønsted Acids

Complex **2.2** has been demonstrate to react with OH^- to produce alcohol like its Re neighbor on the right of the period table. However, complex **2.2** also has a similar structure as $(Cp^*)_2Ta(\eta^2$-$O_2)R$, its other neighbor one left of the period table.

Analogously, will complex 2.2 also react with electrophilic to have O-atom insertion reaction as the Ta complex does? Actually, the formation of alcohol is also observed when complex **2.2** is treated with HCl in 1,4-dioxane. The reaction is complete in 40 hours at room temperature and produces Cp*W(O)$_2$Cl and TMSCH$_2$OH in ~90% yield by ^{1}H NMR spectroscopy (eq 2.4). The acid promoted reaction of **2.2** is slower than the hydroxide-promoted conversion. For example, complex **2.2** with 3 equivalents of NaOH quantitatively forms TMSCH$_2$OH in less than 1 hour at room temperature.

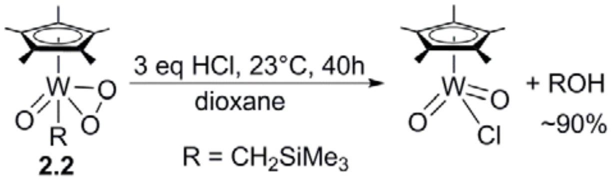

(2.4)

Table 2.2. Reaction conditions and yields for reaction of Cp*W(O)(η^2-O)$_2$(CH$_2$SiMe$_3$) (**2.2**) with Brønsted acid.

No.	Solvent	Acid	T (°C)	t (h)	Yield (%)[a]
1	benzene	none	80	24	0
2	dioxane[b]	3 eq HCl (Et$_2$O)	23	40	~90
3	dioxane	3 eq HCl (dioxane)	23	32	~70
4	dioxane	3 eq HCl (dioxane)	50	2	~60
5	dioxane/water	3 eq HCl (35%)	23	100	~80
6	dioxane/water	5 eq H$_2$SO$_4$ (98%)	23	100	>90
7	dioxane	5 eq H$_2$SO$_4$ (98%)	23	12	Decomp.
8	dioxane/water	None	75	24	~70
9	dioxane	HOTf (99%)	23	12	Decomp.

[a] Yields of TMSCH$_2$OH are based on integration of ^{1}H NMR spectra versus an internal standard. [b] 1,4-dioxane.

Table 2.2 shows the conditions and results for the reactions of complex **2.2** with various proton sources. Without a proton source, when **2.2** is heated in benzene at 80 °C for 24 hours, no alcohol is observed and the starting material decomposes to form complex **2.2** (entry 1). Heating increases the rate of conversion but decreases the yield (entries 3 and 4). The use of strong acid in 1,4-dioxane results in decomposition of the starting material with no alcohol production (entries 7 and 9).

We have considered two roles for the acid in the conversion of **2.2** and HCl to Cp*W(O)$_2$Cl and TMSCH$_2$OH (Scheme 2.15): (1) the proton serves as a catalyst by protonating the η^2-peroxo ligand, which would increase oxygen electrophilicity and facilitate oxy-insertion. A similar mechanism was proposed for the acid-catalyzed rearrangement of an η^2-peroxo Ta alkyl to form oxo-alkoxide derivatives.[24] (2) The proton is not a catalyst, but rather the acid serves to generate free alcohol from Cp*W(O)$_2$(OCH$_2$SiMe$_3$).

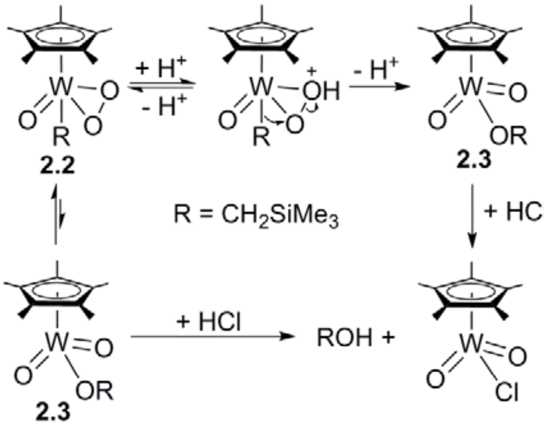

Scheme 2.15. Two possible pathways for the alcohol release reaction of Cp*WO(η^2-O$_2$)(CH$_2$SiMe$_3$) (**2.2**) with HCl.

To investigate rate dependence of the reaction of **2.2** and HCl, we attempted to use excess HCl to achieve pseudo first-order conditions. However, when more than 5 equivalents of HCl are used, complex **2.2** decomposes with little production of $TMSCH_2OH$.

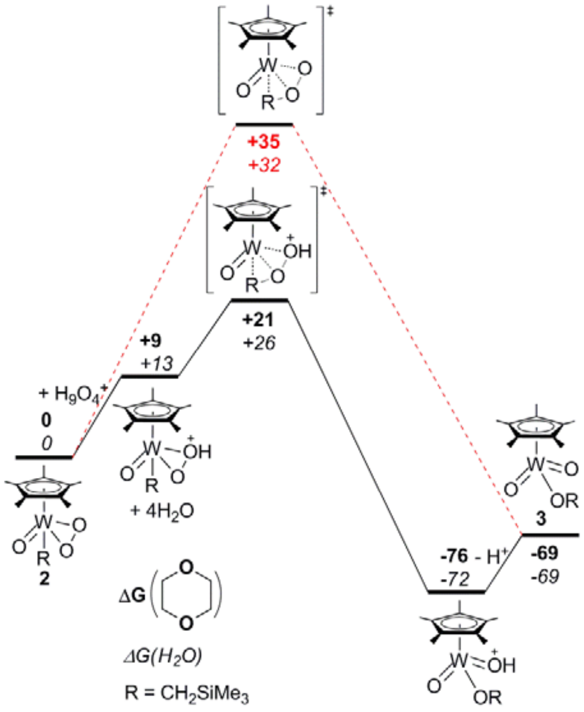

Scheme 2.16. Calculated free energy for the reaction of Cp*WO(η^2-O_2) (CH_2SiMe_3) (**2.2**) with H^+. The Eigen Cation ($H_9O_4^+$) was used to model the proton. Numbers are free energies (kcal/mol) for 1,4-dioxane (top, bold) and water (bottom, italics) and are relative to complex **2.2**.

Reaction coordinates for conversion of **2.1** to **2.3** in the absence and presence of a proton were evaluated computationally to help assess the impact of Brønsted acids upon the proposed mechanisms of oxy-insertion. Various basic sites were evaluated in the starting materials, products, intermediates and transition sites (*e.g.*, protonation of oxo versus peroxo ligands). The discussion focuses on the most stable tautomers (Scheme 2.16). In the absence of a proton, the migration of R to the peroxide moiety has a calculated activation barrier of 35 or 32 kcal/mol in 1,4-dioxane or water, respectively. Upon protonation (the Eigen cation, $H_9O_4^+$, was used to model an aqueous proton), the corresponding barriers were reduced to 21 (1,4-dioxane) or 26 (water) kcal/mol. The results thus support the observation of acceleration of the oxy-insertion reaction upon the introduction of Brønsted acids.

Analysis of the calculated oxy-insertion transition state geometries from **2.2** with and without added proton is revealing (Figure 2.26). The various bond distances in the active site point to an earlier transition state upon the introduction of a proton, which is consistent with a lower barrier according to the Hammond postulate. Additionally, one may hypothesize that the protonation of the incipient oxide group in the peroxo transition state yields a better leaving group (hydroxide). The greater exergonicity for neutral Cp*W(O)(η^2-O_2) R → Cp*W(O)$_2$(OR) versus the protonated variant (–69 kcal/mol in 1,4-dioxane (Scheme 2.16), versus –76 kcal/mol (Scheme 2.16)) provides additional support for these proposals, and the role of Brønsted acids in catalyzing oxy-insertion from **2.2**.

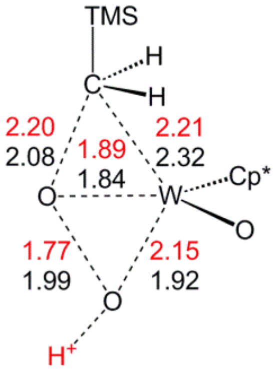

Figure 2.26. Calculated transition state for oxy-insertion of Cp*W(O)(η^2-O_2) (CH_2SiMe_3) (**2.2**) with (red) and without (black) added proton. Bond lengths are given in Å.

2.2.4 Reaction of $Cp^*W(O)_2(CH_2SiMe_3)$ (2.1) with Hydrogen Peroxide in the Presence of Hydroxide

The reaction of complex **2.1** with H_2O_2 (3 equiv) in benzene generates complex **2.2** at room temperature after 24 hours without production of alcohol. However, alcohol production is observed at room temperature when complex **2.1** is treated with a mixture of H_2O_2 (3 equiv) with NaOH (3 equiv) in 1:1 THF-d_8:D_2O (v:v). The reaction is complete in ∼4 hours and produces $TMSCH_2OH$ in >95% yield by ^1H NMR spectroscopy (eq 2.5).

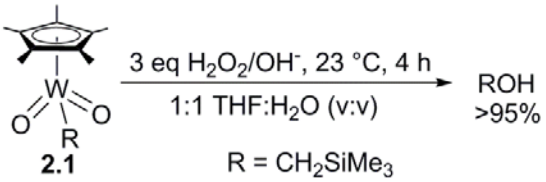

(2.5)

Espenson *et al.* observed faster decomposition and methanol release from MTO with H_2O_2 in basic environment;[35] Periana, Goddard *et al.* studied the mechanism for the reaction of MTO with H_2O_2 in the presence of hydroxide.[15] Calculations show that the OMBV pathway in which OOH^- coordinates to rhenium followed by the migration of the methyl to the coordinated oxygen atom of Re–OOH has the lowest energy barrier. To determine whether the reaction of **2.1** with H_2O_2 in the presence of OH^- proceeds via an OMBV pathway to form the alkoxide complex **2.3**, as the reaction of **2.1** and IO_4^- does (see above), the reaction of complex **2.1** with a mixture of 5 equivalents of H_2O_2 and 5 equivalents of NaOH in 1:1 THF-d_8:D_2O (v:v) was monitored at –1.3 °C by ^1H NMR spectroscopy. Under these conditions, the starting material **2.1** converts to complex **2.2** in 10 min. Complex **2.2** then undergoes slow transformation to $TMSCH_2OH$ over a period of 8 hours. Consequently, alcohol release from complex **2.1** and H_2O_2 in the presence of hydroxide proceeds by an η^2-peroxo pathway that involves two steps: the formation of the η^2-peroxo complex **2.2** and the conversion of **2.2** to $TMSCH_2OH$. Compared to the reaction with H_2O_2 under acidic conditions, the reaction rates of both steps (*i.e.*, formation of **2.2** and release of $TMSCH_2OH$) are faster with hydroxide. For example, the reaction of complex **2.1** with a mixture of H_2O_2 (3 equiv) and HCl (3 equiv) produces complex **2.2** in hours at room temperature, which then converts to $TMSCH_2OH$ in 48 hours (Scheme 2.17).

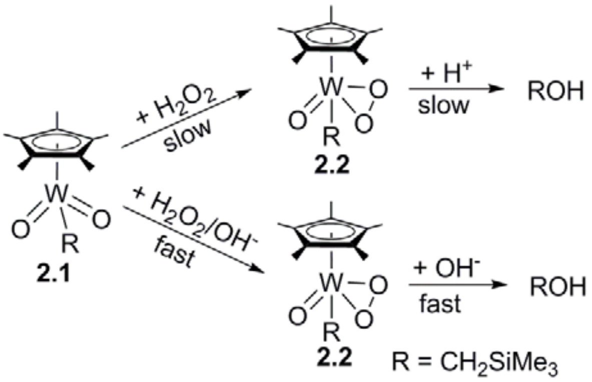

Scheme 2.17. Comparison of alcohol release from $Cp^*W(O)_2(CH_2SiMe_3)$ (**2.1**) with H_2O_2 in the presence of H^+ and OH^-.

DFT calculations were used to probe the conversion of dioxo complex **2.1** and hydrogen peroxide to the η^2-peroxo complex **2.2** (Scheme 2.18). A [2+2] addition of the OH bond of hydrogen peroxide across the W=O bond of **2.1** (red line in Scheme 2.18) has a calculated barrier of 25 and 27 kcal/mol for 1,4-dioxane and water, respectively. This [2+2] transition state leads to the hydroxy/hydroperoxy intermediate $Cp^*W(R)(O)(OH)(OOH)$, which is 10 kcal/mol above complex **2.1**. From this intermediate, a modest barrier of 12 (1,4-dioxane) or 14 (water) kcal/mol must be surmounted to transfer hydrogen from the hydroperoxide to hydroxide ligand to dissociate water and yield complex **2.2**. Overall, with H_2O_2/H_2O as the oxygen-atom transfer couple, the transformation of **2.1** to **2.2** is calculated to be exergonic by –7 kcal/mol in 1,4-dioxane and –8 kcal/mol in water. Deprotonation of hydrogen peroxide and coordination of hydroperoxide gives Cp*W(O)$_2$(R)(OOH), which is higher in energy than **2.1** by 7 and 10 kcal/mol. Conversion of Cp*W(O)$_2$(R)(OOH) to complex **2.2** through an intramolecular proton transfer and dissociation of hydroxide is calculated to occur with an overall activation barrier of 25 and 24 kcal/mol. Thus, the calculations do not reveal any obvious advantage to base promoted conversion of **2.1** and hydrogen peroxide to complex **2.2**.

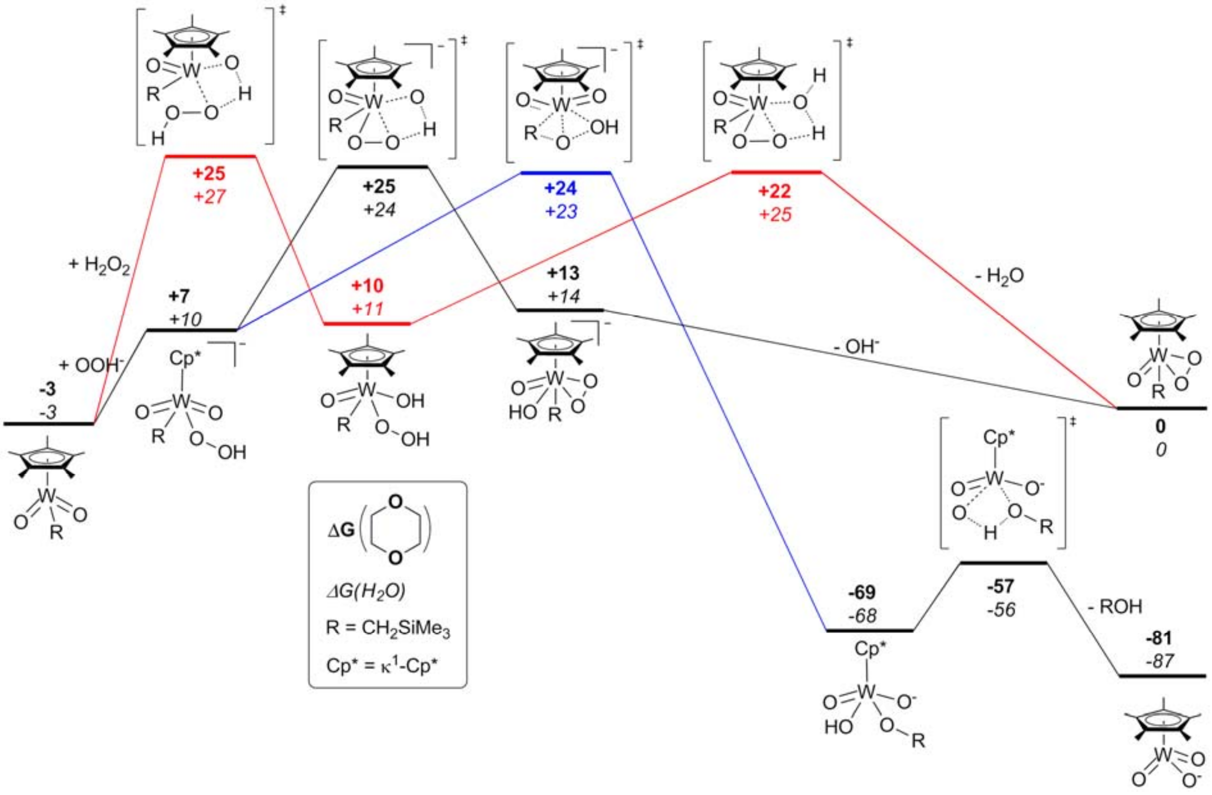

Scheme 2.18 . Calculated free energy for the conversion of Cp*W(O$_2$) (CH$_2$SiMe$_3$) (**2.1**) and H_2O_2 to Cp*WO(η^2-O$_2$) (CH$_2$SiMe$_3$) (**2.2**). Numbers are free energies (kcal/mol) for 1,4-dioxane/water and are relative to complex **2.2** (Cp* = κ^1-Cp*).

2.3 Summary and Discussions

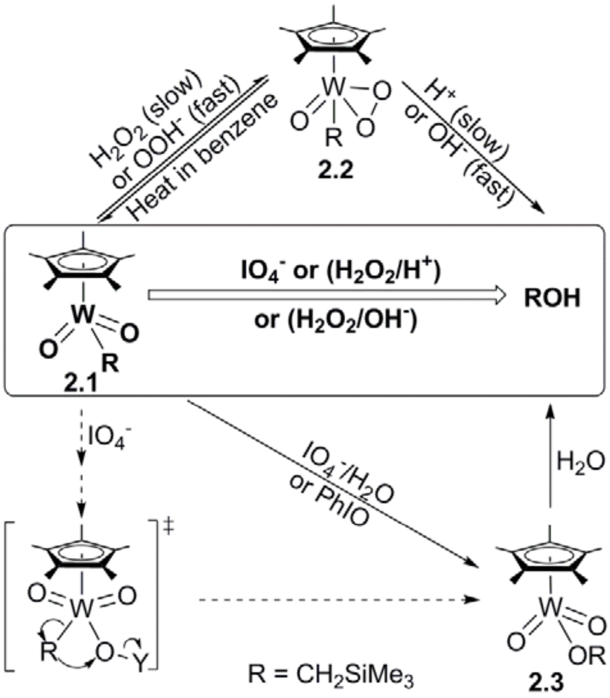

Scheme 2.19. Summary of pathways for the oxygen atom insertion into W–C bonds of Cp*W(O)$_2$(CH$_2$SiMe$_3$) (**2.1)** and Cp*W(O)(η^2-O)$_2$(CH$_2$SiMe$_3$) (**2.2**).

Insertion of oxygen atoms into metal-hydrocarbyl bonds is a potential key step in catalytic oxidation of hydrocarbons. Despite the potential importance of such oxygen atom insertion reactions, there are few examples of non-radical conversion of M–R bonds and oxygen atom transfer reagents to M–OR, and detailed studies of non-radical oxygen atom insertion into M–R bonds are rare. To our surprise, we have established that Cp*W^{VI} complexes can undergo clean oxygen atom insertion reactions by at least *three different pathways* (Scheme 2.19). Oxy-insertion from η^2-peroxide complexes can be promoted by addition of hydroxide or Brønsted acid. DFT calculations lead to the suggestion that protonation of the η^2-peroxide ligand facilitates alkyl migration to the unprotonated oxygen atom. Our calculations suggest that the addition of base leads to a similar transition state in which the alkyl group migrates to the unprotonated oxygen of an η^2-hydroperoxide ligand; however, the base-promoted transition state is overall anionic and has a second oxo ligand (Scheme 2.20). Calculations in water indicate that the $\Delta\Delta G^{\ddagger}$ for the acid- and base-promoted reactions is 3 kcal/mol in favor of the base-promoted conversion. Experiments clearly show that the base-promoted oxy-insertion is faster than the acid-catalyzed reaction. Quantification of such effects is important since most successful transition metal catalyzed alkane oxidations incorporate electrophilic late transition metals that tolerate acidic conditions but are not likely to be amenable to alkaline conditions.[6,43] Some caution is advised when comparing these calculated values since most computations use an implicit water solvation model and calculations for the reaction of **2.1** and IO_4^- with explicit water demonstrate that hydrogen bonding can be important. The third oxy-insertion follows an OMBV pathway. To our knowledge, this is only the second example of an oxygen atom insertion into a M–R bond that likely proceeds by this concerted process.[15] Importantly, the OMBV reaction with **2.1** occurs in neutral water/1,4-dioxane, suggesting that catalysts with nucleophilic hydrocarbyl groups that are tolerant of water should be amenable for this oxy-functionalization process.

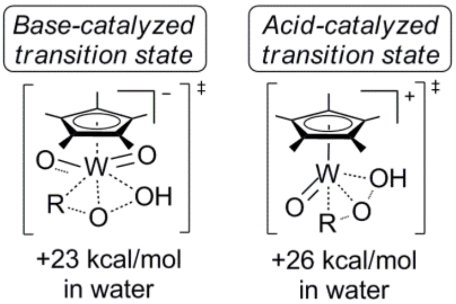

Scheme 2.20. Comparison of transition states for base- and scid-promoted conversion of $Cp^*W(O)(\eta^2\text{-}O)_2(CH_2SiMe_3)$ (**2.2**) to the oxy-insertion products.

We have successfully extended the OMBV reaction form the Re^{VII} to its left neighbor W^{VI} on the periodic table. With the no O-atom insertion reaction from the Pt^{II} and Rh^{III}–R complexes with various oxidants, it more likely that *the nucleophilicity of the* $M–C^{\delta-}$ *bond plays a more important role than the electrophilicity of the bound* $O^{\delta+}$ *does* in the OMBV reactions for O-atom insertion.

2.4 Experimental Section

General Methods. Unless otherwise noted, all synthetic procedures were performed under anaerobic conditions in a nitrogen filled glovebox or by using standard Schlenk techniques. Glovebox purity was maintained by periodic nitrogen purges and was monitored by an oxygen analyzer (O_2 < 15 ppm for all reactions). Tetrahydrofuran and 1,4-dioxane were dried by distillation from sodium/benzophenone and P_2O_5, respectively. Diethyl ether was distilled over CaH_2. THF-d_8, 1,4-dioxane-d_8, D_2O and $H_2{}^{18}O$ were used as received and stored under a N_2 atmosphere over 4 Å molecular sieves (except water). ^{1}H NMR spectra were recorded on a Varian Mercury 300 or Varian Inova 500 MHz spectrometer. All ^{1}H spectra are referenced against residual proton signals of the deuterated solvents. GC/MS was performed using a Shimadzu GCMS-QP2010 Plus system with a 30 mm 0.25 mm SHRXI-5MS column with 0.25 mm film thickness using negative chemical ionization (NCI), which also allows for simulated electron impact (SEI) ionization. The preparation, isolation and characterization of $Cp^*W(O)_2(CH_2SiMe_3)$ and $Cp^*W(O)(\eta^2\text{-}O_2)(CH_2SiMe_3)$ have been previously reported.[36] All other reagents were used as purchased from commercial sources.

Computational methods. Density Functional Theory (DFT) calculations with the B3LYP[44-46] functional employed the Gaussian 09 program[47] in conjunction with the pseudopotentials and valence basis sets of Stevens *et al.*[48,49] for W, Si and I. All 2p elements plus hydrogen were modeled with the 6-311++G(d,p) all-electron basis set. All species were singlet spin states and optimized within the restricted Kohn-Sham formalism with the exception of **1**$^{\bullet-}$and $[IO_4]^{\bullet}$, which are doublets and optimized with unrestricted Kohn-Sham methods. For the latter, spin contamination was minimal. All stationary points were optimized in the gas phase without symmetry constraint and identified as minima or transition states through the calculation of the energy Hessian. Solvent effects were incorporated implicitly through the use of the CPCM[50] model for water and 1,4-dioxane. All quoted energetics are free energies and are reported at STP and were obtained using unscaled vibrational frequencies.

Reaction of Cp*W(O)$_2$(CH$_2$SiMe$_3$) (2.1) with NaIO$_4$. Complex **2.1 (**2.1 mg, 5.0 μmol**)** was dissolved in 300 μL of THF-d_8 in an NMR tube. $NaIO_4$ (3.3 mg, 15 μmol) was dissolved in 300 μL of D_2O and transferred to the solution of **2.1**. The reaction was monitored by ^{1}H NMR spectroscopy until completion. The production of $TMSCH_2OH$ was confirmed using two methods. First, 5 μL of the reaction mixture was analyzed by GC/MS, and $TMSCH_2OH$ was detected (and compared with GC/MS of an authentic sample). Second, 1 μL of $TMSCH_2OH$ was added to the reaction mixture. The intensity of the product peaks increased in ^{1}H NMR spectrum.

Kinetics of reactions of Cp*W(O)$_2$(CH$_2$SiMe$_3$) (2.1) with NaIO$_4$. A representative kinetic experiment is described. Complex **2.1** (32.0 mg 75.0 μmol) was dissolved in 4.5 mL of THF-d_8. Two drops of benzene were added to the solution as an internal standard for ^{1}H NMR integration. A 300 µL aliquot (0.0166 mol/L) was transferred to an NMR tube. $NaIO_4$ (143 mg, 0.667 mmol) was dissolved in 2.0 mL D_2O (0.33 mol/L). D_2O (225 µL) was added to the solution of **2.1** by syringe and cooled in ice water. Then 75 µL (5.0 equiv) of the $NaIO_4$ solution was added to the solution of complex **2.1**. The reaction mixture was then monitored by array ^{1}H NMR spectroscopy on a 500 MHz spectrometer at –1.3 °C. A ^{1}H NMR spectrum was acquired every 26 sec. Integration of the methylene peak of complex **2.1**, $TMSCH_2OH$ and the intermediate **2.3** gave the variation in concentrations. Similar reactions were set up for 10.0, 15.0 and 20.0 equivalents of $NaIO_4$ by adjusting the amounts of the D_2O and $NaIO_4$ solution. To ensure reproducibility, every concentration was repeated in triplicate.

Eyring plot of reaction of $Cp^*W(O)_2(CH_2SiMe_3)$ (2.1) with $NaIO_4$. A representative kinetic experiment is described. Complex **2.1** (13.5 mg, 32.0 µmol) was dissolved in 4.8 mL of THF-*d*$_8$. Two drops of benzene were added to the solution as an internal standard for ^{1}H NMR integration. A 300 µL aliquot (0.0067 mol/L) was transferred to an NMR tube by syringe. $NaIO_4$ (44.8 mg, 0.200 mmol) was dissolved in 6.0 mL D_2O (0.033 mol/L). The solution of complex **2.1** was cooled in ice water. Then 300 µL (5.0 equiv) of the $NaIO_4$ solution was added to the solution of complex **2.1**. The reaction mixture was monitored by array ^{1}H NMR spectroscopy on a 500 MHz spectrometer at 10.7 °C. A ^{1}H NMR spectrum was acquired every 2 min. Integration of the methylene peak of complex **2.1** gave the variation in concentrations. Similar reactions were set up at –1.3, 22.7 and 34.7 °C. The time between every ^{1}H NMR spectrum in the array was adjusted according to the rate of the reaction. To ensure reproducibility, every concentration was repeated at least twice for a minimum of 3 total experiments under each set of conditions.

Oxygen labeling of reaction of $Cp^*W(O)_2(CH_2SiMe_3)$ (2.1) with $NaI^{18}O_4$. $NaIO_4$ (10.7 mg, 50.0 μmol) was dissolved in 300 μL of $H_2{}^{18}O$ and allowed to equilibrate for 1 hour at room temperature with sonication (the exchange of ^{18}O and ^{16}O under such condition is extremely fast).[51] Complex **2.1** (4.2 mg, 10 μmol) was dissolved in 300 μL of THF, and the solution was transferred to the $NaIO_4$ solution. After 20 minutes at room temperature, the color of the solution faded from pale yellow to colorless. A 3.0 μL aliquot of the reaction mixture was analyzed by GC/MS for $TMSCH_2OH$ content. The fragmentation pattern of $TMSCH_2OH$ produced from the reaction was compared to patterns for $TMSCH_2{}^{18}OH$ and $TMSCH_2{}^{16}OH$.

Reaction of $Cp^*W(O)_2(CH_2SiMe_3)$ (2.1) with PhIO. Complex **2.1** (4.2 mg, 10 μmol) and PhIO (8.0 mg, 30 μmol) was dissolved in 400 μL of 1,4-dioxane-d_8 in a J-Young tube. The tube was then taken out of the box and sonicated for 30 min. ^1H NMR spectroscopy was used to monitor the reaction.

Reaction of $Cp^*W(O)_2(CH_2SiMe_3)$ (2.1) with $[Bu_4N][IO_4]$. Complex **2.1** (4.3 mg, 10 μmol) and $[Bu_4N][IO_4]$ (12.9 mg, 30.0 μmol) were dissolved in 300 μL of dry THF-d_8. ^1H NMR spectroscopy was used to monitor the reaction at room temperature. No reaction was observed after 24 hours. D_2O (300 μL) was added to the reaction mixture. A ^1H NMR spectrum was acquired after 2 h, and quantitative formation of $TMSCH_2OH$ was observed.

Kinetics of water dependence in the reaction of $Cp^*W(O)_2(CH_2SiMe_3)$ (2.1) with $[Bu_4N][IO_4]$. A representative kinetic experiment is described. Complex **2.1** (32.0 mg 75.0 μmol) and $[Bu_4N][IO_4]$ (487mg, 1.12 mmol, 15 equiv) were dissolved in 6.0 mL of

THF-d_8. Two drops of benzene were added to the solution as an internal standard for ^{1}H NMR integration. A 400 µL aliquot was transferred to a J-Young tube. D_2O (5.0 µL, 50 equiv) was added to the solution of **2.1** and $[Bu_4N][IO_4]$ by syringe. The reaction mixture was then monitored by array ^{1}H NMR spectroscopy on a 500 MHz spectrometer at 50 °C. A ^{1}H NMR spectrum was acquired every 20 min. Integration of the methylene peak of complex **2.1** gave the variation in concentrations. Similar procedures were used to set up the reaction of **2.1** and 15 equiv of $[Bu_4N][IO_4]$ with 10.0, 20.0, 30.0, 40.0, 60.0 and 100 µL of D_2O (for the reaction with 60.0 and 100 µL of D_2O, the same amount of **2.1** and $[Bu_4N][IO_4]$ were dissolved in 300 µL of THF-d_8 instead of 400 µL). To ensure reproducibility, every concentration was repeated in triplicate.

Reaction of Cp*W(O)(η^2-O_2)(CH_2SiMe_3) (2) with NaOH. Complex **2.2** (4.3 mg, 10 µmol) was dissolved in 300 mL of THF-d_8 in an NMR tube. NaOH (1.2mg, 30 µmol) was dissolved in 300 µL of D_2O and transferred to the solution of complex **2.1**. The reaction mixture was monitored by ^{1}H NMR spectroscopy until completion. The production of $TMSCH_2OH$ was confirmed using two methods. First, 5 µL of the reaction mixture was analyzed by GC/MS, and $TMSCH_2OH$ was detected (and compared with GC/MS of an authentic sample). Second, 1 µL of $TMSCH_2OH$ was added to the reaction mixture. The intensity of the product peaks increased in ^{1}H NMR spectrum.

Kinetics of Cp*W(O)(η^2-O_2)(CH_2SiMe_3) (2.2) with NaOH. A representative kinetic experiment is described. Complex **2.1** (33.0 mg, 75.0 µmol) was dissolved in 4.5 mL of THF-d_8. Several milligrams of hexamethylbenzene were added to the solution as an internal standard for ^{1}H NMR integration. A 300 µL aliquot (0.0166 mol/L) was transferred to an NMR tube. NaOH (26.7 mg, 0.667 mmol) was dissolved in 2.0 mL D_2O

(0.33 mol/L). D_2O (225 μL) was added to the solution of complex **2.1** by syringe and cooled in ice water. Then 75 μL (5.0 equiv) of the NaOH solution was added to the complex **2.1** solution. The reaction mixture was then monitored by array ^{1}H NMR spectroscopy on a 500 MHz spectrometer at 10.7 °C. A ^{1}H NMR spectrum was acquired every 2 min. Integration of the Cp* methyl peak of complex **2.2** and the methylene peak of $TMSCH_2OH$ gave the variation in concentrations. Similar reactions were set up for 10.0, 15.0 and 20.0 equivalents of NaOH by adjusting the amounts of the D_2O and NaOH solution. The time between every ^{1}H NMR spectrum in the array was adjusted according to the rate of the reactions. To ensure reproducibility, every concentration was repeated in triplicate.

Eyring plot of reaction of Cp*W(O)(η^2-O_2)(CH_2SiMe_3) (2.2) with NaOH. A representative kinetic experiment is described. Complex **2.2** (35.2 mg, 80.4 μmol) was dissolved in 4.8 mL of THF-*d*$_8$. Several milligrams of hexamethylbenzene were added to the solution as an internal standard for ^{1}H NMR integration. A 300 μL aliquot (0.0166 mol/L) was transferred to an NMR tube by syringe. NaOH (20.2 mg, 0.505 mmol) was dissolved in 6.0 mL of D_2O (0.083 mol/L). The solution of complex **2.1** was cooled in ice water. Then 300 μL (5.0 equiv) of the NaOH solution was added to the solution of complex **2.1**. The reaction mixture was then monitored by array ^{1}H NMR spectroscopy on a 500 MHz spectrometer at 10.7 °C. A ^{1}H NMR spectrum was acquired every 2 min. Integration of the Cp* methyl peak of complex **2.2** and the methylene peak of $TMSCH_2OH$ gave the variation in concentrations. Similar reactions were set up at –1.3, 22.7 and 34.7 °C. The time between every ^{1}H NMR spectrum in the array was adjusted according to the rate of the reaction. To ensure reproducibility, every concentration was repeated in triplicate.

Oxygen labeling of reaction of Cp*W(O)(η^2-O_2)(CH_2SiMe_3) (2.2) with Li*OH. $H_2{}^{18}O$ (300 μL) was transferred to a vial and frozen in an ^{i}PrOH/dry ice bath. CH_3Li in diethyl ether solution (1M, 30 μL) was added to the frozen $H_2{}^{18}O$. The *i*PrOH/dry ice bath was then removed, and the mixture was warmed up to room temperature to generate the $Li^{18}OH$ in $H_2{}^{18}O$ solution. Complex **2.2** (4.3 mg, 10 μmol) was dissolved in 300 μL of THF, and the solution was added to the $Li^{18}OH$ solution. After 30 min at room temperature, a 3.0 μL aliquot of the reaction mixture was analyzed by GC/MS for $TMSCH_2OH$ content. The fragmentation pattern of $TMSCH_2OH$ from the reaction was compared to patterns for $TMSCH_2{}^{18}OH$ and $TMSCH_2{}^{16}OH$.

Reaction of Cp*W(O)(η^2-O_2)(CH_2SiMe_3) (2.2) with Brønsted acid. A representative reaction is described. Complex **2.2** (2.2 mg, 5.0 μmol) was dissolved in 400 μL of 1,4-dioxane-d_8 in a J-Young tube, and HCl in diethyl ether solution (1N, 15 μL) was added to the solution of **2.2**. The reaction was then monitored by ^{1}H NMR spectroscopy. The reaction was complete after approximately 2 d.

Reaction of Cp*W(O)$_2$(CH_2SiMe_3) (2.1) with H_2O_2/H^+. Complex **2.1** (4.2 mg, 10 μmol) was dissolved in 300 μL of 1,4-dioxane-d_8 in an NMR tube. Hydrochloric acid (35%, 3.0 μL, 33 μmol) and H_2O_2 (30%, 3.0 μL, 29 μmol) were added to 300 μL of D_2O. The mixture of H_2O_2 and HCl was then added to the complex **2.2** solution. ^{1}H NMR spectroscopy was used to monitor the reaction at room temperature.

Reaction of Cp*W(O)$_2$(CH$_2$SiMe$_3$) (2.1) with H$_2$O$_2$/OH$^-$. Complex **2.1 (**4.2 mg, 10 μmol**)** was dissolved in 300 μL of 1,4-dioxane-*d*$_8$ in an NMR tube. NaOH (1.2 mg, 30 μmol) was dissolved in 300 μL of D$_2$O, and H$_2$O$_2$ (30%, 3.0 μL, 29 μmol) was added to the NaOH solution. The mixture of H$_2$O$_2$ and NaOH was then added to the solution of **2.2**. ^{1}H NMR spectroscopy was used to monitor this reaction at room temperature.

Kinetics of reaction of Cp*W(O)$_2$(CH$_2$SiMe$_3$) (2.1) with H$_2$O$_2$/OH$^-$. Complex **2.1 (**4.2 mg, 10 μmol**)** was dissolved in 300 μL of THF-*d*$_8$ in an NMR tube. NaOH (2.0 mg, 50 μmol) was dissolved in 300 μL of D$_2$O and 5 μL (48 μmol) of 30% H$_2$O$_2$ solution was added to the NaOH solution. Both starting materials were cooled in ice water. The mixture of H$_2$O$_2$ and NaOH was then added to the solution of **2.2**. The reaction mixture was then monitored by array ^{1}H NMR spectroscopy on a 500 MHz spectrometer at –1.3 °C. A ^{1}H NMR spectrum was acquired every 26 s.

Kinetics of reaction of Cp*W(O)$_2$(CH$_2$SiMe$_3$) (2.1) and Cp*W(O)(η^2-O$_2$)(CH$_2$SiMe$_3$) (2.2) with H$_2$O$_2$/OH$^-$. A mixture of complex **2.1** (2.1 mg, 5.0 μmol) and complex **2.2 (**2.2 mg, 5.0 μmol**)** were dissolved in 300 μL of THF-*d*$_8$ in an NMR tube. NaOH (2.0 mg, 50 μmol) was dissolved in 300 μL of D$_2$O and 5 μL (48 μmol) of 30% H$_2$O$_2$ solution was added to the NaOH solution. Both starting materials were cooled in ice water. The mixture of H$_2$O$_2$ and NaOH was then added to the solution of **2.2**. The reaction mixture was then monitored by array ^{1}H NMR spectroscopy on a 500 MHz spectrometer at –1.3 °C. A ^{1}H NMR spectrum was acquired every 26 s.

2.5 References

(1) George A. Olah, A. M. *Hydrocarbon Chemistry*; 2nd ed.; John Wiley & Sons, 2003.

(2) Harold A. Wittcoff, B. G. R., Jeffery S. Plotkin *Industrial Organic Chemicals*; 2nd ed.; John Wiley & Sons, 2004.

(3) Conley, B. L.; Tenn, W. J.; Young, K. J. H.; Ganesh, S.; Meier, S.; Ziatdinov, V.; Mironov, O.; Oxgaard, J.; Gonzales, J.; Goddard, W. A.; Periana, R. A. In *Activation of Small Molecules*; Wiley-VCH Verlag GmbH & Co. KGaA: 2006, p 235.

(4) Crabtree, R. H. *J. Chem. Soc., Dalton Trans.* **2001**, 2437.

(5) Labinger, J. A.; Bercaw, J. E. *Nature* **2002**, *417*, 507.

(6) Labinger, J. A. *J. Mol. Catal. A: Chem.* **2004**, *220*, 27.

(7) Periana, R. A.; Bhalla, G.; Tenn III, W. J.; Young, K. J. H.; Liu, X. Y.; Mironov, O.; Jones, C. J.; Ziatdinov, V. R. *J. Mol. Catal. A: Chem.* **2004**, *220*, 7.

(8) Goldberg Karen, I.; Goldman Alan, S. In *Activation and Functionalization of C-H Bonds*; American Chemical Society: 2004.

(9) Conley, B. L.; Tenn Iii, W. J.; Young, K. J. H.; Ganesh, S. K.; Meier, S. K.; Ziatdinov, V. R.; Mironov, O.; Oxgaard, J.; Gonzales, J.; Goddard Iii, W. A.; Periana, R. A. *J. Mol. Catal. A: Chem.* **2006**, *251*, 8.

(10) Webb, J. R.; Bolaño, T.; Gunnoe, T. B. *ChemSusChem* **2011**, *4*, 37.

(11) Chepaikin, E. G. *Usp. Khim.* **2011**, *80*, 363.

(12) Shilov, A. E.; Shul'pin, G. B. *Chem. Rev.* **1997**, *97*, 2879.

(13) Stahl, S. S.; Labinger, J. A.; Bercaw, J. E. *Angew. Chem. Int. Ed.* **1998**, *37*, 2180.

(14) Lersch, M.; Tilset, M. *Chem. Rev.* **2005**, *105*, 2471.

(15) Conley, B. L.; Ganesh, S. K.; Gonzales, J. M.; Tenn, W. J.; Young, K. J. H.; Oxgaard, J.; Goddard, W. A.; Periana, R. A. *J. Am. Chem. Soc.* **2006**, *128*, 9018.

(16) Tenn, W. J.; Young, K. J. H.; Bhalla, G.; Oxgaard, J.; Goddard, W. A.; Periana, R. A. *J. Am. Chem. Soc.* **2005**, *127*, 14172.

(17) Feng, Y.; Lail, M.; Barakat, K. A.; Cundari, T. R.; Gunnoe, T. B.; Petersen, J. L. *J. Am. Chem. Soc.* **2005**, *127*, 14174.

(18) Figg, T. M.; Webb, J. R.; Cundari, T. R.; Gunnoe, T. B. *J. Am. Chem. Soc.* **2011**, *134*, 2332.

(19) Conner, D.; Jayaprakash, K. N.; Wells, M. B.; Manzer, S.; Gunnoe, T. B.; Boyle, P. D. *Inorg. Chem.* **2003**, *42*, 4759.

(20) Feng, Y.; Lail, M.; Foley, N. A.; Gunnoe, T. B.; Barakat, K. A.; Cundari, T. R.; Petersen, J. L. *J. Am. Chem. Soc.* **2006**, *128*, 7982.

(21) Hashiguchi, B. G.; Young, K. J. H.; Yousufuddin, M.; Goddard, W. A.; Periana, R. A. *J. Am. Chem. Soc.* **2010**, *132*, 12542.

(22) Kloek, S. M.; Heinekey, D. M.; Goldberg, K. I. *Angew. Chem. Int. Ed.* **2007**, *46*, 4736.

(23) Bercaw, J. E.; Hazari, N.; Labinger, J. A. *Organometallics* **2009**, *28*, 5489.

(24) Van Asselt, A.; Trimmer, M. S.; Henling, L. M.; Bercaw, J. E. *J. Am. Chem. Soc.* **1988**, *110*, 8254.

(25) Matsunaga, P. T.; Hillhouse, G. L.; Rheingold, A. L. *J. Am. Chem. Soc.* **1993**, *115*, 2075.

(26) Alsters, P. L.; Boersma, J.; van Koten, G. *Organometallics* **1993**, *12*, 1629.

(27) Brown, S. N.; Mayer, J. M. *J. Am. Chem. Soc.* **1994**, *116*, 2219.

(28) Koo, K.; Hillhouse, G. L.; Rheingold, A. L. *Organometallics* **1995**, *14*, 456.

(29) Brown, S. N.; Mayer, J. M. *J. Am. Chem. Soc.* **1996**, *118*, 12119.

(30) Pouy, M. J.; Milczek, E. M.; Figg, T. M.; Otten, B. M.; Prince, B. M.; Gunnoe, T. B.; Cundari, T. R.; Groves, J. T. *J. Am. Chem. Soc.* **2012**, *134*, 12920.

(31) Blackburn, T. F.; Labinger, J. A.; Schwartz, J. *Tetrahedron Lett.* **1975**, *16*, 3041.

(32) Brindley, P. B.; Scotton, M. J. *J. Chem. Soc., Perkin Trans. 2* **1981**, 419.

(33) Kamaraj, K.; Bandyopadhyay, D. *Organometallics* **1999**, *18*, 438.

(34) Vaughan, G. A.; Rupert, P. B.; Hillhouse, G. L. *J. Am. Chem. Soc.* **1987**, *109*, 5538.

(35) Abu-Omar, M. M.; Hansen, P. J.; Espenson, J. H. *J. Am. Chem. Soc.* **1996**, *118*, 4966.

(36) Legzdins, P.; Phillips, E. C.; Sanchez, L. *Organometallics* **1989**, *8*, 940.

(37) Mei, J.; Carsch, K. M.; Freitag, C. R.; Gunnoe, T. B.; Cundari, T. R. *J. Am. Chem. Soc.* **2013**, *135*, 424.

(38) Kim, G. S.; Huffman, D.; DeKock, C. W. *Inorg. Chem.* **1989**, *28*, 1279.

(39) Chisholm, M. H.; Folting, K.; Huffman, J. C.; Kirkpatrick, C. C. *Inorg. Chem.* **1984**, *23*, 1021.

(40) Richardson, D. E. In *Kinetica98*; Department of Chemistry, University of Florida: 1998.

(41) Kassim, A. Y.; Sulfab, Y. *Inorg. Chem.* **1981**, *20*, 506.

(42) Wang, W.-D.; Espenson, J. H. *J. Am. Chem. Soc.* **1998**, *120*, 11335.

(43) Hashiguchi, B. G.; Bischof, S. M.; Konnick, M. M.; Periana, R. A. *Acc. Chem. Res.* **2012**, *45*, 885.

(44) Lee, C.; Yang, W.; Parr, R. G. *Physical Review B* **1988**, *37*, 785.

(45) Becke, A. D. *J. Chem. Phys.* **1993**, *98*, 5648.

(46) Becke, A. D. *J. Chem. Phys.* **1993**, *98*, 1372.

(47) Frisch, M. J., G.W. Trucks, H.B. Schlegel, G.E. Scuseria, M.A. Robb, J.R. Cheeseman, G. Scalmani, V. Barone, B. Mennucci, G.A. Petersson, H. Nakatsuji, M. Caricato, X. Li, H.P. Hratchian, A.F. Izmaylov, J. Bloino, G. Zheng, J.L. Sonnenberg, M. Hada, M. Ehara, K. Toyota, R. Fukuda, J. Hasegawa, M. Ishida, T. Nakajima, Y. Honda, O. Kitao, H. Nakai, T. Vreven, J. Montgomery, J. A., J.E. Peralta, F. Ogliaro, M. Bearpark, J.J. Heyd, E. Brothers, K.N. Kudin, V.N. Staroverov, R. Kobayashi, J.R. Normand, K., A. Rendell, J.C. Burant, S.S. Iyengar, J. Tomasi, M. Cossi, N. Rega, N.J. Millam, M. Klene, J.E. Knox, J.B. Cross, V. Bakken, C. Adamo, J. Jaramillo, R. Gomperts, R.E. Stratmann, O. Yazyev, A.J. Austin, R. Cammi, C. Pomelli, J.W. Ochterski, R.L. Martin, K. Morokuma, V.G. Zakrzewski, G.A. Voth, P. Salvador, J.J. Dannenberg, S. Dapprich, A.D. Daniels, Ö. Farkas, J.B. Foresman, J.V. Ortiz, J. Cioslowski, D.J. Fox, Gaussian; Revision B.01 ed.; Gaussian Inc: Wallinford, CT, 2009.

(48) Stevens, W. J.; Basch, H.; Krauss, M. *J. Chem. Phys.* **1984**, *81*, 6026.

(49) Stevens, W. J.; Krauss, M.; Basch, H.; Jasien, P. G. *Can. J. Chem.* **1992**, *70*, 612.

(50) Cossi, M.; Rega, N.; Scalmani, G.; Barone, V. *J. Comput. Chem.* **2003**, *24*, 669.

(51) Pecht, I.; Luz, Z. *J. Am. Chem. Soc.* **1965**, *87*, 4068.

3 Oxygen Atom Insertion into Iron(II) Phenyl and Methyl Bonds

3.1 Rationale for Study of Oxygen Atom Insertion into Fe–C bonds

The selective catalytic oxidation of hydrocarbons is an important but challenging process.[1-14] As discussed in Chapter One, transition metal catalysts for the partial oxidation of alkanes to form alcohols must be able to perform two key steps: C–H bond activation and C–O bond formation. One strategy is using the Pt-based Shilov systems, which perform the C–H bond activation and C–O bond formation at two different oxidation state of the catalysts. The stringent requirements for the metal centers and oxidants limit the utility of this system.

Another strategy we discussed involves C–H activation by metal–alkoxide (M–OR) complexes and C–O bond formation involves net oxygen atom insertion into metal–alkyl bonds (Scheme 3.1). Two pathways for the C–O bond formation through O-atom insertion into M–R bonds have been introduced. One pathway is an organometallic Baeyer-Villiger (OMBV) type reaction,[6,15-20] involving the migration of the hydrocarbyl ligand (R) to the coordinated O atom of YO to form M–OR with the release of Y group (Scheme 3.2). The other pathway proceeds through the migration of the R group to a M=O intermediate. Since the activation of C–H bonds via 1,2-addition across M–X (X = OR, NR, NR_2) bonds has been reported,[15,21-27] the development of catalytic cycles is potentially viable (Scheme 3.1).

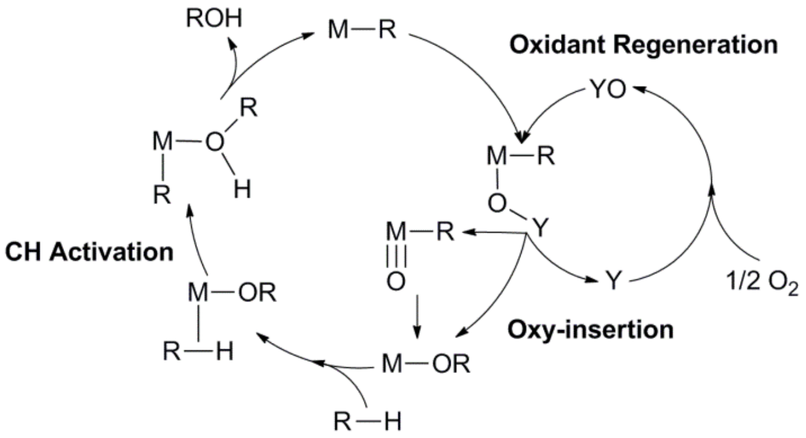

Scheme 3.1. Proposed pathways for partial oxidation of hydrocarbons involving oxygen atom insertion into a M–R bond and 1,2-CH-Addition across a M–OR bond.

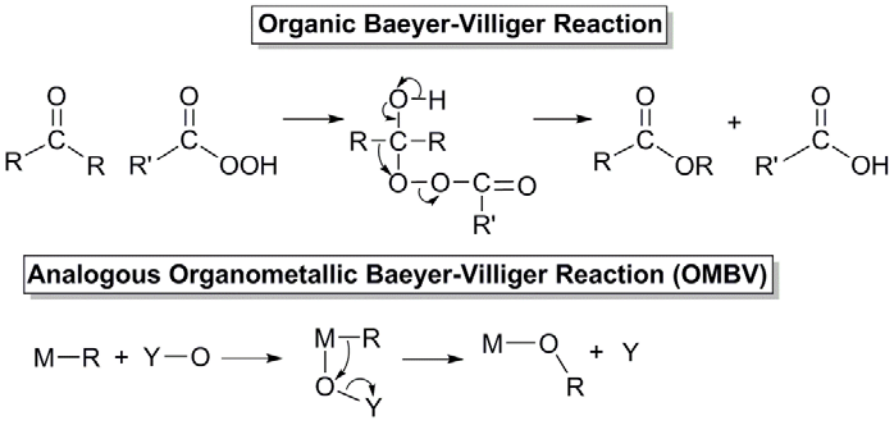

Scheme 3.2. Generic mechanisms for the organic Baeyer-Villiger reaction and the analogous organometallic Baeyer-Villiger reaction (OMBV).

Insertions of oxygen atoms into M–C bonds via non-radical routes are rare. Bercaw and co-workers reported oxygen atom insertion into Ta(V) hydrocarbyl bonds int the presence of elctrophiles.[28] Espenson and co-workers reported that methyltrioxorhenium (MTO) reacts with oxidants to release methanol.[29] Periana, Goddard and co-workers extended the MTO reaction and reported facile conversion of Re–Me bond of MTO to a Re–OMe bond upon treatment of various oxidants (H_2O_2, PyO, PhIO and IO_4^-).[15] They studied the mechanism of these reactions experimentally and computationally and pointed out that the O-atom insertion in MTO does not likely occur by the migration of the methyl ligand to the oxo ligand of MTO. An organometallic Baeyer-Villiger (OMBV) involving the migration of the nucleophilic methyl ligand to the coordinated O atom of the oxidants to the MTO was proposed (Scheme 3.3). This O-atom insertion into MTO is the first well-defined OMBV reaction. It was proposed that the reaction was facilitated by the migration of the nucleophilic polarized $–R^{\delta-}$ group to the electrophilic bound O-atom of YO (Scheme 3.4).

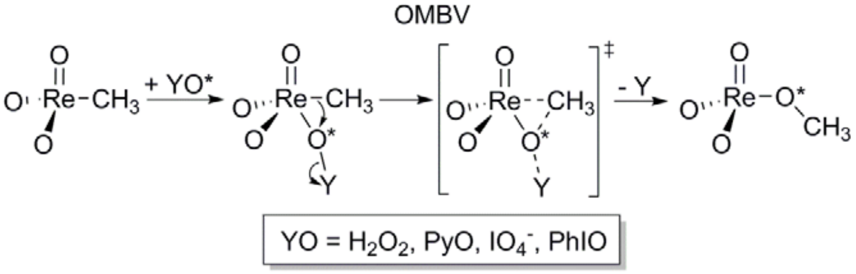

Scheme 3.3. Proposed mechanism for the O-atom insertion into MTO with various oxidants.

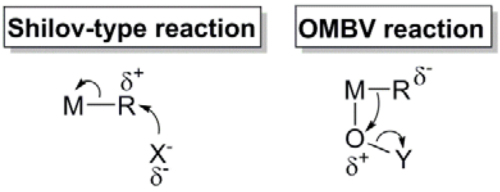

Scheme 3.4. Electronic properties for the C–X bond formation in the Shilov-type systems and C–O bond formation via organometallic Baeyer-Villiger reaction (OMBV).

Extension of this O-atom insertion reaction to the Re–aryl complexes also results in a faster formation of the O-atom insertion products than MTO with oxidants.[16] The faster migration of more nucleophilic Ar group than the Me group to the Re–OY ligand is consistent with the $R^{\delta-}$ to $M–O^{\delta+}–Y$ migration analysis.

We later attempted to extend the OMBV type reactions to a range oxidants and M–R complexes and to elucidate the roles of nucleophilicity of the $M–C^{\delta-}$ bond or the electrophilicity of the bound $O^{\delta+}$ in the O-atom insertion reactions. With no success of the attempt to extended the OMBV reaction to the late transition Rb^{III}– and Pt^{II}–R complexes,[30] we moved our search to the left of the periodic table and reported the second OMBV type O-atom insertion reaction into W^{VI}–R bonds.[20] $Cp^*W(O)_2(CH_2SiMe_3)$ was observed to react with 1 equivalent of $NaIO_4$ in 1:1 THF-d_8:D_2O or 1:1 1,4-dioxane-d_8:D_2O (v:v) to produce quantitative $TMSCH_2OH$ at room temperature. An OMBV type mechanism was proposed involves periodate coordinates to the W complex, followed by concerted migration of the alkyl ligand to the coordinated oxygen atom of IO_4^- and loss of IO_3^-. Protonation of W–OR generates the alcohol product (Scheme 3.5).

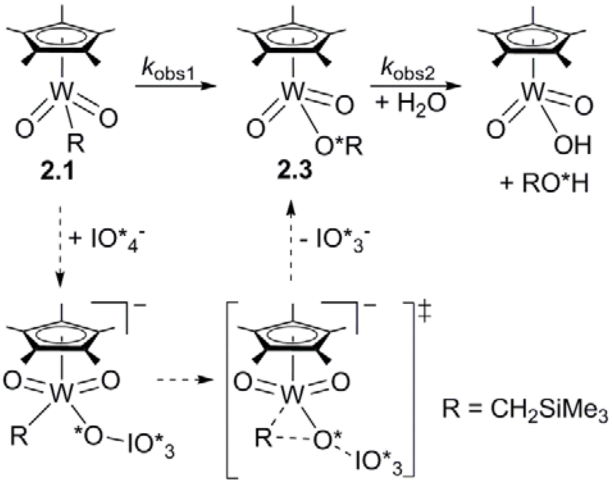

Scheme 3.5. Proposed mechanism for the formation of $TMSCH_2OH$ from the reaction of $Cp^*W(O)_2(CH_2SiMe_3)$ (**2.1**) and $NaIO_4$ in 1:1 THF-d_8:D_2O (v:v).

With the previous result of the extension of the OMBV reaction form the Re^{VII} to the late 4d and 5d Rh^{III} and Pt^{II}–R and middle transition W^{VI} complexes, it more likely that the nucleophilicity of the M–$C^{\delta-}$ bond plays a more important role than the electrophilicity of the bound $O^{\delta+}$ does in the OMBV reactions for O-atom insertion.

Neither of the d^0 Re^{VII} or W^{VI}–R active C–H bond of hydrocarbons, we more sought to focus our investigation on the late d^6 and d^8 3d M–R complexes. Additionally, computational studied by Cundari Group suggested low energy barriers for the O-atom insertion into late 3d M–R bonds.[31]

The other pathway for the O-atom insertion into M–R bonds proceeds through the migration of the R group to a M=O intermediate. Very few examples of well-defined alkyl or aryl migration to oxo ligands to form M–OR products have been reported. Brown and Mayer reported high valent Re^{VII}–oxo complexes that undergo insertion of an oxo ligand, probably best considered as an electrophilic oxene type ligand, into Re–Ph bonds under photolytic and thermal conditions.[32-34] In 1994, they first reported the C–H activation by Re^V complex TpRe(O)(Cl)I under photolysis to form TpRe(O)(Cl)Ph, which was followed by a photolytic phenyl-to-oxo migration to produce the O-atom insertion product TpRe(OPh)(Cl)L (L = Py, MeCN, Me_3PO) in the presence of L (Scheme 3.6).

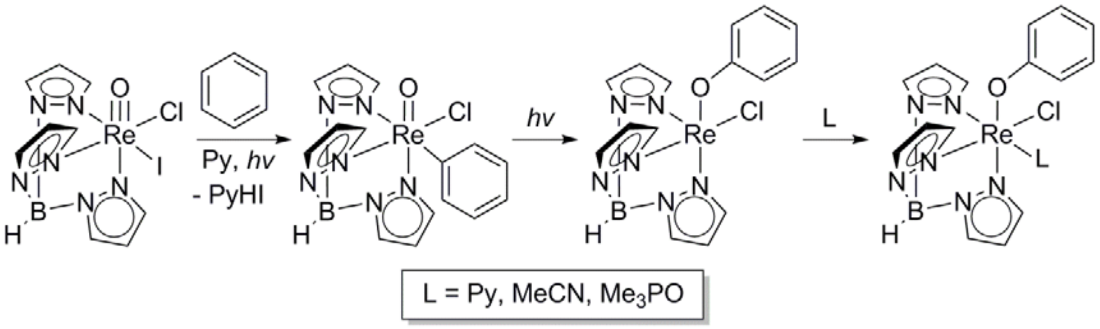

Scheme 3.6. O-atom insertion into Re–Ar bonds by migration of Ar to Re^V=O.

Brown and Mayer later synthesized the Re^{VII}-dioxo-aryl complex $[TpRe(O)_2](Ph)[OTf]$ from the reaction of the Re^V-oxo and pyridine-*N*-oxide at low temperature.[34] Phenyl-to-oxo migration to generate a Re^{VII}-phenoxide complex was observed from this Re^{VII}-dioxo-phenyl complex at room temperature. When using Me_2SO, the adduct $[TpRe(O)(OSMe_2)Ph][OTf]$ is generated and in a rapid equilibrium with the dioxo complex via dissociation of Me_2S. Phenyl-to-oxo migration was observed is this case to produce the phenoxide complex $[TpRe(O)(OSMe_2)(OPh)][OTf]$ (Scheme 3.7).[34] It was proposed that the strong oxo-to-Re π-donation enhances the electrophilicity of the oxo ligand, which facilitates the nucleophilic attack of the $R^{\delta-}$ group to the $M{\equiv}O^{\delta+}$ ligand to produce the phenyl-to-oxo migration product (Scheme 1.22). This $R^{\delta-}$ to $M{\equiv}O^{\delta+}$ migration is similar as the $R^{\delta-}$ to $M–O^{\delta+}–Y$ migration in the OMBV reaction, which are different from the nucleophilic attack of X^- to the $M–R^{\delta+}$ in the Shilov-type reaction (see above, Scheme 3.8). Similar mechanisms have been proposed for the O-atom insertion into Ni^{II} and Pd^{II}–C bonds.[35-42]

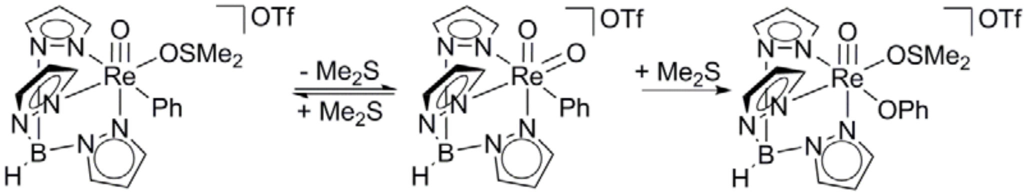

Scheme 3.7. O atom insertion into Re–Ar bonds by migration of Ar to Re=O.

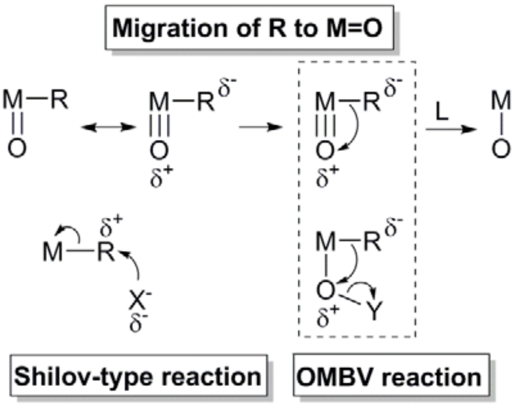

Scheme 3.8. Comparison of the migrations in the R to M=O, Organometallic Baeyer-Villiger (OMBV) reaction and Shilov-type reaction.

A transition for the nucleophilicity of the M–C$^{\delta-}$ bond or the electrophilicity of the bound O$^{\delta+}$ in the periodic table is shown in Scheme 3.9. Since OMBV reaction and R to M=O migration both prefer metal–alkyls that are more M–C$^{\delta-}$ polarized and have the same trend in metal selectivity, they can be competitive. If our search on the O-atom insertion into late 3d M–R complexes succeeds, which pathway will it undergo?

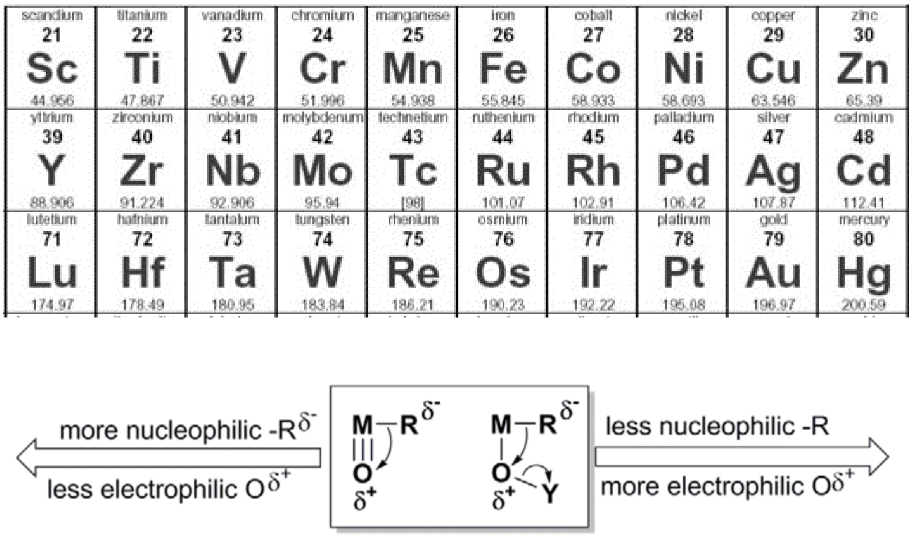

scandium 21 Sc 44.956	titanium 22 Ti 47.867	vanadium 23 V 50.942	chromium 24 Cr 51.996	manganese 25 Mn 54.938	iron 26 Fe 55.845	cobalt 27 Co 58.933	nickel 28 Ni 58.693	copper 29 Cu 63.546	zinc 30 Zn 65.39
yttrium 39 Y 88.906	zirconium 40 Zr 91.224	niobium 41 Nb 92.906	molybdenum 42 Mo 95.94	technetium 43 Tc [98]	ruthenium 44 Ru 101.07	rhodium 45 Rh 102.91	palladium 46 Pd 106.42	silver 47 Ag 107.87	cadmium 48 Cd 112.41
lutetium 71 Lu 174.97	hafnium 72 Hf 178.49	tantalum 73 Ta 180.95	tungsten 74 W 183.84	rhenium 75 Re 186.21	osmium 76 Os 190.23	iridium 77 Ir 192.22	platinum 78 Pt 195.08	gold 79 Au 196.97	mercury 80 Hg 200.59

Scheme 3.9. Transitions for the nucleophilicity of the M–C$^{\delta-}$ bond or the electrophilicity of the bound O$^{\delta+}$ in the periodic table.

Cundari group (University of North Texas) studied the comparison between the OMBV pathway and R to M=O migration pathway for the O-atom insertion into late 3d M–R complexes.[43] Relatively lower active energy barriers are calculated for the R to M=O migration pathway. Fe–R complexes possess the lowest energy barrier for R to M=O migration.[43] Moreover, enzymes perform C–H oxidation via high-valent Fe–oxo complexes, which initiate net H atom abstraction to generate a transient radical.[44-46] A C–O bond forming "rebound" step followed by alcohol dissociation completes the conversion (Scheme 3.10).[47]

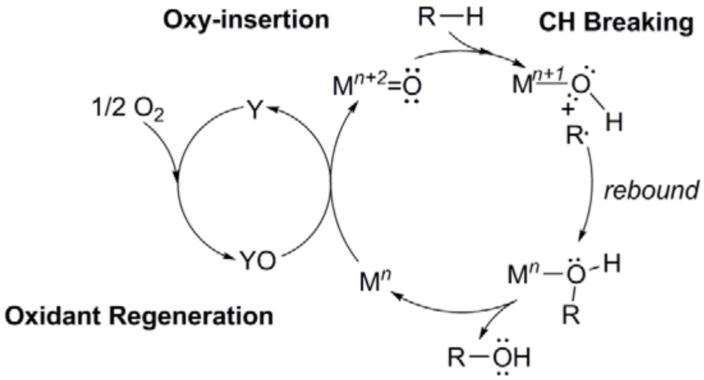

Scheme 3.10. Hydrocarbon functionalization involving a C–H bond breaking by M=O step and a C–O bond forming "rebound" step.

The Gunnoe Group recently reported facile C–H activation by Cp*Fe(CO)(NCMe)Ph (Cp* = 1,2,3,4,5-pentamethylcyclopentadienyl) (**3.1**).[48] Steven Kalman working in our group demonstrated C–H activation by complex **3.1** for aromatic bonds including benzne, furan and thiophene (Scheme 3.11). The mechanism involves dissociation of the CH_3CN ligand, coordination of the arenes to Fe and C–H activation via σ-bond metathesis.

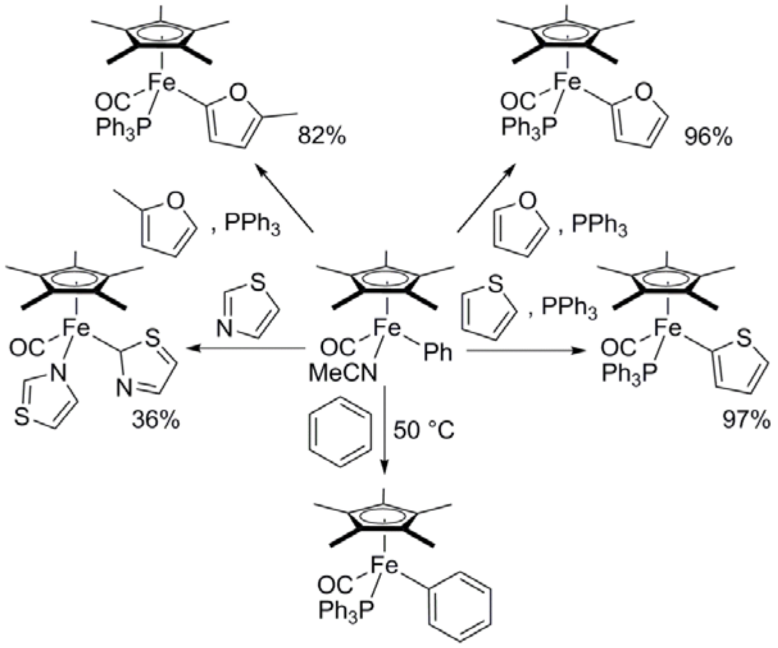

Scheme 3.11. Activation of aromatic C–H bond by Cp*Fe(CO)(NCMe)Ph (**3.1**).

Having observed C–H activation by Cp*Fe(L)(L')Ph complexes, this class of complex was deemed a good starting point to pursue Fe-mediated C–O bond formation. A computational study, performed in collaboration with the Cundari group (University of North Texas), of metal-mediated C–O bond formation by Cp*Fe(CO)(NCMe)R (R = Me or Ph) indicated that O-atom insertion to form Fe–OR should be kinetically feasible.[43] The calculations reveal that the pathway via the formation of the Fe=O intermediate and immigration of the R group to the oxo group to form the M–OR has the lowest activation barrier (22 kcal/mol) (Scheme 3.12). Consistent with the prediction based on theory, herein we report the observation of conversion of Fe–R bonds and oxidants into alcohols. The major contents of this chapter are from our research article published in *Organometallics*.[49] Daniel Purdue and Professor did the computation study is this chapter, Steven Kalman initiated the synthesis of complexes 3.1 and 3.2. Michal Sabat worked on the single crystal X-ray diffraction.

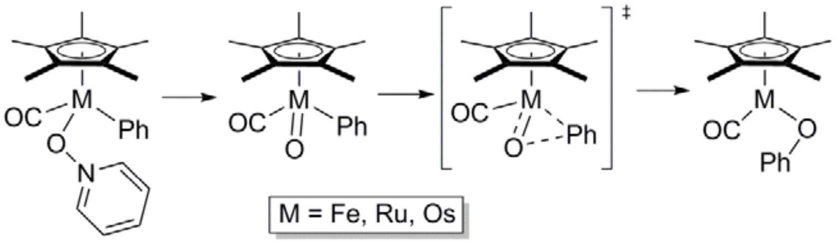

Scheme 3.12. O-atom insertion into Cp*M(CO)(NCMe)R via formation of the M=O.

3.2 Results and Discussion

3.2.1 The Reaction of Cp*Fe(CO)(NCMe)Ph (3.1) with Oxidants

The reaction of Cp*Fe(CO)(NCMe)Ph (**3.1**) with various oxidants results in either decomposition or the production of benzoic acid (eq 3.1 and Table 3.1). For some oxidants, the Cp* ligand is oxidized to 1,2,3,4-tetramethylfulvene (Table 3.1, entries 1-6). Benzene is formed many cases (Table 3.1, entries 1-3 and 5-8), which is presumed to result from protonation (protic oxidants) of the Fe–Ph bond or Fe–Ph bond homolysis from an oxidized intermediate (likely Fe^{III}).[50] Although previous calculations showed that the formation of Cp*Fe(CO)(NCMe)OPh from reaction of Cp*Fe(CO)(NCMe)Ph and pyridine-*N*-oxide should be kinetically accessible.[43] The formation of benzoic acid suggested that CO insertion into the Fe–Ph bond apparently competes with O atom insertion. Consistent with this suggestion, a computational study predicts a $\Delta G^\ddagger$ of 12.7 kcal/mol for CO insertion into the Fe–Ph bond of Cp*Fe(CO)(NCMe)Ph (Scheme 3.13). In contrast, the overall calculated $\Delta G^\ddagger$ for conversion of Cp*Fe(CO)(NCMe)Ph and pyridine-*N*-oxide to Cp*Fe(CO)(OPh) is approximately 33.1 kcal/mol. Because of the competition of CO insertion, the reactivity with a Cp*Fe(L)$_2$R complex without a CO co-ligand was probed.

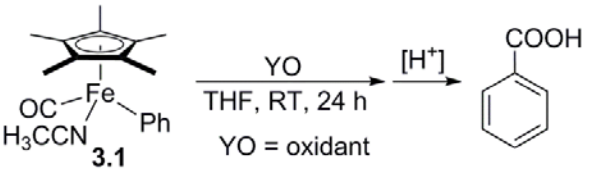

(3.1)

Table 3.1. Reaction conditions, products and yields for the reactions of Cp*Fe(CO)(NCMe)Ph (**3.1**) with various oxidants.[a]

no.	Oxidant	T (°C)	t (h)	PhCOOH (%)[b]	benzene (%)	fulvene[c] (%)
1	O_2 (15 psi)	21	24	60	20	> 90
2	Me_3NO	21	0.5	0	> 90	> 90
3	PyO	60	24	0	10	10
4	PyO	hv	1.5	0	0	15

5	*m*-CPBA[d]	21	0.5	0	> 90	<10
6	^{n}BuN$_4$IO$_4$	21	0.5	10	10	> 90
7	H_2O_2	21	0.5	60	<10	0
8	^{t}BuOOH	21	24	0	90	0

[a] Reactions are with 3 equiv of oxidant in THF-d_8 in NMR tubes. [b] Yields of products are based on integration of ^{1}H NMR spectra versus an internal standard. [c] Fulvene = 1,2,3,4-tetramethylfulvene. [d] *m*-CPBA = *meta*-chloroperoxybenzoic acid.

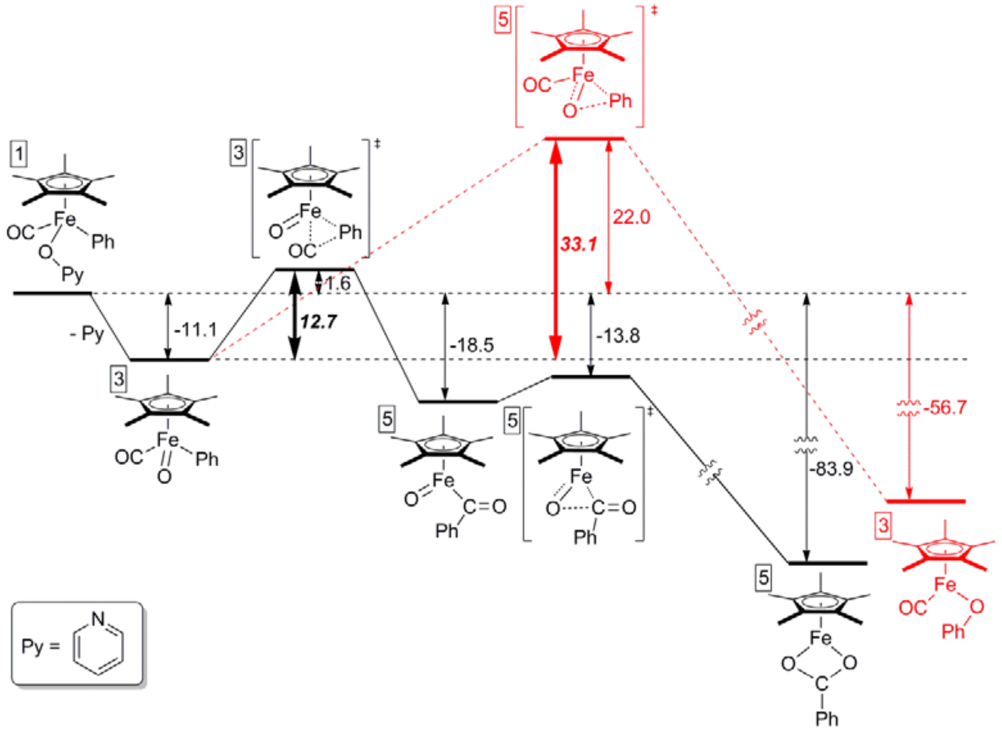

Scheme 3.13. Calculated (Cundari group, U. of North Texas) free energies for the reaction of Cp*Fe(CO)(NCMe)Ph (**3.1**) and pyridine-*N*-oxide (PyO) in THF-d_8. Numbers are free energies (kcal/mol) relative to Cp*Fe(CO)(ONMe$_3$)Ph. Lowest energy spin states are labeled in the boxes on the top left of structures.

3.2.2 The reaction of Cp*Fe(P(OCH$_2$)$_3$CEt)$_2$Ph (3.3) with Me$_3$NO

Steven Kalman in Gunnoe group synthesized Cp*Fe(P(OCH$_2$)$_3$CEt)$_2$Ph (**3.3**). The reaction of [(TMEDA)FeCl$_2$]$_n$ (n = 1, 2) (TMEDA = tetramethylethylenediamine) with $P(OCH_2)_3CEt$ and Cp*Li produces $Cp^*Fe[P(OCH_2)_3CEt]_2Cl$ (**3.2**) in 70% isolated yield. Although the experimental elementary analysis (EA) data did not match the theoretic value, a ^1H NMR spectrum of **3.2** is shown in Figure 3.1. Complex **3.2** reacts with PhLi to give $Cp^*Fe(P(OCH_2)_3CEt)_2Ph$ (**3.3**) in 62% isolated yield (Scheme 3.14). Complex **3.3** was characterized by single crystal X-ray diffraction and the details are shown in Figure 3.2.

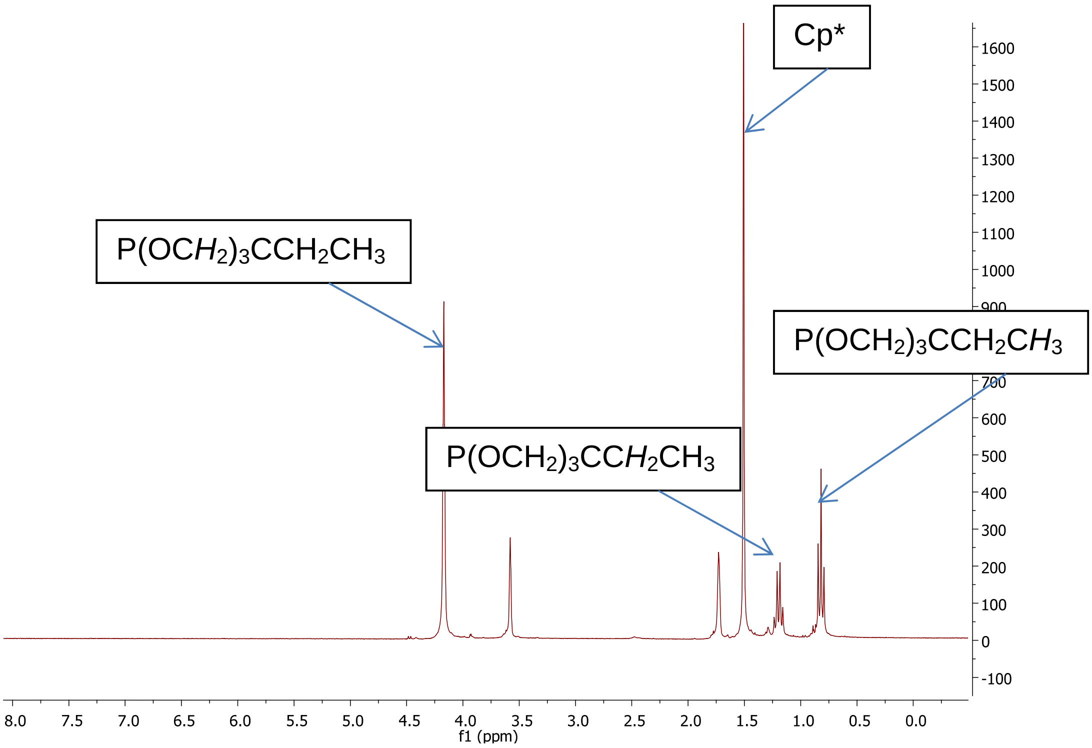

Figure 3.1. ^1H NMR spectrum of $Cp^*Fe(P(OCH_2)_3CEt)_2Cl$ (**3.2**) in THF-d_8.

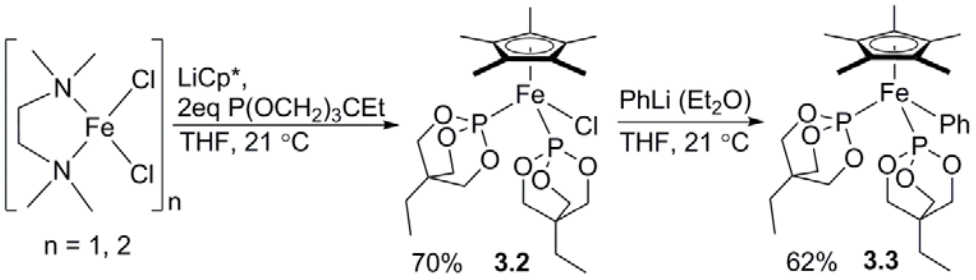

Scheme 3.14. Synthesis of $Cp^*Fe(P(OCH_2)_3CEt)_2Ph$ (**3.3**).

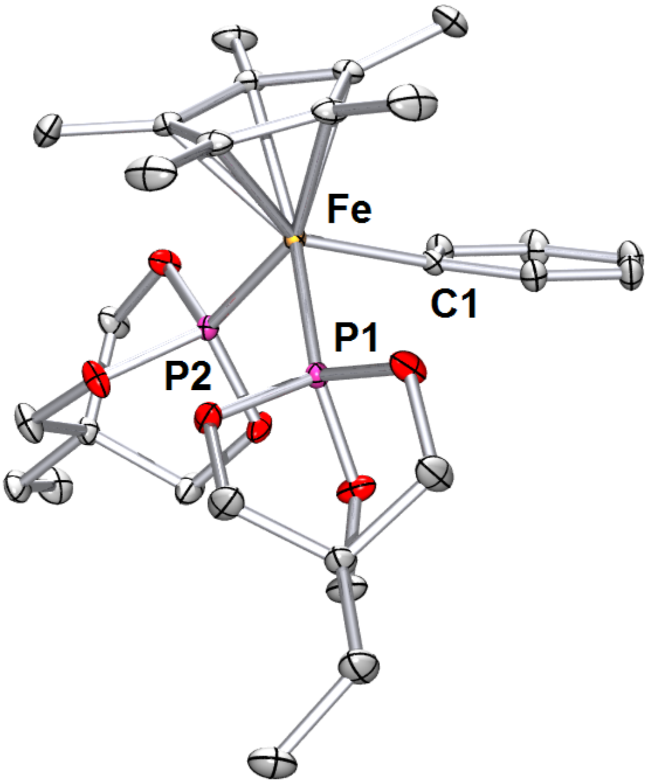

Figure 3.2. ORTEP drawing of Cp*Fe(P(OCH$_2$)$_3$CEt)$_2$Ph (**3.3**) (50% probability ellipsoids; H atoms omitted). Selected bond lengths (Å): Fe–C1 1.9993(2), Fe–P1 2.0854(4), Fe–P2 2.0996(4). Selected bond angles (°): C1–Fe–P1 92.91(4), C1–Fe–P2 92.73(4), P1–Fe–P2 91.65(2).

Under ambient light, monitoring the reaction of Cp*Fe(P(OCH$_2$)$_3$CEt)$_2$Ph (**3.3**) with excess Me$_3$NO in THF-*d*$_8$ by ^{1}H NMR spectroscopy reveals the transformation of **3.3** to several products after four days at room temperature. The addition of Brønsted acid (*e.g.*, H$_2$O or HCl) results in the production of PhOH in 70% yield (^{1}H NMR) relative to **3.3**. Phenol production has been confirmed by ^{1}H NMR spectroscopy and GC-MS. The control reaction of **3.3** and water (THF-*d*$_8$, room temperature) produces benzene without observation of phenol. During the reaction of **3.3** with Me$_3$NO, prior to addition of acid, the phenyl ligand of **3.3** is converted to a new species that has been identified as

PhOH·ONMe$_3$. The addition of Me$_3$NO to a solution of PhOH gives the same NMR spectra (Figure 3.3-3.5).

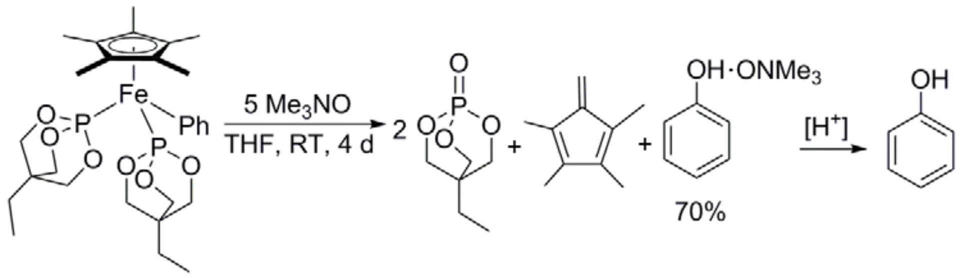

3.3

(3.2)

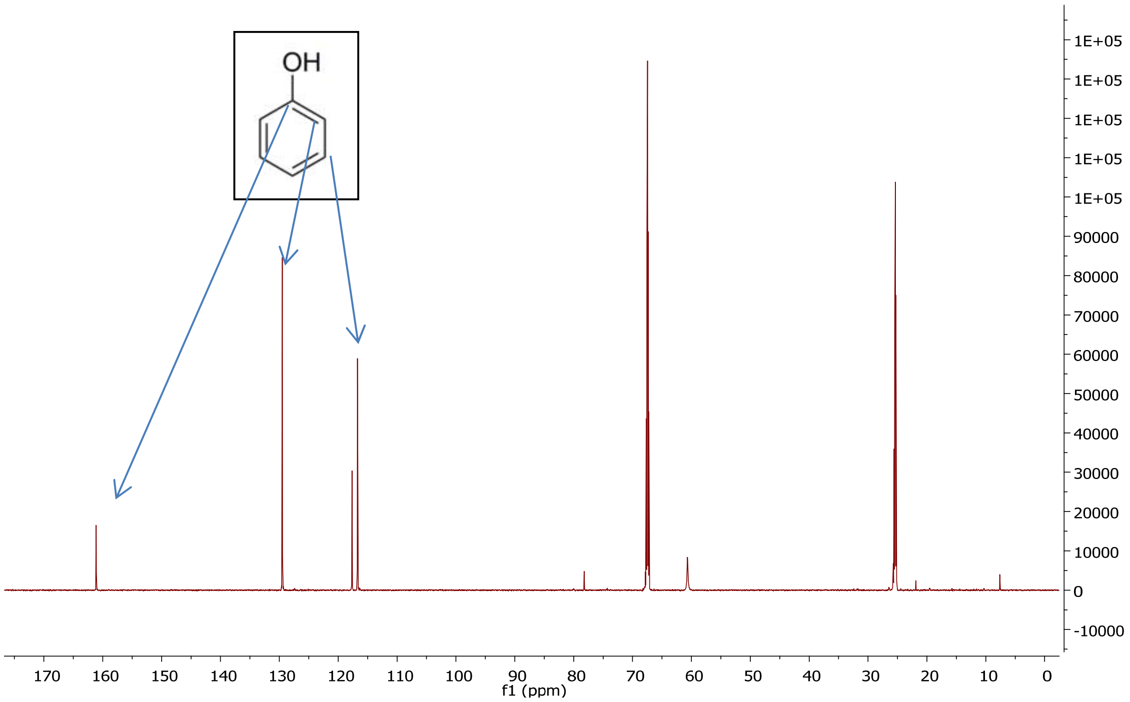

Figure 3.3. ^{13}C NMR spectrum of PhOH·OMe$_3$ from the reaction of Cp*Fe(P(OCH$_2$)$_3$CEt)$_2$Ph (**3.3**) with 5 *equiv* of Me$_3$NO in THF-d_8.

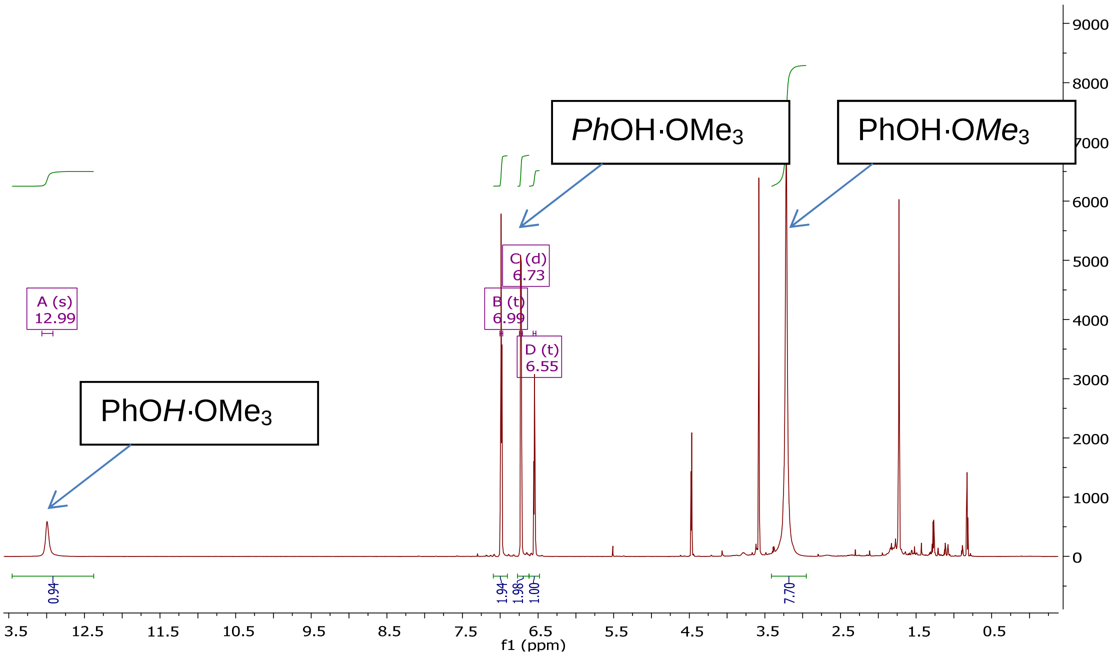

Figure 3.4. ^{1}H NMR spectrum of PhOH·ONMe$_3$ generated from the reaction of Cp*Fe(P(OCH$_2$)$_3$CEt)$_2$Ph (**3.3**) with 5 equiv of Me$_3$NO in THF-d_8.

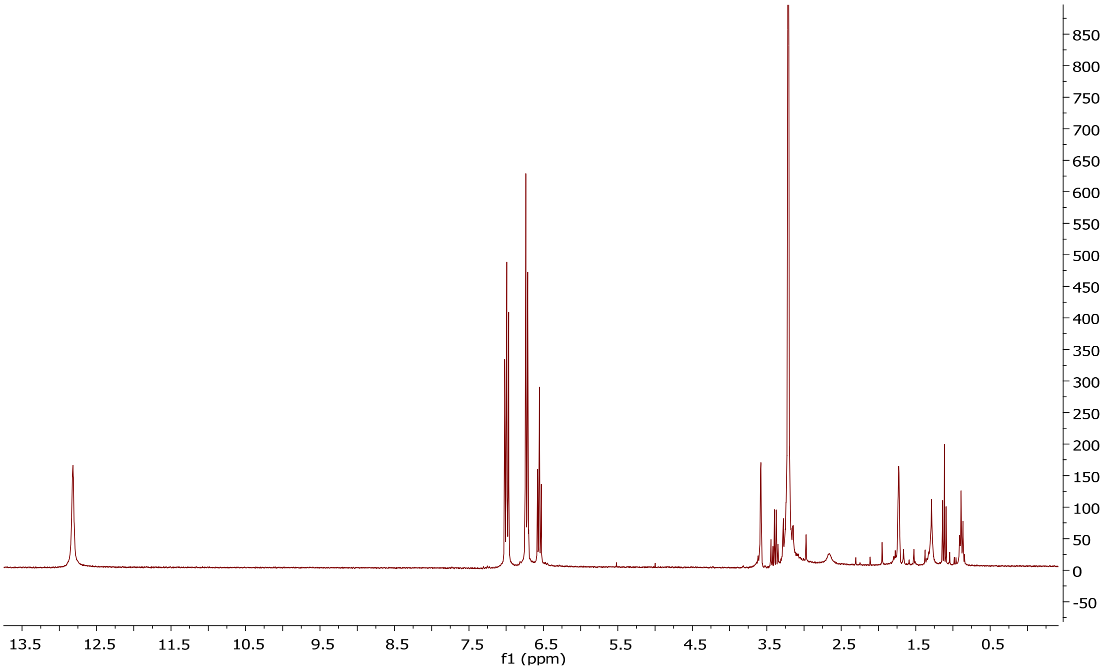

Figure 3.5. ^{1}H NMR spectrum of PhOH·OMe$_3$ from the reaction of PhOH with excess Me$_3$NO in THF-d_8.

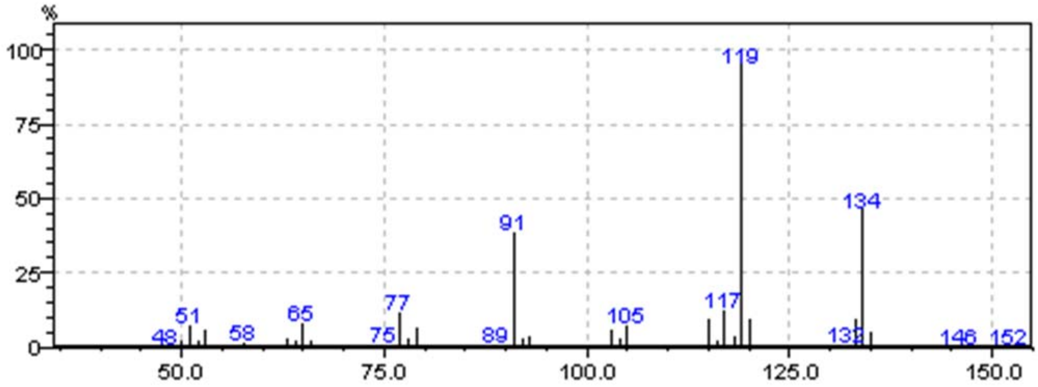

Figure 3.6. Mass spectrum for 1,2,3,4-tetramethylfulvene ($C_{10}H_{14}$, MW = 134) from the reaction of Cp*Fe(P(OCH_2)$_3$CEt)$_2$Ph (**3.3**) with excess Me_3NO in THF-*d*$_8$.

For the reaction of **3.3** with Me_3NO, in addition to PhOH production, the Cp* ligand is oxidized to 1,2,3,4-tetramethylfulvene (Figure 3.6) and the phosphite ligands are oxidized to phosphate as indicated by a resonance in the ^{31}P NMR spectrum at –8.2 ppm.[51] A brown precipitate is also observed, but we have been unable to characterize this material. Thus, the reaction of **3.3** and Me_3NO results in the oxidation of Cp*, both P(OCH_2)$_3$CEt ligands and the phenyl ligand (eq 3.2). When **3.3** is treated with only 1 equiv of Me_3NO, partial conversion of **3.3** to the same products occurs.

No reaction is observed for **3.3** and Me_3NO after one week in the absence of light even upon heating at 80 °C. When photolyzed, the reaction of **3.3** and Me_3NO is complete within 2 h to produce PhOH·$ONMe_3$ (compared to 4 days in ambient light). The addition of Brønsted acid (*e.g.,* H_2O or HCl) to the reaction mixture results in the formation of PhOH (eq 3.3). Further studies showed that light is required for dissociation of a phosphite ligand (see below) in the conversion of **3.3** and Me_3NO.

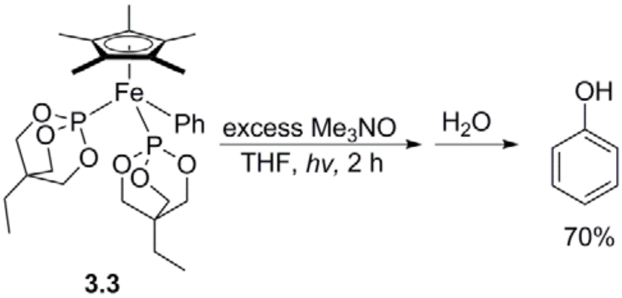

3.3

(3.3)

We first considered a radical pathway for the conversion of the Fe–Ph bond. The Fe^{II}–Ph might be oxidized by Me_3NO to produce Fe^{III}–Ph which then undergoes bond homolysis to give Fe^{II} and Ph•, oxidation of the Ph• generate PhOH. However, no significant change in the product or rate is observed when the same reaction is performed in the presence of radical traps such as TEMPO [(2,2,6,6-tetramethylpiperidin-1-yl)oxyl] or 1,4-cyclohexadiene. Since TEMPO is known to trap phenyl radical,[52] this suggests that free phenyl radical is not formed in the reaction of **3.3** with Me_3NO. However, these experiments cannot rule out a short-lived phenyl radical that rapidly recombines with an Fe–O moiety. We also considered a pathway involving decomposition of complex **3.3** in the presence of light to form an unobserved Fe catalyst (*e.g.*, Fe nanoparticles), which then catalyzes the oxidation of benzene to phenol. Complex **3.3** and excess Me_3NO were reacted in the presence of excess benzene, but the catalytic conversion of benzene to phenol was not observed. We also performed this reaction in the presence of excess 1,4-cyclohexadiene (to provide a source of hydrogen) and, again, did not observe catalytic production of PhOH. Thus, if an *in situ* Fe catalyst for benzene oxidation is formed, it is limited to < 1 turnover. While they do not definitively eliminate *in situ* formation of an Fe catalyst from consideration, these experimental results are most consistent with a stoichiometric oxidation reaction.

It was hypothesized that light might promote $P(OCH_2)_3CEt$ dissociation from **3.3** as a key step for the formation of PhOH. In the dark, there is no reaction between complex **3.3** and excess PMe_3 (THF-d_8) after one week at 80 °C. In contrast, complex **3.3** is quantitatively converted to $Cp^*Fe(P(OCH_2)_3CEt)(PMe_3)Ph$ (**3.4**) within 2 hours under photolysis at room temperature (eq 3.4). Under pseudo-first-order conditions (*i.e.*, excess PMe_3), complex **3.2** was treated with a series of concentrations of PMe_3 in THF-d_8 under photolysis, and a first-order rate constant for the disappearance of complex **3.3** was determined for each reaction. Sample kinetics plots reactions of $Cp^*Fe(P(OCH_2)_3CEt)_2Ph$ (**3.3**) with PMe_3 in THF-d_8 photolyzed at 21 °C (note: one plot is shown for each [PMe_3], but multiple experiments were performed) are shown in Figures 3.7-3.10.

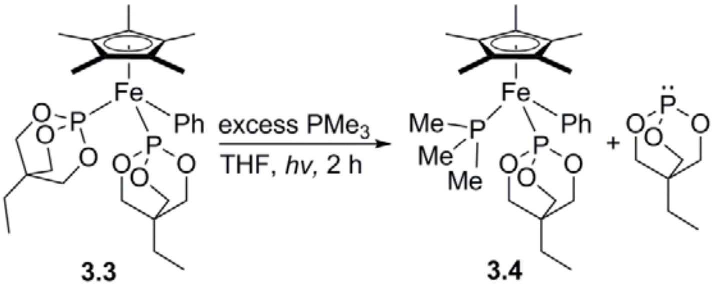

(3.4)

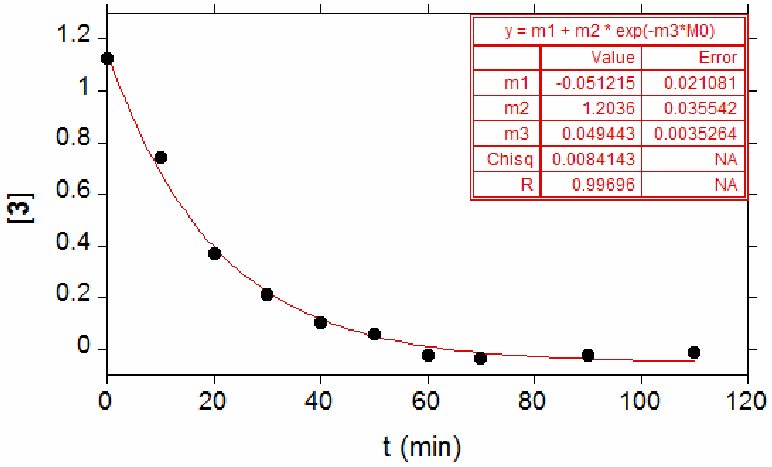

Figure 3.7. First order decay of $Cp^*Fe(P(OCH_2)_3CEt)_2Ph$ (**3.3**) with 5 equiv. of PMe_3 in THF-d_8 photolyzed at 21 °C with $k_{obs} = 0.049\ min^{-1} = 0.82 \times 10^{-3}\ s^{-1}$.

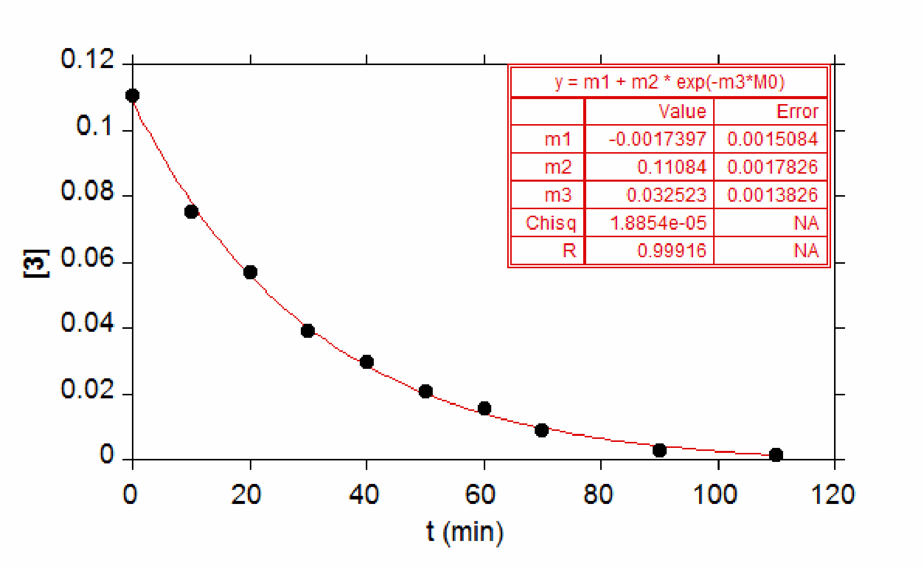

y = m1 + m2 * exp(-m3*M0)

	Value	Error
m1	-0.0017397	0.0015084
m2	0.11084	0.0017826
m3	0.032523	0.0013826
Chisq	1.8854e-05	NA
R	0.99916	NA

Figure 3.8. First order decay of Cp*Fe(P(OCH$_2$)$_3$CEt)$_2$Ph (**3.3**) with 10 equiv. of PMe$_3$ in THF-d_8 photolyzed at 21 °C with $k_{obs} = 0.033$ min^{-1} = 0.55 ×10^{-3} s^{-1}.

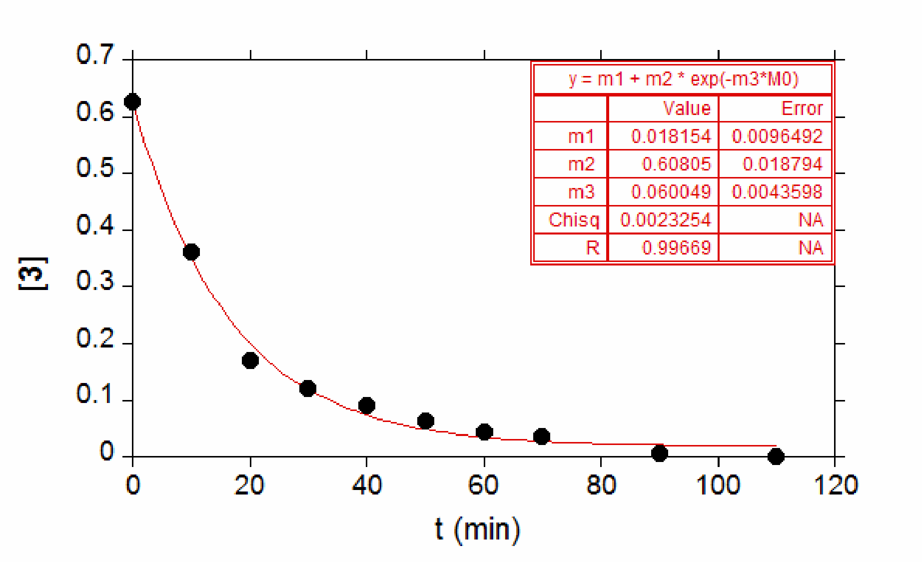

y = m1 + m2 * exp(-m3*M0)

	Value	Error
m1	0.018154	0.0096492
m2	0.60805	0.018794
m3	0.060049	0.0043598
Chisq	0.0023254	NA
R	0.99669	NA

Figure 3.9. First order decay of Cp*Fe(P(OCH$_2$)$_3$CEt)$_2$Ph (**3.3**) with 15 equiv. of PMe$_3$ in THF-d_8 photolyzed at 21 °C with $k_{obs} = 0.060$ min^{-1} = 1.0 ×10^{-3} s^{-1}.

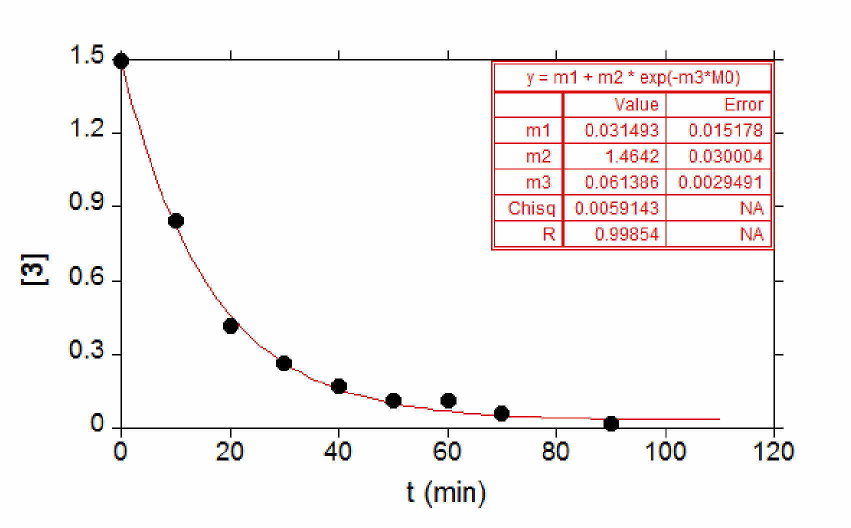

Figure 3.10. First order decay of Cp*Fe(P(OCH$_2$)$_3$CEt)$_2$Ph (**3.3**) with 20 equiv. of PMe$_3$ in THF-d_8 photolyzed at 21 °C with k_{obs} = 0.061 min^{-1} = 1.0 ×10^{-3} s^{-1}.

Within deviation of the data, a plot of k_{obs} as a function of [PMe$_3$] shows a zero-order dependence on [PMe$_3$] (Figure 3.11). The average k_{obs} value is 0.8(3) × 10^{-3} s^{-1}. The large deviations in k_{obs} are likely a result of challenges associated with reproducibility using the photolysis lamp (*e.g.*, rate changes as a function of distance from the lamp). As expected for an 18-electron complex, the kinetic data are consistent with a dissociative ligand exchange with P(OCH$_2$)$_3$CEt dissociation as the rate-limiting step.

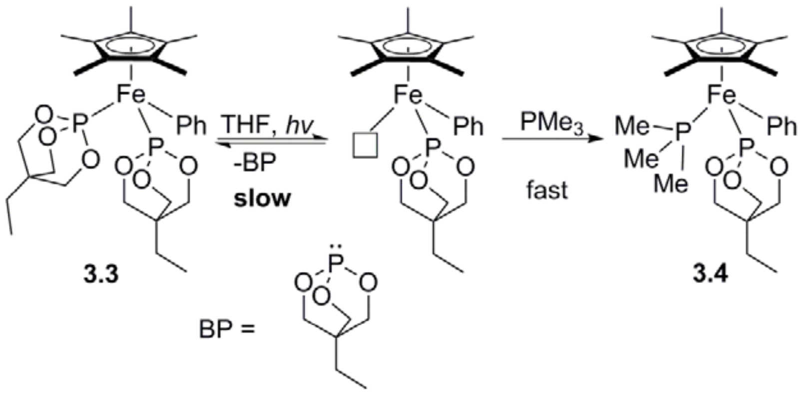

Scheme 3.15. Dissociate mechanism for the reaction of Cp*Fe(P(OCH$_2$)$_3$CEt)$_2$Ph (**3.3**) with PMe$_3$.

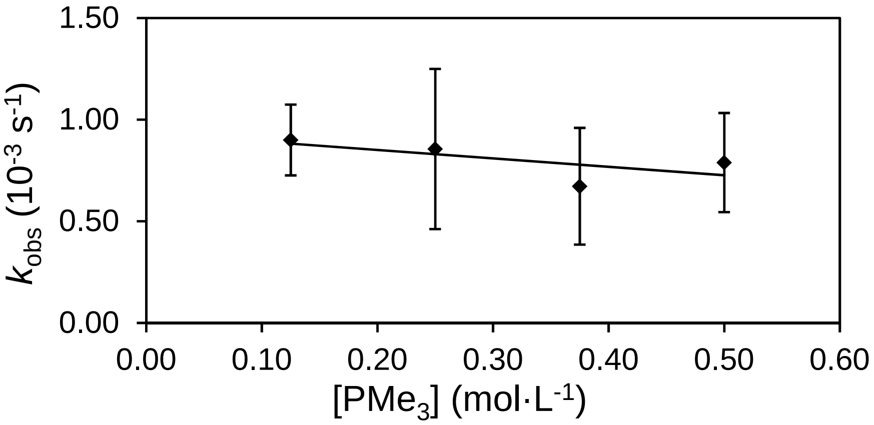

Figure 3.11. Plot of k_{obs} vs. [PMe_3] for the reaction of Cp*Fe($P(OCH_2)_3CEt)_2Ph$ (**3.3**) with PMe_3 showing a zero order dependence on [PMe_3].

The reaction of **3.3** and Me_3NO in THF-d_8 was monitored by ^{1}H and ^{31}P NMR spectroscopy under the same photolysis conditions as the reaction of **3.3** and PMe_3. Free $P(OCH_2)_3CEt$ is formed and then converted to O=$P(OCH_2)_3CEt$, which supports dissociation of $P(OCH_2)_3CEt$ under photolysis as the first step of oxygen atom insertion into the Fe–Ph bond.

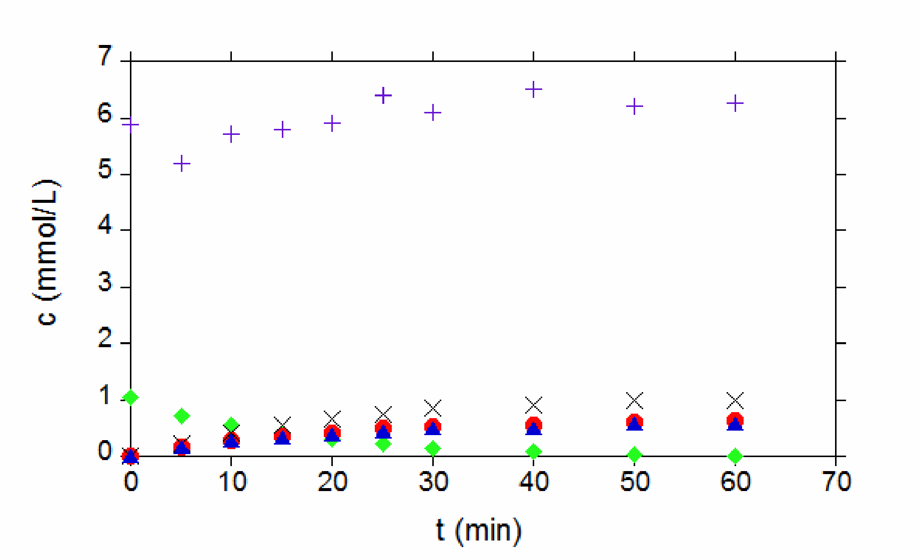

Figure 3.12. Plot of concentration versus time for the reaction of Cp*Fe($P(OCH_2)_3CEt)_2Ph$ (**3.3**) with 6 equiv. of Me_3NO photolyzed at 21 °C in THF-d_8 including complex **3.3** (green, diamonds), Me_3NO (purple, crosses), O=$P(OCH_2)_3CEt$ (black, x), 1,2,3,4-tetramethylfulvene (blue, triangles) and PhOH·$ONMe_3$ (red, circles).

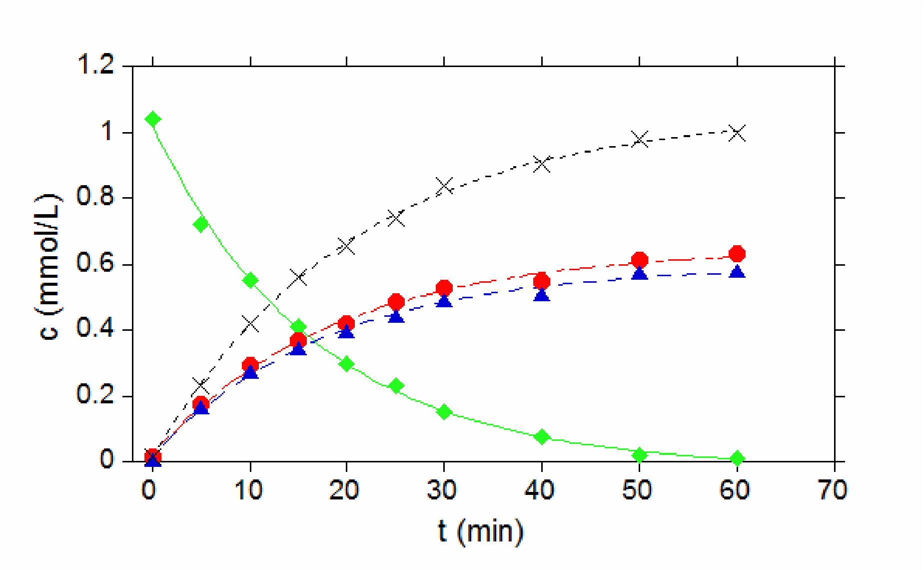

Figure 3.13. Plot of concentration versus time for the starting material and three products observed during the reaction of Cp*Fe(P(OCH$_2$)$_3$CEt)$_2$Ph (**3.3**) with Me$_3$NO photolyzed at 21 °C in THF-d_8 including complex **3.3** (green, diamonds), O=P(OCH$_2$)$_3$CEt (black, x), 1,2,3,4-tetramethylfulvene (blue, triangles) and PhOH·ONMe$_3$ (red, circles).

A sample kinetic plots of the Rate for reactions of Cp*Fe(P(OCH$_2$)$_3$CEt)$_2$Ph (**3.3**) with 6 equiv of Me$_3$NO in THF-d_8 photolyzed at 21 °C are shown in Figures 3.12 and 3.13, which depict the concentration versus time plot for the starting material **3.3** and the three products shown in eq 3.2 (based on the integrations of ^{1}H NMR spectra). Excess Me$_3$NO is used and saturated in the solution, which is consistent to the integration in Figure 3.12. Since oxidation of free P(OCH$_2$)$_3$CEt by Me$_3$NO occurs in the absence of photolysis, we did not monitor the concentration of free P(OCH$_2$)$_3$CEt. In the plot, in order to keep to y-scale similar for all compounds, the concentration of O=P(OCH$_2$)$_3$CEt is divided by two. Using a first-order fit for the disappearance of **3.3** gave $k_{obs} = 1.0(1) \times 10^{-3}$ s^{-1} (Figure 3.14), which is almost identical to the k_{obs} for phosphite/PMe$_3$ exchange (see above). This is consistent with rate limiting phosphite dissociation during the formation of PhOH from reaction of **3.3** with Me$_3$NO. The generation of PhOH·ONMe$_3$ and 1,2,3,4-tetramethylfulvene have almost identical rates with a $k_{obs} = 0.9(1) \times 10^{-3}$ s^{-1}

as the decay of **3.3** (Figures 3.15 and 3.16). The oxidation of free P(OCH$_2$)$_3$CEt with Me$_3$NO (P(OCH$_2$)$_3$CEt + Me$_3$NO → O=P(OCH$_2$)$_3$CEt + Me$_3$N, under same pseudo-first-order conditions,) in THF-*d*$_8$ was independently determined by ^{1}H NMR spectroscopy at room temperature, and $k_{obs} = 0.55(1) \times 10^{-3}$ s^{-1} was determined (Figures 3.17 and 3.18), which is consistent with the observation of a low concentration of free phosphite that is ultimately converted to phosphate. The plot in Figure 3.13 shows no evidence of an induction period.

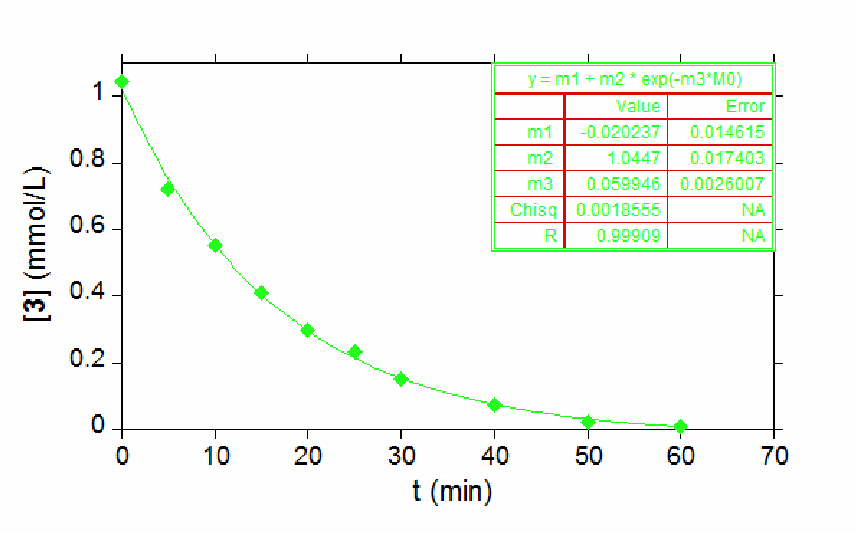

Figure 3.14. First order decay of Cp*Fe(P(OCH$_2$)$_3$CEt)$_2$Ph (**3.3**) with 6 equiv. of Me$_3$NO in THF-*d*$_8$ photolyzed at 21 °C with $k_{obs} = 0.060$ min^{-1} = 1.0×10^{-3} s^{-1}.

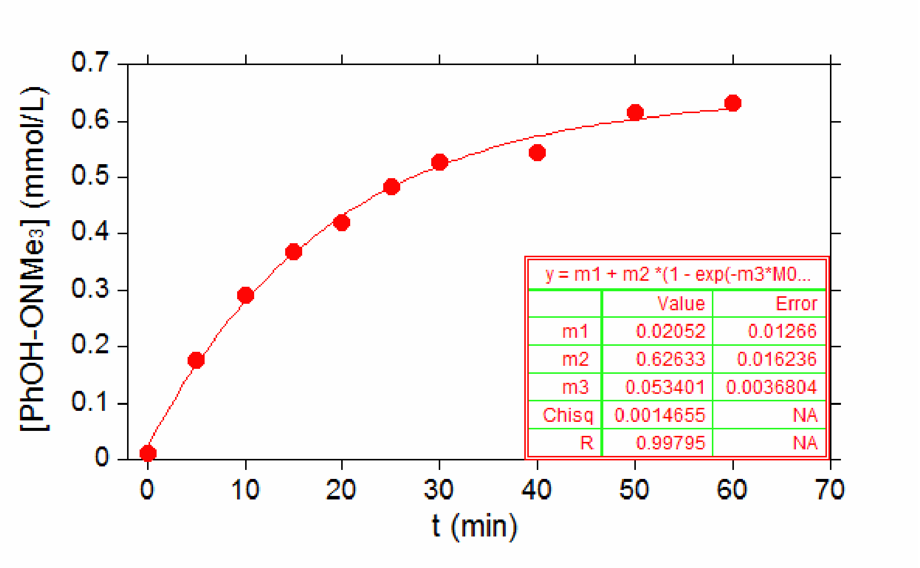

y = m1 + m2 *(1 - exp(-m3*M0...

	Value	Error
m1	0.02052	0.01266
m2	0.62633	0.016236
m3	0.053401	0.0036804
Chisq	0.0014655	NA
R	0.99795	NA

Figure 3.15. First order growth of PhOH·ONMe$_3$ in the reaction of Cp*Fe(P(OCH$_2$)$_3$CEt)$_2$Ph (**3.3**) with 6 equiv. of Me$_3$NO in THF-d_8 photolyzed at 21 °C with k_{obs} = 0.053 min^{-1} = 0.90 ×10^{-3} s^{-1}.

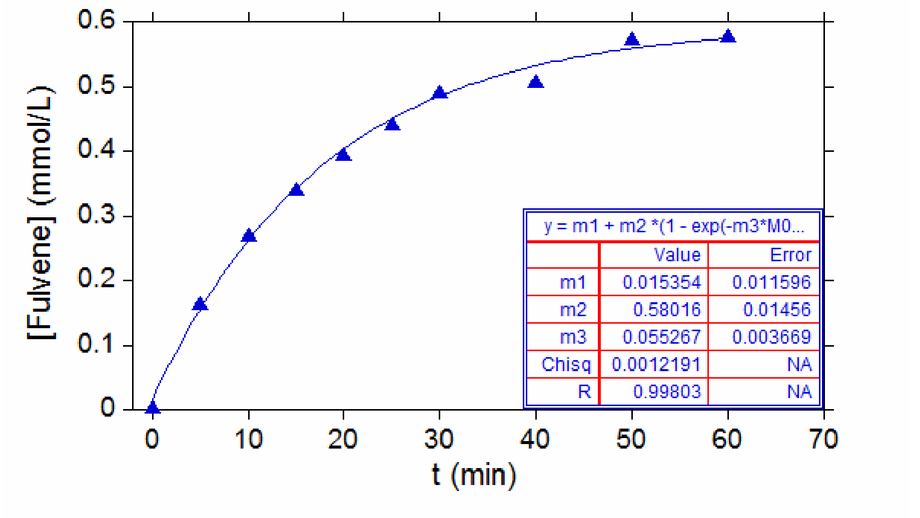

y = m1 + m2 *(1 - exp(-m3*M0...

	Value	Error
m1	0.015354	0.011596
m2	0.58016	0.01456
m3	0.055267	0.003669
Chisq	0.0012191	NA
R	0.99803	NA

Figure 3.16. First order growth of 1,2,3,4-tetramethylfulvene in the reaction of Cp*Fe(P(OCH$_2$)$_3$CEt)$_2$Ph (**3.3**) with 6 equiv. of Me$_3$NO in THF-d_8 photolyzed at 21 °C with k_{obs} = 0.055 min^{-1} = 0.91 ×10^{-3} s^{-1}.

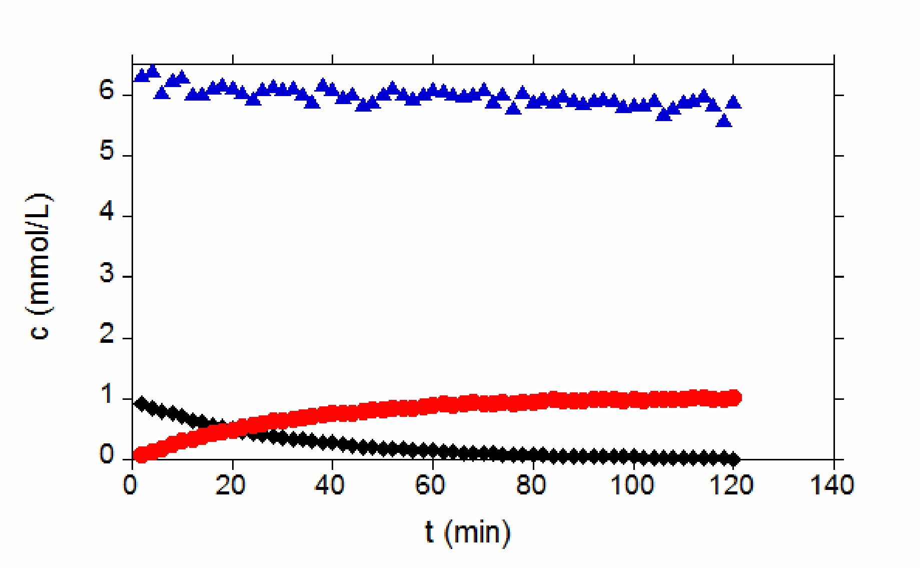

Figure 3.17. Plot of concentration versus time for the reaction of $P(OCH_2)_3CEt$ with 6 equiv. of Me_3NO at 21 °C in THF-d_8 including $P(OCH_2)_3CEt$ (black, diamonds), $O{=}P(OCH_2)_3CEt$ (red, circles), Me_3NO (blue, triangles).

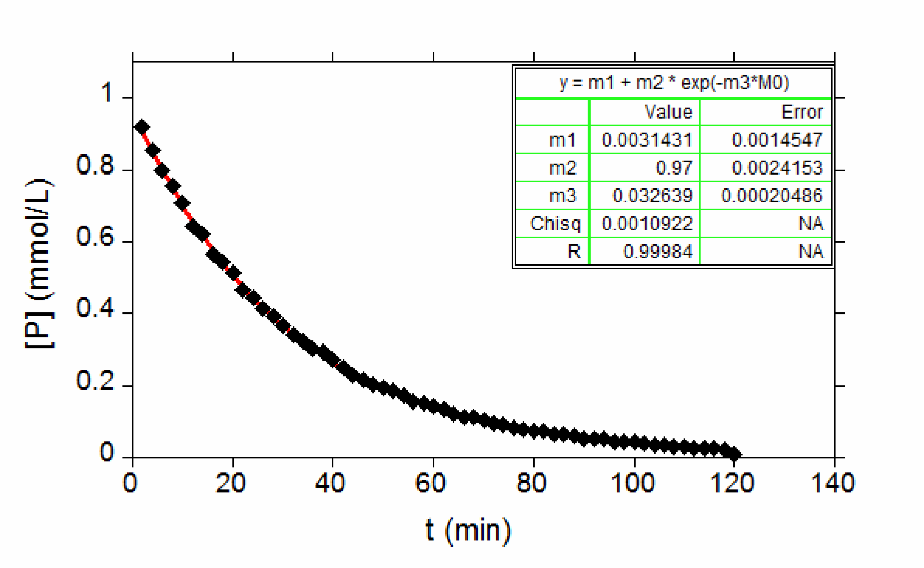

Figure 3.18. First order decay of $P(OCH_2)_3CEt$ with 6 equiv. of Me_3NO in THF-d_8 photolyzed at 21 °C with $k_{obs} = 0.033\ min^{-1} = 0.55 \times 10^{-3}\ s^{-1}$.

Previous computational studies of O atom insertion into the Fe–R bonds of Cp*Fe(CO)(NCMe)R from reactions with oxidants revealed that the most favorable pathway would likely involve formation of the Fe–oxo intermediate Cp*Fe(CO)(O)R followed by migratory insertion of the hydrocarbyl ligand to the oxo ligand.[43] We extended the computational studies to $Cp^*Fe(P(OCH_2)_3CEt)_2Ph$ using Me_3NO as oxidant, with the assumption that the analogous Fe-oxo complex, $Cp^*Fe(P(OCH_2)_3CEt)(O)Ph$, is an intermediate. Density functional theory (DFT) calculations were carried out by the Cundari Group to determine the energy barriers for the three observed oxidation reactions following the dissociation of the $P(OCH_2)_3CEt$ and the formation of the Fe=O intermediate: the oxidation of coordinated $P(OCH_2)_3CEt$ to form $O{=}P(OCH_2)_3CEt$, conversion of Ph–Fe=O to form Fe–OPh and oxidation of Cp* to form 1,2,3,4-tetramethylfulvene (Scheme 3.16).

Complex **3.3** is calculated to possess a singlet spin ground state. Fe remains bonded to Cp* in an η^5 fashion throughout the reaction coordinate. Overall, the oxy-insertion product $Cp^*Fe(P(OCH_2)_3CEt)(OPh)$ is calculated to be highly exergonic relative to the starting materials (ΔG = –65.4 kcal/mol). Upon dissociation of the phosphite ligand from **3.3**, which is found to be endergonic by 1.7 kcal/mol, a spin flip from the singlet to a triplet occurs. The minimum energy crossing point (MECP) for the "spin flip" for phosphine loss was calculated using Harvey's method.[53,54] The singlet → triplet "spin flip" associated with phosphite dissociation was calculated to be energetically demanding, lying ~20 kcal/mol above complex **3.3**, and hence engendering a barrier that is similar to the OAT barrier (*vide infra*) and consistent with the experimental proposal of rate determining phosphite dissociation.

Coordination of Me_3NO to $Cp^*Fe(P(OCH_2)_3CEt)Ph$ was calculated to stabilize the complex by 2.2 kcal/mol with $\Delta G = 0.5$ kcal/mol compared to the starting complex **3.3**. Another spin flip (triplet → quintet) accompanies the transformation of $Cp^*Fe(P(OCH_2)_3CEt)Ph$ → $Cp^*Fe(P(OCH_2)_3CEt)(ONMe_3)Ph$. Attempts to find phosphite/ONMe$_3$ ligand exchange via an associative mechanism were not successful, and thus, consistent with kinetic study of P(OCH$_2$)$_3$CEt/PMe$_3$ exchange (see above), the simulations imply a dissociative mechanism.

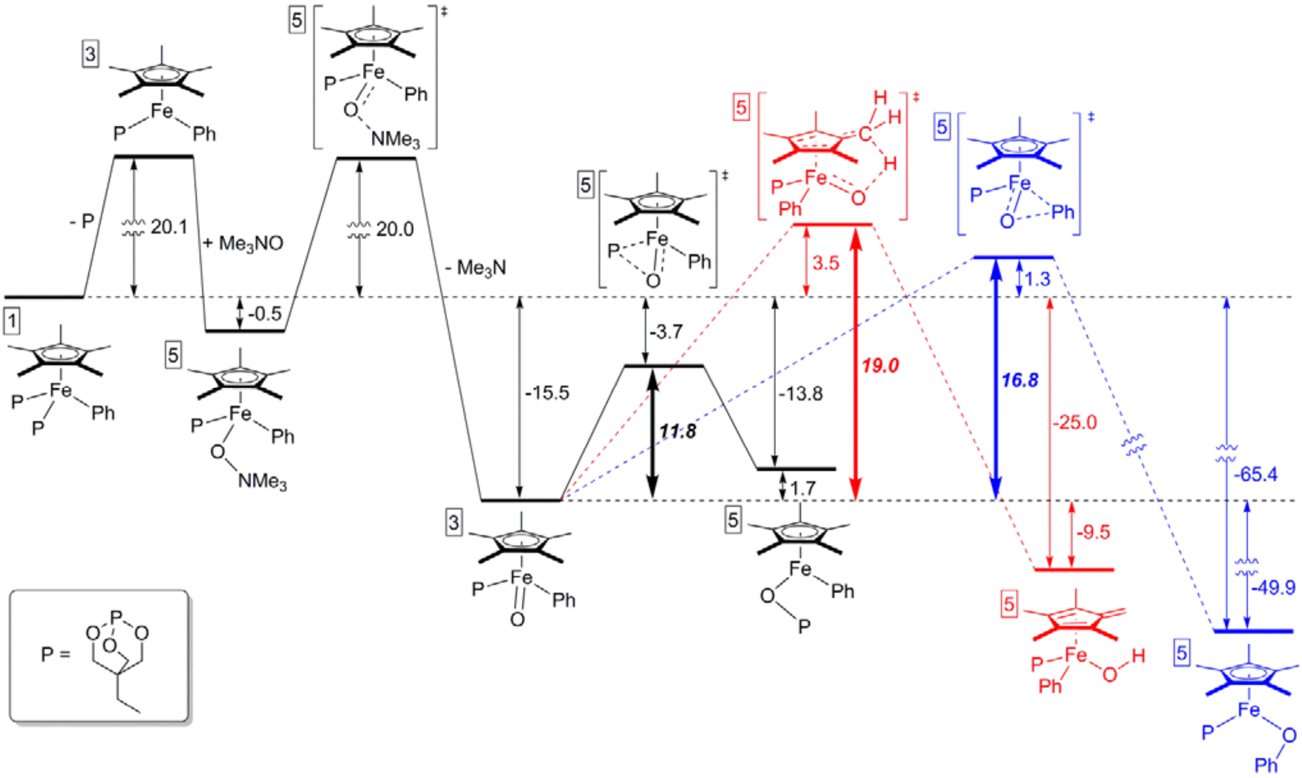

Scheme 3.16. Calculated free energies for the reaction of Cp*Fe(P(OCH$_2$)$_3$CEt)$_2$Ph (**3.3**) and Me$_3$NO in THF-d_8. Numbers are free energies (kcal/mol) relative to complex **3.3**. Lowest energy spin states are labeled in the boxes on the top left of structures.

Conversion of Cp*Fe(P(OCH$_2$)$_3$CEt)(ONMe$_3$)Ph to the Fe–oxo complex Cp*Fe(P(OCH$_2$)$_3$CEt)(O)Ph is calculated to be exergonic (ΔG = –15.5 kcal/mol relative to **3**). The transition state for the oxygen atom transfer was calculated to be 20.0 kcal/mol above Cp*Fe(P(OCH$_2$)$_3$CEt)(ONMe$_3$)Ph with a quintet spin state. Formation of Cp*Fe(P(OCH$_2$)$_3$CEt)(O)Ph entails another spin flip to a triplet. The Fe of Cp*Fe(P(OCH$_2$)$_3$CEt)(O)Ph has a spin density of 1.315 e^-, while the oxo has a 0.819 e^- spin density. This suggests the oxo intermediate possesses oxyl ($O^{-\bullet}$) character. The spin density plot can be seen in Figure 3.19, showing the alpha spin (orange) being shared between the oxyl and Fe while a small amount of beta spin (purple) is on the phenyl ligand.

Migration of the phenyl ligand to the Fe–oxo bond (Scheme 3.16, blue pathway) results in a calculated free energy barrier of 16.8 kcal/mol and was found to be exergonic by 65.4 kcal/mol upon formation of the quintet phenoxide product Cp*Fe(P(OCH_2)$_3$CEt)(OPh). Thus, the calculations predict that formation of the oxo complex occurs with a more substantial free energy of activation than the phenyl migration step. Similar to calculations of oxy-insertion into the Fe–Ph bond of Cp*Fe(CO)(NCMe)Ph,[43] the calculations predict that conversion of Cp*Fe(P(OCH_2)$_3$CEt)$_2$Ph and Me_3NO to Cp*Fe(P(OCH_2)$_3$CEt)(OPh) is kinetically feasible.

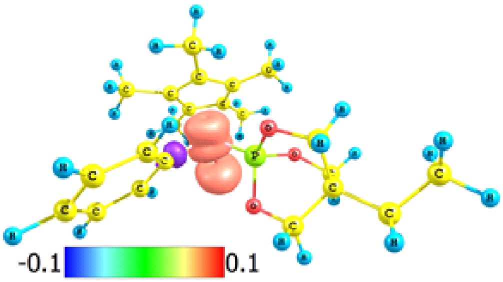

Figure 3.19. Spin density plot of oxo intermediate, Cp*Fe(P(OCH_2)$_3$CEt)(O)Ph, [scale: 0.33, contour value: 0.006943].

From the oxo complex Cp*Fe(P(OCH_2)$_3$CEt)(O)Ph, the phosphite can migrate to the oxo ligand to form phosphate (Scheme 3.16, black pathway). The calculated free energy barrier to form phosphate from Cp*Fe(P(OCH_2)$_3$CEt)(O)Ph is 11.8 kcal/mol. The formation of the phosphate product Cp*Fe(O=P(OCH_2)$_3$CEt)Ph is 13.8 kcal/mol exergonic in relation to the starting material Cp*Fe(P(OCH_2)$_3$CEt)$_2$Ph. These results suggest that phosphate formation can originate from Cp*Fe(P(OCH$_2$)$_3$CEt)(O)Ph or free phosphite (see above).

Oxidation of Cp* was also modeled computationally (Scheme 3.16, red pathway). From Cp*Fe(P(OCH$_2$)$_3$CEt)(O)Ph, the formation of 1,2,3,4-tetramethylfulvene via H atom transfer to the oxo ligand was calculated to have a free energy barrier of 19.0 kcal/mol.

3.2.3 The Reaction of Cp*Fe(P(OCH$_2$)$_3$CEt)$_2$Ph (3.3) with Other Oxidants

In contrast to the reaction of **3.3** with Me$_3$NO, the reaction of **3.3** with sodium periodate in a THF/H$_2$O mixture results in the quantitative production of 1,2,3,4,5-pentamethyl-5-phenyl-cyclopentadiene (Cp*Ph) after 24 h by ^{1}H NMR spectroscopy (eq 3.5). The product Cp*Ph was isolated and analyzed by ^{1}H, ^{13}C NMR spectroscopy and GC-MS (Figures 3.20-3.22).

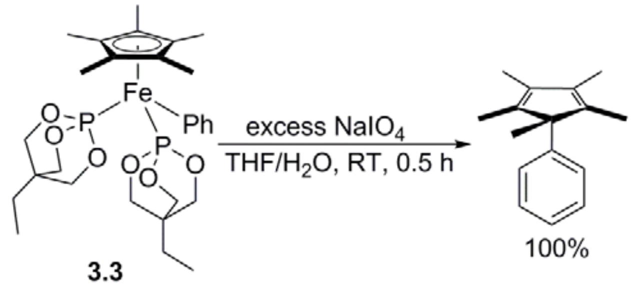

(3.5)

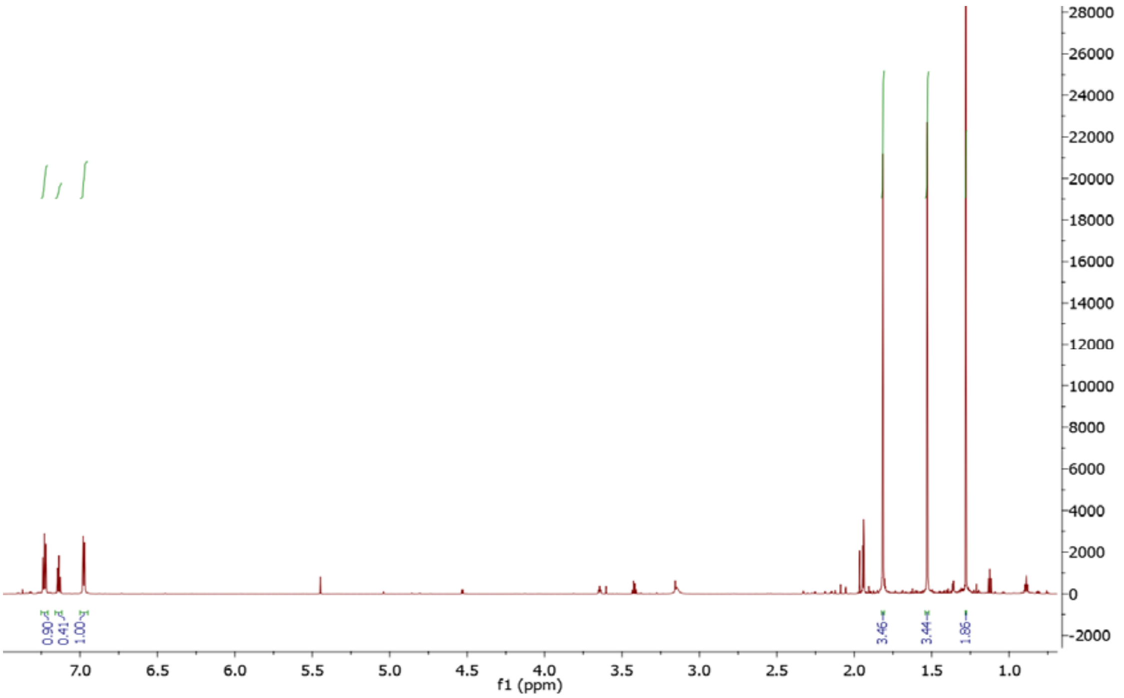

Figure 3.20. ^{1}H NMR spectrum of 1,2,3,4,5-pentamethly-5-phenyl-cyclopentadiene (Cp*Ph) isolated from the reaction of Cp*Fe(P(OCH$_2$)$_3$CEt)$_2$Ph (**3.3**) and AgOTf in CD$_3$CN.

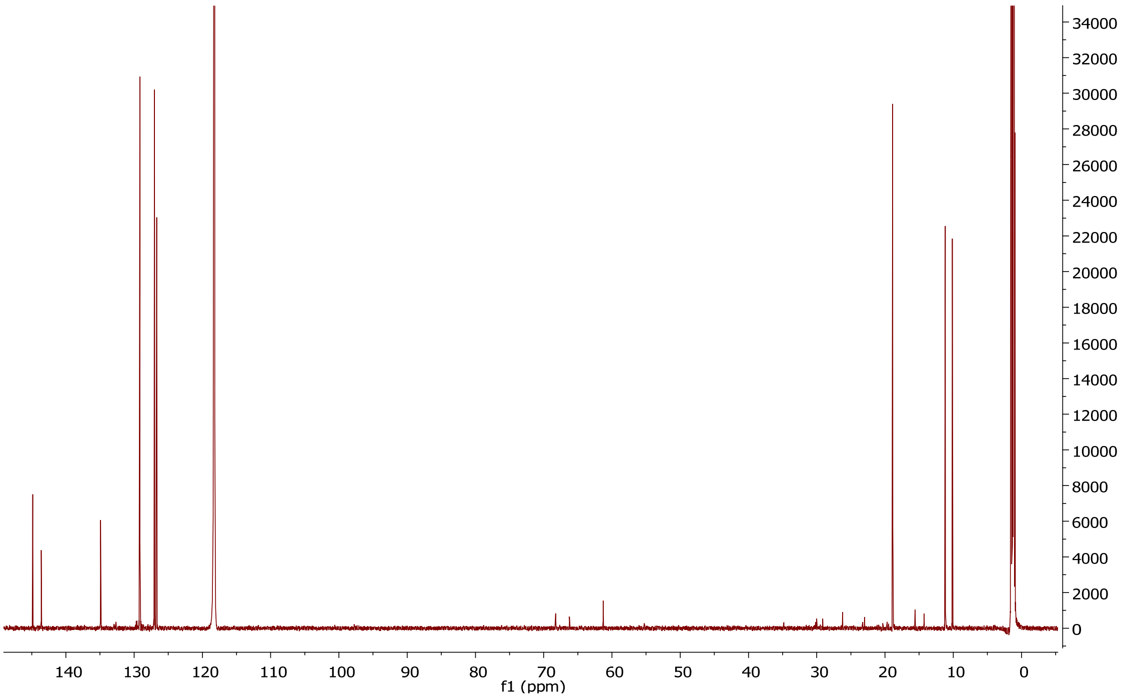

Figure 3.21. ^{13}C NMR spectrum for 1,2,3, 4,5-pentamethly-5-phenyl-cyclopentadiene (Cp*Ph) isolated from the reaction of Cp*Fe(P(OCH$_2$)$_3$CEt)$_2$Ph (**3.3**) and AgOTf in CD$_3$CN.

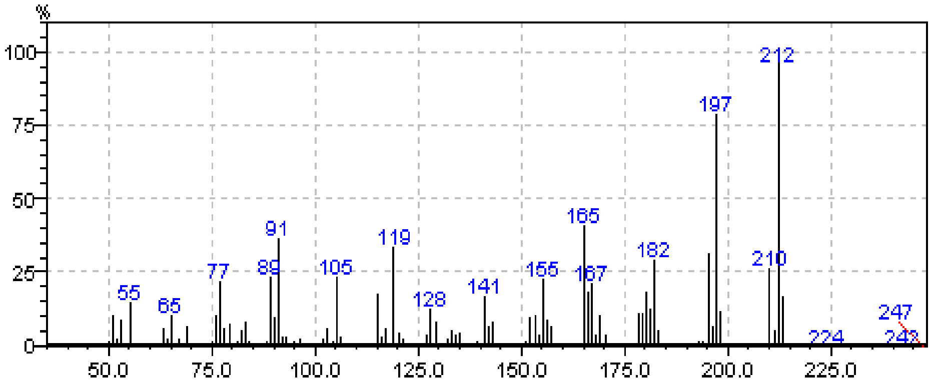

Figure 3.22. Mass spectrum for 1,2,3,4,5-pentamethly-5-phenyl-cyclopentadiene (Cp*Ph) ($C_{14}H_{20}$, MW = 212).

We considered that the formation of Cp*Ph might result from an initial electron transfer to form the Fe^{III} complex $[Cp^*Fe(P(OCH_2)_3CEt)_2Ph]^+$ followed by C–C reductive elimination. Consistent with this proposal, the reaction of **3.3** with AgOTf (OTf = trifluoromethanesulfonate), a known single electron oxidant, results in the formation of Cp*Ph in quantitative yield (Scheme 3.17). DFT calculations reveal that the free energy barrier for the formation of Cp*Ph via direct C–C reductive elimination is 40.1 kcal/mol from the Fe^{II} complex **3.3**, but the calculated free energy barrier is reduced to 19.4 kcal/mol for the cationic formally Fe^{III} complex $[Cp^*Fe(P(OCH_2)_3CEt)_2Ph]^+$ (Scheme 3.18).

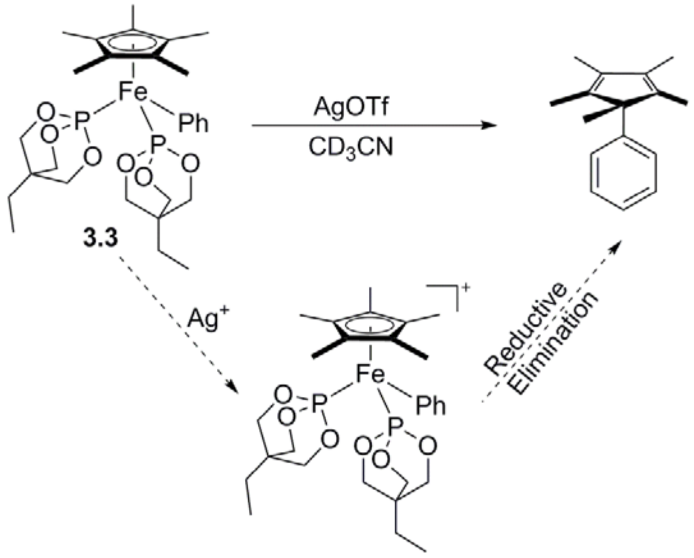

Scheme 3.17. Proposed Pathway for the Reaction of Cp*Fe(P(OCH$_2$)$_3$CEt)$_2$Ph (**3.3**) and AgOTf.

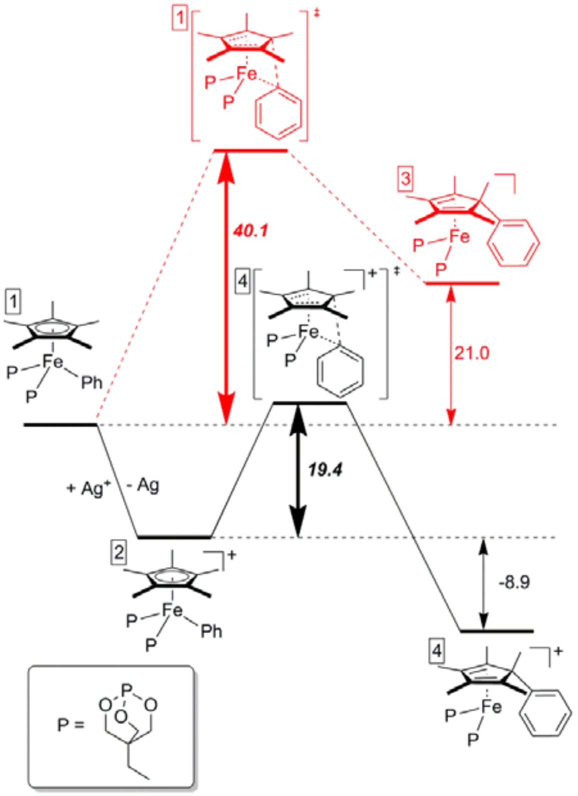

Scheme 3.18. Calculated Free Energies for the Reaction of Cp*Fe(P(OCH$_2$)$_3$CEt)$_2$Ph (**3.3**) and AgOTf in THF-d_8. Numbers are free energies (kcal/mol) relative to complex **3.3**. Lowest energy spin states are labeled in the boxes on the top left of structures.

Table 3.2 shows the yields of PhOH and Cp*Ph for the reactions of **3.3** with a range of oxidants and solvents. The production of PhOH requires light (either ambient or photolysis lamp); however, Cp*Ph formation occurs in the absence of light. These observations are consistent with light induced dissociation of phosphite as key step in the formation of PhOH but not Cp*Ph. The reaction of **3.3** with pyridine-*N*-oxide produces Cp*Ph. Although pyridine-*N*-oxides are not typically considered single electron oxidants, such reactivity has precedent.[55] Complex **3.3** reacts with Me_3NO in THF to produce a high yield of PhOH either under photolysis or ambient light (Table 3.2, entries 1 & 2), but only the C–C coupling product is observed in MeCN (Table 3.2, entry 3). Although we do not have a definitive explanation for the solvent effect, it is possible the MeCN may promote electron transfer due to its polar nature by stabilizing incipient charge in the transition states for the formation of $[Cp^*Fe(P(OCH_2)_3CEt)_2Ph]^+$. Alternatively, MeCN might inhibit coordination of Me_3NO to Fe and suppress the oxy-insertion reaction while the proposed mechanism for formation of Cp*Ph does not require a vacant coordination site on Fe. $^nBu_4NIO_4$ and H_2O_2 also generate PhOH in THF (Table 3.2, entries 8, 11 and 12). Aerobic oxidation of the Fe–Ph to form PhOH is also observed, although the yield is low (Table 3.2, entries 6 & 7). Taken together, these results suggest that PhOH formation does not likely occur by an initial single electron transfer to generate an Fe^{III} intermediate. Rather, the reaction is hypothesized to occur by initial $P(OCH_2)_3CEt/Me_3NO$ ligand exchange to generate $Cp^*Fe(P(OCH_2)_3CEt)(Me_3NO)Ph$, which then undergoes net O atom transfer to the phenyl ligand.

Table 3.2. Reaction conditions and yields for $Cp^*Fe(P(OCH_2)_3CEt)_2Ph$ (**3.3**) with various oxidants.[a]

no.	oxidant	solvent	T (°C)[b]	t (h)	PhOH (%)[c]	Cp*Ph (%)
1	Me_3NO	THF	21	96	70	10
2	Me_3NO	THF	21(*hv*)	2	70	10
3	Me_3NO	CH_3CN	21	96	0	80
4	NMO[d]	THF	21	72	70	10
5	O_2 (15 psi)	CH_3CN	21	24	0	90
6	O_2 (15 psi)	THF	21	24	15	20
7	O_2 (15 psi)	THF	21(*hv*)	1	15	20
8	$^nBU_4NIO_4$	THF	21(*hv*)	4	25	12
9	$NaIO_4$	THF/H_2O	21	0.5	0	100
10	$^nBU_4NIO_4$	CH_3CN	21	24	0	90
11	H_2O_2	THF	21	72	10	80
12	H_2O_2	THF	21(*hv*)	4	13	15
13	PyO	THF	21(*hv*)	4	0	0
14	PyO	THF	70	96	0	70
15	4-NO_2-PyO	CH_3CN	50	24	0	90
16	AgOTf	CH_3CN	21	0.5	0	100

[a] Reactions incorporate 5 equiv of oxidant in deuterated solvents. [b] All reactions in were performed under ambient or UV light. *hv* is used to show reactions performed under UV light. PhOH is not observed when reactions are performed in the absence of light. [c] Yields of products are based on integration of ^{1}H NMR spectra versus an internal standard. [d] NMO = *N*-methyl-morpholine *N*-oxide.

3.2.4 The reactivity of Cp*Fe(P(OCH$_2$)$_3$CEt)$_2$Me (3.5)

We have also prepared and isolated the methyl complex Cp*Fe(P(OCH$_2$)$_3$CEt)$_2$Me (**3.5**) by using the analogous procedures for synthesizing complex **3.4**. The ^{1}H and ^{13}C NMR spectra are shown in Figures 3.23 and 3.24.

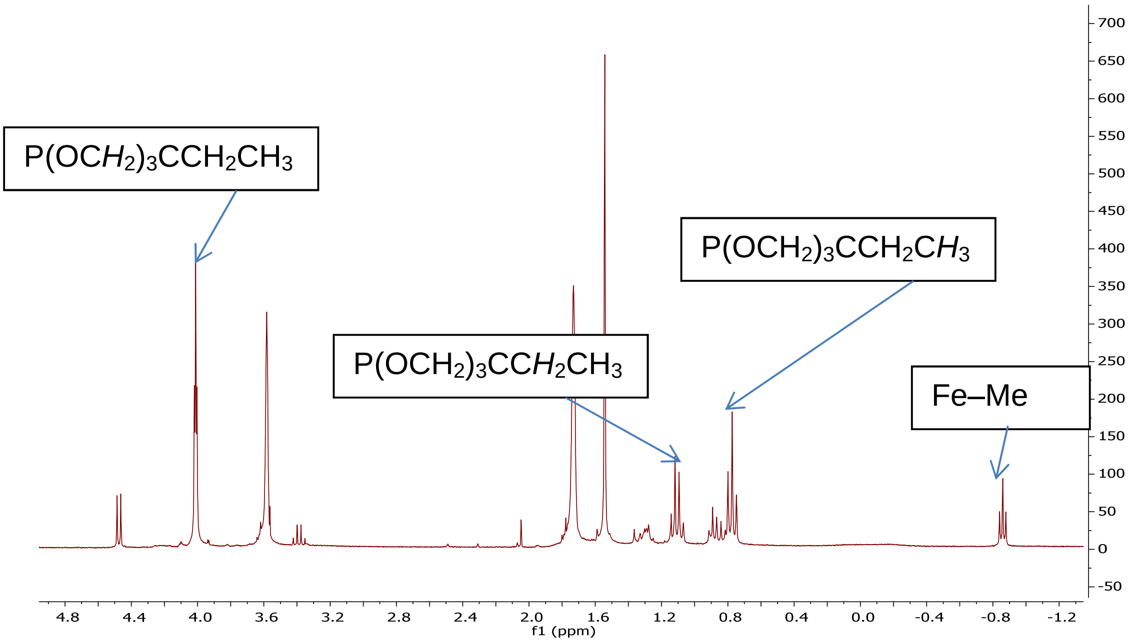

Figure 3.23. ^{1}H NMR spectrum for Cp*Fe(P(OCH$_2$)$_3$CEt)$_2$Me (**3.5**) in CD$_3$CN.

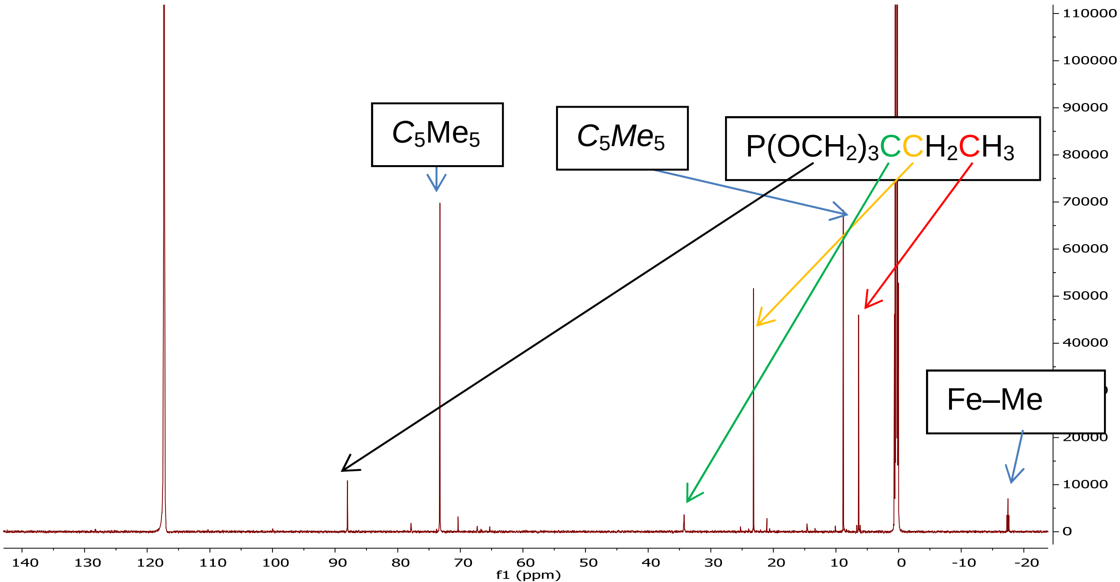

Figure 3.24. ^{13}C NMR spectrum for Cp*Fe(P(OCH$_2$)$_3$CEt)$_2$Me (**3.5**) in CD$_3$CN.

When treated with Me_3NO in THF, complex **3.5** displays analogous reactivity to **3.3** to produce MeOH, but with a lower yield (~ 25%) by ^1H NMR spectroscopy (eq 3.6). The lower yield of the alcohol production for the Fe–Me than the Fe–Ph complex is explained by the less nucleophilic –Me and smaller stabilization of charge by delocalizationin the transition state that is possible in arkyl versus aryl migration (Scheme 3.19).

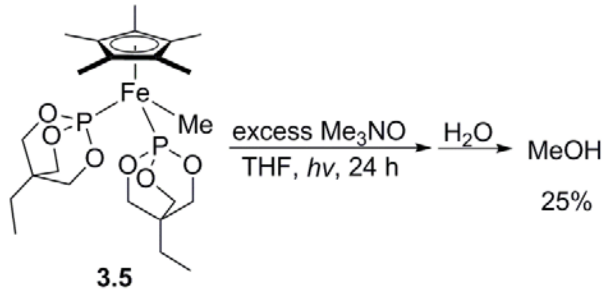

3.5

(3.6)

Scheme 3.19. Nucleophilic migration of $R^{\delta-}$ to $M\equiv O^{\delta+}$.

The C–C reductive elimination product 1,2,3,4,5,5-hexamethyl-cyclopentadiene (Cp*Me) is also observed when **3.5** reacts with Me_3NO or O_2 in CD_3CN, with MeOH as the co-product (eq 3.7). Table 3.3 shows the results of the reactions of **3.5** with various oxidants. The reaction of **3.6** with pyridine-*N*-oxide produces high yield of Cp*Me upon heating at 70 °C (entry 14), although pyridine-*N*-oxides are not typically considered single electron oxidants (see above). Complex **3.5** reacts with Me_3NO in THF to produce MeOH either under photolysis or ambient light (Table 3.3, entries 1 & 2). Same yield of MeOH was produced in MeCN as in THF, which is significantly different from the

PhOH production from **3.3** with Me_3NO in CD_3CN (Table 3.3, entry 3). $^nBu_4NIO_4$ and H_2O_2 also generate MeOH in THF (Table 3.3, entries 8, 11 and 12) under photolysis. Aerobic oxidation of the Fe–Me to form MeOH is also observed in approximately same yield as Me_3NO (Table 3.3, entries 6 & 7). Taken together, these results suggest that MeOH formations from the reaction of **3.5** with oxidants are similar as the PhOH releases from **3.3** with oxidants but with lower yields.

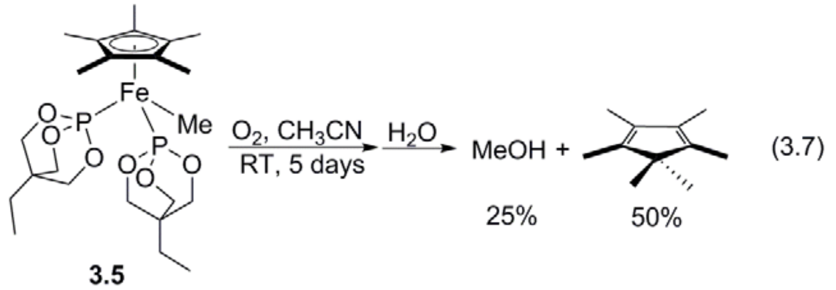

3.5

(3.7)

Table 3.3. Reaction conditions and yields for reaction of $Cp^*Fe(P(OCH_2)_3CEt)_2Me$ (3.5) with various oxidants.[a]

no.	Oxidant	Solvent	T (°C)	t (h)	MeOH (%)[b]	Cp*Me (%)
1	Me_3NO	THF	21	96	25	0
2	Me_3NO	THF	21 (*hv*)	24	25	0
3	Me_3NO	CH_3CN	21	96	25	0
4	NMO[c]	THF	21	96	25	0
5	O_2 (15 psi)	CH_3CN	21	24	0	90
6	O_2 (15 psi)	THF	21	24	16	70
7	O_2 (15 psi)	THF	21 (*hv*)	24	22	0
8	$^nBu_4NIO_4$	THF	21 (*hv*)	4	10	0
9	$NaIO_4$	THF/H_2O	21	0.5	0	100

10	${}^{n}Bu_4NIO_4$	CH_3CN	21	24	0	83
11	H_2O_2	THF	21	24	26	0
12	H_2O_2	THF	21(*hv*)	2	20	0
13	PyO	THF	21(*hv*)	4	0	0
14	PyO	THF	70	96	0	70
15	4-NO_2-PyO	CH_3CN	50	24	0	76
16	AgOTf	CH_3CN	21	0.5	0	100

[a]Reactions are with 5 equiv of oxidant in deuterated solvents. [b]Yields of products are based on integration of ${}^1H$ NMR spectra versus an internal standard. [c]NMO = *N*-methylmorpholine *N*-oxide.

3.3 Summary and Conclusions

Insertion of oxygen atoms into metal-hydrocarbyl bonds is a key step in the development of potential catalysts for the oxidation of hydrocarbons as shown in Scheme 3.2. Despite the potential importance of such oxygen atom insertion reactions, there are few examples of non-radical conversion of M–R bonds and oxygen atom transfer reagents to M–OR. Herein, it is demonstrated demonstrate that Fe^{II} hydrocarbyl (phenyl and methyl) complexes undergo C–O bond formation upon reaction with certain oxidants. The experimental observations were augmented by computational studies that indicate Fe-oxo complexes as viable intermediates that precede net oxo insertion into the Fe–R bond. The reaction requires light, presumably to initiate ligand exchange between phosphite and the oxidant. The calculations indicate that both Fe–oxo formation and the oxy-insertion into Fe–R bonds are thermally viable processes. Although the previous (limited) examples of O atom insertion into M–R bonds occur with metals that will not activate C–H bonds, use of Cp*Fe(P(OCH_2)$_3$CEt)$_2$R complexes is promising because of the demonstrated ability of the related Cp*Fe(CO)(NCMe)Ph to activate C–H bonds.[48] These studies establish the ability of d^6 complexes to mediate O atom insertion into M–R bonds. Importantly, they also point the way to new ligand motifs that avoid: 1) C–C coupling products, and 2) ligand oxidation.

3.4 Experimental Section

General Methods. Unless otherwise noted, all synthetic procedures were performed under anaerobic conditions in a nitrogen filled glovebox or by using standard Schlenk techniques. Glovebox purity was maintained by periodic nitrogen purges and was monitored by an oxygen analyzer (O_2 < 15 ppm for all reactions). Tetrahydrofuran was dried by distillation from sodium/benzophenone. Diethyl ether was distilled over CaH_2. THF-d_8, CD_3CN, D_2O were used as received and stored under a N_2 atmosphere over 4 Å molecular sieves (except water). ^{1}H NMR spectra were recorded on a Varian Mercury 300 MHz, Varian Inova 500 MHz, or Bruker 800 MHz spectrometer. ^{13}C NMR spectra were recorded using a Varian Mercury 300 MHz (operating frequency 75 MHz), Varian Inova 500 MHz (operating frequency 125 MHz), or Bruker 800 MHz (operating frequency 201 MHz) spectrometer. ^{31}P NMR spectra were recorded using a Varian Mercury 300 MHz (operating frequency 121 MHz) referenced against an external standard of H_3PO_4 ($\delta = 0$). All ^{1}H and ^{13}C [^{1}H] spectra are referenced against residual proton signals (^{1}H NMR) or the ^{13}C signals of the deuterated solvents (^{13}C [^{1}H[NMR). GC/MS was performed using a Shimadzu GCMS-QP2010 Plus system with a 30 m ×

0.25 mm RTx-Qbond column with 8 μm thickness using electron impact ionization. Photolysis experiments were performed using UV−vis radiation generated by a 450 W power supply (Model #l7830, Ace Glass, Inc.) equipped with a water-cooled 450 W 5 in. arc IMMER UV−vis lamp (Model #7825-34, Ace Glass, Inc.). All other reagents were used as purchased from commercial sources. Elemental analyses were performed by Atlantic Microlabs, Inc. $[(TMEDA)FeCl_2]_n$ (n = 1, 2) (TMEDA = tetramethylethylenediamine) and Cp*Fe(CO)(NCMe)Ph (**3.1**) was prepared according to the literature procedure.[48,56]

Reaction of Cp*Fe(CO)(NCMe)Ph (3.1) with oxidants. A representative experiment is described. Complex **3.1** (3.5 mg, 10 μmol) and pyridine-*N*-oxide (2.9 mg, 30 μmol) were dissolved in 400 μL of THF-d_8 in an NMR tube. The reaction mixture was placed in an oil bath at 60 °C. The reaction was periodically removed from the oil bath and analyzed by ^{1}H NMR spectroscopy. D_2O (2 μL) was added to the reaction mixture and the products were analyzed by ^{1}H NMR spectroscopy and/or GC-MS.

Cp*Fe(P(OCH$_2$)$_3$CEt)$_2$Cl (3.2) THF (50 mL) was cooled in a glovebox freezer at –30 °C for 30 min. After the cooling time period, the solution was added to a mixture of Cp*Li (1.01 g, 7.1 mmol), $[(TMEDA)FeCl_2]_n$ (n = 1, 2) (1.10 g, 4.53 mmol) and $P(OCH_2)_3CEt$ (2.01 g, 12.3 mmol) in a round bottom flask. The mixture was stirred and allowed to warm to room temperature over a period of approximately 30 min. The red brown mixture was eluted through silica gel on a fine porosity frit using THF. A red brown band was collected, and most of the solvent was removed under vacuum. Hexanes (50 mL) were added to form a precipitate. The red brown solid was collected via vacuum filtration, washed with hexanes and dried in vacuum (1.79 g, 70% yield). ^{1}H NMR (300 MHz, THF-d_8): δ 4.17 (12H, s, P(OC*H*$_2$)$_3$CCH$_2$CH$_3$), 1.51 (15H, s, C$_5$(C*H*$_3$)$_5$), 1.20 (4H, q, $^3J_{HH}$ = 8 Hz, P(OCH$_2$)$_3$CC*H*$_2$CH$_3$), 0.82 (6H, t, $^3J_{HH}$ = 8 Hz, P(OCH$_2$)$_3$CCH$_2$C*H*$_3$). ^{13}C NMR (201 MHz, CD$_3$CN): δ 88.7 (P(O*C*H$_2$)$_3$CCH$_2$CH$_3$), 74.4 (*C*$_5$(CH$_3$)$_5$), 35.5 (P(OCH$_2$)$_3$*C*CH$_2$CH$_3$), 23.7 (P(OCH$_2$)$_3$C*C*H$_2$CH$_3$), 9.3 (C$_5$(*C*H$_3$)$_5$), 7.0 (P(OCH$_2$)$_3$CCH$_2$*C*H$_3$). ^{31}P NMR (121 MHz, CD$_3$CN): δ 163.8 (s).

Cp*Fe(P(OCH$_2$)$_3$CEt)$_2$Ph (3.3) Complex **3.2** (1.02 g, 1.80 mmol) was dissolved in THF (50 mL) in a Schlenk flask. The solution was then cooled in an isopropanol/dry ice bath. A diethyl ether solution of PhLi (1.8 M, 2.2 mL, 4.0 mmol) was added to the solution of **3.2** with stirring. Upon addition of PhLi the mixture turned to yellow from red brown. The mixture was allowed to warm to room temperature. In a glovebox, the solution was eluted through silica gel using THF. A yellow band was collected, and most of the solvent was removed under vacuum. Hexanes (50 mL) were added to form a precipitate. The yellow solid was collected via filtration, washed with hexanes and dried under vacuum (0.71 g, 65% yield). Single crystals suitable for X-ray diffraction were grown by slowly diffusion of pentane into a THF solution of **3.3**. ^{1}H NMR (800 MHz, CD$_3$CN): δ 7.56 (2H, d, $^3J_{HH}$ = 7 Hz, phenyl *ortho*), 6.60 (2H, t, $^3J_{HH}$ = 7 Hz, phenyl *meta*), 6.60 (1H, t, $^3J_{HH}$ = 7 Hz, phenyl *para*), 4.07 (12H, s, P(OC*H*$_2$)$_3$CCH$_2$CH$_3$), 1.42 (15H, s, C$_5$(C*H*$_3$)$_5$), 1.15 (4H, q, $^3J_{HH}$ = 8 Hz, P(OCH$_2$)$_3$CC*H*$_2$CH$_3$), 0.77 (6H, t, $^3J_{HH}$ = 8 Hz, P(OCH$_2$)$_3$CCH$_2$C*H*$_3$). ^{13}C NMR (201 MHz, CD$_3$CN): δ 171.2 (ipso Ph, t, $^2J_{PC}$ = 34 Hz), 146.9, 125.2, 119.9 (Ph), 91.0 (P(O*C*H$_2$)$_3$CCH$_2$CH$_3$), 74.3 (*C*$_5$(CH$_3$)$_5$), 35.5 (P(OCH$_2$)$_3$*C*CH$_2$CH$_3$, t, $^3J_{PC}$ = 15 Hz), 24.0 (P(OCH$_2$)$_3$C*C*H$_2$CH$_3$), 10.0 (C$_5$(*C*H$_3$)$_5$), 7.3

($P(OCH_2)_3CCH_2CH_3$). ^{31}P NMR (121 MHz, CD_3CN): δ 167.3 (s). Anal. Calcd for $C_{28}H_{42}O_6P_2Fe$: C 56.78, H 7.15; found C 56.88, H 7.20.

Cp*Fe(P(OCH$_2$)$_3$CEt)$_2$Me (3.5) Complex **3.5** was made by the same procedure as **3.3** but using MeLi instead of PhLi solution (65% isolated yield). ^1H NMR (300 MHz, CD_3CN): δ 4.02 (12H, s, $P(OCH_2)_3CCH_2CH_3$), 1.53 (15H, s, $C_5(CH_3)_5$), 1.13 (4H, q, $^3J_{HH}$ = 8 Hz, $P(OCH_2)_3CCH_2CH_3$), 0.76 (6H, t, $^3J_{HH}$ = 8 Hz, $P(OCH_2)_3CCH_2CH_3$), –0.96 (3H, t, $^3J_{PH}$ = 6 Hz, CH_3). ^{13}C NMR (201 MHz, CD_3CN): δ 89.0 ($P(OCH_2)_3CCH_2CH_3$), 74.3 ($C_5(CH_3)_5$), 35.3 ($P(OCH_2)_3CCH_2CH_3$, t, $^3J_{PC}$ = 15 Hz), 24.3 ($P(OCH_2)_3CCH_2CH_3$), 9.8 ($C_5(CH_3)_5$), 7.4 ($P(OCH_2)_3CCH_2CH_3$), –16.5 (CH_3, t, $^2J_{PC}$ = 30 Hz). ^{31}P NMR (121 MHz, CD_3CN): δ 167.5 (s). Anal. Calcd for $C_{23}H_{40}O_6P_2Fe$: C 52.21, H 7.60; found C 51.99, H 7.55.

Reaction of Cp*Fe(P(OCH$_2$)$_3$CEt)$_2$Ph (3.3) with Me$_3$NO. Complex **3.3** (3 mg, 5 μmol) and Me_3NO (2 mg, 25 μmol) were mixed in ~ 400 μL of THF-d_8 in an NMR tube with ambient light. The reaction was periodically analyzed by ^1H NMR spectroscopy. The reaction was complete in 4 days. D_2O (2 μL) was added to the reaction mixture and the products were analyzed by ^1H NMR spectroscopy and GC-MS.

Reaction of Cp*Fe(P(OCH$_2$)$_3$CEt)$_2$Ph (3.3) with Me$_3$NO under photolysis. Complex **3.3** (3 mg, 5 μmol) and Me_3NO (2 mg, 25 μmol) were mixed in ~ 400 μL of THF-d_8 in an NMR tube. The solution was placed in a photolysis cabinet with a Hg vapor lamp. The reaction was complete within 2 hour (the products were analyzed by ^1H NMR spectroscopy).

Attempted Catalytic oxidation of benzene by Cp*Fe(P(OCH$_2$)$_3$CEt)$_2$Ph (3.3) with Me$_3$NO. Complex **3.3** (3 mg, 5 μmol) and Me$_3$NO (2 mg, 25 μmol) were mixed in ~ 400 μL of THF-d_8 in an NMR tube. Benzene (2 μL, 22 μmol) and 1,4-cyclohexadiene (2 μL, 21 μmol) was added to the solution. Me$_3$SiSiMe$_3$ (~ 1 μL) was added as an internal standard for ^{1}H NMR spectroscopy. The solution was placed in a photolysis cabinet with a Hg vapor lamp. The reaction was complete within 20 min (the products were analyzed by ^{1}H NMR spectroscopy).

Reaction of Cp*Fe(P(OCH$_2$)$_3$CEt)$_2$Ph (3.3) with O$_2$. Complex **3.3** (3.0 mg, 5. μmol) was dissolved in 400 μL of THF-d_8. The reaction mixture was opened to air under ambient light for 1 day and periodically monitored by ^{1}H NMR spectroscopy. The products were analyzed by ^{1}H and ^{13}C NMR spectroscopy and GC-MS.

Reaction of Cp*Fe(P(OCH$_2$)$_3$CEt)$_2$Ph (3.3) with oxidants. A representative experiment is described. Complex **3.3** (6.0 mg 10.1 μmol) and pyridine-*N*-oxide (4.8 mg 50.0 μmol) were dissolved in 400 μL of THF-d_8 in an NMR tube. The reaction mixture was placed in an oil bath at 70 °C. The reaction was periodically removed from the oil bath and analyzed by ^{1}H NMR spectroscopy. Brønsted acid (D$_2$O or HCl) was added to the reaction mixture and the products were analyzed by ^{1}H NMR spectroscopy and/or GC-MS.

Kinetics for reaction of Cp*Fe(P(OCH$_2$)$_3$CEt)$_2$Ph (3.3) with PMe$_3$. A representative kinetic experiment is described. Complex **3.3** (6.0 mg 10 μmol) and 5 μL of PMe$_3$ (3.6 mg, 50 μmol) were dissolved in 400 μL of THF-d_8. The compound OPPh$_3$ (~ 3 mg) was added as an internal standard for ^{31}P NMR spectroscopy. The reaction mixture was placed in the photolysis cabinet 40 cm away from the Hg vapor lamp (the distance is important). A ^{31}P NMR spectrum was acquired every 10 min. Integration of the ^{31}P NMR peak of complex **3.3** gave the variation in concentration. Similar reactions were set up for 10.0, 15.0 and 20.0 μL of PMe_3. To ensure reproducibility, every concentration was repeated in triplicate.

Kinetics for reaction of $Cp^*Fe(P(OCH_2)_3CEt)_2Ph$ (3.3) with Me_3NO. A representative kinetic experiment is described. Complex **3.3** (0.3 mg, 0.5 μmol) and Me_3NO (3.0 mg, 40 μmol) were dissolved in 500 μL of THF-*d*$_8$ (Me_3NO is partially dissolved and saturated in the solution). The compound $Me_3SiSiMe_3$ (~ 1 μL) was added as an internal standard for ^{1}H NMR spectroscopy. The reaction mixture was placed in the photolysis cabinet 40 cm away from the Hg vapor lamp. A ^{1}H NMR spectrum was acquired every 5 min for the first 30 min and every 10 min thereafter. Integration of the ^{1}H NMR spectra gave the variation in concentration of complex **3.3,** $P(OCH_2)_3CEt$, $PhOH{\cdot}ONMe_3$ and 1,2,3,4-tetramethylfulvene. To ensure reproducibility, each experiment was repeated in triplicate.

Kinetics for reaction of $P(OCH_2)_3CEt$ with Me_3NO. A representative kinetic experiment is described. $P(OCH_2)_3CEt$ (0.3 mg, 0.5 μmol) was dissolved in 1.6 mL of THF-*d*$_8$. The compound $Me_3SiSiMe_3$ (3.0 μL) was added as an internal standard for ^{1}H NMR spectroscopy. Me_3NO (3.0 mg, 40 μmol) was added to a screw-cap tube. A 500 μL aliquot of the $P(OCH_2)_3CEt$ solution was transferred to the Me_3NO in the tube and timed as the start of the reaction. The tube was shaken for about 30 s to help dissolve the Me_3NO (Me_3NO is partially dissolved and saturated in the solution). The reaction mixture was then monitored by array ^{1}H NMR spectroscopy on a 500 MHz spectrometer at room temperature (20.4 °C). ^{1}H NMR spectra were acquired every 2 min for 120 min total. Integration of the ^{1}H NMR spectra gave the variation in concentration of $P(OCH_2)_3CEt$. To ensure reproducibility, each experiment was repeated in triplicate.

Computational Methods. Density functional theory (DFT) within the Gaussian 09 package[57] was used for geometry optimization and vibrational frequency calculations. The hybrid meta-GGA functional – wB97XD[58] was employed with a double zeta basis set with pseudopotentials and added d functions for group elements (*e.g.*, CEP-31G(d)).[59] This functional contains empirical dispersion terms, and also long-range corrections. Tests with a larger, all-electron basis set – including diffuse functions on main group elements (B3LYP/6-31+G(d)) – as well as Truhlar's M06[60] functional (M06/6-31+G(d)) did not yield significantly different calculated geometries or free energies. MECP calculations on full models of **3.3** were carried out at the wB97XD/6-31+G(d) level of theory. Calculations were carried out in the continuum SMD[61] solvation method with THF ($\varepsilon = 7.58$) being the solvent.

The energies quoted are free energies that were calculated at 298.15 K and 1 atm. The stationary points were defined as minima or transition states (TSs) by the presence of 0 or 1 imaginary frequencies, respectively, as obtained from the calculated energy Hessians. Various spin states were studied with only results for the lowest energy spin state reported.

3.5 References

(1) Crabtree, R. H. *J. Chem. Soc., Dalton Trans.* **2001**, 2437.

(2) Harold A. Wittcoff, B. G. R., Jeffery S. Plotkin *Industrial Organic Chemicals*; 2nd ed.; John Wiley & Sons, 2004.

(3) George A. Olah, A. M. *Hydrocarbon Chemistry*; 2nd ed.; John Wiley & Sons, 2003.

(4) Conley, B. L.; Tenn, W. J.; Young, K. J. H.; Ganesh, S.; Meier, S.; Ziatdinov, V.; Mironov, O.; Oxgaard, J.; Gonzales, J.; Goddard, W. A.; Periana, R. A. In *Activation of Small Molecules*; Wiley-VCH Verlag GmbH & Co. KGaA: 2006, p 235.

(5) Goldberg Karen, I.; Goldman Alan, S. In *Activation and Functionalization of C-H Bonds*; American Chemical Society: 2004.

(6) Webb, J. R.; Bolaño, T.; Gunnoe, T. B. *ChemSusChem* **2011**, *4*, 37.

(7) Labinger, J. A.; Bercaw, J. E. *Nature* **2002**, *417*, 507.

(8) Labinger, J. A. *J. Mol. Catal. A: Chem.* **2004**, *220*, 27.

(9) Crabtree, R. H. *Chem. Rev.* **1985**, *85*, 245.

(10) Cavaliere, V. N.; Mindiola, D. J. *Chemical Science* **2012**, *3*, 3356.

(11) Sen, A. *Acc. Chem. Res.* **1998**, *31*, 550.

(12) Periana, R. A.; Taube, D. J.; Evitt, E. R.; Löffler, D. G.; Wentrcek, P. R.; Voss, G.; Masuda, T. *Science* **1993**, *259*, 340.

(13) Muehlhofer, M.; Strassner, T.; Herrmann, W. A. *Angew. Chem. Int. Ed.* **2002**, *41*, 1745.

(14) Shilov, A. E.; Shul'pin, G. B. *Chem. Rev.* **1997**, *97*, 2879.

(15) Conley, B. L.; Ganesh, S. K.; Gonzales, J. M.; Tenn, W. J.; Young, K. J. H.; Oxgaard, J.; Goddard, W. A.; Periana, R. A. *J. Am. Chem. Soc.* **2006**, *128*, 9018.

(16) Bischof, S. M.; Cheng, M.-J.; Nielsen, R. J.; Gunnoe, T. B.; Goddard, W. A.; Periana, R. A. *Organometallics* **2011**, *30*, 2079.

(17) Gonzales, J. M.; Distasio, R.; Periana, R. A.; Goddard, W. A.; Oxgaard, J. *J. Am. Chem. Soc.* **2007**, *129*, 15794.

(18) Tenn, W. J.; Conley, B. L.; Hövelmann, C. H.; Ahlquist, M. r.; Nielsen, R. J.; Ess, D. H.; Oxgaard, J.; Bischof, S. M.; Goddard, W. A.; Periana, R. A. *J. Am. Chem. Soc.* **2009**, *131*, 2466.

(19) Pouy, M. J.; Milczek, E. M.; Figg, T. M.; Otten, B. M.; Prince, B. M.; Gunnoe, T. B.; Cundari, T. R.; Groves, J. T. *J. Am. Chem. Soc.* **2012**, *134*, 12920.

(20) Mei, J.; Carsch, K. M.; Freitag, C. R.; Gunnoe, T. B.; Cundari, T. R. *J. Am. Chem. Soc.* **2013**, *135*, 424.

(21) Feng, Y.; Lail, M.; Barakat, K. A.; Cundari, T. R.; Gunnoe, T. B.; Petersen, J. L. *J. Am. Chem. Soc.* **2005**, *127*, 14174.

(22) Tenn, W. J.; Young, K. J. H.; Bhalla, G.; Oxgaard, J.; Goddard, W. A.; Periana, R. A. *J. Am. Chem. Soc.* **2005**, *127*, 14172.

(23) Kloek, S. M.; Heinekey, D. M.; Goldberg, K. I. *Angew. Chem. Int. Ed.* **2007**, *46*, 4736.

(24) Webb, J. R.; Burgess, S. A.; Cundari, T. R.; Gunnoe, T. B. *Dalton Transactions* **2013**, *42*, 16646.

(25) Bercaw, J. E.; Hazari, N.; Labinger, J. A. *Organometallics* **2009**, *28*, 5489.

(26) Feng, Y.; Lail, M.; Foley, N. A.; Gunnoe, T. B.; Barakat, K. A.; Cundari, T. R.; Petersen, J. L. *J. Am. Chem. Soc.* **2006**, *128*, 7982.

(27) Cundari, T. R.; Grimes, T. V.; Gunnoe, T. B. *J. Am. Chem. Soc.* **2007**, *129*, 13172.

(28) Van Asselt, A.; Trimmer, M. S.; Henling, L. M.; Bercaw, J. E. *J. Am. Chem. Soc.* **1988**, *110*, 8254.

(29) Abu-Omar, M. M.; Hansen, P. J.; Espenson, J. H. *J. Am. Chem. Soc.* **1996**, *118*, 4966.

(30) Webb, J. R.; Figg, T. M.; Otten, B. M.; Cundari, T. R.; Gunnoe, T. B.; Sabat, M. *Eur. J. Inorg. Chem.* **2013**, *2013*, 4515.

(31) Figg, T. M.; Webb, J. R.; Cundari, T. R.; Gunnoe, T. B. *J. Am. Chem. Soc.* **2011**, *134*, 2332.

(32) Brown, S. N.; Mayer, J. M. *J. Am. Chem. Soc.* **1994**, *116*, 2219.

(33) Brown, S. N.; Mayer, J. M. *Organometallics* **1995**, *14*, 2951.

(34) Brown, S. N.; Mayer, J. M. *J. Am. Chem. Soc.* **1996**, *118*, 12119.

(35) Matsunaga, P. T.; Hillhouse, G. L.; Rheingold, A. L. *J. Am. Chem. Soc.* **1993**, *115*, 2075.

(36) Koo, K.; Hillhouse, G. L.; Rheingold, A. L. *Organometallics* **1995**, *14*, 456.

(37) Matsunaga, P. T.; Mavropoulos, J. C.; Hillhouse, G. L. *Polyhedron* **1995**, *14*, 175.

(38) Alsters, P. L.; Boersma, J.; van Koten, G. *Organometallics* **1993**, *12*, 1629.

(39) Alsters, P. L.; Teunissen, H. T.; Boersma, J.; Spek, A. L.; van Koten, G. *Organometallics* **1993**, *12*, 4691.

(40) Figg, T. M.; Cundari, T. R. *Organometallics* **2012**, *31*, 4998.

(41) Kamaraj, K.; Bandyopadhyay, D. *Organometallics* **1999**, *18*, 438.

(42) Wadhwani, P.; Bandyopadhyay, D. *Organometallics* **2000**, *19*, 4435.

(43) Pardue, D. B.; Mei, J.; Cundari, T. R.; Gunnoe, T. B. *Inorg. Chem.* **2014**, *53*, 2968.

(44) Shu, L.; Nesheim, J. C.; Kauffmann, K.; Münck, E.; Lipscomb, J. D.; Que Jr, L. *Science* **1997**, *275*, 515.

(45) Liu, K. E.; Lippard, S. J. In *Adv. Inorg. Chem.*; Sykes, A. G., Ed.; Academic Press: 1995; Vol. Volume 42, p 263.

(46) Wallar, B. J.; Lipscomb, J. D. *Chem. Rev.* **1996**, *96*, 2625.

(47) Groves, J. T.; McClusky, G. A. *J. Am. Chem. Soc.* **1976**, *98*, 859.

(48) Kalman, S. E.; Petit, A.; Gunnoe, T. B.; Ess, D. H.; Cundari, T. R.; Sabat, M. *Organometallics* **2013**, *32*, 1797.

(49) Mei, J.; Pardue, D. B.; Kalman, S. E.; Gunnoe, T. B.; Cundari, T. R.; Sabat, M. *Organometallics* **2014**, *33*, 5597.

(50) Tilset, M.; Fjeldahl, I.; Hamon, J.-R.; Hamon, P.; Toupet, L.; Saillard, J.-Y.; Costuas, K.; Haynes, A. *J. Am. Chem. Soc.* **2001**, *123*, 9984.

(51) Mendenhall, G. D.; Kessick, R. F.; Dobrzelewski, M. *Journal of Photochemistry* **1984**, *25*, 227.

(52) Beckwith, A. L. J.; Bowry, V. W.; Ingold, K. U. *J. Am. Chem. Soc.* **1992**, *114*, 4983.

(53) Harvey, J. N.; Aschi, M.; Schwarz, H.; Koch, W. *Theor. Chem. Acc.* **1998**, *99*, 95.

(54) N. Harvey, J.; Aschi, M. *PCCP* **1999**, *1*, 5555.

(55) Sako, M.; Shimada, K.; Hirota, K.; Maki, Y. *J. Am. Chem. Soc.* **1986**, *108*, 6039.

(56) C. Davies, S.; L. Hughes, D.; Jeffery Leigh, G.; Roger Sanders, J.; S. de Souza, J. *J. Chem. Soc., Dalton Trans.* **1997**, 1981.

(57) Frisch, M. J., G.W. Trucks, H.B. Schlegel, G.E. Scuseria, M.A. Robb, J.R. Cheeseman, G. Scalmani, V. Barone, B. Mennucci, G.A. Petersson, H. Nakatsuji, M. Caricato, X. Li, H.P. Hratchian, A.F. Izmaylov, J. Bloino, G. Zheng, J.L. Sonnenberg, M. Hada, M. Ehara, K. Toyota, R. Fukuda, J. Hasegawa, M. Ishida, T. Nakajima, Y. Honda, O. Kitao, H. Nakai, T. Vreven, J. Montgomery, J. A., J.E. Peralta, F. Ogliaro, M. Bearpark, J.J. Heyd, E. Brothers, K.N. Kudin, V.N. Staroverov, R. Kobayashi, J.R. Normand, K., A. Rendell, J.C. Burant, S.S. Iyengar, J. Tomasi, M. Cossi, N. Rega, N.J. Millam, M. Klene, J.E. Knox, J.B. Cross, V. Bakken, C. Adamo, J. Jaramillo, R. Gomperts, R.E. Stratmann, O. Yazyev, A.J. Austin, R. Cammi, C. Pomelli, J.W. Ochterski, R.L. Martin, K. Morokuma, V.G. Zakrzewski, G.A. Voth, P. Salvador, J.J. Dannenberg, S. Dapprich, A.D. Daniels, Ö. Farkas, J.B. Foresman, J.V. Ortiz, J. Cioslowski, D.J. Fox, Gaussian; Revision B.01 ed.; Gaussian Inc: Wallinford, CT, 2009.

(58) Grimme, S. *J. Comput. Chem.* **2006**, *27*, 1787.

(59) Stevens, W. J.; Krauss, M.; Basch, H.; Jasien, P. G. *Can. J. Chem.* **1992**, *70*, 612.

(60) Zhao, Y.; Truhlar, D. *Theor. Chem. Acc.* **2008**, *120*, 215.

(61) Marenich, A. V.; Cramer, C. J.; Truhlar, D. G. *The Journal of Physical Chemistry B* **2009**, *113*, 6378.

4 Oxygen Atom Insertion into Cobalt(I) Methyl Bond

4.1 Rationale for study of Oxygen Atom Insertion into Co–C bonds

The catalytic selective oxidation of hydrocarbons to functionalized products is a fundamentally important process in chemical industry.[1-14] As discussed in Chapter One, the transformation of methane to methanol is one of the most attractive targets. However, because of the inert nature of alkanes and over oxidation of the more reactive products, partial oxidation of methane to methanol is one of the most challenging processes.

As discussed in Chapter One, transition metal catalysts for the partial oxidation of alkanes to form alcohols must be able to perform two key steps: C–H bond activation and C–O bond formation. One strategy is the Shilov-type systems[14,15], which perform the C–H bond activation and C–O bond formation at two different oxidation states and involves three steps: 1) a low oxidation state metal catalyst serves to activate the C–H bond of hydrocarbons to form the meta–hydrocarbyl (M–R); 2) oxidation of the metal center to a high oxidation state (generally via a net 2 e^- process); 3) reductive elimination of the M–R and X^- from the metal center to form the C–X bond and generate the functionalized product. In the Shilov system, it has been proposed that C–H bond activation occurs at Pt^{II} and C–X (X = OH or Cl) bond formation at Pt^{IV}–alkyl by reductive (i.e., reduction of Pt^{IV} to Pt^{II}) nucleophilic addition to an electrophilic Pt^{IV}–alkyl ligand. The use of expensive Pt^{IV} as a stoichiometric oxidant to convert Pt^{II}–alkyl to Pt^{IV}–alkyl limits the utility of this catalyst (Scheme 4.1)[14-16]. Periana and co-workers improved this system by using concentrated sulfate acid as the oxidants but the new catalyst still suffers from the inhibition by the accumulated methyl bisulfate product. [17]

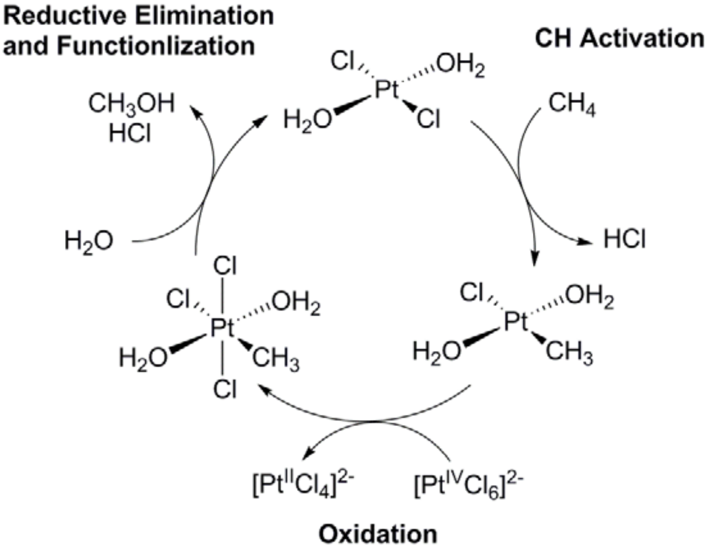

Scheme 4.1. Proposed catalytic cycle for methane functionalization by Shilov system.

Another strategy is to serve C–H bond activation and C–O bond formation at the same oxidation state via a non-redox pathway (Scheme 4.2).[6,18-21] This catalytic cycle has C–H bond activation by 1,2-addition across a metal-alkoxide bond (M–OR) to generate the functionalized alcohol and M–R, a net oxygen atom insertion into the M–R bond from oxygen donor YO to reform the M–OR completes the catalytic cycle. Recycling YO by O_2 would lower the cost of the process. The C–O bond formation involves net oxygen atom insertion into metal–alkyl bonds, which can occur via a metal–oxo intermediate or a Baeyer-Villiger type pathway.[6,18,19,22,23] The Baeyer-Villiger pathway involves concerted C–O bond formation with Y–O bond breaking (Scheme 4.2).

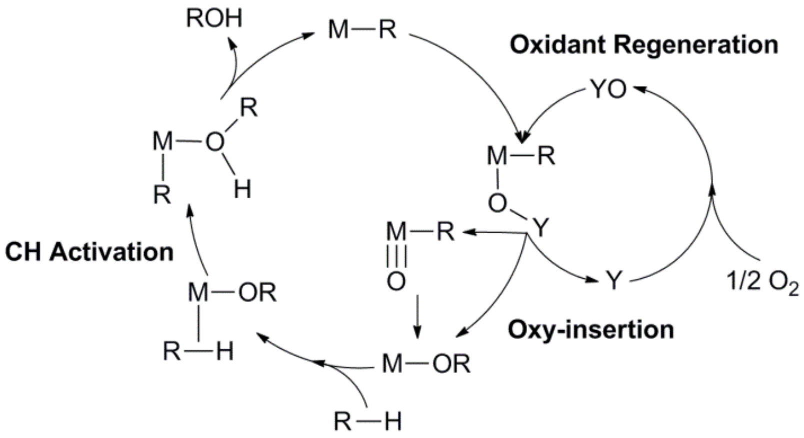

Scheme 4.2. Proposed pathways for partial oxidation of hydrocarbons involving oxygen atom insertion into a M–R bond and 1,2-CH-Addition across a M–OR bond.

In Chapter One, we discussed the examples of C–H bonds via 1,2-addition across M–OR bonds including the intermolecular benzene C–H activation by Ru^{II} hydroxide and anilide complexes by our group,[20,24] an Ir^{III} complex and Ru^{II} complexes by Periana, Goddard *et al.*,[25,26] a Rh^{I} complex reported by Heinekey, Goldberg *et al.*,[27] and a Rh^{I} complex reported by Bercaw, Labinger *et al.*[28] Examples of C–O bond formation via O-atom insertion into M–C bonds were also discussed. The insertions of oxygen atoms into M–C bonds via non-radical routes are rare. The majority of examples of O-atom insertion into M–T bonds involve high valent d^0 metals including Ta^{IV}, Cr^{VI}, Re^{VII} and our W^{VI} complexes,[18,22,29-34] which are incapable of C–H activation. To our knowledge, O-atom insertion into M–R bonds for non-d^0 metals include only Ni^{II}, Pd^{II} and one example of a two-coordinate Fe^{II}, our Fe^{II} complex, and a recently reported Ir^{III} complex. [35-40]

Computational studies for O-atom insertion into late(r) transition metal–carbon bonds by Cundari group indicate that the first row metals (Fe, Co, Ni) possess the lowest activation barriers for the O-atom insertion via the migration of R group to a M=O intermediate.[41] As discussed in Chapter One, computational studies for the O-atom insertion into Ni–C bond in the Hillhouse system reveal the pathway involving the metal-oxo intermediate has the lowest activation barrier (Scheme 4.3).[42] In Chapter Three, calculations for the O-insertion into Fe–C bond also prefer the pathway via Fe=O intermediate (Scheme 4.4).[40] However, O-atom insertion into Co–C bond has never been reported. Co^I complexes have been reported to perform C–H activation and catalyze reactions via C–H activation for a long time. Herein, we reported our attempts to perform O-atom insertion into Co^I–C bonds via the reactions of $(N_3)CoMe$ (N_3 = 2,6-diacetylpyridinebis(2,6-diisopropylanil)) (**4.1**) with a series of oxidants.

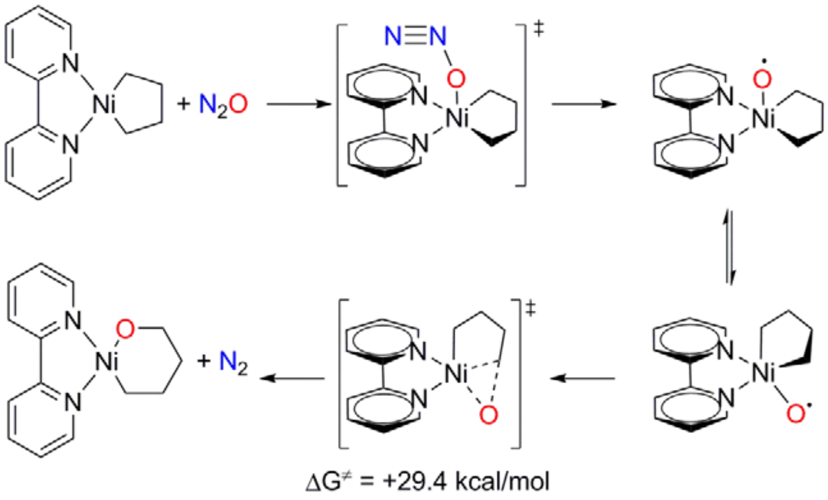

Scheme 4.3. Calculated pathway for oxygen atom insertion into Ni–C bond in Hillhouse reaction.

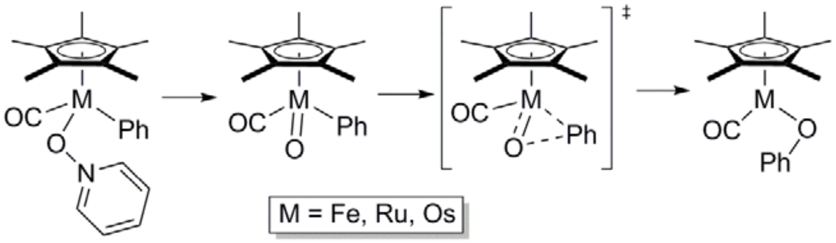

Scheme 4.4. O-atom insertion into Cp*M(CO)(NCMe)R via formation of the M=O.

4.2 Results and Discussion

4.2.1 Synthesis of (N_3)CoMe (4.1)

The 2,6-diacetylpyridinebis(2,6-diisopropylanil) ligand was prepared by the reported procedures.[43] The condensation of 2,6-diacetylpyridine and 2,6-diisopropylaniline was catalyzed by acetic acid in pure ethanol to produce the high yield product. Reaction of the N_3 ligand and $CoCl_2$ in THF to generated the (N_3)$CoCl_2$, which is methylated and reduced by 2 equiv. of MeLi to produce the (N_3)CoMe (**4.1**) in 90% yield by ^{1}H NMR (Scheme 4.5). ^{1}H NMR spectrum of (N_3)CoMe is shown in Figure 4.1. Attempt at recrystallization of **4.1** in toluene at –65 °C resulted in no pure crystals.

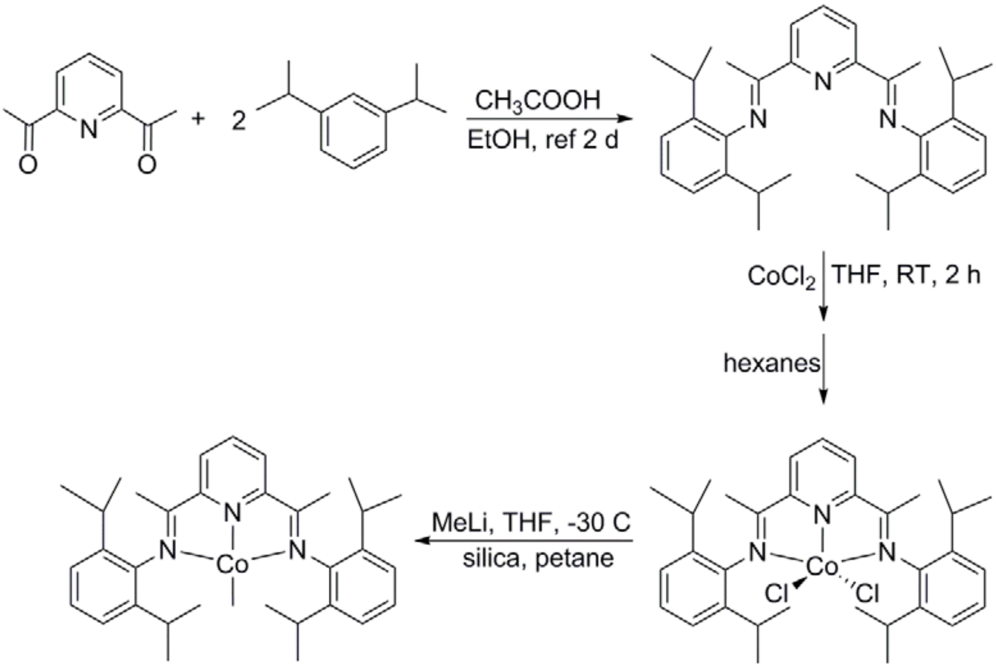

Scheme 4.5. Synthesis of (N_3)CoMe (**4.1**).

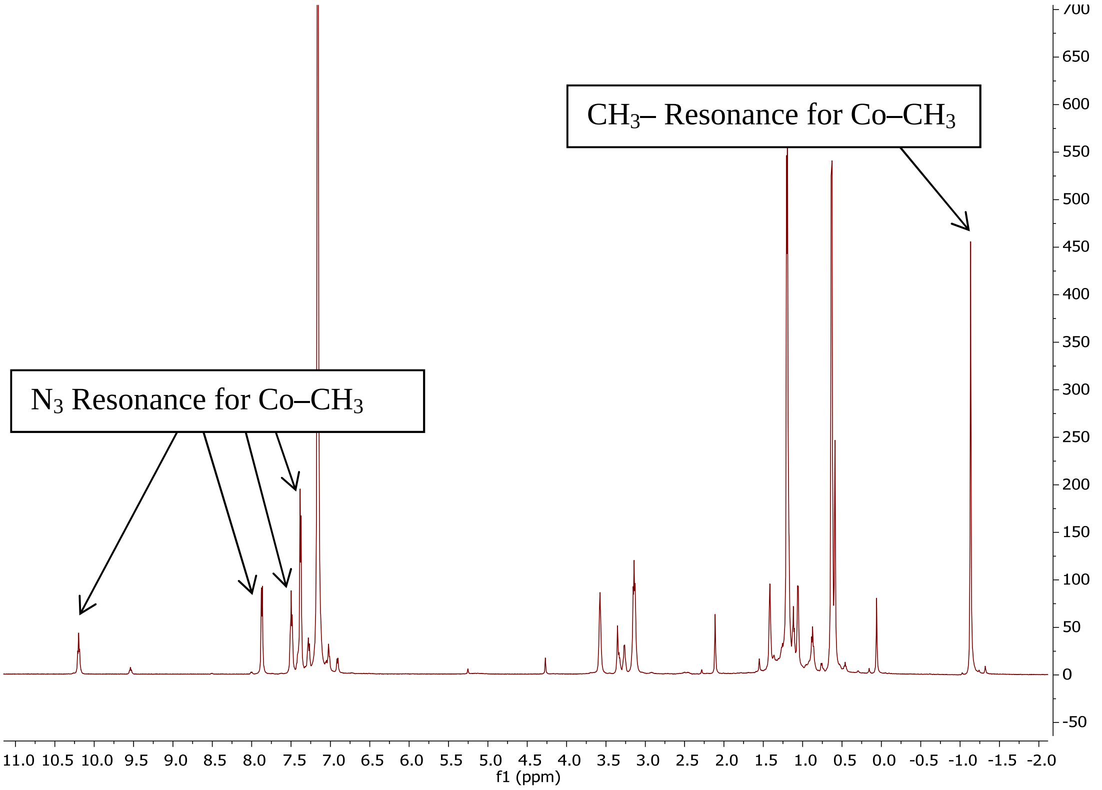

Figure 4.1. ^{1}H NMR spectrum of (N_3)CoMe (**4.1**) in C_6D_6 at room temperature.

4.2 Reactions of (N_3)CoMe (4.1) with Oxidants

Complex **4.1** reacted with more than 1 equiv. of H_2O_2 (~35% aqueous solution) in THF immediately. The color of the reaction mixture changed from purple to dark green. The mixture then converted to light green solution and dark precipitations. ^{1}H NMR spectra reveal that free N_3 ligand was produced, along with ~20% yield of MeOH in the solution (eq 4.1). When less than 1 equiv. of H_2O_2 was used, partial starting material reacted and resulted in the same products.

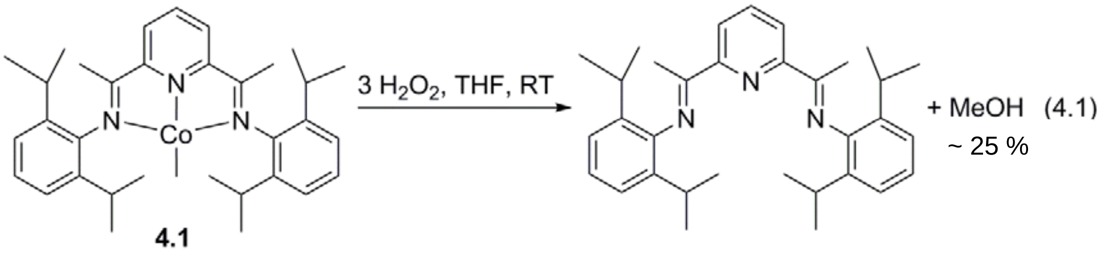

(4.1)

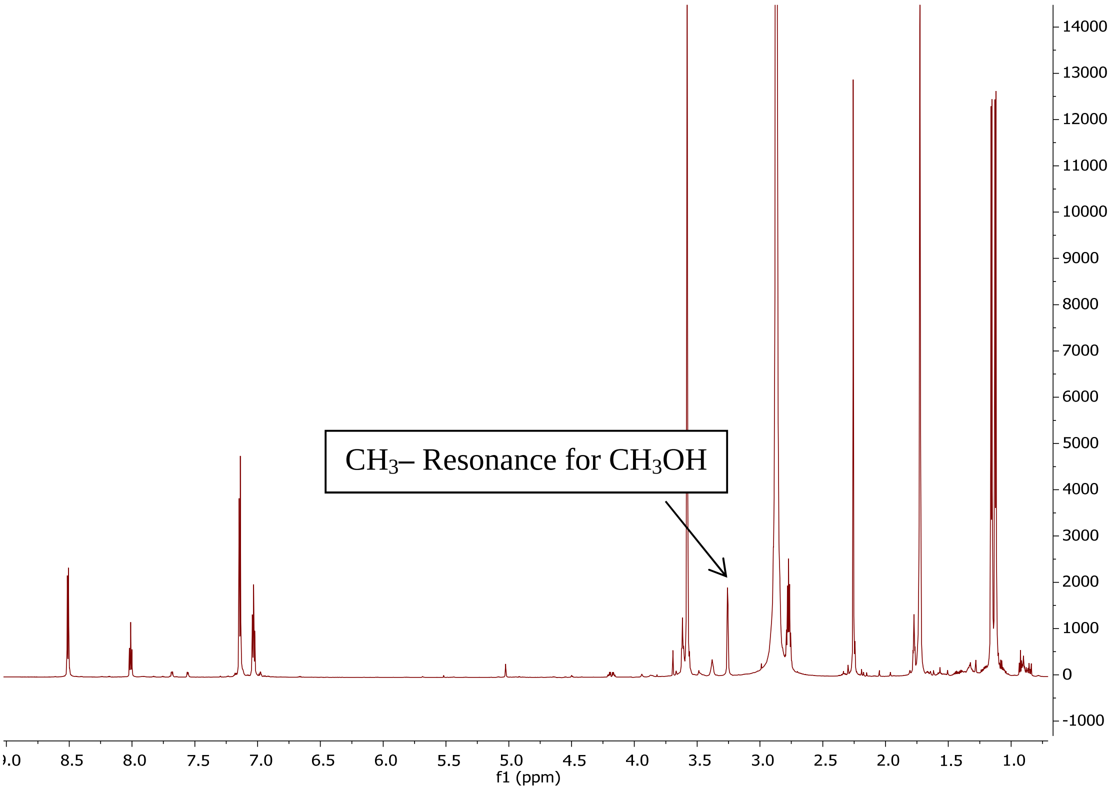

Figure 4.2. ^{1}H NMR spectrum for the reaction of $(N_3)CoMe$ (**4.1**) and H_2O_2 (~35% aq) in THF-d_8.

We first considered a radical pathway for the methanol release reaction from complex **4.1** and H_2O_2. However, no significant change in the product or rate is observed when the same reaction is performed in the presence of radical traps such as TEMPO [(2,2,6,6-tetramethylpiperidin-1-yl)oxyl] or 1,4-cyclohexadiene. Since TEMPO is known to trap methyl radical,[44] this suggests that free methyl radical is not formed in the reaction of **4.1** with H_2O_2. However, these experiments cannot rule out a short-lived methyl radical that rapidly recombines with a Co–O moiety. Then we considered that the methanol release from **4.1** and H_2O_2 was formed by protonlysis of the methoxide which was from the O-atom insertion into Co–C bond via the formation of a Co-oxo intermediate. The same reaction was set up at low temperature (–65 °C) to trap this assumed Co-oxo intermediate. Dark green solution was formed intermediately after the H_2O_2 was added to the solution of complex **4.1**. The solution was stable at –65 °C for hours without any precipitation. However, the reaction mixture started to decompose as it warmed up when taken to monitor by NMR spectroscopy or IR spectroscopy.

Complex **4.1** reacts with *m*-CPBA (*m*-CPBA = *meta*-chloroperoxybenzoic acid) and Me_3NO in THF-d_8 at room temperature to give unknown products with precipitation. ^{1}H NMR spectra showed a singlet at ~4.6 ppm, which is likely for a methylene resonance of a Co–OMe to show up. Adding proton source (D_2O) to the reaction mixture yielded ~20% MeOH by ^{1}H NMR spectroscopy (Figure 4.3). Low temperature reactions resulted in the similar decomposition as the low temperature reaction of **4.1** with H_2O_2 (see above). When less than 1 equiv. of *m*-CPBA was used, partial reaction occurred.

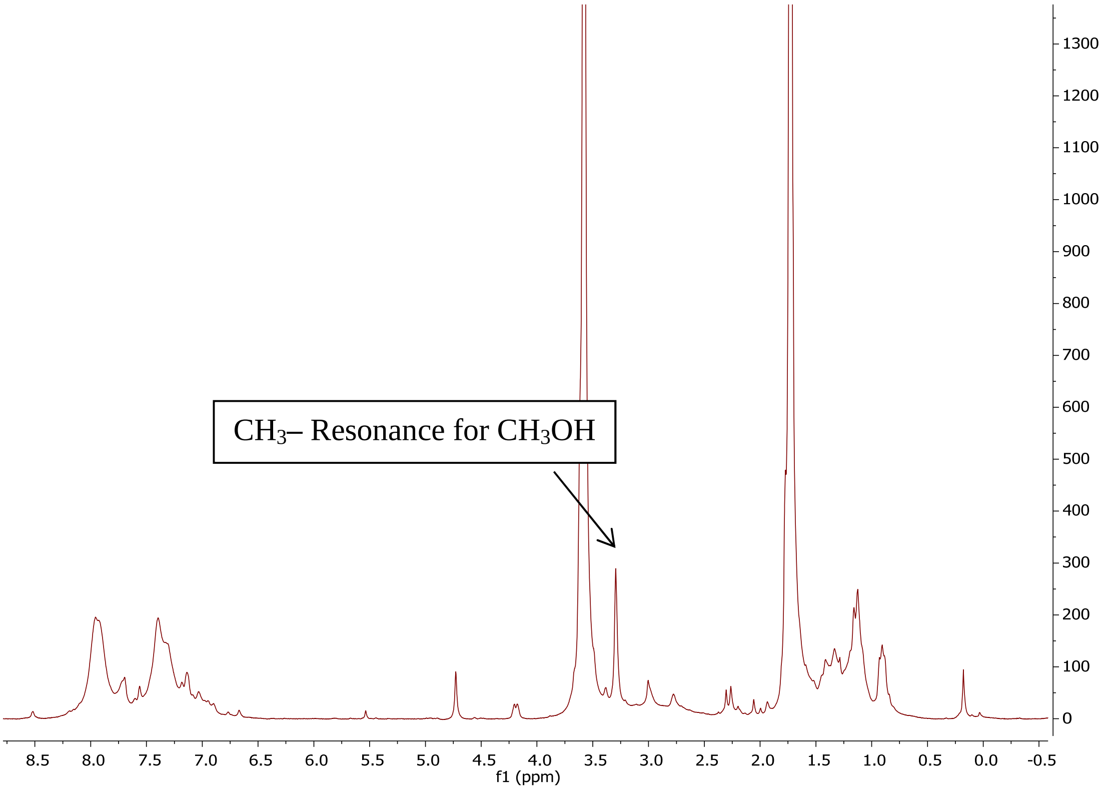

Figure 4.3. ^{1}H NMR spectrum for the reaction of (N$_3$)CoMe (**4.1**) and excess *m*CPBA in THF-d_8 at room temperature after added 1 μL D_2O.

Complex **4.1** also reacted intermediately with Me_3NO in THF-d_8 at room temperature to generate precipitates, free ligand, partial yield of MeOH and partial yield of unknown product with asinglet resonance at 4.5 ppm in ^{1}H NMR spectrum. Adding D_2O to the reaction mixture resulted in the disappearance of the peak at 4.5 ppm and the generation of MeOH (Figure 4.4). The reactions of complex **4.1** and *m*-CPBA and Me_3NO are summarized in eq 4.2.

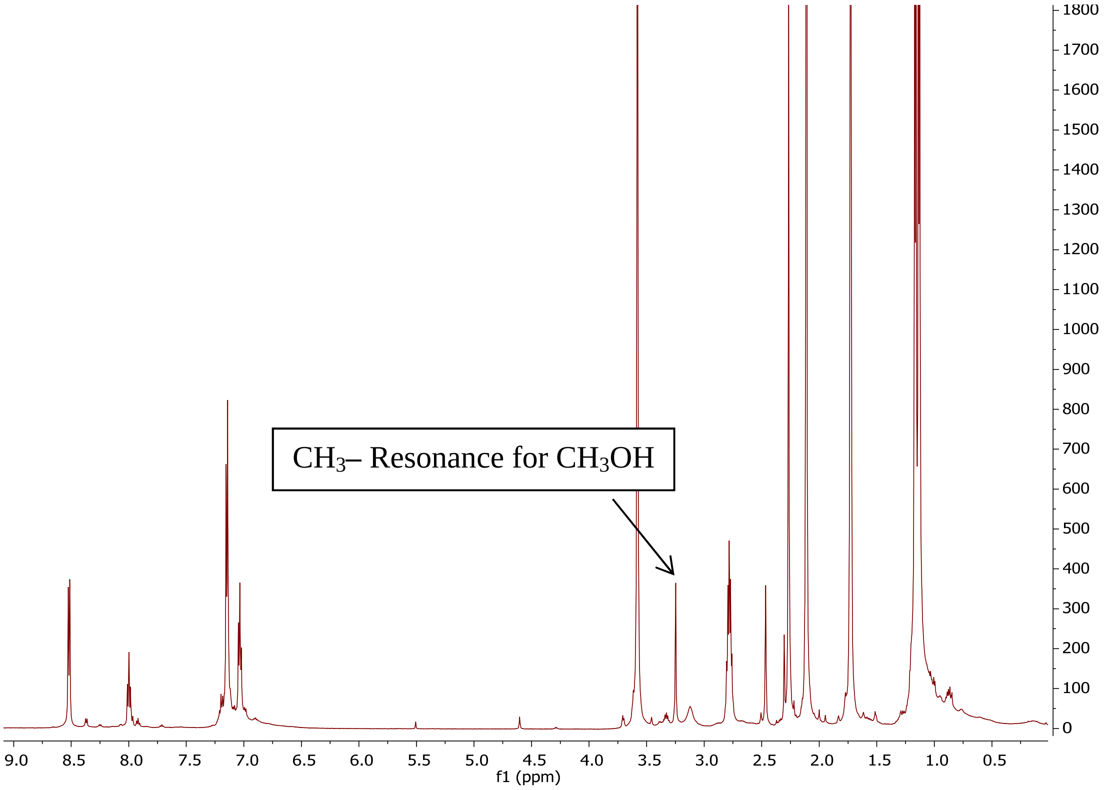

Figure 4.4. ^{1}H NMR spectrum for the reaction of (N_3)CoMe (**4.1**) and excess Me_3NO in THF-d_8 at room temprature.

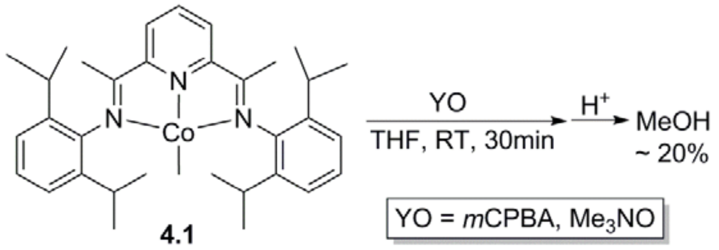

4.1

(4.2)

Complex **4.1** did not react with PyO until heating at 90 °C for 20 h. ^{1}H NMR spectra showed that **4.1** decomposed to generate free N_3 ligand and CH_3CH_3 (Figure 4.5) (eq 4.3). Thermolysis of **4.1** in THF-d_8 at 90 °C for 24 h did not result in decomposition. The CH_3CH_3 is probably produced via a radical pathway initiated by the decomposition of PyO in THF-d_8 at 90 °C.

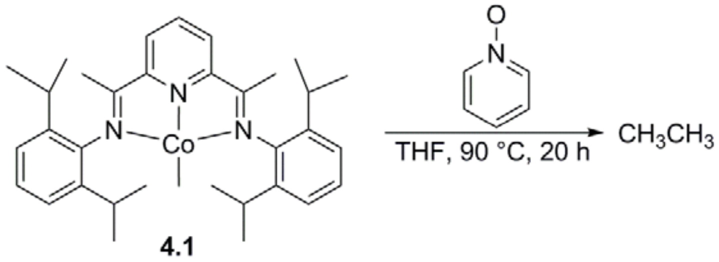

(4.3)

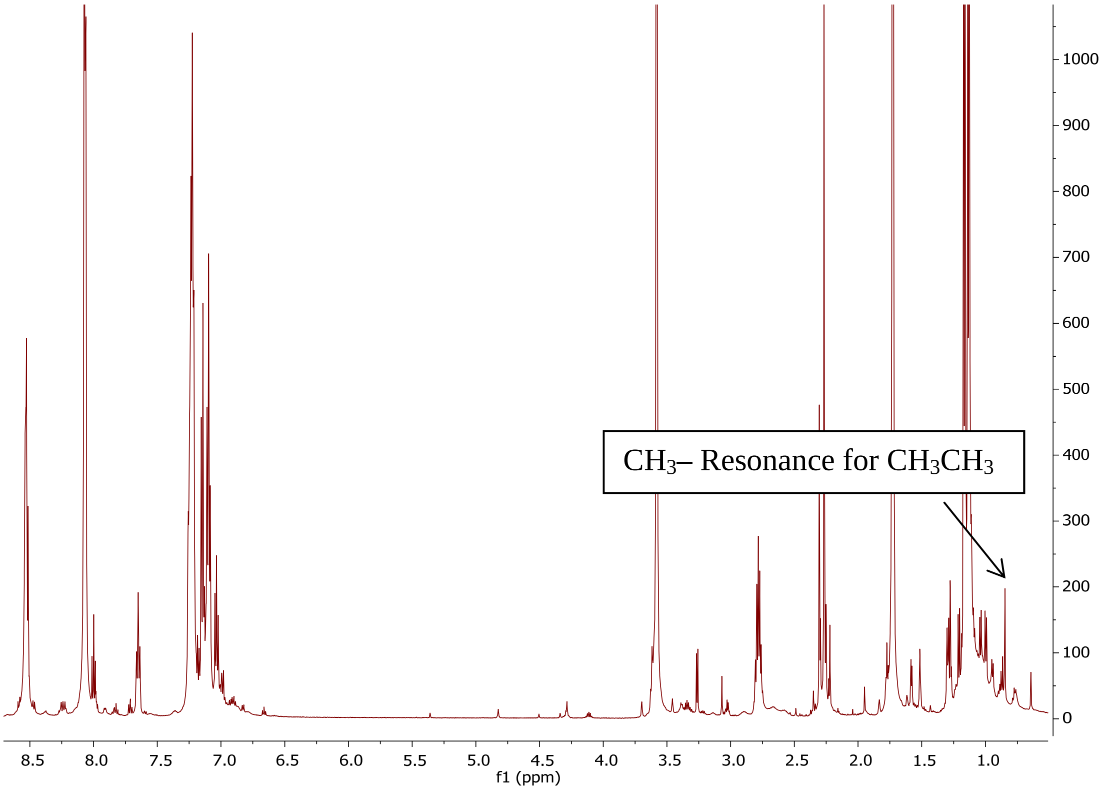

Figure 4.5. ^{1}H NMR spectrum for the reaction of (N_3)CoMe (**4.1**) and excess PyO in THF-d_8 at 90 °C for 20 hours.

Complex **4.1** reacted with ^{t}BuOOH intermediately in THF-d_8 at room temperature to generate a paramagnetic mixture, which decomposed when heated. The reaction conditions and results of complex **4.1** and various of oxidants discussed above are summarized in Table **4.1**.

Table 4.1. Reaction conditions and products for $(N_3)CoMe$ (**4.1**) and oxidants[a]

No.	Oxidant[b]	T (°C)	t (min)	Product[c]
1	H_2O_2	23	30	~25% MeOH
2	H_2O_2 (TEMPO)	23	30	~25% MeOH
3	H_2O_2 (CHD)	23	30	~25% MeOH
4	mCPBA	23	30	~20% MeOH
5	Me_3NO	23	30	~20% MeOH
6	PyO	90	24 h	CH_3CH_3
7	^tBuOOH	23	30	decompose

[a] The reactions are in THF-d_8 with trace D_2O added to the reaction mixture. [b] Excess oxidants are used in the reactions. [c] Yields are based on ^1H NMR integration.

4.3. Summary and Discussion

The production of MeOH from the reactions of complex **4.1** and oxidants (H_2O_2, *m*-CPBA, Me_3NO, see above) with proton source provides a promising result for O-atom insertion into Co–CH_3 bond, although few data have been collected. However, further study of the O-atom insertion into complex **4.1** and study of selective oxidation of hydrocarbons catalyzed by **4.1** were abandoned for two following reason: 1) Complex **4.1** is not feasible for C–H activation under common conditions. There was no reaction for **4.1** heating in C_6D_6 at 140 °C for 24 hours. 2) For all the promising results that involve methanol production, complex **4.1** decomposed with the N_3 ligand no longer coordinated with the Co center, which would terminate the catalytic reaction. Actually, no catalysis was observed for the selective oxidation of benzene with various of oxidants in the presence of complex **4.1**. Thus, the studies of O-atom insertion into complex **4.1** point us the direction for O-atom insertion into Co–C bond and catalyst design for selective oxidation of hydrocarbons: a more electron donating ligand to provide a stronger coordination with the metal center which might be survive with oxidants involved.

4.4. Experimental Section

General Methods. Unless otherwise noted, all synthetic procedures were performed under anaerobic conditions in a nitrogen filled glovebox or by using standard Schlenk techniques. Glovebox purity was maintained by periodic nitrogen purges and was monitored by an oxygen analyzer (O_2 < 15 ppm for all reactions). Tetrahydrofuran was dried by distillation from sodium/benzophenone. Diethyl ether was distilled over CaH_2. THF-d_8, CD_3CN, THF-d_8 were used as received and stored under a N_2 atmosphere over 4 Å molecular sieves (except water). ^1H NMR spectra were recorded on a Varian Mercury 300 MHz, Varian Inova 500 MHz, or Bruker 800 MHz spectrometer. ^{13}C NMR spectra were recorded using a Varian Mercury 300 MHz (operating frequency 75 MHz), Varian Inova 500 MHz (operating frequency 125 MHz), or Bruker 800 MHz (operating frequency 201 MHz) spectrometer. All ^1H and ^{13}C [^1H} spectra are referenced against residual proton signals (^1H NMR) or the ^{13}C signals of the deuterated solvents (^{13}C [^1H} NMR). GC/MS was performed using a Shimadzu GCMS-QP2010 Plus system with a 30 m × 0.25 mm RTx-Qbond column with 8 µm thickness using electron impact ionization. All other reagents were used as purchased from commercial sources. Elemental analyses were performed by Atlantic Microlabs, Inc. N_3 ligand (N_3 = 2,6-diacetylpyridinebis(2,6-diisopropylanil)) and $(N_3)CoCl_2$ were prepared according to the literature procedure.[43,45]

Synthesis of (N_3)CoMe) (4.1) (N_3)$CoCl_2$ (0.41g, 0.65mmol) was dissolved in ~50 mL THF in the flask and the solution was put in the cold well at –65 °C for an hour. The solution of was taken out and stirred vigorously. MeLi in Et_2O solution (1.6 M, 0.80 mL, 1.3 mmol) was added to the solution and stirred for about 20 min. The color of the reaction mixture changed from brown to purple intermediately. The reaction mixture was then run though a frit with Celite and the solvent was removed under vacuum to yield the purple solid (0.31g, 72%).

Reactions of (N_3)CoMe (4.1) with hydrogen peroxide. Complex **4.1** (6.0 mg 10.1 µmol) was dissolved in 400 µL of THF-d_8 in a screw-up NMR tube and taken out of the box. H_2O_2 solution (~35%, 2.0 µL, 22 µmol) was injected to the solution of **4.1**. The reaction mixture was periodically removed from the oil bath and analyzed by ^1H NMR spectroscopy. Brønsted acid (D_2O or HCl) was added to the reaction mixture and the products were analyzed by ^1H NMR spectroscopy and/or GC-MS.

Reactions of (N_3)CoMe (4.1) with oxidants. A representative experiment is described. Complex **4.1** (6.0 mg 10.1 µmol) and pyridine-*N*-oxide (2.0 mg 21 µmol) were dissolved in 400 µL of THF-d_8 in an NMR tube. The reaction mixture was placed in an oil bath at 70 °C. The reaction was periodically removed from the oil bath and analyzed by ^1H NMR spectroscopy. Brønsted acid (D_2O or HCl) was added to the reaction mixture and the products were analyzed by ^1H NMR spectroscopy and/or GC-MS.

4.5. References

(1) Harold A. Wittcoff, B. G. R., Jeffery S. Plotkin *Industrial Organic Chemicals*; 2nd ed.; John Wiley & Sons, 2004.

(2) Crabtree, R. H. *J. Chem. Soc., Dalton Trans.* **2001**, 2437.

(3) George A. Olah, A. M. *Hydrocarbon Chemistry*; 2nd ed.; John Wiley & Sons, 2003.

(4) Conley, B. L.; Tenn, W. J.; Young, K. J. H.; Ganesh, S.; Meier, S.; Ziatdinov, V.; Mironov, O.; Oxgaard, J.; Gonzales, J.; Goddard, W. A.; Periana, R. A. In *Activation of Small Molecules*; Wiley-VCH Verlag GmbH & Co. KGaA: 2006, p 235.

(5) Goldberg Karen, I.; Goldman Alan, S. In *Activation and Functionalization of C-H Bonds*; American Chemical Society: 2004.

(6) Webb, J. R.; Bolaño, T.; Gunnoe, T. B. *ChemSusChem* **2011**, *4*, 37.

(7) Labinger, J. A.; Bercaw, J. E. *Nature* **2002**, *417*, 507.

(8) Labinger, J. A. *J. Mol. Catal. A: Chem.* **2004**, *220*, 27.

(9) Crabtree, R. H. *Chem. Rev.* **1985**, *85*, 245.

(10) Cavaliere, V. N.; Mindiola, D. J. *Chemical Science* **2012**, *3*, 3356.

(11) Sen, A. *Acc. Chem. Res.* **1998**, *31*, 550.

(12) Periana, R. A.; Taube, D. J.; Evitt, E. R.; Löffler, D. G.; Wentrcek, P. R.; Voss, G.; Masuda, T. *Science* **1993**, *259*, 340.

(13) Muehlhofer, M.; Strassner, T.; Herrmann, W. A. *Angew. Chem. Int. Ed.* **2002**, *41*, 1745.

(14) Shilov, A. E.; Shul'pin, G. B. *Chem. Rev.* **1997**, *97*, 2879.

(15) Stahl, S. S.; Labinger, J. A.; Bercaw, J. E. *Angew. Chem. Int. Ed.* **1998**, *37*, 2180.

(16) Lersch, M.; Tilset, M. *Chem. Rev.* **2005**, *105*, 2471.

(17) Periana, R. A.; Taube, D. J.; Gamble, S.; Taube, H.; Satoh, T.; Fujii, H. *Science* **1998**, *280*, 560.

(18) Conley, B. L.; Ganesh, S. K.; Gonzales, J. M.; Tenn, W. J.; Young, K. J. H.; Oxgaard, J.; Goddard, W. A.; Periana, R. A. *J. Am. Chem. Soc.* **2006**, *128*, 9018.

(19) Tenn, W. J.; Conley, B. L.; Hövelmann, C. H.; Ahlquist, M. R.; Nielsen, R. J.; Ess, D. H.; Oxgaard, J.; Bischof, S. M.; Goddard, W. A.; Periana, R. A. *J. Am. Chem. Soc.* **2009**, *131*, 2466.

(20) Feng, Y.; Lail, M.; Barakat, K. A.; Cundari, T. R.; Gunnoe, T. B.; Petersen, J. L. *J. Am. Chem. Soc.* **2005**, *127*, 14174.

(21) Figg, T. M.; Webb, J. R.; Cundari, T. R.; Gunnoe, T. B. *J. Am. Chem. Soc.* **2011**, *134*, 2332.

(22) Bischof, S. M.; Cheng, M.-J.; Nielsen, R. J.; Gunnoe, T. B.; Goddard, W. A.; Periana, R. A. *Organometallics* **2011**, *30*, 2079.

(23) Gonzales, J. M.; Distasio, R.; Periana, R. A.; Goddard, W. A.; Oxgaard, J. *J. Am. Chem. Soc.* **2007**, *129*, 15794.

(24) Feng, Y.; Lail, M.; Foley, N. A.; Gunnoe, T. B.; Barakat, K. A.; Cundari, T. R.; Petersen, J. L. *J. Am. Chem. Soc.* **2006**, *128*, 7982.

(25) Tenn, W. J.; Young, K. J. H.; Bhalla, G.; Oxgaard, J.; Goddard, W. A.; Periana, R. A. *J. Am. Chem. Soc.* **2005**, *127*, 14172.

(26) Hashiguchi, B. G.; Young, K. J. H.; Yousufuddin, M.; Goddard, W. A.; Periana, R. A. *J. Am. Chem. Soc.* **2010**, *132*, 12542.

(27) Kloek, S. M.; Heinekey, D. M.; Goldberg, K. I. *Angew. Chem. Int. Ed.* **2007**, *46*, 4736.

(28) Bercaw, J. E.; Hazari, N.; Labinger, J. A. *Organometallics* **2009**, *28*, 5489.

(29) Van Asselt, A.; Trimmer, M. S.; Henling, L. M.; Bercaw, J. E. *J. Am. Chem. Soc.* **1988**, *110*, 8254.

(30) Hess, A.; Hörz, M. R.; Liable-Sands, L. M.; Lindner, D. C.; Rheingold, A. L.; Theopold, K. H. *Angew. Chem. Int. Ed.* **1999**, *38*, 166.

(31) Brown, S. N.; Mayer, J. M. *J. Am. Chem. Soc.* **1994**, *116*, 2219.

(32) Brown, S. N.; Mayer, J. M. *Organometallics* **1995**, *14*, 2951.

(33) Brown, S. N.; Mayer, J. M. *J. Am. Chem. Soc.* **1996**, *118*, 12119.

(34) Mei, J.; Carsch, K. M.; Freitag, C. R.; Gunnoe, T. B.; Cundari, T. R. *J. Am. Chem. Soc.* **2013**, *135*, 424.

(35) Matsunaga, P. T.; Hillhouse, G. L.; Rheingold, A. L. *J. Am. Chem. Soc.* **1993**, *115*, 2075.

(36) Koo, K.; Hillhouse, G. L.; Rheingold, A. L. *Organometallics* **1995**, *14*, 456.

(37) Matsunaga, P. T.; Mavropoulos, J. C.; Hillhouse, G. L. *Polyhedron* **1995**, *14*, 175.

(38) Alsters, P. L.; Teunissen, H. T.; Boersma, J.; Spek, A. L.; van Koten, G. *Organometallics* **1993**, *12*, 4691.

(39) Ni, C.; Power, P. P. *Chem. Commun.* **2009**, 5543.

(40) Mei, J.; Pardue, D. B.; Kalman, S. E.; Gunnoe, T. B.; Cundari, T. R.; Sabat, M. *Organometallics* **2014**, *33*, 5597.

(41) Unpublished data by Tom Cundari Group

(42) Figg, T. M.; Cundari, T. R. *Organometallics* **2012**, *31*, 4998.

(43) Britovsek, G. J. P.; Bruce, M.; Gibson, V. C.; Kimberley, B. S.; Maddox, P. J.; Mastroianni, S.; McTavish, S. J.; Redshaw, C.; Solan, G. A.; Strömberg, S.; White, A. J. P.; Williams, D. J. *J. Am. Chem. Soc.* **1999**, *121*, 8728.

(44) Beckwith, A. L. J.; Bowry, V. W.; Ingold, K. U. *J. Am. Chem. Soc.* **1992**, *114*, 4983.

(45) Small, B. L.; Brookhart, M.; Bennett, A. M. A. *J. Am. Chem. Soc.* **1998**, *120*, 4049.

5. Summary and Outlook

Metal centers that perform both C–H bond activation/C–O bonds formation via O-atom insertion have the potential as catalysts for selective oxy-functionalization of hydrocarbons. Two pathways for the oxygen atom insertion into M–R bonds, the organometallic Baeyer-Villiger (OMBV) type pathway and the migration of R to M=O pathway, are promising and under investigation.

5.1 Early 3d *vs* late 4d and 5d (nucleophilicity of the $R^{\delta-}$ *vs* electrophilicity of $O^{\delta+}$)

As discussed above, metal–alkyls that are $M–C^{\delta+}$ polarized likely undergo reductive functionalization with X^- nucleophiles, but $M–C^{\delta-}$ polarized systems do not. Metal–alkyls that are $M–C^{\delta-}$ polarized likely undergo migration of $R^{\delta-}$ to the electrophilic $M–O^{\delta+}–Y$ in OMBV reactions or to the electrophilic $M\equiv O^{\delta+}$ in the R to M=O reactions. Early transition metals are more likely to generate a nucleophilic $M–R^{\delta-}$ but also seems to generate less nucleophilic $O^{\delta+}$, while late transition metals are more likely to generate an electrophilic $M–R^{\delta+}$ but also seems to generate more nucleophilic $O^{\delta+}$ (Scheme 5.1). Relatively little is known about the O-atom insertion reactions with few examples demonstrated, hence we have three questions at the beginning (see above): *Which plays a more important role, the nucleophilicity of the* $M–C^{\delta-}$ *bond or the electrophilicity of the bound* $O^{\delta+}$*? Can we extend the OMBV reaction to a series of M–R complexes with different electronic configurations and geometries and other oxidants? If more OMBV reaction are discovered, Is there any transition series between early transition metals with generally more nucleophilic* $–R^{\delta-}$ *groups and later transition metals with generally less nucleophilic –R group but more electrophilic* $O^{\delta+}$ *group that is likely to facilitate the*

O-atom insertion reaction? With the studies of O-atom insertion reactions into the early/middle W–R complex, the late first row $\mathrm{Fe^{II}}$ and $\mathrm{Co^{I}}$–R complexes and the previously studied late $\mathrm{Rh^{III}}$ and $\mathrm{Pt^{II}}$–R complexes, the answers seem almost elucidated, if not totally.

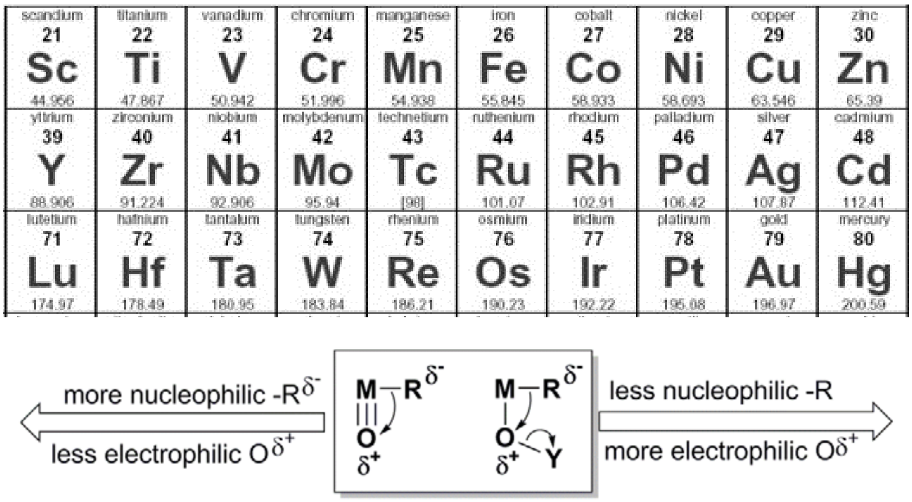

Scheme 5.1. Transitions for the nucleophilicity of the $\mathrm{M{-}C^{\delta-}}$ bond or the electrophilicity of the bound $\mathrm{O^{\delta+}}$ in the periodic table.

Experimental and computational studies of oxy-insertion indicate that the OMBV reaction with the late 2nd and 3rd row transition metal $\mathrm{Rh^{III}}$– and $\mathrm{Pt^{II}}$–hydrocarbonyl complexes occur with extremely large activation barriers. DFT calculation indicate activation barrier greater than 40 kcal/mol for the OMBV-type oxygen insertion reaction, and experimental work performed by Joanna Webb in our group resulted in no O-atom insertion product, despite the fact that $\mathrm{Pt^{II}}$ and $\mathrm{Rh^{III}}$ hydrocarbyl complexes with coordinated oxidants have been isolated.[1,2] To the contrast, facile O-atom insertion into early/middle $\mathrm{W^{VI}}$–R complexes via OMBV pathway has been demonstrated experimentally and computationally. O-atom insertion products have also been observed from the reactions of middle transition metal first row $\mathrm{Fe^{II}}$ and $\mathrm{Co^{I}}$–R complexes with oxidants. We successfully *extended the O-atom insertion reaction to a range oxidants and more M–R complexes with other geometries and electronic configurations. The experimental and theoretical results indicate that the nucleophilicity of the M–C*$^{\delta-}$ *bond seems to be a more important factor than the electrophilicity of the bound O*$^{\delta+}$ *in the OMBV reaction.*

5.2 OMBV *vs* R to M=O

It should be noticed that, for the two well-defined OMBV reactions of Re^{VII} and W^{VI}–R complexes, the metal centers are at their highest oxidation state with no d electrons, thus, competitive oxidation by YO of the metal center versus the R group is not possible. However, Re^{VII} and W^{VI}–R complexes are unlikely to facilitate C–H activation of hydrocarbons. Since low oxidation state metal centers with more d electron counts are more active for C–H activation, we consequently sought to extend the OMBV reaction to the d^6 or d^8 later transition metals.

As discussed in Chapter One, Density Functional Theory (DFT) computational study performed by Cundari Group in University of North Texas shows that, the OMBV insertions of $[(bpy)_xM(Me)(OOH)]_n \rightarrow [(bpy)_xM(OMe)(OH)]_n$ (x = 1 or 2; bpy = 2,2'-bipyridyl; n is varied to maintain the d-electron count at d^6 or d^8) are favored by lower coordination numbers (x = 1 versus x = 2), earlier transition metals, and first-row (3d) transition metals,[1] which is consistent with the analysis above. Actually, the activation barrier is as low as ~25 kcal/mol for the OMBV reaction of the late 3d metals.[1] However, experimental results indicate the oxidation of the metal center (Fe^{II} and Co^{I}) as well as producing the O-atom insertion products. Further calculations by the Cundari Group show that the migration of R to M=O pathway has even lower activation barriers than the OMBV pathway for the O-atom insertion reaction for late 3d metals.

Since OMBV reaction and R to M=O migration both prefer metal–alkyls that are more M–C$^{\delta-}$ polarized and have the same trend in metal selectivity, they can be competitive. There is no change for the oxidation state of the metal center in the OMBV reaction, hence the competitive oxidation of the metal center by YO is undesirable and could be a key challenge in utilizing this type of functionalization reaction to design new hydrocarbon functionalization catalysts based on a C–H activation/C–O bond formation cycle. Low oxidation state late 3d and 4d metal complexes are likely to be oxidized by YO to give a higher oxidation state M=O; middle transition metal complexes are also likely to lose all their d electrons to reach their highest oxidation state before they undergo OMBV reaction (such as W^{VI} and Re^{VII}); late 5d and high oxidation state 4d metal–alkyl are almost always M–C$^{\delta+}$ polarized and unlikely to undergo OMBV reaction. Thus, *if a C–H activation capable d^6 or d^8 metal complex also undergoes O-atom insertion, it is unlikely to proceed through the OMBV pathway. A migration or R to M=O pathway would be more reasonable.*

5.3. Trends for the O-atom Insertion into Middle and Late Metal–Carbon Bonds

Scheme 5.2 shows a summary of examples for the O-atom insertion into middle and late metal–carbonyl bonds so far. The reported O-atom insertion into Ta–C bonds in Group (V), is proposed to proceed through the migration of the R to the η^2-peroxo ligand.[3] The O-atom insertion reaction of Cr with O_2 is also proposed to have this mechanism.[4] Both migration of R to the η^2-peroxo ligand and OMBV pathway are observed in the O-atom insertion in the W system in Group (VI).[5] Moreover, the O-atom insertion in the Re–C bond in MTO is demonstrated to proceed via OMBV pathway and the migration of R to Re-oxo is also observed in Brown and Mayer's system in Group(VII).[6,7] Finally, O-atom insertion and related products have been observed in the Group (VIII to X) complexes (*i.e.*, Fe, Co, Ni, Pd), though no solid experimental evidence has been provided to demonstrate the mechanisms for these O-atom insertion reactions. Computational studies indicate that all these reactions prefer the migration of the aryl or alkyl to the metal-oxo pathway.[8-10] The colored arrow in Scheme 5.2 summarizes the transition of the mechanisms for O-atom insertion reaction: from left to right in the period table, the favored mechanism transit from migration of R to η^2-O_2 ligand to migration of R to M–OY, and finally to migration of R to M=O.

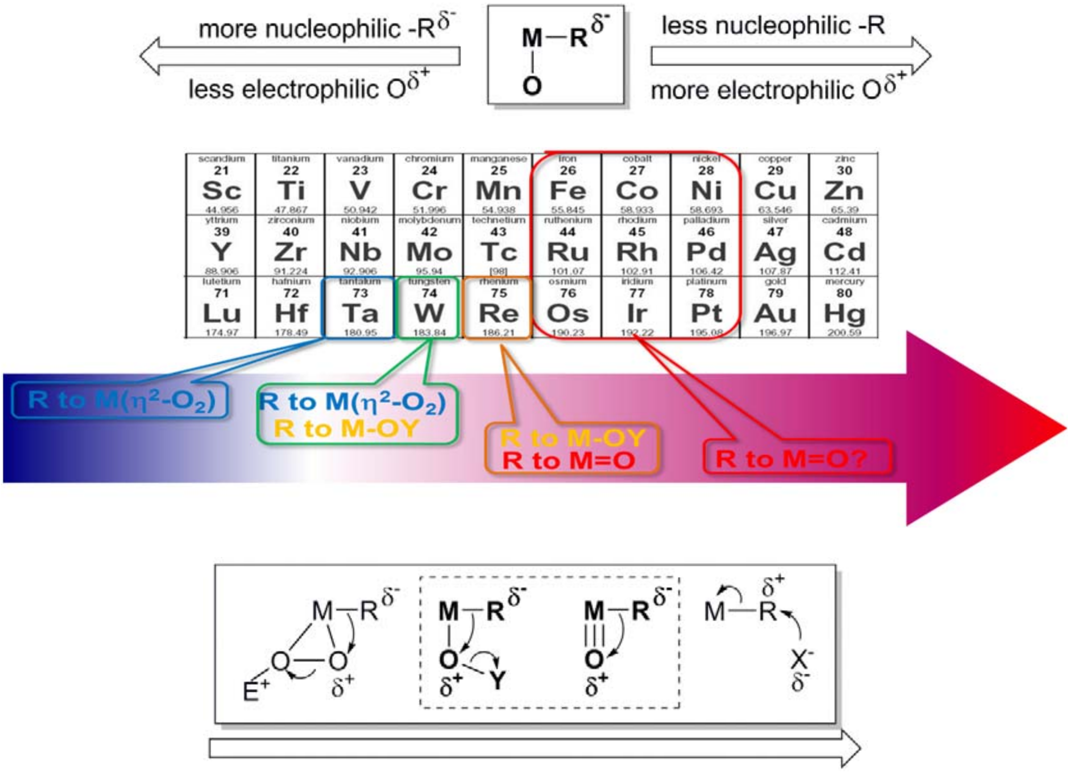

Scheme 5.2. Summary for the O-atom insertion into middle and late metal–carbonyl bonds.

From left to right on the periodic table, the metal–alkyls are from more M–R$^{\delta-}$ polarized to less M–R$^{\delta-}$ polarized to M–R$^{\delta+}$ polarized (above arrow in Scheme 5.2) . As discussed above, the OMBV reaction and R to M=O migration both prefer metal–alkyls that are more M–C$^{\delta-}$ polarized and have the same trend in metal selectivity, and hence they can be competitive. In the migration of R to η^2-O_2 ligand reaction, including the reported Ta^{V}, W^{VI} and Re^{VII}–(η^2-O_2) complexes, electrophiles such as proton are required to enhance the electrophilicity of the bound η^2-O_2 ligand to facilitate the nucleophilic attack of the R$^{\delta-}$ group. Thus, the R to η^2-O_2 migration is more facile for metal-hydrocarbyl bonds that are polarized M–C$^{\delta-}$, making it competitive with the OMBV reaction and R to M=O migration. In addition, oxidation of the metal center by YO can compete with O-atom insertion reactions above. Herein, we are trying to answer the question that searches for a section of transition series between early transition metals with generally more nucleophilic –R$^{\delta-}$ groups and late transition metals with generally less nucleophilic –R group (see above). *For non-d^0 early/middle transition metal–alkyl complexes, oxidation of the metal centers is often facile, and low oxidation state early/middle metal centers will lose all of their d-electrons to achieve their highest oxidation state (i.e., attempted O-atom insertion with W^{II}–R complex resulted in oxidation to W^{VI}–R complex). With peroxide oxidants (or O_2 in some case), early/middle M(η^2-O_2)–R might be generated and likely to undergo O-atom insertion via R to η^2-O_2 migration in the presence of electrophiles. Middle d^0 metal–alkyls are likely to undergo O-atom insertion via OMBV pathway. Low oxidation state late d^6 or d^8 3d and 4d metal-alkyls* *are likely to have O-atom insertion via R to M=O migration. High oxidation state late 4d or 5d metal–alkyls are more likely M–R*$^{\delta+}$ *polarized and less likely to undergo any O-atom insertion reaction. Reductive functionalization is more promising for them.* The trends of this transition are summarized in the bottom arrow in Scheme 5.2.

5.4 Ligands

Computational studies by Cundari for the O-atom insertion into first row (3d) metal–alkyl bonds indicate low energy barriers.[1,10] However, experimental attempts to observe O-atom insertion into Cp*Fe(CO)(CH_3CN)Ph resulted in the more competitive CO insertion.[10] The Cp*Fe(P(OCH_2)$_3$CEt)$_2$Ph complex without CO ligand was reacted with oxidants. Although high yield of O-atom insertion product PhOH was observed, the other ligands coordinated to the metal center were all oxidized and caused the decomposition of the starting complex. Similar observations were made for reactions of a Co^I complex with oxidants. The triamine (N3 = 2,6-diacetylpyridinebis(2,6-diisopropylanil)) ligand dissociates from the metal center in the reactions of (N_3)CoMe with oxidants.

Our results provide suggestions for future catalyst design: 1) First row transition metals are capable of O-atom insertion into M–R bonds and should be a focus for catalyst development; 2) ligands that can insert into M–R bonds or be oxidized, such as CO, should be avoided; 3) the ligands coordinated to the metal center should be resistant to the oxidation (e.g.,. *N*- or *O*-based ligands are viable). As an example, based on these considerations, the reported ($^{tBu}N_4$)Fe ($^{tBu}N_4$ = (N,N’-di-tert-butyl-2,11-diaza[3.3](2,6)pyridinophane) complexes are potential choicees to perform O-atom insertion and catalytic oxidation of hydrocarbons. Former studies by Mirica and co-workers show that the $^{tBu}N_4$ ligand stays coordination with the Fe center when reacting with oxidants such as H_2O_2 (Scheme 5.3).[11] As a result, the alkylated ($^{tBu}N_4$)FeR_2 and ($^{tBu}N_4$)Fe(CH_3CN)R(OTf) complexes would be promising for O-atom insertion and catalytic selective oxidation of hydrocarbon studies.

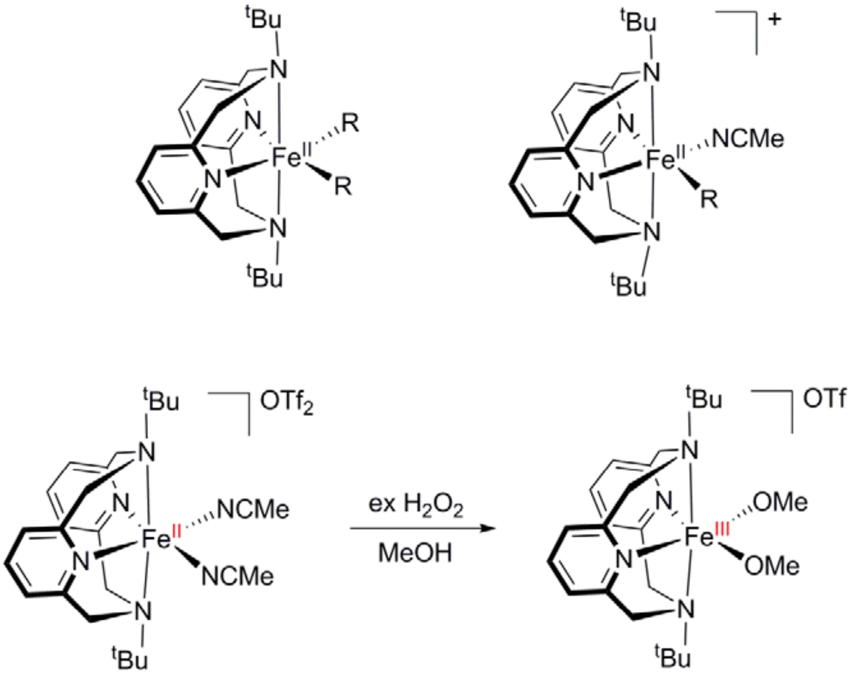

Scheme 5.3. Proposed ($^{tBu}N_4$)FeR_2 and ($^{tBu}N_4$)Fe(CH_3CN)R(OTf) ($^{tBu}N_4$ = (N,N'-di-tert-butyl-2,11-diaza[3.3](2,6)pyridinophane) complexes for future O-atom insertion reaction and the $^{tBu}N_4$ ligand stays coordination with the Fe center when reacting with oxidants such as H_2O_2.

5.5 Outlook and Future Directions

Our studies suggest that a catalyst that can perform both C–H bond activation and C–O bond formation via O-atom insertion to catalyze the partial oxidation of hydrocarbon should likely be a d^6 or d^8 later transition metal complex with oxidative-resistant and strongly coordinating ligands. As electrophiles facilitate the R to η^2-O_2 migration type O-atom insertion reaction, they might also catalyze the OMBV reaction or R to M=O migration, by coordinating the YO or oxo ligand to enhance the electrophilicity of the bound O^- For example, water facilitates the OMBV reaction of the W^{VI}–R with IO_4^- by enhancing the electrophilicity of the bound O of IO_4^-. Thus, electrophiles have the potential to be the co-catalyst for hydrocarbon oxy-functionalization.

5.6 References

(1) Figg, T. M.; Webb, J. R.; Cundari, T. R.; Gunnoe, T. B. *J. Am. Chem. Soc.* **2011**, *134*, 2332.

(2) Webb, J. R.; Figg, T. M.; Otten, B. M.; Cundari, T. R.; Gunnoe, T. B.; Sabat, M. *Eur. J. Inorg. Chem.* **2013**, *2013*, 4515.

(3) Van Asselt, A.; Trimmer, M. S.; Henling, L. M.; Bercaw, J. E. *J. Am. Chem. Soc.* **1988**, *110*, 8254.

(4) Hess, A.; Hörz, M. R.; Liable-Sands, L. M.; Lindner, D. C.; Rheingold, A. L.; Theopold, K. H. *Angew. Chem. Int. Ed.* **1999**, *38*, 166.

(5) Mei, J.; Carsch, K. M.; Freitag, C. R.; Gunnoe, T. B.; Cundari, T. R. *J. Am. Chem. Soc.* **2013**, *135*, 424.

(6) Conley, B. L.; Ganesh, S. K.; Gonzales, J. M.; Tenn, W. J.; Young, K. J. H.; Oxgaard, J.; Goddard, W. A.; Periana, R. A. *J. Am. Chem. Soc.* **2006**, *128,* 9018.

(7) Brown, S. N.; Mayer, J. M. *J. Am. Chem. Soc.* **1996**, *118,* 12119.

(8) Matsunaga, P. T.; Hillhouse, G. L.; Rheingold, A. L. *J. Am. Chem. Soc.* **1993**, *115*, 2075.

(9) Alsters, P. L.; Boersma, J.; van Koten, G. *Organometallics* **1993**, *12*, 1629.

(10) Mei, J.; Pardue, D. B.; Kalman, S. E.; Gunnoe, T. B.; Cundari, T. R.; Sabat, M. *Organometallics* **2014**, *33*, 5597.

(11) Khusnutdinova, J. R.; Luo, J.; Rath, N. P.; Mirica, L. M. *Inorg. Chem.* **2013**, *52*, 3920.